MEASUREMENT OF TWO-PHASE FLOWS BY PHASE SEPARATION

by

T.S. Whitaker

Thesis submitted in accordance with
the requirements of The University
of Liverpool for the Degree
of Doctor of Philosophy

Department of Mechanical Engineering,
The University of Liverpool.

November 1992

SUMMARY

The aim of this programme of research was to produce a prototype two-phase flowmeter by separating a mixture of gas and liquid to the constituent phases and passing each through a conventional flowmeter.

The performance characteristics of a novel gas/liquid separator were determined for single-phase and two-phase flow conditions. Static pressure and velocity profiles in the helical passages showed secondary flows to be present. Testing using air/water mixtures demonstrated that the gas and liquid phases were separated by the centrifugal forces generated by the motion of the two-phase mixture through helical passages.

The separator was modified to permit the collection of the separated phases. The performance was quantified in terms of the gas separation efficiency and the liquid draw-off. Air/water and air/kerosene flows were used in the experimental work, which examined several different separator configurations. The flow rate and quality of the separated mixture were found to be a maximum at low residence time (high flow velocity).

A model simulating separated flow was used to predict the position of the phase interface in the helical passages. This model was validated from the separator friction pressure loss data in two-phase flow. Flow in helically coiled tubes was examined to determine the effects of helix angle on the flow structure and pressure losses.

Experimental data from individual take-off slots in the separator was found to be in close agreement with the Schrock correlation for flow through an upward branch in a tee junction. The take-off flow quality depended on the phase interface position below the slot and the axial location of the slot.

A combination of annular and classical venturimeters was selected for measurement of phase flow rate. The annular venturimeter provided total volume flow rate measurements with an uncertainty lower than ± 10%, given that the gas and liquid were well-mixed. The classical venturimeter results were less good due to more demanding flow conditions.

The separator and venturimeters were combined to form the prototype two-phase flowmeter. The total volume flow rate was measured to within ± 10% of the reference. Void fraction was found to be related to the ratio of the pressure drops at each venturimeter. The liquid flow rate was measured to within ± 10% of the reference. The prototype two-phase flowmeter successfully demonstrated measurement of the total and liquid phase flow rates to limits acceptable in many practical situations.

ACKNOWLEDGEMENTS

The author's thanks go to Dr Ieuan Owen for his advice and encouragement, which was invaluable during the course of this research.

The author also wishes to thank the members of the Mechanical Engineering Workshop at Liverpool University for their assistance, in particular Mr Geoff Williams.

The latter part of this research was conducted at NEL and the author thanks Dr Brian Millington for his advice and support.

My thanks also to my wife, Elizabeth, for her support, understanding and encouragement during this period.

This work was carried out with financial support from the Department of Trade and Industry under Grant No. NPX/7/030.

CONTENTS

NOMENCLATURE

A	Area
Cd	Discharge Coefficient
d	Internal Diameter
D	Outer Diameter
f	Friction Factor
F	Force
g	Acceleration due to gravity
G	Mass Flux
h	Phase Height
H	Duct Height
l	Length
L	Length
m	Mass Flow Rate
n	Integer Number
P	Pressure
Q	Volume Flow Rate
r	Radius
R	Radius
s	Perimeter
t	Time
T	Temperature
U	Mean Velocity
v	Local Velocity
x	Distance

X^2	Lockhart-Martinelli Parameter
z	Distance

Greek Symbols

α	Volume Void Fraction
β	Diameter Ratio (d/D)
δ	Small Quantity
Δ	Difference
θ	Angle
η	Efficiency
μ	Kinematic Viscosity
ν	Dynamic Viscosity
π	Constant
ϕ^2	Two-phase Multiplier
ρ	Density
σ	Surface Tension
Σ	Sum of
τ	Shear Stress

Subscripts

a	Annular
eq	Equivalent
g	Gas Phase
i	Interfacial Quantity
k	k^{th} Phase
l	Liquid Phase

CHAPTER 1: INTRODUCTION

1.1 The Nature Of Multiphase Flow in Practice

1.1.1 Introduction to Multiphase Flow

Multiphase flow is encountered when fluids of two or more different phases flow together simultaneously in any continuous volume. For example, when a gas, liquid and solid phase flow together in a pipe. There may also be more than one component in the mixture, this most commonly occurs when the gas phase is not the vapour of the liquid phase, such as in an air/water mixture.

Multiphase flows tend to adopt differing geometrical flow patterns depending on the mass and volume fractions, the total volume flow rate of each phase, the orientation of the flow space and the pressure of the mixture. The most commonly occurring flow patterns have been observed under laboratory conditions and identified, those typical of vertical and horizontal tubes are shown in Fig. 1.1.

Single component flows such as steam/water can raise problems of flashing or condensation, due to either decrease or increase in the pressure of the fluid mixture, resulting in the creation of significant quantities of vapour or liquid condensate in a mixture. This phenomenon is often caused by passage through components, such as valves, resulting in changes of pressure and velocity of the mixture. In multiphase flows these changes in phase,

allied to simultaneous changes in volume fraction and interphase slip ratio caused by changes in the mixture pressure, may result in flow pattern or regime changes which are difficult to predict and, in the absence of optically clear sections, can be difficult to detect.

1.1.2 Definition of Void Fraction

To deal with multiphase flow in practice is a difficult problem, particularly when attempting to measure the individual phase mass flow rates and velocities. The determination of void fraction is also difficult, not least because it may defined by three different methods: the line void fraction is defined as the percentage of a straight line through a mixture which passes through the gas phase, the area void fraction is defined as the percentage of the area of a plane cross-section which is occupied by the gas phase and the volume void fraction is defined as the proportion of a fixed volume which is taken up by the gas phase. For the purposes of this work the void fraction will be defined as the volume void fraction unless otherwise stated.

1.1.3 Multiphase Flow Modelling

The theoretical treatment of multiphase flows is far more complex than that of single-phase flows; there are many more variables and the knowledge of such flow is so limited that for any practical analysis it is normal to use numerous simplifying assumptions and empirical correlations. Most of the simpler theories

assume that a given type of flow pattern exists and then base the analysis upon this premise, see for example Baroczy (1966).

Of these flow theories, the most commonly used is probably the homogeneous model. The homogeneous model assumes that the flow consists of a homogeneous mixture in thermal equilibrium which can be treated as a single fluid with the area or volume averaged properties of its two components. Other models usually relate to other identifiable quasi-steady flow regimes such as separated flows (stratified or annular flows) and dispersed flows (bubble, mist and churn flows). The main difficulty with most of these models is in being certain of which flow regime exists in the time and space in which the interest lies and of knowing which of the assumptions made in the model selected are valid under the conditions prevalent in the flow.

Attempts have been made to predict the changes in flow pattern using flow regime maps which plot the various experimentally defined regime boundaries against parameters which are independent of tube diameter and fluid pressure. The efforts of many early workers in the multiphase flow field were directed towards producing flow regime maps based on empirical data. The best known of these flow maps are those of Baker (1954) and of Mandhane et al (1974) for horizontal flow, Fig. 1.2, and Oshinowo and Charles (1974) for vertical flow.

Flow pattern maps, of course, are only valid for the conditions prevalent during the experiments and the configuration of the apparatus used to collect the data from which the maps were constructed. Those, such as the Mandhane flow map, constructed from large data bases are more reliable than the maps made using small

data sets. It is generally difficult to be precise in predicting flow patterns using these techniques, particularly near the flow regime boundaries. The flow regime may also change while passing through the region of interest, this is particularly true if any body forces are applied or if the flow is accelerated by passage through a component or pipe constriction.

The main problem with the homogeneous model, even when the flow is apparently homogeneous, is that there is almost certain to be some slip, or relative velocity, between the phases. The assumption of no slip is one of bases of this theory, allowing the mixture to be treated as a single fluid, and any variation from the no slip condition leads to errors in the analysis. Recent flow theories have concentrated on a multidimensional approach to a general solution, using closure equations which are flow regime dependent, to enable solutions to be obtained. General agreement has been obtained on the form of the three-dimensional conservation equations using this approach [Ishii, 1975] and debate now centres on the forms of the closure equations [Boure, 1987] which usually involve simplifying assumptions such as no interfacial slip or constant pressure through the cross-section of the flow. Often the form of the closure equations is also flow regime dependent. Even with the use of these closure equations specific solutions in more than one dimension are problematic. For problems involving pipework or other devices which contain flow passages of complex shape modelling approaches are often used which depend on correlations from previous experiments.

1.2 The Difficulties Presented by Multiphase Flow in the Oil Industry

1.2.1 Production Problems

The majority of oil wells produce not just oil but often natural gas and contaminants such as sand, chemical 'mud' and water. The 'live' crude oil will contain many different fractions which may also tend to flash into gases as the well-head is approached and the mixture pressure drops, thus increasing the void fraction of the mixture. Some wells which produce mainly natural gas may have problems involving condensate as the mixture temperature drops. These deviations from single-phase flow will affect conventional flowmeters to varying degrees, as demonstrated by Kinghorn and McHugh (1981) for a turbine flowmeter.

1.2.2 Flowmetering Problems

The oil industry has flowmetering requirements in three different areas; fiscal metering, custody transfer and reservoir management. Fiscal metering, which would be required to allow the transportation of the oil of two or more different producers simultaneously through one pipeline, will require multiphase flowmeters to measure mass or volume flowrates to ± 0.25% accuracy for high value fluids such as oil while ± 1% will be adequate for fluids such as natural gas and water which have a lower value to the oil producer. Custody transfer metering is used to allow produced streams of oil from the subsea wells of a number of different

operators to be tied back to a single platform. Custody transfer meters will be required to achieve the best possible accuracy. In the case of the chemical process industry this accuracy may be variable and will probably depend on the value of the fluids concerned or the required accuracy of their proportions.

1.2.3 Future Flowmetering Requirements

Multiphase meters for reservoir management will be used to find the rates of withdrawal of the constituent fluids from an oil well; this knowledge will then allow the petroleum engineer to manage his total resources effectively. It is important to know if an oil well develops water breakthrough, which occurs when water pumped down-hole to force the oil out of the reservoir returns to the surface. Water breakthrough reduces the production efficiency of a well and increases the production costs. At present all the wells on one platform are sampled in rotation and it can be several weeks between tests on each individual well. An inexpensive multiphase flowmeter could be fitted to each well and calibrated against the platform test separator. This type of meter could also be used to provide checks against test separators on exploration rigs.

Repeatability is probably more important than accuracy in the context of reservoir management as the meter can be calibrated against the meters on the production platform. For reservoir management an accuracy of ± 10% would be considered adequate, as long as the unit cost of the flowmeter was relatively low. Multiphase flowmeters for these purposes could also be suitable for subsea use.

1.2.4 Potential Applications

Subsea multiphase flowmeters will allow the development of presently uneconomic reserves by removing the need for a dedicated platform at each field. As oil reserves become depleted and oil prices rise previously uneconomic or marginal fields may be considered for production. The economic case for this type of development may not justify the use of a dedicated platform at the field. The wells may be drilled from a mobile rig and produced from a subsea wellhead, Fig. 1.3. Each well could then be controlled from a nearby existing production platform using the information from the subsea multiphase flowmeters. The production from these subsea wells will then be pumped back to that platform, thus improving the economic viability of the entire system, particularly if the platform is relatively mature and the original field is becoming uneconomic. Due to lack of space on the platform for individual separators for each well these subsea wells will need to be monitored and controlled by subsea flowmeters and pumps, Sasanow (1989).

Subsea separators are likely to be too bulky and so the flowmeters will have to be tolerant of multiphase flow whilst maintaining at least sufficient accuracy to allow their use for reservoir management. Thus the greatest fixed cost of new oil field development, the cost of a new production platform, will be eliminated. This economy will immediately make marginal fields more attractive for development.

Fiscal metering requirements will be difficult to achieve, the accuracy required is often only achieved in single-phase flow with great care over installation and calibration of the flowmeter. Multiphase flow is, as yet, not as well understood and consequently repeatable results are still more difficult to achieve than for single-phase fluids. Problems are caused particularly by the often intermittent nature of the flows encountered.

The most promising applications for a multiphase flowmeter appear to be for reservoir management and for custody transfer, where the required accuracy of the flowmeter is less stringent. The practical application of such flowmeters is complicated by the presence of solid phases in the mixture to be metered and, often, the presence of more than one liquid phase.

The solid phases cause abrasion, impact damage and wear to the exposed parts of flowmeters and so intrusive parts, particularly moving parts, are prone to excessive wear causing flowmeters to rapidly lose their calibration. These problems can be exacerbated by waxing, causing the formation of solid particles in the flow and deposition on wetted parts or blocking of small flow passages such as pressure tappings.

As many of the applications envisaged for multiphase technology are subsea there is a minimum acceptable mean time between failures typically 2-3 years as diver servicing/replacement is expensive in terms of time and lost production. The oil industry would also like to see no calibration being necessary once the flowmeter is in-situ.

1.3 Existing Technology

1.3.1 Conventional Flowmeters in Multiphase Flow

Conventional flowmeters for single-phase flows fall into several groups. The most commonly used are devices which infer the volume flowrate of the fluid from a measure of the change in momentum through the meter; typical of such devices are the orifice plate and the venturimeter. Positive displacement meters measure the throughput of known volumes of the fluid and non-intrusive flowmeters, such as electromagnetic and acoustic flowmeters, infer fluid velocity from either proportionally induced voltages or cross-correlation of acoustic signatures. There are also mass flow meters of which the Coriolis type meter is probably the most widely used. All these types of flowmeter have their performance adversely affected to some extent by the presence of both gas and liquid phases together. The presence of a second liquid phase or a solid phase is less problematic.

The main problem for momentum change meters is measuring the total volume flowrate when the meter signal, often in the form of a differential pressure, varies considerably as the instantaneous local void fraction changes. The changes in void fraction may be characteristic of the prevalent flow pattern or due to pressure loss through the meter. Void fraction measurement still presents a difficult problem especially in separated flow regimes where there will be significant slip between the phases. Positive displacement meters will still measure set volumes, but again a measure of the void fraction is necessary. Inferential flowmeters tend to produce

poor readings due to the disparity in the densities and discontinuities of the phases and the presence of slip. Those flowmeters with moving or non-moving parts, which are in contact with the fluid, tend to be very inaccurate. This is particularly true of those which rely on fluid-dynamic effects such as vortex shedding, here the gas voids in the flow are usually counted in addition to the vortices or stimulate unpredictable rates of vortex production which are no longer proportional to the flow rate of the fluids.

The problem breaks down into two distinct areas; firstly the problem of noise in the signal from the flowmeter and secondly the interpretation of the signal. The effects of noise on the signal may be reduced by filtering the signal to remove readings which are well away from the mean signal or by taking the signal over a long time base to average out the noise. This type of technique makes transient analysis of the signal difficult and the flowmeter readings have to be taken as mean values.

1.3.1 Flowmetering by Phase Separation

Compared with the flowmetering of multiphase mixtures, the metering of single-phase fluids presents few difficulties. Indeed under ideal conditions a repeatability of 0.05% can be achieved and flowmeter manufacturers often claim accuracies of 0.25% of full scale for turn down ratios of up to 10:1. The technologies associated with these accuracies have usually been seen to be more sensitive, and so less accurate when used in multiphase flows, or to

involve delicate moving parts which are vulnerable to heavy scouring wear or impact damage leading to loss of calibration.

One method of measuring multiphase flow is to separate the component fluids and, using the mature single-phase technology, measure the flow rates of each separated stream. Separation techniques are usually associated with the use of natural gravity or with some method of enhanced gravity, involving a rotating type of flow field to generate a centrifugal gradient as in a hydrocyclone, Nebrensky et al (1980). These techniques rely on the use of acceleration fields on mixtures of fluids of different densities to effect separation [see Helgeson et al, 1984]. Normally those mixtures with the greatest differences in densities will be separated most successfully. Hence the separation of a gas or a solid from a liquid is considerably easier than the separation of two liquids.

Separators which rely solely on the action of gravity tend to be of large volume in relation to their throughput. This is due to the length of residence time required to achieve good separation. Such separators are often found on oil rigs, Fig. 1.4. Because the size, weight and cost of these separators prohibits the use of dedicated equipment for each production train a single separator is used to sample between many different wells and analyse the output of each.

Separators which make use of artificial gravity are devices such as centrifuges and hydrocyclones, Fig. 1.5. Both of these types are more compact than gravity separators but are still too bulky to be considered as in-line separators. Hydrocyclones have advantages over centrifuges in that they have no moving parts and

will accept greater throughput for a given size but they are sensitive to flowrate and voidage, and large deviation from their design operating point tends to lead to carry-under of gas or carry-over of liquid.

1.4 Separator Origins and Principle

1.4.1 Gas/Oil Separator

It is proposed that a new type of multiphase flowmeter, of compact design, can be developed using a compact type of separator with a continuous helical flow path. Conventional flowmetering technology could then be used on the separated phase flow streams to obtain the flow rates of the individual phases. The separator to be used has demonstrated that it can achieve some separation of two-phase gas/liquid flows, King and Purfit (1984), although the effectiveness of this separator, prior to the present work, was unknown.

The separator was designed by INCO Ltd and consisted of a profiled body which is inserted into a plain tube. The insert has six helical passages of triangular cross-section cut into its outer diameter, Fig. 1.6. These passages have a total cross-sectional area of 18% of that of the 100mm diameter pipe in which the centrebody is placed. Thus the fluid mixture which enters these passages undergoes an increase in velocity, due to the decrease in flow area and the mixture is also forced to rotate around the centrebody due to the helical nature of the passages. The rotation of the flow in turn induces a centrifugal field which will act to separate fluids of

differing densities, the more dense fluid will pass to the passage outer wall and the less dense fluid will move radially inward. The phase distribution in the separator has been investigated by King and Purfit (1984) and shown to be similar to that described above. King and Purfit also showed that an improvement in the quality of separation can be achieved by reducing the pitch of the separator. This increased the influence of the centrifugal gradient relative to the influence of the buoyancy forces acting on the gas phase by increasing the tangential velocity of the mixture.

1.4.2 State of Development of Separator/Flowmeter

Prior to the present project the Gas/Oil Separator had been developed to the point at which a visual assessment of the underlying principle could be made. There had been no attempt to describe the type of flows existing in the separator beyond the intuition that separation would be achieved between gases and liquids by a combination of gravity and centrifugal forces. It was apparent that separation of some degree was achieved. From early work using a small sampling type of probe King and Purfit described the phase distribution in the helical passages.

A second generation device was then manufactured with a reduced flow area and reduced pitch. The effect of these modifications was to increase the influence of centrifugal forces on the separation relative to the gravity forces. Similar experiments to determine the phase distribution in the helical passages appeared to show that a better separation was achieved by the modified

device. No attempt was made to collect the separated phases and thus to estimate the efficiency of the device.

1.5 Proposed Multiphase Flowmeter

The objective of the present work is to develop a multiphase flow meter to the highest possible accuracy. To achieve this the Gas/Oil separator described above will be used in conjunction with conventional flowmeters. An attempt will be made to meet practical requirements for robustness. The underlying principles of the multiphase flowmeter will be analysed in as much depth as possible in order to improve the function of the device.

The separator will be used to separate the two phases entering the flowmeter. In the present work gas and liquid will be used as the two phases inside the helical passages. The problem is then how to pass each phase to different flowmeters. The proposed solution to this problem is to produce a passage internally in the separator. This passage will be open to the separator exit and so to the pressure at the separator exit plane. The pressure at this plane being lower than at a point, say, mid-way along the separator, due to the frictional losses in the helical passages. If slots or holes are then cut through the wall of the separator between the helical passage roots and the internal passage there should be sufficient pressure differential, Fig. 1.7, to drive the separated gas phase through the slots into the internal passage. The far greater centrifugal force on the liquid phase, due to its much greater density, will tend to prevent the liquid from passing through the slots into the internal passage.

The gas and liquid phases are then physically divided by the wall of the separator and may then be passed to different flowmeters. There is unlikely to be complete separation of the gas and liquid streams using this, or any other, method. Therefore the flowmeters which are to be used to measure the phase flow rates will encounter two-phase flow conditions, although these conditions will be much closer to single-phase flow than those of the main flow stream. Due to the presence of more than one phase passing through the flowmeters, a less accurate measure of the total flow rate can be anticipated. Even so, to have practical applications, an accuracy of ± 10% may be acceptable if the overall cost of the device is reasonably low. The individual flow rates of each phase may also be measured if the void fraction of the flow through the separator is known. In the following chapters the results of experimental and theoretical investigations of the separator/flowmeter package are presented and discussed.

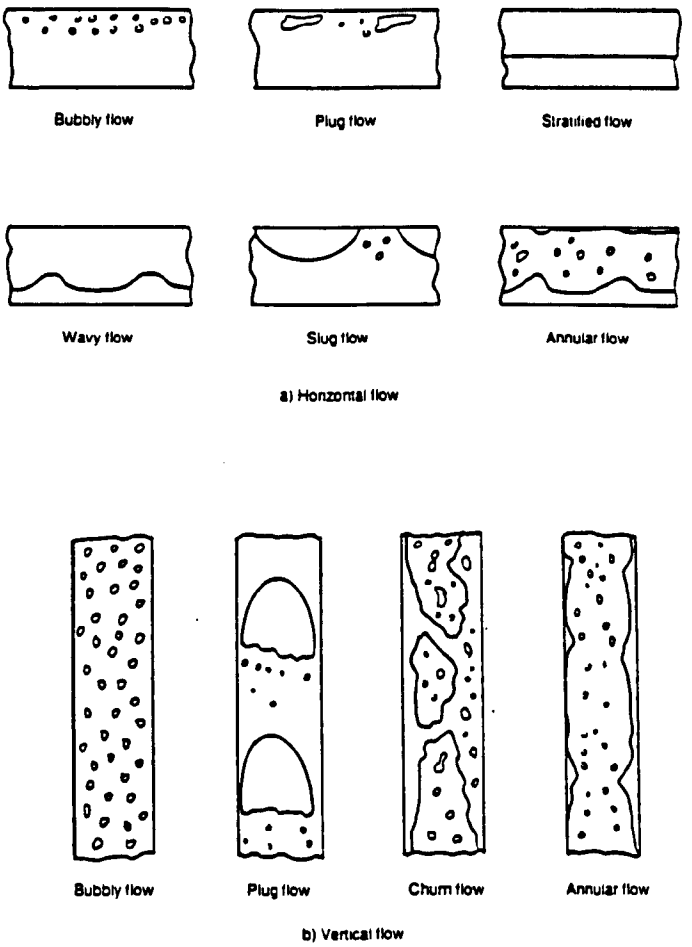

Figure 1.1 Flow patterns in horizontal and vertical flow

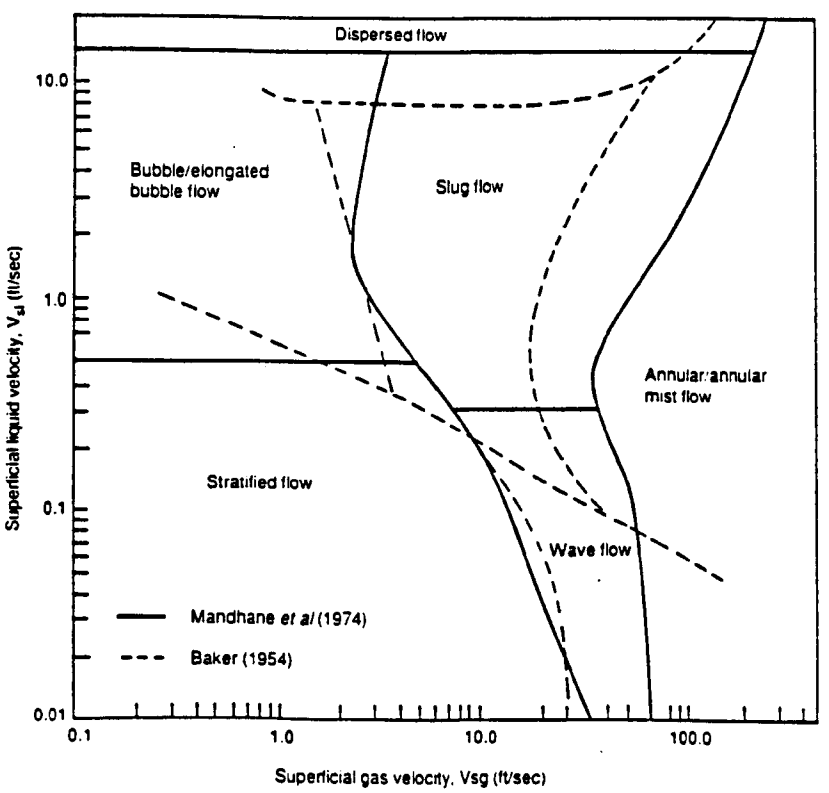

Figure 1.2 Horizontal flow pattern map

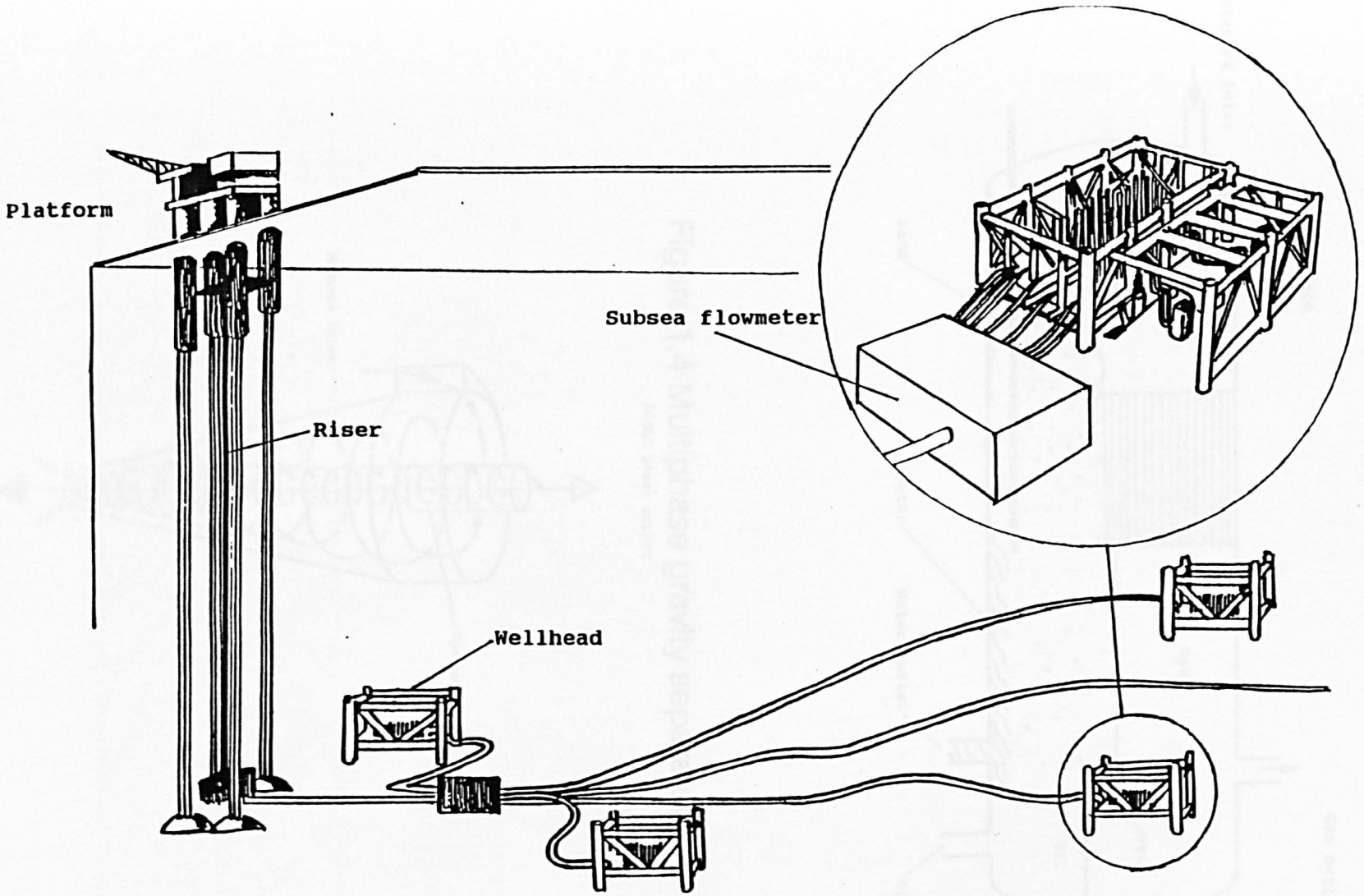

Figure 1.3 Subsea oil production

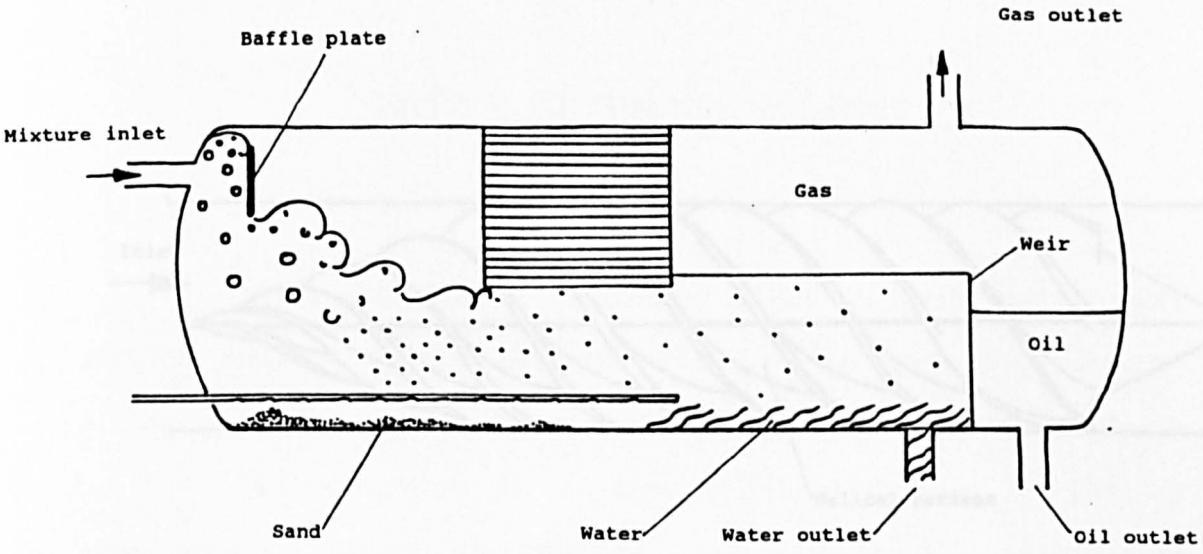

Figure 1.4 Multiphase gravity separator

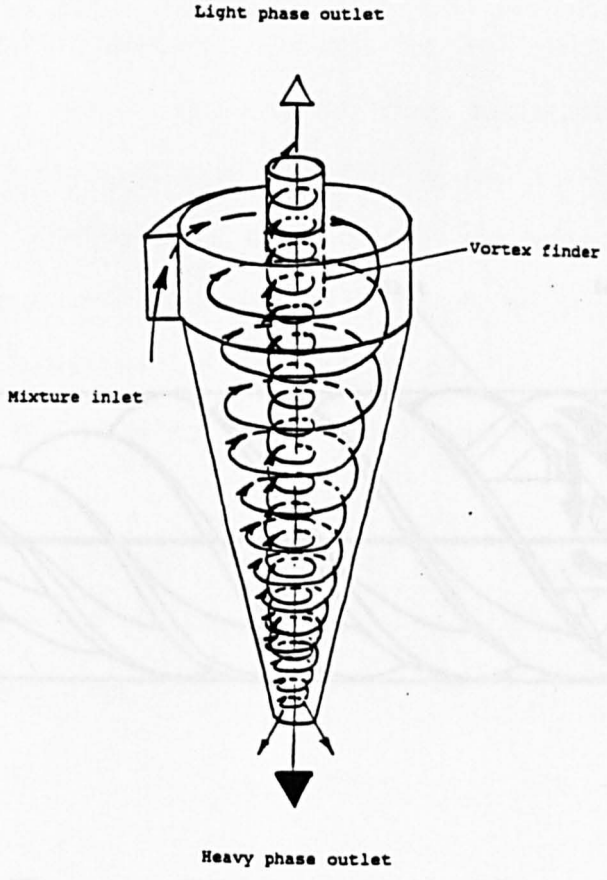

Figure 1.5 Cyclone separator

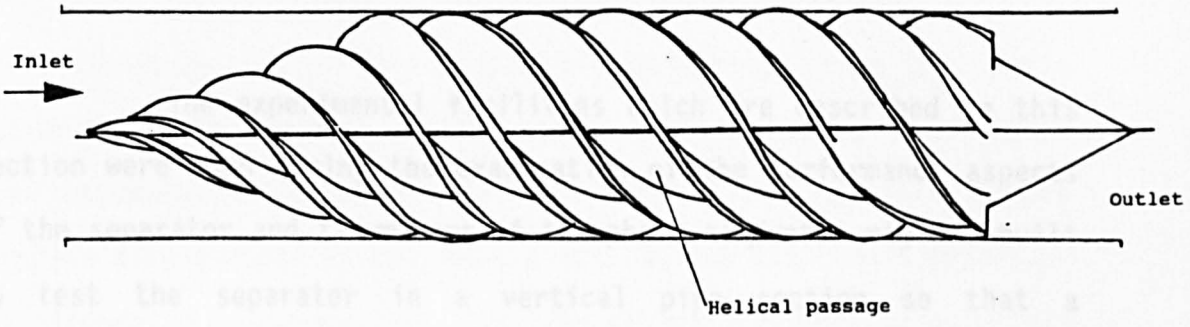

Figure 1.6 Gas/oil separator

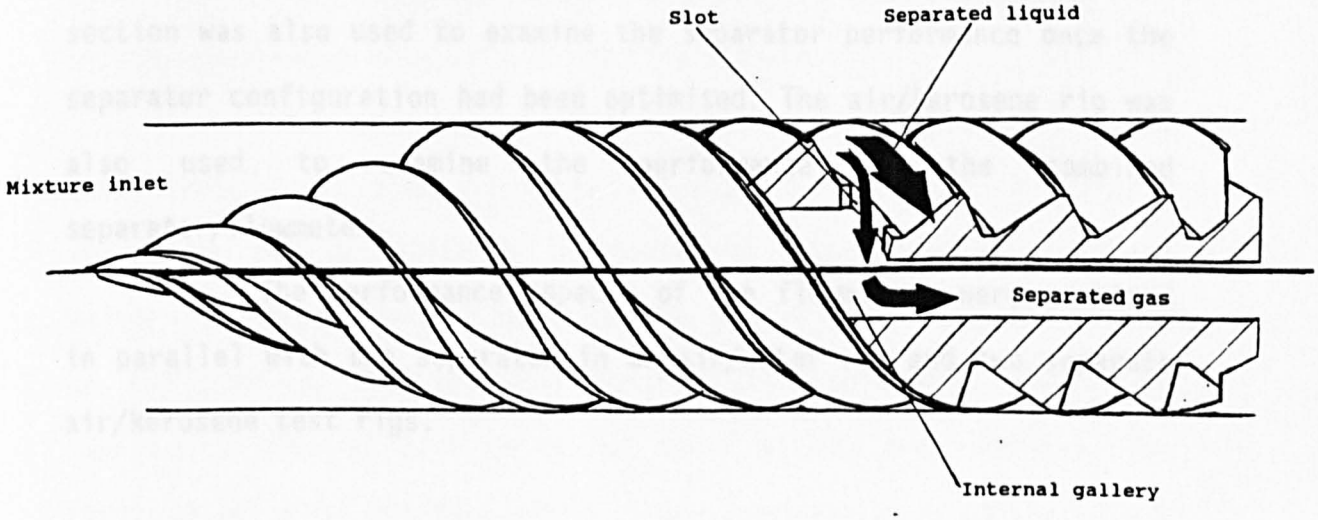

Figure 1.7 Separated gas flow path

CHAPTER 2: EXPERIMENTAL FACILITIES

The experimental facilities which are described in this section were used during the examination of the performance aspects of the separator and flowmeters. A two-phase air/water rig was built to test the separator in a vertical pipe section so that a symmetrical phase distribution was obtained, eliminating gravitational effects on the flow structure. A second experimental rig was built to investigate the effects of the helix angle of the helical passages on the pressure losses in the separator. This experimental rig was built using coils of flexible reinforced PVC tube of differing diameters. Changing the helix angle of such a coil is considerably easier and cheaper than manufacturing several new separators with flow passages of differing helix angles.

An air/kerosene experimental rig with a vertical test section was also used to examine the separator performance once the separator configuration had been optimised. The air/kerosene rig was also used to examine the performance of the combined separator/flowmeter.

The performance aspects of the flowmeters were examined in parallel with the separator in an air/water rig and two separate air/kerosene test rigs.

2.1 Experimental Rig for Air/Water Separator Tests

2.1.1 General Description

The experimental rig which was required to test the two-phase separator had to be capable of delivering both gas and a liquid phases to the test section. These fluids were supplied either simultaneously, or independently, to the test section in order to simulate single-phase or two-phase flows. As the gas/liquid separator was already in existence, Fig. 2.1, the rig was designed to suit this and to be flexible enough to accommodate other devices of similar size. To this end the rig was designed with three parallel lines connecting with an inlet and an exhaust manifold, Fig. 2.2. The manifold connections for these lines were 2", 4" and 6" respectively. To reduce the potential number of flow patterns which could form at the test section entrance, the test sections and working lines were installed in a vertical plane, Govier and Aziz (1972). For the range of void fractions which were used during the experiments this ensured that the flow at the test section was always either a homogeneous/bubbly flow or a churn flow regime.

Water was used as the liquid (continuous) phase in the experimental rig, compressed air was used for the gas (dispersed) phase. The rig was built in the Hydraulics Laboratory at Liverpool University. The water was supplied from a large tank (capacity 95 m^3) on the roof of the building housing the laboratory. This tank supplied a head of 37.5 metres of water at the test section. The level in the tank and thus the delivery head was kept constant by a recirculating pump which returned the water exhausting from the rig, via a sump, to the supply tank. The compressed air was supplied from

the laboratory main at a pressure of 6.8 bar gauge. This pressure was kept constant using a pressure regulator and, after passing through the experimental rig, the air was exhausted to atmosphere.

The main rig pipework was constructed from PVC pipe and fittings, the main supply and return pipe being of 6" bore. The vertical height of the experimental working sections ran to 6 m above floor level. The rig was fitted with a drain at the lowest level of the pipework, to ease the changing of the test section and orifice plates. The liquid flow into the rig and the pressure in the rig and at the test sections was controlled by gate valves at the rig inlet and outlet. Those test sections which were not in use during experiments were isolated using ball valves.

The compressed air was injected into the pipe before the test section in the vertical leg of the rig and each leg had an individual air injection point. The air injectors consisted of a valve and a short length of tube which passed through the rig pipe wall to the centreline of the pipe, Fig. 2.3(a). The velocity of the incoming gas flow was considered to be sufficient to achieve good mixing at the injection point and as the test section was preceded by a length of optically clear tube it was possible to confirm the quality of gas/liquid mixing during the commissioning of the rig. As the rig pipework undergoes a transition involving two out of plane 90° bends at the entry to the vertical leg some degree of residual swirl was expected at this section. During the commissioning of the rig this swirl was observed by noting the path of individual gas bubbles. To reduce the swirl a cruciform type flow straightener, Fig. 2.4, was added at the entrance to the vertical leg. The flow straightener was observed, from the motion of gas bubbles in the flow, to alleviate this problem.

2.1.2 Liquid-phase Flow Measurement

The range of water flow rates which were potentially required in the test section were too large for the use of one reference flowmeter; the turn-down ratio required would have been too great for the desired accuracy. To achieve the required overall turn-down ratio, several orifice plates of different diameters were used in one installation. The installation of the orifice plates was designed in accordance with the requirements of BS.1042 (1981), using the minimum recommended number of pipeline diameters upstream and downstream of the orifice plates due to space limitations. The orifice plates were installed in two parallel horizontal pipes of 4" and 6" internal diameter. The orifice plates for use in the 4" line were designed for the lower end of the water flow range to be used and those in the 6" line were for the higher flow rates.

A differential pressure transducer was used to measure the pressure difference across each of the orifice plates using D and D/2 tappings. The pressure transducer had a working range of 0 - 70 kN/m^2 with an output signal of 0-1 volt DC. The output signal was passed to a 13 bit analogue to digital converter (ADC) which gave a resolution of 1 in 4096. The signal from the ADC was then read by a microcomputer. The digital signal was sampled over a period of 100 seconds so that a repeatable mean could be found with the signal noise and the noise from the flow eliminated.

2.1.3 Gas Flow Measurement

The gas phase in the experimental rig was compressed air which was supplied at a constant but adjustable pressure from the laboratory main via a pressure regulator. The air flow rate was measured using a bank of parallel mounted Rotameters. These flowmeters were calibrated for use at a pressure of 6.8 bar gauge and a correction factor was used when the supply could not be kept at the correct pressure for any reason. The pressure in the rig just downstream of the air injection point was also measured, as this governed the actual volume of air in the test section during the experimental work. The air supply was sufficient to allow experiments to be performed using up to 30% volume void fractions at the highest attainable total flow rates. The air was injected into the rig at a pressure higher than that in the rig itself to prevent any back-flow of liquid into the air flowmeters. Valves were installed after each Rotameter to cause choking downstream of the flowmeters and eliminate rig pressure pulsations from the Rotameters.

2.1.4 Test Section and Instrumentation

The test section instrumentation consisted mainly of pressure measurement devices. These were used for either measuring the static or total pressures at various points in the test section. The test section consisted of clear Perspex blocks inside which the separator was suspended in a 4" bore, Fig. 2.5. These blocks were clamped between two steel flanges and located together using spigots; an 'O' ring seal was used between each of the blocks to contain the fluid pressure within the rig. The lengths of tube before and after

the test section were also constructed from clear Perspex tube to enable the entrance and exit flow patterns to the test section to be observed. At several points the Perspex blocks were pierced by pressure tappings and by small bore access holes to allow the insertion of either static or total pressure probes. The Perspex blocks could be arranged in differing orders to permit investigations to be carried out at several horizontal planes between the entrance to the test section and the exit plane. Individual blocks could also be rotated to allow investigations to be carried out in different passages of the separator.

The pressure probes were connected to either mercury or water filled manometers, or to pressure gauges depending on whether the measurements to be taken were for differential or static pressures. A Pitot static type of probe, Fig. 2.6, was also used in the separator passages to measure the local fluid velocities and velocity profiles. For single-phase flow this probe was used with a water manometer and for two-phase flow data was gathered from a differential pressure transducer.

For the experiments designed to measure the gas separation performance of the separator, the separated air and water were collected in a sealed tank (described later in section 2.2.3). The time taken to collect 10kg of water was measured to give the water flow rate and simultaneously the separated air was passed out of the tank through a Rotameter to give the air flow rate.

2.1.5 Calibration of Instrumentation

The orifice plates, which were used to measure the water flow rates, were calibrated in-situ once the test rig had been

constructed. The calibration was obtained by setting the liquid flow rate and then recording the differential pressure from the orifice plate. The differential pressure was measured using a 0 - 70 kN/m^2 differential pressure transducer, the output voltage from which was read on to a microcomputer via an ADC. This signal was then averaged over 100 readings and stored in the computer. The mass flow rate from the rig was measured simultaneously with the differential pressure across the orifice plate using a dynamic weighing system to collect the water at the rig exhaust - the mass flow rate being found from the time taken to collect a specific mass of water.

An equation was fitted to each set of data from the orifice plates, Fig. 2.7, this equation was then used in a computer program to find the flow rate from the averaged differential pressure across the orifice plate. The data from the orifice plates was used to compare the discharge coefficients found experimentally with those predicted by BS.1042. The discharge coefficients found experimentally for a typical orifice plate, installed and designed in accordance with BS.1042, were 1.55% lower than those predicted by the British Standard, Fig 2.8. The British Standard also shows an increase in discharge coefficient for a given β ratio orifice plate at lower Reynolds number. The calibration data for the orifice plate show a decreasing trend for the discharge coefficient as the Reynolds number decreases. This suggests that slight discrepancies from the conditions used to carry out the experiments on which the British Standard is based can cause variations from predicted discharge coefficients, this highlights the value of an in-situ calibration where this is practicable.

The calibration of the Rotameters for the gas phase of the rig was more difficult to achieve. There was no satisfactory

standard available against which to calibrate these meters and so the manufacturer's calibration had to be relied upon. This was that at a constant pressure of 6.8 bar the maximum error was of ± 2% of full scale: thus by not using these flowmeters in their low range, the errors were minimised. The Rotameters were supplied with air via short tubes from a manifold arrangement, control of flow rate was achieved by use of a valve downstream of each Rotameter. The assumption was made that each of the Rotameters was operating at the manifold pressure which was measured using a pressure gauge. Any deviation from the calibration pressure of the flowmeters was corrected for. All the pressure gauges used were calibrated against a deadweight tester, the differential pressure transducers were factory calibrated over their full range and supplied with a calibration certificate stating an accuracy of ± 0.15% of full scale.

2.2 Error Analysis for Flow Metering Devices

2.2.1 Orifice Plates

Most devices which are used to measure physical quantities have sources of error which are associated with them. These errors are of four different types: random errors, constant systematic errors, spurious errors and variable systematic errors. Spurious errors, often due to data transfer or transcription faults, are usually easily picked out at the analysis stage where the data may be discarded. Constant systematic errors may be due to transducer zero errors or 'range' error on the calibration. Variable systematic errors may be due to component wear, such as orifice bore wear, or due to temperature effects on transducers. Random errors are caused

by variations in the measured quantity of a variable even when that variable is constant. Kinghorn (1990) showed that the uncertainty arising from random and systematic errors can be easily dealt with. The random uncertainty of a set of results may be obtained by multiplying the standard deviation of the data set by the value of Student's t at the required confidence level. The 95% confidence level is usually applied in flow measurement and t_{95} can be found from the equation

$$t_{95} = 1.96 + \frac{2.36}{\nu} + \frac{3.2}{\nu^2} + \frac{5.2}{\nu^{3.84}} \qquad (2.1)$$

where ν = n-1

n = no. of readings

The uncertainty associated with the flow measurement from an orifice plate is a combination of several uncertainties. The mass flow rate , which is the desired result from an orifice type device, is a function of several different variables. Each of these subsidiary variables has an associated uncertainty and the uncertainty in the mass flow rate is a combination of the subsidiary uncertainties. The standard orifice equation gives

$$\dot{m} = Cd.A_0\left[\frac{2\rho.\Delta P}{(1-\beta^4)}\right]^{0.5} \qquad (2.2)$$

The variables which have associated uncertainty in the case of the orifice are the discharge coefficient, Cd; the fluid density, ρ; the differential pressure, ΔP; and the diameter ratio,

β. The uncertainty associated with each of these variables must now be estimated or measured.

For the discharge coefficient the standard deviation of the measurements taken during the calibration was used in conjunction with Student's t_{95} for the size of the data set. For the orifice bore and pipe bore diameters the manufacturing tolerances were used; these were ± 0.1mm and ± 0.25mm respectively. The uncertainty for the fluid density was estimated from the variation of water density across the temperature range used in the experiments. For the random error in the differential pressure measurement the standard deviation for a set of readings was taken with t_{95} for the data set.

The combined uncertainty was found using the 'root sum square' method which is defined as

$$e^2(y) = \left\{\frac{\partial y}{\partial x_1}\right\}^2 e^2(x_1) + \left\{\frac{\partial y}{\partial x_2}\right\}^2 e^2(x_2) + \ldots + \left\{\frac{\partial y}{\partial x_n}\right\}^2 e^2(x_n) \qquad (2.3)$$

For the case of the orifice plate this equation can be written in terms of the percentage uncertainty for each of the variables and the sensitivity coefficients for each of the variables. [See Appendix 1 for derivation]

$$E^2(m) = E^2(Cd) + \left[\frac{2\beta^4}{1-\beta^4}\right]^2 E^2(D) + \left[\frac{2}{1-\beta^4}\right]^2 E^2(d) +$$

$$\frac{1}{4} E^2(\Delta P) + \frac{1}{4} E^2(\rho) \qquad (2.4)$$

Inspection of this equation shows that the flow rate measurement is more sensitive to the errors in the discharge coefficient and the bore diameters than to the errors in the differential pressure and the fluid density. Using the above techniques the orifice plates used for the water flow measurement in the air/water experimental rig were found to have a random uncertainty of ± 1.58% at a confidence level of 95% under single-phase flow conditions. The component error with the largest uncertainty and greatest influence was the discharge coefficient.

The uncertainty associated with the differential pressure across the orifice increased when the rig was used under two-phase flow conditions, Fig. 2.9. The increase in uncertainty was due to the small pressure fluctuations caused by the gas injection downstream of the orifice plate installation. The increase in the uncertainty of the differential pressure measurement did not affect the overall uncertainty associated with the orifice plates, due to the low sensitivity coefficient associated with the differential pressure measurement in equation 2.4.

2.2.2 Rotameter Errors

The error for the Rotameters claimed by the manufacturers was ± 2% of the full scale reading of the flowmeter. Thus for a Rotameter of 100 l/min capacity the error was ± 2 l/min across the flow range of the flowmeter. The percentage error in the reading of the Rotameter would thus be ± 20% at 10 l/min reducing to ± 2% at 100 l/min. Providing the Rotameters were not used in the lower 30% of their capacity the flow measurement uncertainty was kept to less than ± 6% of the air volumetric flow rate. The error in the air flow measurement was not of great significance in the overall mixture mass flow rate due to the relatively low density of the gas compared to the liquid phase.

2.3 Two-phase Air/Kerosene Test Rig

2.3.1 Liquid Flow Measurement and Test Section

The air/kerosene flow rig was also based on 4" pipework, although for safety reasons it was constructed from welded steel pipe, Fig. 2.10. This test rig was in the Oil Laboratory at NEL. The same test section which was used in the air/water experiments was used in this rig. The kerosene supply was from an 18 m^3 tank at ground level. Kerosene was supplied to the rig by a variable speed centrifugal pump which meant that, due to the characteristics of the pump, the supply pressure at the inlet to the test section varied with the flow rate. The flow rate of the kerosene was measured by a reference 4" turbine meter, this meter was calibrated against a gravimetric facility to give a polynomial expression for the meter

factor in terms of the number of litres passing through the meter per pulse read. The pulse output from the meter was read onto a microcomputer via a datalogger, the frequency was then converted to a reading of litres per second of fluid which was then output by the computer on the display screen. The reading error of the turbine meter was ± 0.06 l/s. This corresponded to a error of ± 1.0% at the lowest kerosene flow rate used, 6 l/s. The error was ± 0.35% for the highest kerosene flow rates used, 17.5 l/s.

2.3.2 Air Flow Measurement

The second phase used in the kerosene test rig was compressed air, at a supply pressure of 3 bar gauge. The air supply to the test section was injected at the base of the vertical leg which contained the test section. The air entered the side of the rig pipework through a T-piece and mixed with the kerosene, Fig. 2.3(b). The mixture which was achieved by this method was observed to be either a bubbly or churn type of well-mixed flow at the test section entrance. The air was metered using a bank of parallel mounted Rotameters which were supplied with air through the same manifold. These flowmeters were calibrated in air against a set of turbine meters which had been calibrated against traceable choked nozzles.

The pressure and temperature of the air in the manifold were measured using a pressure gauge and a platinum resistance thermometer, the readings from the Rotameters were then corrected for the difference between the calibration and working temperature and pressure. The supply pressure to the manifold was controlled using a pressure regulator, this made the task of maintaining the calibration pressure of 3 bar gauge considerably easier. The supply flowmeters

were calibrated, by the manufacturer, to supply free air at 2 bar absolute, whenever the test section varied from this pressure a second correction had to be applied. The uncertainty of the Rotameters was ± 2% of full scale. As shown in section 2.2.2 the error in the air reference flow rate was less significant than the Rotameter error would suggest as the mass flow rate of the gas phase was always much less than that of the liquid phase. In order to minimise the error in the gas flow measurement the Rotameters were not used at the lower end of their range.

The pressure in the test section inlet was also measured so that the actual volume of the gas present at this section could be found. The pressure at the separator exit plane was measured so that the driving pressure for the air separation was known. The temperature of the kerosene increased during a test due to heat input at the pump. The mixture temperature in the test rig was therefore measured, as it affected the mixture density slightly. A second platinum resistance thermometer was therefore placed a short distance downstream of the test section where the air and kerosene were well mixed. The temperature at this point was taken to be the same as in the test section.

2.3.3 Collection of Separated Fluids

The kerosene and air separated from the helical passages into the internal gallery of the separator were passed out of the rig independently of the main flow, Fig. 2.11. This mixture then passed to a gravity separation unit where it then flowed into the top of a large sealed vessel. At the entrance to the vessel gravity separated the kerosene from the mixture due to its relatively large density.

The kerosene fell to the bottom of the vessel whilst the air passed out via an exit tube in the top of the vessel. The air was then passed through a bank of Rotameters before exhausting to atmosphere. The gravity separation vessel was mounted on a gravimetric facility which was used for dynamic weighing of the kerosene collected over a timed interval to give the separated kerosene mass flow rate.

The Rotameters which were used to measure the air flow rate were calibrated against the same air turbine meters as the flowmeters used to measure the inlet air flow rate to the test section. The pressure of the manifold to which the Rotameters were connected was monitored by a pressure gauge. The gravity separation vessel was kept at the same pressure as that at the exit plane of the helical separator in the test section, in order to obtain representative results. This back pressure was adjusted using the valves mounted downstream of the Rotameters. This increased the pressure in the gravity separator above atmospheric pressure on some occasions and so a pressure relief valve was fitted to prevent over pressurisation of the vessel. The rig back-pressure to the rear of the test section was applied by closure of a valve downstream of the test section.

The separator did not remove all the air from the flow through the test section; the remaining air was returned to the main tank with the kerosene. The air quickly separated out from the kerosene under the influence of gravity in this tank. The capacity of the tank was much greater than required for the flow rates at which the rig was operated and gave a long residence time for the kerosene. In addition the exhaust entered at the top of the tank while the inlet to the pump was drawn from the bottom of the tank. This ensured that none of the air carried back to the tank from the test section

was carried under in the main kerosene flow to cause a source of error.

2.4 Annular Flowmeter Test Rig

The proposed multiphase flowmeter separated the gas and liquid phases into an internal and external flow path respectively. The external flow path was of an annular cross-section and so the flowmeter used in this passage had to be of an annular design. As described later in Chapter 5 an annular venturimeter was developed for the purpose.

2.4.1 Flow Measurement

The two fluids used in the annular flowmeter test rig were air and water, the water being supplied from a large tank with a constant 37.5 m head and the compressed air from the laboratory main. The water flow rate to the test section containing the annular venturimeter was measured using a reference vortex shedding meter of 4" nominal bore, the same diameter as the rig pipeline and test section. The vortex shedding meter was mounted 20 diameters upstream of the test section and 50 diameters downstream of the valve and bend at the rig inlet, Fig. 2.12. The valve was used to control the rate of water flow to the test section in conjunction with a valve situated immediately before the rig exhaust, thus the back-pressure could be varied at the test section.

The calibration for the vortex shedding meter was carried out with the flowmeter in-situ, the calibration method made use of the dynamic weighing system described earlier (Section 2.1.5). The

output signal from the vortex shedding meter was a frequency which was directly proportional to the volume flow rate passing through the meter, the constant of proportionality is known as the meter factor and was constant across the range of the meter. The meter factor was found to be 0.802 l/pulse with a maximum error of ± 1.6%. The air flow rate was metered using the same bank of variable area flow meters as for the separator test rig described earlier (Section 2.1.3), these were used at the manufacturers calibration pressure and temperature with any deviation from the calibrated condition being corrected for.

2.4.2 Instrumentation and Test Section

The test section was mounted horizontally in the test rig downstream of the reference meter, the air was injected 10 pipe diameters downstream of this meter to avoid influencing its calibration. The test section was mounted 10 diameters further downstream from the air injection point to allow the gas and liquid phases time to mix well, the air being injected vertically downwards from the top of the pipe.

The differential pressure across the venturi was measured using sets of static pressure tappings connected with piezometer rings, these averaged out any circumferential variations in the pressure measurement. The inlet pressure tappings were connected to one side of a manometer and to a pressure gauge whilst the throat pressure tappings were connected to the opposite side of the manometer. The inlet static pressure and throat differential pressure were measured in this way, the inlet pressure being used to calculate the gas volume flow rate at the inlet plane of the test section.

As the test section was constructed from clear acrylic tube, visual observations showed that although the flow entering the meter was well mixed, at lower flow rates it tended to become stratified during its passage through the meter. A mixer, consisting of a thin plate drilled with small diameter holes, was fitted between the flanges immediately upstream of the test section. This device ensured that the flow had a homogeneous flow pattern throughout the test section at all the flow conditions. The well-mixed flow was similar to that observed at the separator exit plane after the air/water mixture had left the helical passages.

2.5 Internal Flowmeter Test Rig

The internal flowmeter measured the gas phase flow rate and so the internal flowmeter test rig was required to operate using the gas phase as the single-phase flow and at high void fraction under two-phase conditions. A rig suitable for the two-phase experiments was available and the single-phase work was carried out on a separate rig. A classical venturimeter, described in Chapter 5, was designed to measure the internal flow.

2.5.1 Single-phase Internal Flowmeter Test Rig

A similar layout to that occupied by the internal flowmeter in the separator was constructed in the single-phase test section, Fig. 2.13. The air flow was supplied at a constant 3 bar gauge from a bank of Rotameters to the venturimeter which then exhausted to atmosphere. The Rotameters had previously been calibrated against a set of turbine meters (section 2.3.2). The

supply pressure was maintained at a constant value using a pressure regulator. The pressure differential was measured across the venturi throat using a 4 - 20 mA current loop pressure transducer. The current was converted to a voltage across a 50Ω precision resistor and read onto a microcomputer using an ADC. The voltage output from the transducer was averaged over 100 readings to give a mean value.

2.5.2 Air/Kerosene Internal Flowmeter Test Rig

The experimental rig for two-phase air/kerosene flow calibration of the internal venturimeter was required to produce sufficiently high void fractions to reproduce the experimental conditions which occur in the separator central gallery. The only available test rig capable of producing these large void fractions at the low mass flux required had an inclined test section which was near horizontal. Due to the near horizontal orientation of the test section the churn flow regime expected in the separator internal gallery would not be reproduced in the internal flowmeter test rig. The work of Taitel and Dukler (1976) indicated that an intermittent flow regime would dominate at the test conditions.

The kerosene phase was supplied from a tank by a centrifugal pump. To give the required kerosene flow rate through the test section at the required pressure a bypass system was used to divert the majority of the flow delivered by the pump straight back to the supply tank. The remaining liquid flow passed to the test section. The kerosene flow rate was measured by collecting a fixed mass of the liquid efflux from the rig in a weightank over a timed period. The air and kerosene were mixed in a tee 90 diameters upstream of the test section, Fig. 2.14. The air flow rate was

measured using a bank of Rotameters which had been calibrated against a set of traceable turbine meters. The pressure differential across the venturimeter throat was measured using a differential pressure transducer connected to a microcomputer with an ADC and voltmeter. The readings from the pressure transducer were time-averaged over 100 readings. The local pressure at the test section inlet was measured using a pressure gauge. The temperature immediately downstream of the test section was monitored using a PRT, the resistance of which was measured using a bridge circuit.

2.6 Helical Coil Test Rig

2.6.1 Description of Apparatus

The helical coil test rig was designed as an experiment to find the pressure losses in helically coiled tubes of differing helix angles in two-phase flow. The constituent fluids were compressed air for the gas phase and water for the liquid phase. The air was supplied from a large reservoir held at 6.8 bar gauge. The water was supplied from the laboratory water main at mains pressure. For experiments requiring large liquid flow rates a small centrifugal pump was used to increase the available water flow rate, Fig. 2.15. The air and water flow rates were independently metered before mixing in an equal T immediately before entering the test section. After the test section the flow from the rig passed into a weightank and then to a drain. A valve was situated between the test section and the weightank to enable the test section pressure to be varied.

2.6.2 Helical Coil Test Sections

The helical coils were constructed from clear nylon reinforced PVC tubes which were wound around specially constructed mandrels. Two different coils were used, one with 25.4mm internal diameter tube and the second of 38.1mm internal diameter. The ratio of the tube diameter to the helix diameter was around 0.09 for both the 25.4mm coil and the 38.1mm helical coil. The mandrels were constructed from steel sheet perforated with regularly spaced 8mm diameter holes. The sheet steel was rolled to the required diameter and welded along the seam to form a tube. The perforations allowed the pipe clips which secured the coil to the mandrel to be easily positioned to suit a number of different helix angles for the coil.

The two mandrel diameters used were 254mm and 419mm and the wound coils then had approximately 30 diameters per turn, Fig. 2.16. Each mandrel was long enough to allow 4 turns per coil, giving a 60 diameter development length before the first pressure tapping. This was sufficient to allow a fully developed flow in single-phase flow and was shown by Akagawa et al (1971) to allow a stable flow pattern to develop in two-phase flow. The pressure differential was measured across 1 turn, approximately 30 diameters, giving a further turn before exhaust from the rig. The pressure tappings were formed by drilling through the tube wall, removing any burrs, and then glueing brass tappings flush with the internal diameter using epoxy resin. The coil axis was horizontal during the experiments and by measuring the pressure differential across one pitch of the coil no static pressure difference correction was necessary to the pressure measurement.

2.6.3 Instrumentation

The water flow rate was measured using a set of Rotameters which were initially calibrated using the weightank into which the flow from the rig exhausted. If the water flow exceeded the range of the flowmeters the gravimetric facility was used. The air flow rate was measured using another set of two Rotameters, these were calibrated for use at 6.8 and 5.44 bar gauge respectively. The delivery pressure from the air reservoir varied considerably with time between 6.8 and 4 bar gauge. The pressure at which the flowmeters were operating was carefully monitored using a pressure gauge in order that the true mass flow rate of the air passing through the Rotameters could be found using the square root of the ratio of the working pressure to the calibration pressure. The pressure differential at the coil was measured using a water manometer with the pressure tappings positioned at the outer diameter of the tube at the lowest position in each coil to ensure that no air became entrapped in the pressure lines to the manometer. A pressure gauge was used to measure the static pressure at the first pressure tapping, this allowed the actual flow rate of the air at this point to be calculated.

Figure 2.1 Gas/liquid separator

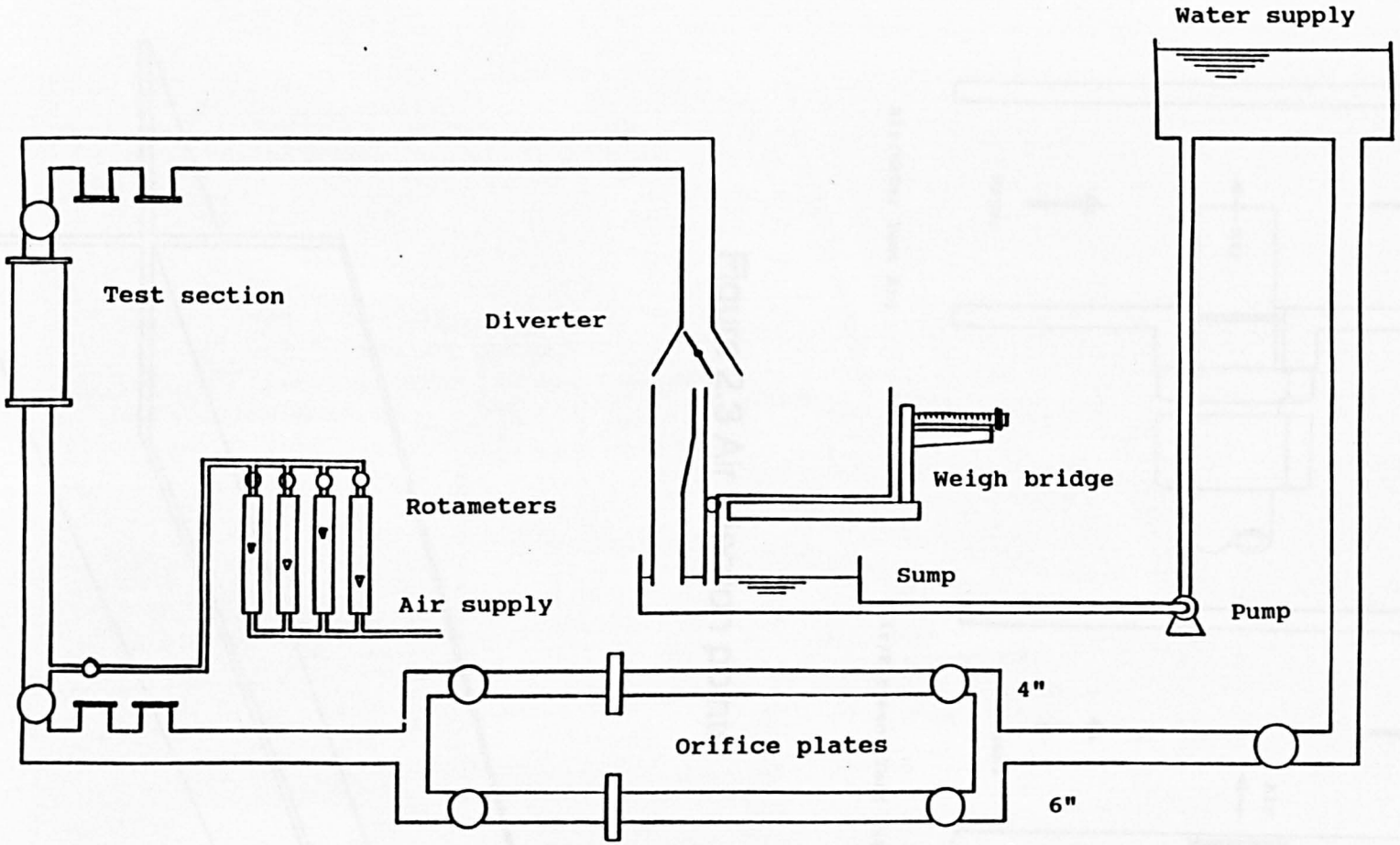

Figure 2.2 Air/water test rig

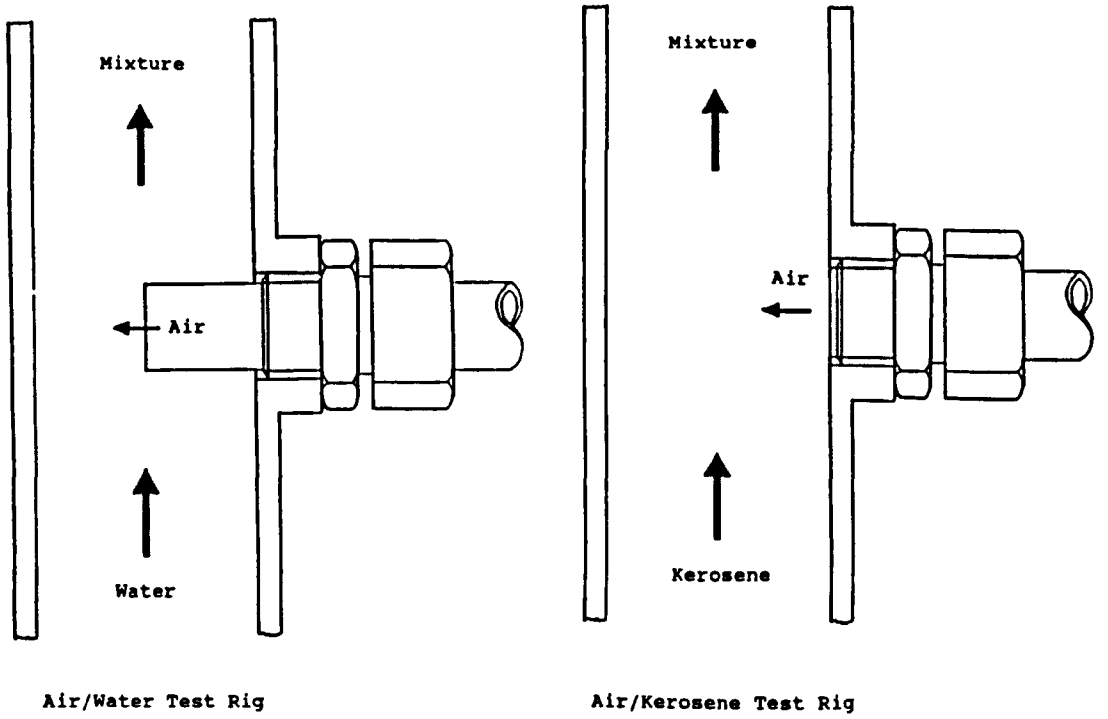

Figure 2.3 Air injection points

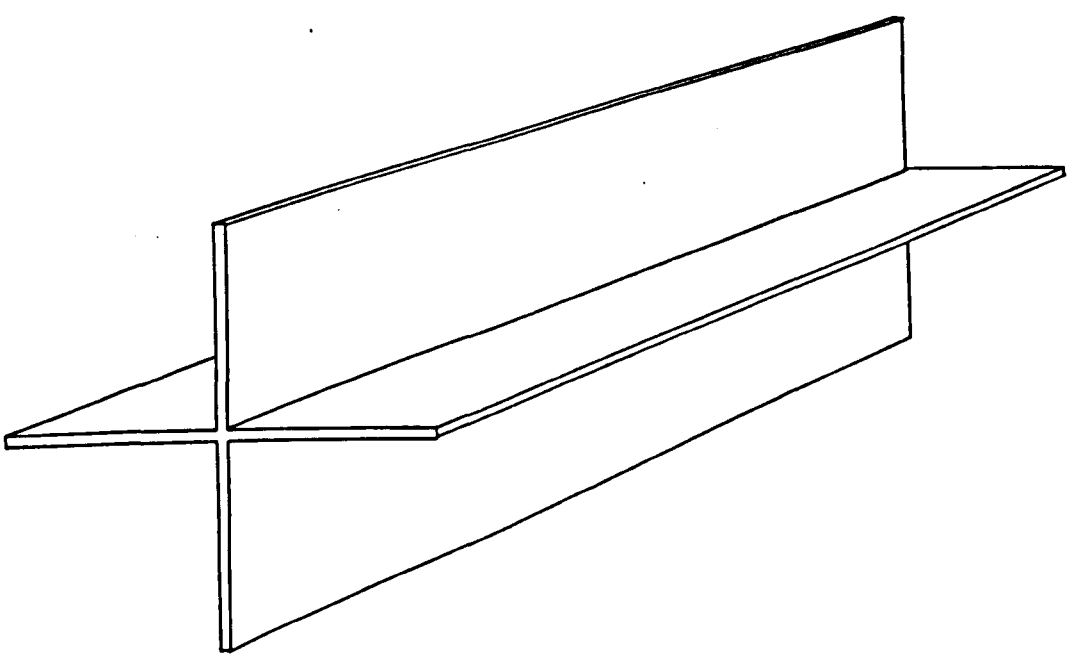

Figure 2.4 Cruciform flow straightener

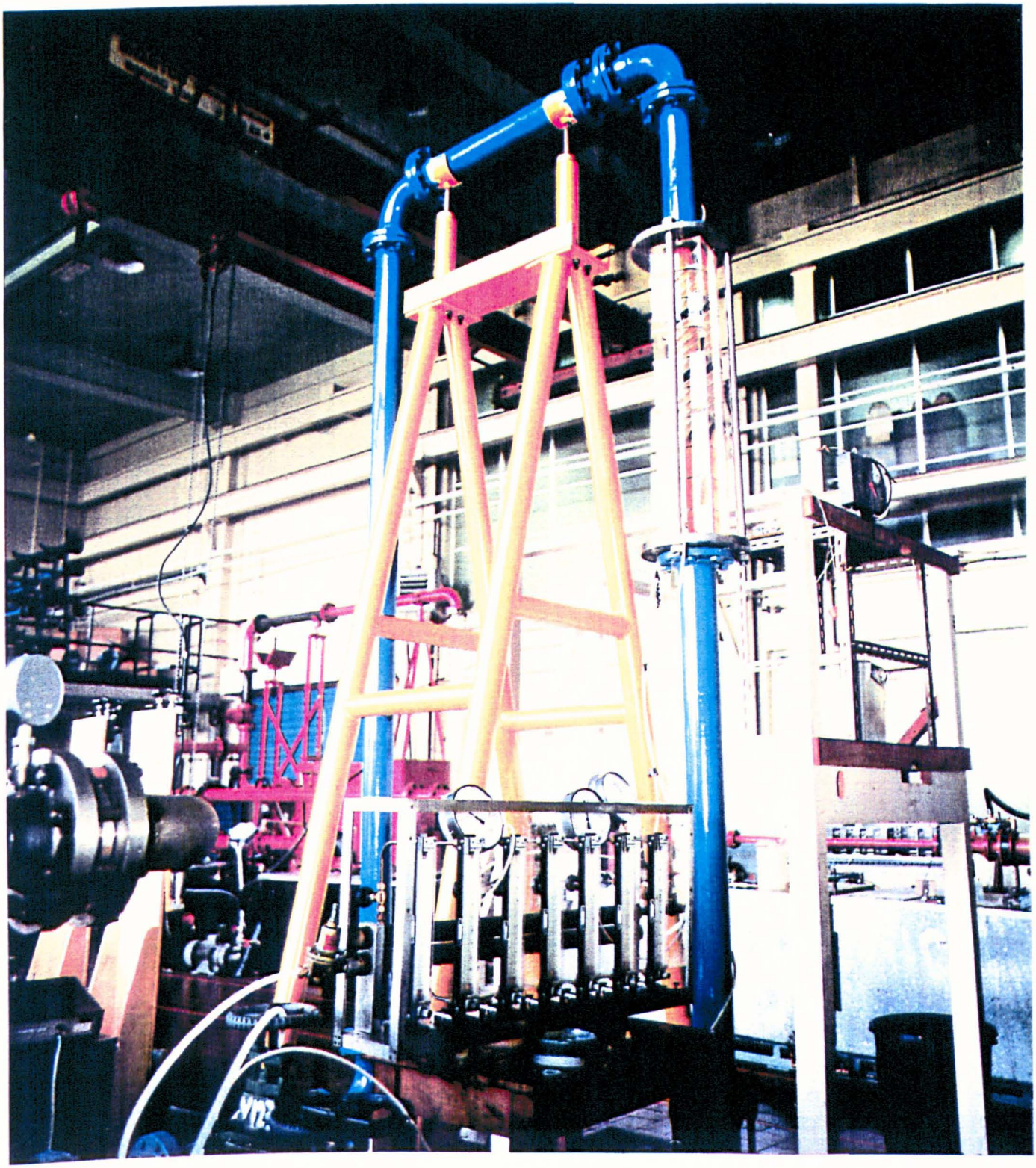

Figure 2.5 Gas/liquid separator test section

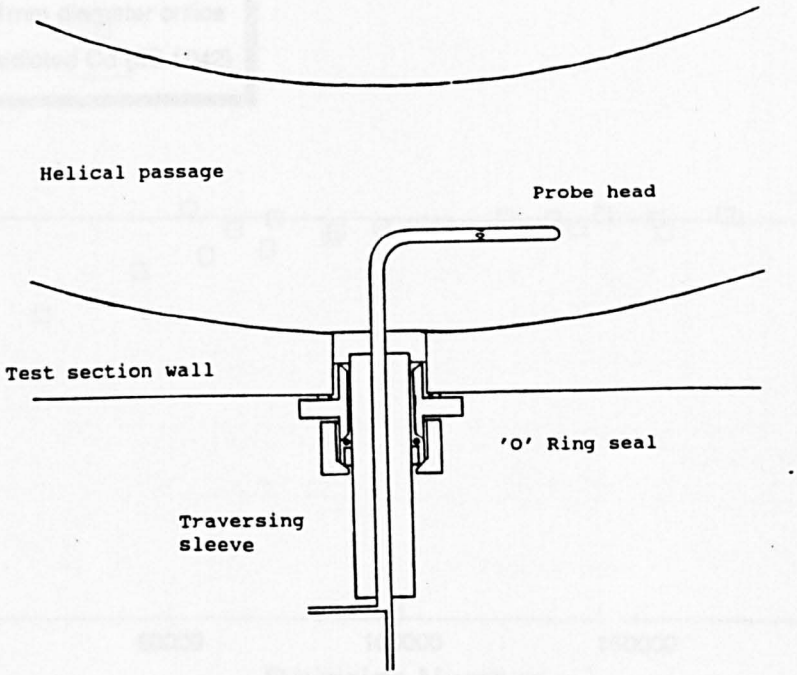

Figure 2.6 Pitot static probe

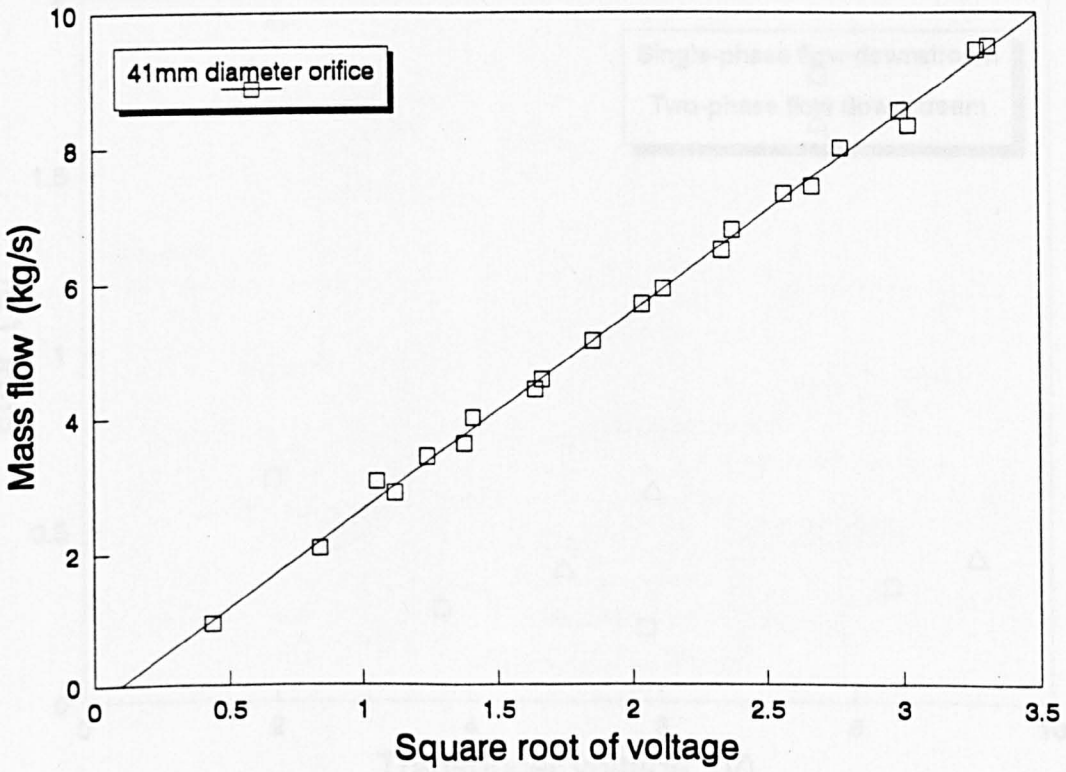

Figure 2.7 Typical orifice plate calibration

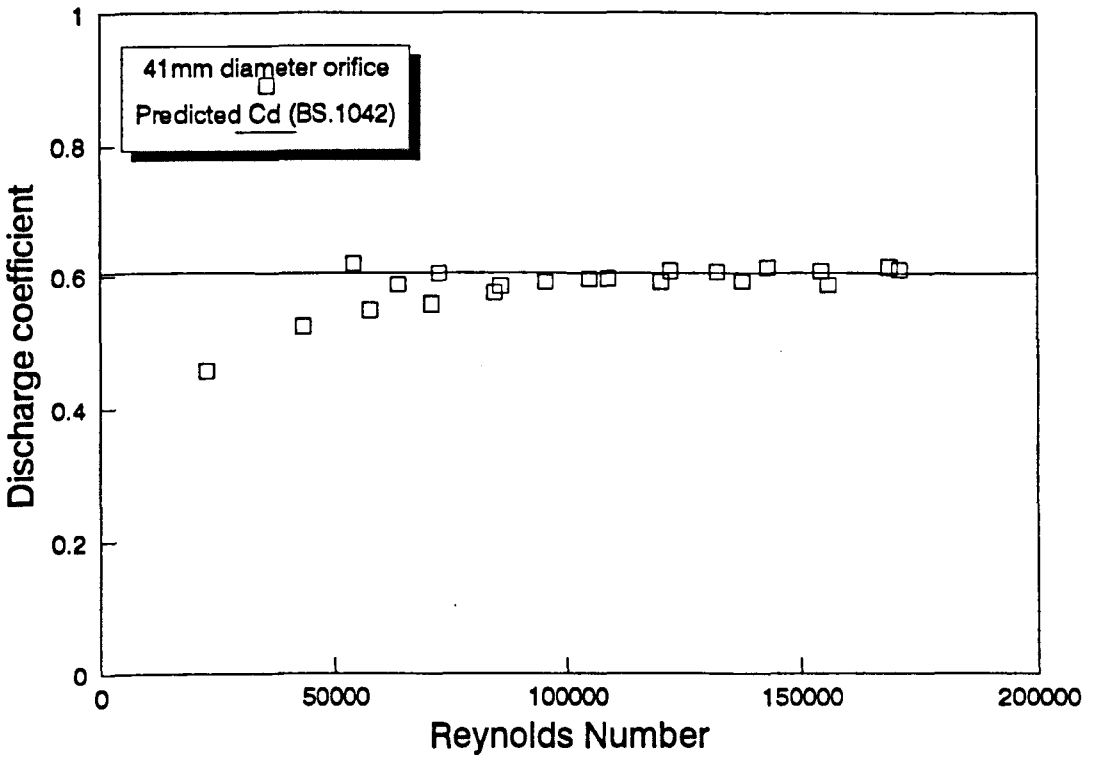

Figure 2.8 Typical orifice discharge coefficient

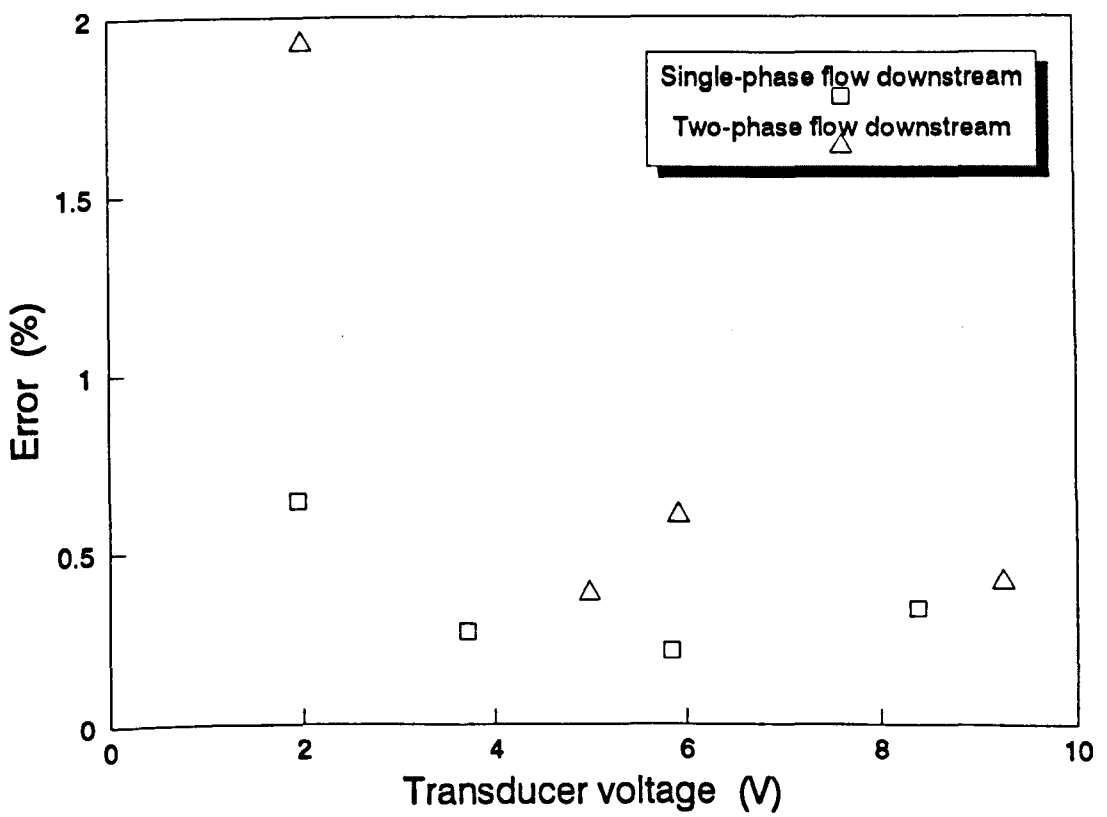

Figure 2.9 Orifice plate uncertainty

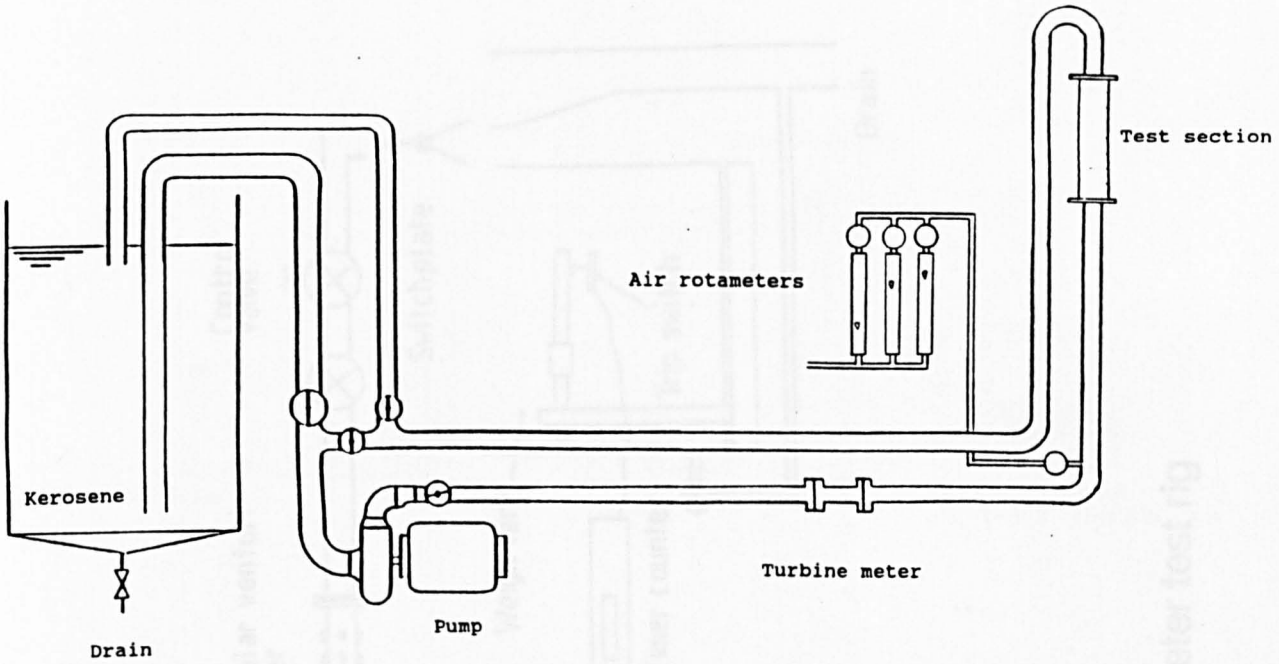

Figure 2.10 Air/kerosene test rig

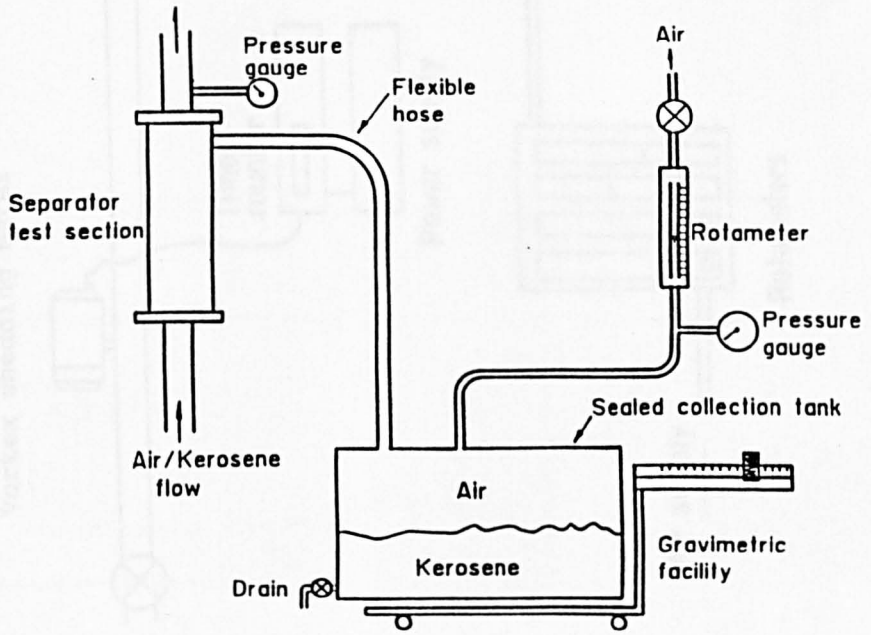

Figure 2.11 Separated air/kerosene collection

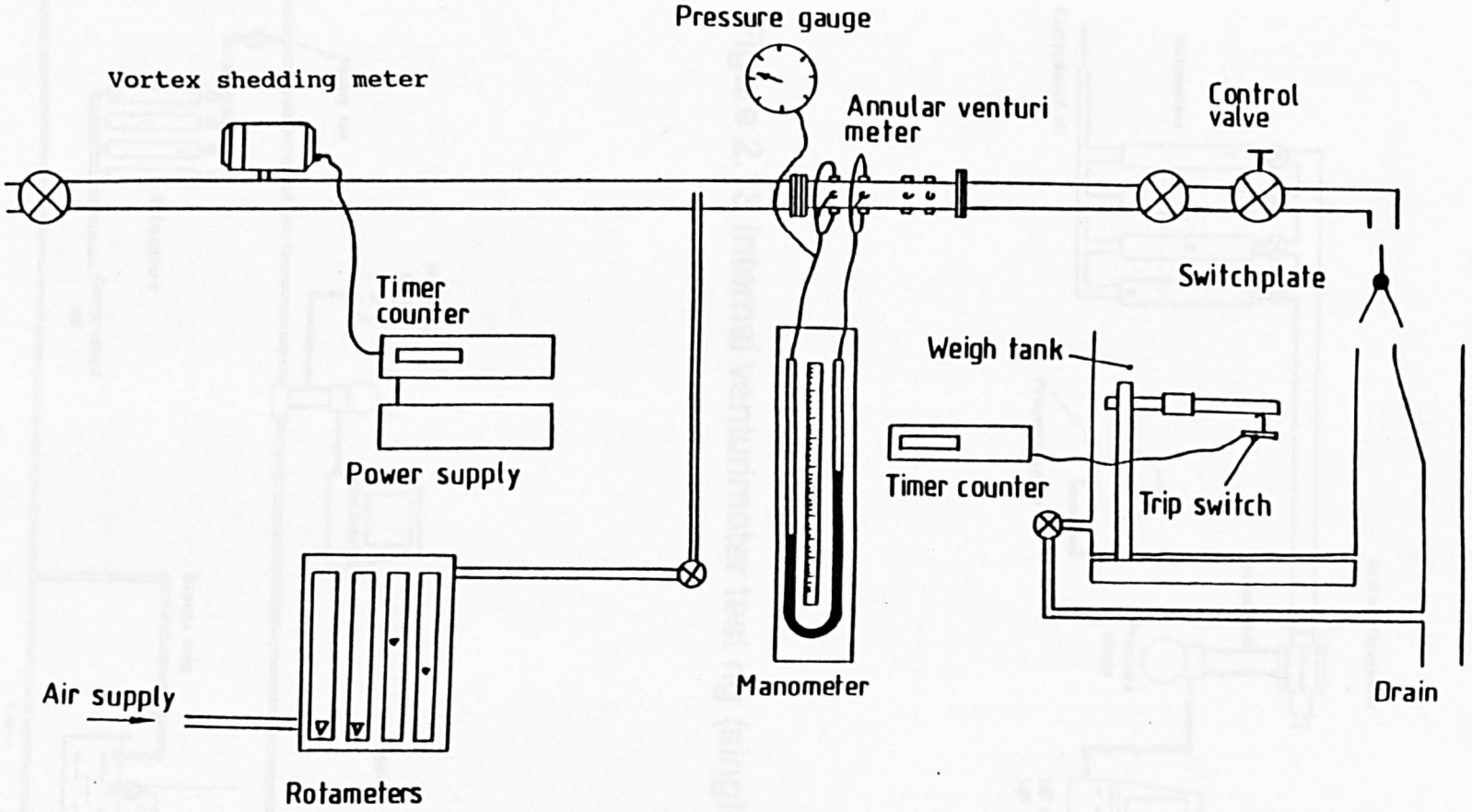

Figure 2.12 Annular venturimeter test rig

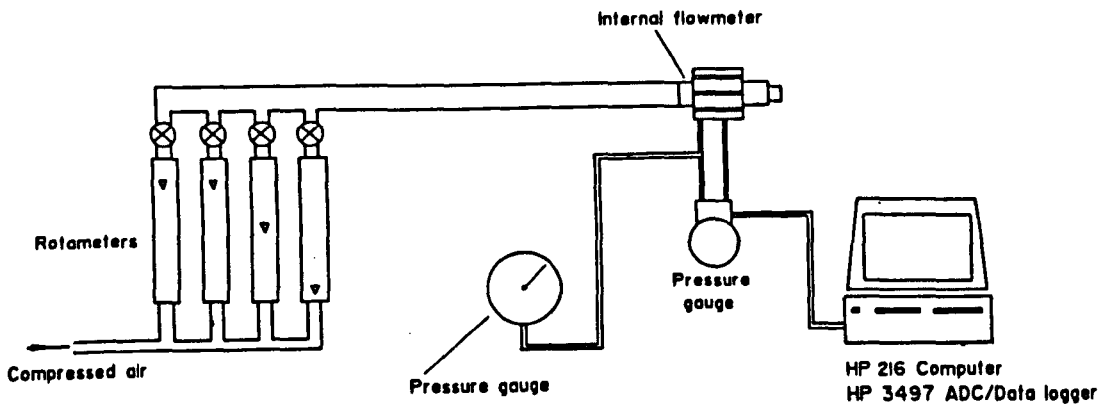

Figure 2.13 Internal venturimeter test rig (single-phase)

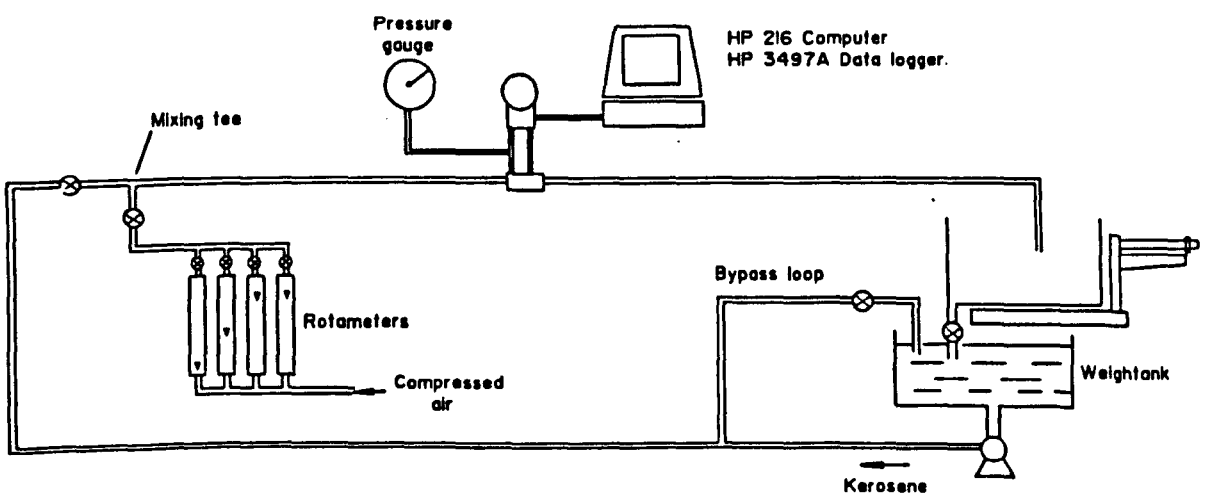

Figure 2.14 Internal venturimeter test rig (two-phase)

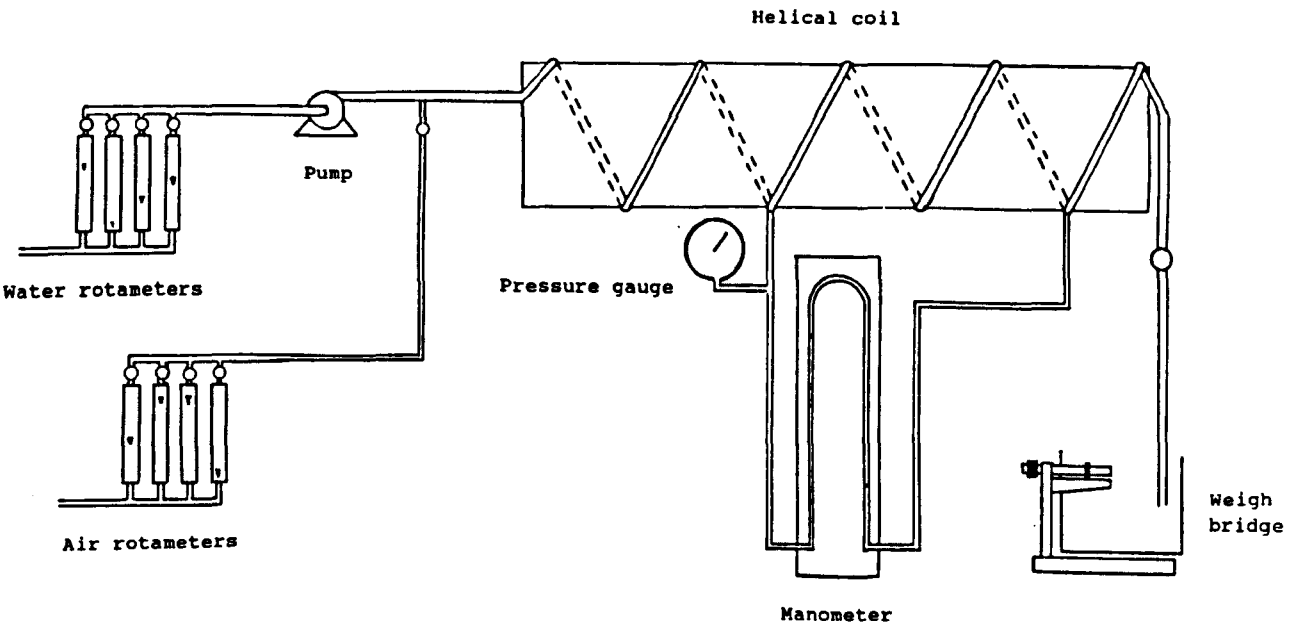

Figure 2.15 Helical coil test rig

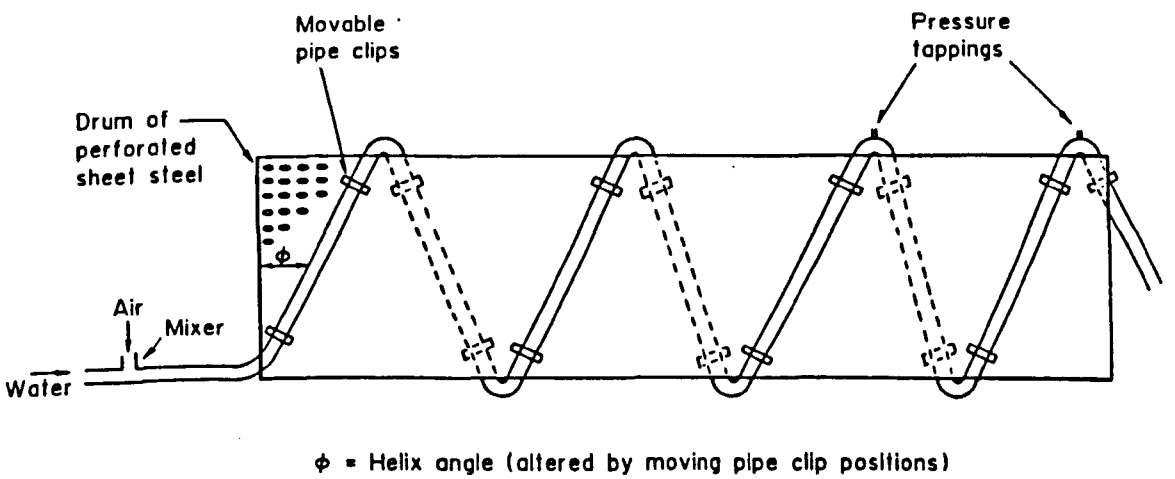

Figure 2.16 Helical coils

CHAPTER 3: THE SEPARATOR PERFORMANCE

3.1 Introduction

There are two critical aspects of the separator performance. The first is the separation performance (see Svarovsky, 1984), which is measured using two different parameters. The gas separation efficiency is defined as the percentage of the gas phase removed from the two-phase mixture by the separator. The second parameter, the liquid draw-off, is defined as the percentage of the liquid phase which is separated off with the gas phase. The separation performance governs the quality of the flow which will pass through the annular and internal flowmeters. Ideally all the gas phase would pass through the internal flowmeter (100% gas separation efficiency) and all the liquid phase would pass through the annular flowmeter (zero liquid draw-off).

The second important aspect is the head lost to friction in the separator. As the flow enters the helical passages there is an increase in its average velocity. The velocity increase is caused by the reduction in the flow area of 81% from the full 4" pipe area. The friction losses are proportional to the square of the mean velocity and so too great a flow rate will lead to high pressure losses through the device. The pressure losses will limit the operating range of the separator for a given passage area.

3.2 Single-Phase Investigations

3.2.1 Pressure Drop

The preliminary experimental work on the separator was conducted to find the pressure drop across the device in a single-phase fluid. The pressure drop across the separator was measured between two static pressure tappings, one at the entrance plane to the separator and one at the exit plane. The pressure drop, using water as the working fluid, is plotted against the mass flux, G, of the flow through the helical passages in Fig. 3.1. The pressure drop was also shown to be proportional to the square of the mean fluid velocity. The Reynolds number of the flow, using the equivalent diameter of the helical passage, was always greater than 2×10^5, showing that the flow was in the fully turbulent regime throughout the flow range tested.

The total pressure drop through the separator may be expected to be comprised of three components: the entry losses, the friction losses and the exit losses. As the total pressure loss is proportional to the square of the velocity then each of the components may also be assumed to obey a similar relationship. These three component losses are analagous to those in a contraction, a plain tube and an expansion in single-phase turbulent pipe flow. For water flows, at the maximum available driving pressure of 3.5 bar gauge, the maximum obtainable flow rate through the separator was 17.5 l/s.

In order to isolate the pressure loss in the separator due to friction, the test section was arranged to locate two static pressure tappings in one helical passage; the first tapping was

located 20mm after the entry to the helical passage and the second a similar distance before the passage exit. The vertical height difference between the tappings was 435mm. The friction pressure drop measured in this way was plotted against the mass flux, Fig. 3.2, and was also found to be directly proportional to the square of the mean fluid velocity. The friction losses for a straight duct are given by the Darcy equation, Massey (1983),

$$\Delta P = \frac{4f\delta l V^2 \rho}{2d_{eq}} \qquad (3.1)$$

where d_{eq} = 4 × Area/Perimeter
= Equivalent Diameter

which shows the dependency of the losses on the friction coefficient, f, for the duct. The friction losses were found to be higher in the helical passage than for an equivalent area straight circular duct with a friction factor taken from the Moody diagram for a duct of similar relative roughness. The friction factors for the helical passage were around 1.3 times greater than those predicted for a smooth straight tube. Similar results have been obtained by Ito (1959), Rogers and Mayhew (1964), Anglesea et al (1974) and Srinivasan et al (1968), who found friction factors in helically coiled tubes to be around 1.2 times greater than for the straight tubes before coiling, and dependent upon the curvature ratio of the coil or bend.

The slight differences between these results and those for the helical passages are probably due to the use of a poor

estimate of the relative roughness of the helical passage walls in calculating the theoretical friction coefficient. The friction coefficient of Srinivasan et al (1970) predicted the experimental data well (see Fig. 3.2) and so the triangular cross-section shape of the separator passages did not appear to significantly influence the single-phase frictional pressure losses in turbulent flow. The majority of the work done on helical coils has concentrated on coils with small helix angles, generally less than 10°, whereas the separator helical passages have a helix angle of 32°. From an extrapolation of the friction pressure losses for the entire length of the helical passages the total of the entry and exit losses are seen to be of the same magnitude as the friction losses.

3.2.2 Helical Passage Radial Pressure Profile

The pressure in a straight horizontal tube flowing full is generally considered to be uniform across a section perpendicular to the tube axis. Due to the helical form of the separator flow passages the fluid motion is influenced by centrifugal body forces caused by the curved path of the fluid. These forces are proportional to the square of the fluid velocity and will create a radial pressure difference between the root and outer wall of the passage. Hart et al (1988) and Banerjee et al (1967) found evidence of these pressure gradients and used them to predict the position of a flowing liquid ribbon on the tube wall in two-phase flow.

To investigate the form of this pressure gradient between the passage root and outer wall, a static pressure probe, Fig. 3.3, was traversed radially across the passage from the outer wall to the root at several different flow rates. This type of probe is not of a

very high accuracy for measurement of absolute values of static pressure, because the flow accelerates across the end of the tube giving a reduced static pressure reading. Absolute values were not necessarily required, however, because the parameter of interest was the ratio of two readings taken at different radii.

The static pressure was found to increase with increasing radius from the passage root to the passage outer wall, Figs. 3.4 - 3.8. This contrasted with the flow in a straight duct where the transverse pressure profile is usually of constant magnitude. The static pressure between the root and the mid-passage had a lower pressure gradient than the readings taken between the mid-passage and the outer wall of the passage.

The mean of the static pressure measured between r = 34mm (root) and r = 45mm (mid-passage) was used to define the average static pressure in the passages. This average was then used to normalise the static pressure across the entire passage radius and compare the pressure gradients in the outer passage at different flow rates, Fig. 3.9. At all the flow rates examined, the static pressure increased with radius. The static pressure difference between the root and outer passage wall increased with the average flow velocity. All the radial pressure distribution curves exhibited an increase in gradient in the immediate vicinity of the outer passage wall, thus indicating the presence of an undetected effect such as a recirculation zone. Similar secondary flows were shown to exist in curved ducts by Dean (1927) and Hawthorne (1950). Hart et al (1988) found similar static pressure differences in a helically coiled tube between the inner and outer tube walls. Hart attributed these to the influence of the centrifugal forces acting on the fluid flow. The static pressure difference between the root and the outer wall of the

passage in the separator, Fig. 3.10, was proportional to the square of the passage velocity showing the same influence of centrifugal forces as that found by Hart.

Static pressure probes are prone to influence by their own presence in the flow, as mentioned above. To check the probe readings at the wall, a comparison was made with the readings from wall static pressure tappings at the same axial location. The static pressure measurements were consistent with those taken using the probe, demonstrating that the probe did not greatly influence the static pressure in the vicinity of the wall.

3.2.3 Helical Passage Streamwise Velocity Profile

The static pressure has been shown to vary with radius in the helical passages and it is reasonable to suppose that some variation of streamwise velocity may also occur. The streamwise velocity is defined as the velocity along a path parallel to the passage axis, Fig. 3.11. A total pressure probe was used in conjunction with a static pressure probe to investigate the radial variation of velocity through the helical passage. The total pressure probe, Fig. 3.12, was installed in a helical passage with the static pressure probe in an adjacent helical passage at the same axial distance from the separator inlet. Mutual interaction of the static and total pressure probes was thus avoided. This installation assumed that the static pressure was the same in all the helical passages at the same axial station.

The reading quality of the total pressure probe was tested by deliberately misaligning the probe to be at an angle to the mean flow direction, this produced no significant difference to the

readings obtained from the probe. Thus small pressure probe misalignments were shown not to produce variations in the probe readings. The pressure difference between the static and total pressure probes was measured using a manometer. The local streamline velocity was calculated from the pressure difference where

$$V = \left[\frac{2g\Delta P}{\rho}\right]^{0.5} \qquad (3.2)$$

The local streamline velocity was found to be near constant between the passage root and r = 40mm, Fig. 3.13, for each of the water flow rates. The streamline velocity then reduced towards the outer wall of the helical passage to a value of approximately 0.85 times the average at each condition. The profiles for each of the flow rates examined appear to be very similar, differing in magnitude but each with the same underlying trend. The values obtained near to the passage walls, at around r = 50mm, are the least reliable due to the disturbance effect on the total pressure probe from the passage wall. The geometry of the total pressure probe and the passage were not ideally matched, the passage being curved in three planes while the probe was straight, and it was impossible for the probe to follow the geometry of the root or wall exactly.

The streamline velocity can be seen to decrease from a near constant value at approximately the same radius as the static pressure gradient in the helical passage begins to increase. The increase of the static pressure from the passage root to the passage outer wall is characteristic of that seen in a forced vortex where the pressure increase is proportional to the square of the tangential velocity (see Fig. 3.10). The decrease in the streamline velocity

near to the outer wall and the simultaneous increase in the static pressure gradient point to the existence of a zone of secondary flow at the outer wall.

3.3 Two-phase Separator Investigations

In air/water flow the mixture in the separator passages became separated with the liquid phase occupying the outer sector of the passage. The gas phase flowed in the root of the passage. The separation was caused by the centrifugal force generated by the swirling motion of the mixture in the helical passages, similar to that noted in static centrifugal separator vanes by Kalra et al (1983).

3.3.1 Two-phase Pressure Drop

The overall two-phase pressure drop for the separator was examined using a similar procedure to that for the single-phase flow experiments. The pressure tappings used were at the test section entry plane and at the separator exit plane. The pressure drop across the separator was measured for several different volume void fractions over a range of flow rates. The pressure drops were found to be proportional to the mass flux, Fig. 3.14. The mass flux, G, was defined as the total mass flow rate per unit area in the helical passages.

$$G = \frac{m_g + m_l}{A} \qquad (3.3)$$

For each of the nominal void fractions, the two-phase pressure drop follows a slightly different curve, showing that the pressure drop is also dependent on the void fraction of the flow. The gradient of the pressure loss curves increased as the void fraction increased. The scatter in the data increases as the pressure drop increases, indicating a tendency for the flow regime to become more intermittent as the gas phase undergoes expansion through the separator and the void fraction increases through the helical passages.

The frictional pressure loss in two-phase flow was measured by using two static pressure tappings in the outer wall of one helical passage. The pressure losses in two-phase flow are made up from three components; the gravitational pressure loss, the accelerational pressure loss and the friction pressure loss.

$$\Delta P_{tp} = \Delta P_{grav} + \Delta P_{acc} + \Delta P_{frict} \qquad (3.4)$$

The pressure loss within the air/water flow in the passage due to change of phase is zero. The gravitational pressure loss is known from the vertical height difference between the static pressure tappings, assuming a negligible change in the mixture density. Taking into account the gravitational pressure loss, the measured pressure loss is that due to friction and acceleration. The accelerational pressure loss in a two-phase system with separated flow is given by Whalley (1987) as

$$\Delta P_{acc} = G^2 \frac{\partial}{\partial z}\left[\frac{x^2}{\alpha\rho_g} + \frac{(1-x)^2}{(1-\alpha)\rho_l}\right] \qquad (3.5)$$

The pressure loss in the helical passage due to the acceleration of the mixture, ΔP_{acc}, can be estimated, using equation 3.5, from the known test section inlet conditions. The friction pressure loss is the measured two-phase pressure loss minus the accelerational pressure loss. The accelerational pressure loss was less than 2% of the friction pressure loss, Fig. 3.15, at all the conditions in the separator passage. Jensen et al (1985) also found that the accelerational pressure drop in air/water swirling flow was negligible. The pressure losses increased with increasing mass flux and, as the void fraction increased, the two-phase pressure losses also increased.

The friction pressure losses in two-phase flow through the separator were greater than those for single-phase flow, the ratio between the two-phase friction pressure loss and the friction loss for the total mass flux flowing as one phase in the same passage is known as the two-phase multiplier, ϕ^2_{lo}, [Lockhart and Martinelli (1949), Wallis (1969)].

$$\phi^2_{lo} = \frac{\Delta P_{tpf}}{\Delta P_{lo}} \qquad (3.6)$$

The two-phase multiplier increased from around 1.05 to 1.7 across the range of the flow rates and void fractions used. These results are similar in magnitude to those found by Akagawa et

al (1971) for a helical coil. The two-phase pressure drop also increases as the void fraction increases, this effect was noted by Anglesea et al (1974) in experiments on pressure losses in helical coils with steam/water flow.

3.3.2 Two-phase Radial Pressure Profile

To find the static pressure variation across the helical passage in two-phase flow a static pressure probe was traversed across the passage radially. The static pressure was measured using a pressure gauge, at the same time the probe was observed and the radius at which the interface zone between the two phases was pierced by the probe tip was noted. The pressure traverse results, Fig. 3.16, show that between the passage root and the point at which the interface is met, at around r = 44mm, there is little variation in the static pressure.

The local static pressure at each radius was normalised using this near constant pressure. The results shown in Fig. 3.16 are for a nominal volume void fraction of around 30% only. The near constant static pressure in the separated gas phase is due to the relatively small centrifugal force which acts on the air, because of its low density, causing no significant static pressure rise. The static pressure in the separated liquid phase increased with radius between the gas/liquid interface and the passage outer wall. The pressure gradient in each phase is given by

$$\frac{\Delta P}{\Delta r} = \frac{\rho V^2}{r} \qquad (3.7)$$

The higher pressure gradient in the separated liquid phase is caused by the much greater centrifugal force on the liquid because of its much higher density, typically 400 times that of air at 2.5 bar.

The phase areas occupied by each phase can be estimated from the observation of the phase boundary position. These results are not very accurate, however, given the uncertain thickness of the interface region and the unsteady nature of the flow. At a given axial plane in the separator the radial position of the air/water interface appeared to remain constant, for a constant void fraction, as the mixture flow rate was increased. This indicates that the slip ratio between the separated fluids is constant for a given void fraction at any one cross-section in the separator.

The increase in flow rate in the separator did not increase the separated gas velocity sufficiently to create a significant radial pressure gradient in the gas phase at any condition. For the radial pressure gradient in the gas phase to approach that of the liquid phase the mean gas phase velocity would need to be much greater than the liquid phase velocity, Whalley (1980). In the separated liquid phase the pressure gradient becomes steeper as the flow velocity is increased.

During the experiments the presence of a secondary flow in each phase was noted from the observation that both separated phases appeared to be forming streamwise vortices. Johnson (1989)

showed that in a rectangular cross-section bend the secondary flow consisted of a single recirculation, unlike that in a tube bend which forms a double recirculation. From the evidence of the experimental observations it seems likely that the flow through the triangular cross-section passages in the separator forms a single recirculation secondary flow pattern similar to those found in rectangular cross-section bends.

3.3.3 Streamwise Velocity Profile

The streamwise velocity in each of the separated flows is of interest, if only to confirm the slip ratio between the two phases experimentally. A Pitot-static tube (Fig. 2.6) was used in an attempt to investigate the magnitude of the phase velocities in the separated two-phase flow and the radial variation of these velocities. The initial experiments showed that as there was an incomplete separation of the gas and liquid phases in the separator passages there was a large fluctuation of the probe reading due to the difference in the momentum of the two fluids in which the probe was operating.

In an attempt to analyse the pressure signal from the probe a differential pressure transducer was used to produce a proportional voltage signal. Ideally the signal would have two values, high and low, proportional to the energy of the phase impinging on the tube. This was not the case during the experiments which were performed, the signal being made up of several different values not apparently related to the momentum of either phase, Fig. 3.17. The physical size of the probe determined that rather than either gas only or liquid only impinging on the probe an indeterminately proportioned mixture was more frequently sensed.

Davis (1980) also found that the pitot response was between the stagnation and momentum flux values in two-phase flow with a probe smaller than the predicted mean bubble size.

This technique, then, failed to supply the velocity distribution in the separated phases. The velocity in the gas phase was assumed not to vary radially as the static pressure showed no radial variation. The separated liquid phase velocity was assumed to have a distribution similar to that for the single-phase flow as the static pressure distribution was similar to that for the single-phase flow.

3.3.4 Passage Root Pressure Survey

The gas-liquid separator has been demonstrated to separate the fluids [see also King and Purfit, 1984]. To quantitatively assess the separation performance of the separator physical modifications were necessary. The modifications consisted of drilling a central gallery from the rear of the separator upstream along the axis. The separator wall, between the passage root and the gallery outer diameter was then pierced by slots which enabled the separated air to pass from the helical passages into the central gallery (see Fig. 1.7). For the air to pass through these slots a pressure differential must exist across them. To aid the siting of these slots a pressure survey of the passage root was performed, in two-phase flow, to find the locations in the passage root likely to have the highest pressure differential.

The pressure survey was performed by traversing the static pressure probe into the passage root at several axial locations and measuring the static pressure at these points at the

same flow conditions. The static pressure was also measured at the separator exit plane and at 10mm downstream of the separator exit plane at the passage root radius, to discover whether there was static pressure recovery at the separator exit. The static pressures were measured at several flow rates for a constant inlet pressure. As the flow velocity was increased, Fig. 3.18, the local static pressures decreased and the pressure difference between the exit plane (z = 630mm) and the mid (z = 403mm) and low (z = 161mm) separator positions increased. The increase in pressure differences between the horizontal planes was due to the increase of the friction pressure losses with flow rate. The pressure difference between the low/mid points on the separator and the exit plane varied between 0.41 and 0.61 bar across the flow range.

The higher pressure differential between the low slot position and the exit plane is likely to give a better separation performance at this position than further downstream in the passages, but it is likely that there will be sufficient pressure differential at all the potential slot positions to drive some of the air flow through the slots and into the central gallery. The volume flow rate through the slots will depend on the differential pressure across them.

3.4 Investigations with Kerosene Liquid Phase

3.4.1 Single-phase Kerosene Pressure Drops

The single-phase friction pressure losses in the separator were examined using kerosene as the working fluid. The kerosene flow rig has been described in Chapter 2. Two static

pressure tappings were inserted in the same helical passage wall a vertical distance of 172mm apart. A differential pressure transducer was connected across these tappings and linked to a microcomputer via an ADC. The readings from the transducer were averaged over 100 measurements.

The single-phase pressure losses across the separator were examined to provide a comparison with the results from the single-phase water system. The friction pressure drop, Fig. 3.19, was lower than that predicted using the friction factor correlation of Srinivasan et al (1970) for helically coiled tubes. This may be an effect of the passage geometry, causing a single recirculation zone in the helical passages rather than the double recirculation found in helically coiled tubes. The friction pressure drop along the helical passage increased as the mass flux was increased, this was also the case for the single-phase water flow. The friction pressure drop agreed with that found in the water flow. The percentage difference between the measured and predicted pressure drops decreased slightly as the mass flux was increased.

The friction factors calculated from the single-phase kerosene flow were compared with those found from the single-phase water flow, Fig.3.20. The majority of the friction factor points gained from the water experiments were at higher Reynolds Number than those from the kerosene flow because of the lower density and higher kinematic viscosity of the kerosene. The magnitude of the friction factors from both experiments were found to be in close agreement.

3.4.2 Two-phase Air/Kerosene Pressure Drops

The friction pressure drop was also examined in two-phase air/kerosene flow. The acceleration pressure drop was calculated using equation 3.5. The friction and acceleration pressure losses for each of the void fraction conditions used are shown in Fig. 3.21 and 3.22. The highest pressure losses were given by the 30% void fraction condition. The friction pressure losses reduced as the void fraction of the flow was reduced, the lowest being at 10% void fraction. The trend of the results was similar to that seen in the air/water flow where the highest pressure losses were at the largest void fractions. The pressure losses also reduced with decreasing void fraction in the air/water system. The acceleration pressure losses in the air/kerosene system were similar in magnitude to those in the air/water system and were around 6% of the friction losses. Inspection of equation 3.5 showed that the acceleration pressure losses in the air/kerosene system were slightly higher than in the air/water system because the density of kerosene is lower than that of the water.

The similarity of the results from both the water and the kerosene based systems showed that, as expected, the pressure losses are not dependent on the fluid characteristics. The agreement of both the single-phase systems with the predictions based on the friction factor correlation of Srinivasan (1970) showed that a secondary flow exists in the helical passages.

3.4.3 Entry Losses

The pressure losses caused by the separator entry were also examined in air/kerosene flow. The pressure losses followed a similar pattern, Fig. 3.23, to the friction pressure drop in the helical passages. As the mass flux was increased the entry pressure losses increased. The highest pressure losses were again at the greatest void fraction conditions. The lowest void fractions gave the lowest entry pressure losses. Knowledge of both the entry and frictional pressure losses enabled the calculation of the local static pressure at any point in the helical passages between the entry and the exit plane.

3.5 Take-off Slot Performance

3.5.1 Visual Assessment of Take-off Slots

The air take-off slots, Fig. 3.24, in the helical passage roots were initially assessed visually over a range of two-phase flow conditions. The observations were recorded by video camera for later analysis. The initial position of the slots was known as Configuration 'a'. The first slot, located axially 80mm after the separator entry, did not appear to ingest any of the gas stream. Although at this point the air stream had separated from the water it had not yet migrated to the passage root, in consequence there appeared to be a region of water flowing between it and the take-off slot which prevented the gas stream flowing into the slot.

At the next slot, located at the mid-height position of the separator, the air stream was observed to be entering the slot at

all the two-phase flow conditions. Not all the separated air passed into the slot however, a part of the gas stream continued to flow in the helical passage downstream of the slot. The take-off slot immediately before the separator exit was also observed to extract air from the helical passage root at some of the flow conditions used.

The visual assessments were not capable of estimating the quantative performance of the slots beyond the simple conclusion that the position of the slots influenced their effectiveness. The first slot was apparently ineffective due to the separated gas stream being near the centre of the helical passage. The mid-slot appeared to work at all the flow conditions and the slot immediately before the exit of the separator worked at some flow conditions. The exit slot has the lowest pressure differential and there was probably only sufficient driving pressure across the slot to extract the gas stream at higher flow rates.

3.5.2 Gas Take-off Slot Configuration 'a'

For quantative analysis of the separator performance the separated gas and liquid phases were collected and the flow rate of each was measured (section 2.1.4).

The separator and test section were vertically orientated to give a phase distribution unaffected by gravity at the test section entry. The phase distribution in bubbly upward flow in a vertical pipe is generally such that the gas phase is concentrated toward the pipe axis with the liquid phase distributed nearer to the pipe wall. This type of distribution, which is not biased toward any particular sector of the pipe [Serizawa and Kataoka, 1988], should

then give a uniform distribution at the separator entry plane. The flow entering each helical passage is then assumed to have an equal proportion of both the liquid and the gas phase from the main tube. From this assumption the gas and liquid which was collected from two of the helical passages was taken to be one third of the total which would have been separated by the full complement of six helical passages. The gas separation efficiency was then defined as

$$\eta_g = \frac{3Q_{gs}}{Q_{gt}} \qquad (3.8)$$

Air and water were used to provide the gas and liquid phases. The performance of the separator was assessed at several different void fractions between 5% and 35% across the full flow range available (2 - 17.5 l/s of water). The percentage of the air separated, by mass, was plotted against the mass flux, G, of the two-phase flow. The residence time of the flow in the separator is related to the mass flux.

The gas separation efficiency results, Fig. 3.25, tended to reduce from between 55% and 90% to around 45% as the mass flux through the separator increased. The flow void fraction had no clear influence on the results, although the lower void fractions appeared to give a higher gas separation efficiency. The liquid draw-off, Fig. 3.26, was generally 4% of the total liquid flow, or less, across the flow range.

3.5.3 Configuration 'b'

Each of the take-off slots in Configuration 'a' was increased to 100mm in length, the new arrangement was known as Configuration 'b'. The gas separation efficiency, Fig. 3.27, was found to reduce slightly from between 60% and 95% to between 50% to 75% as the mass flux increased. For the same mass flow conditions the liquid draw-off, Fig. 3.28, was lower than 5% of the separator liquid flow.

3.5.4 Configuration 'c'

An additional take-off slot was cut into each of the helical passages upstream of the existing slots, the new arrangement being known as Configuration 'c'. The gas separation efficiency, Fig. 3.29, was found to reduce from between 80% and 95% to between 45% and 80% as the mass flux through the separator increased. Generally the results indicated that, for a given mass flux, the separation efficiency increased as the flow void fraction decreased. The liquid draw-off , Fig. 3.30, was lower than 6% across the range of mass flux used. The results at the lower void fractions gave the highest liquid draw-off.

3.5.5 Comparison of Different Configurations

From the results of the three take-off slot configurations it can be seen that the gas separation performance of Configurations 'b' and 'c' was very similar. The gas separation efficiency results from Configuration 'a' were generally inferior to

those from 'b' and 'c'. The liquid draw-off results for Configurations 'a' and 'b' were similar while those for 'c' were slightly greater. Generally Configuration 'b' gave the best combination of high gas separation efficiency and low liquid draw-off.

The improvement in the gas separation efficiency from Configuration 'a' to that for 'b' and 'c' was due to the increase in length of the take-off slots from 50mm to 100mm which gave an increased residence time of the flow across the slots. The increased liquid draw-off results from Configuration 'c' were due to the additional upstream slot. This slot was at a position where, although the gas and liquid were separated, the gas phase had not migrated to the passage root. There was a greater proportion of the liquid phase adjacent to the slot which was then drawn into the central gallery.

3.6 Separator Performance in Air/Kerosene Flows

3.6.1 Experimental Layout of Take-off Slots

After consideration of the air/water experimental investigation the optimal slot arrangement was decided to be Configuration 'b', Fig. 3.31. The performance of the individual slots and that of the complete arrangement was examined in air/kerosene flow. During the investigation of the individual slots the redundant take-off slots were blocked with acrylic resin filler paste, sculpted to the form of the helical passage root.

A similar system to that used for the air/water experiments was used for the collection and measurement of the separated air and kerosene, Fig. 3.32. The Rotameters used to measure

the separated air flow rate were of lower capacity than those used in the air/water experiments. At the lowest recorded air flow rate the error was ± 2.66%, less than the equivalent errors in the air/water experiments.

3.6.2 Slot 1

The gas separation efficiency for Slot 1, Fig. 3.33, decreased from between 40% and 80% to between 40% and 60% as the mass flux increased. Across the same mass flux range the liquid draw-off, Fig. 3.34, remained at less than 5%.

3.6.3 Slot 2

The experimental data taken using Slot 2 show that the gas separation efficiency, Fig. 3.35, remains between 25% and 60% across the majority of the mass flux range. The liquid draw-off, Fig. 3.36, was generally lower than 4% across the range of mass flux.

3.6.4 Slot 3

The gas separation efficiency measured during the Slot 3 experiments was generally lower than 40%, Fig. 3.37, over the range of mass flux. Across the same range of mass flux the liquid draw-off, Fig. 3.38, was generally lower than 1%.

3.6.5 Configuration 'b'

After each slot had been tested individually the complete arrangement was examined. As the mass flux was increased, Fig. 3.39, the gas separation efficiency reduced from between 30% and 80% to between 40% and 50%. Over the same range of mass flux the liquid draw-off, Fig.3.40, was generally less than 4.5%.

3.7 Separator Effectiveness

3.7.1 Effectiveness of Air/Water Separation

As discussed in section 3.5.5 the Configuration 'b' gave a better combination of high gas separation efficiency and low liquid draw-off than 'a' and 'c'. It was noted that the gas take-off rate was significantly improved by lengthening the slots, without incurring a simultaneous increase in the liquid draw-off rate. This indicated that the percentage of the gas which will flow through a take-off slot is dependent on the residence time of the gas above the slot.

3.7.2 Effectiveness of Air/Kerosene Separation

Each of the slot locations was examined individually in the air/kerosene flow. The performance of each, physically identical, slot was dependent upon its axial location. Slot 1, which was closest to the separator inlet, had the highest gas separation performance but also removed a large proportion of the kerosene from the flow. The mid axial slot, Slot 2, had a lower gas separation efficiency and

liquid draw-off than Slot 1. The slot immediately before the separator exit, Slot 3, returned the lowest gas separation efficiency and liquid draw-off. The performance of the combined slots in two helical passages was not as good as the sum performance of the individual slots. The performance of a slot must, therefore, be affected by the presence of a slot either upstream or downstream of itself.

The most important parameters by which the separation performance of each individual take-off slot may be judged are the total flow rate of the mixture through the slot and the quality of that mixture. Madden and St. Pierre (1970) found that the flow rate through a slot, which had its longitudinal axis parallel to the direction of the flow across it, was proportional to the pressure drop across the slot. This was a similar result to that for any orifice. Other workers (Section 4.4.3) have noted a relationship between the quality of the flow through a branch above a stratified two-phase flow and the distance of the gas/liquid interface below the branch entrance.

The experimental data from the separator was examined to find whether similar relationships held for the take-off slots in helical passages. The variables likely to affect the separation performance of the slots were examined using dimensional analysis to find likely dimensionless groupings. The flow of the mixture through the slot was taken to be a function of several variables

$$Q_{slot} = f(Q_{total}, \Delta P, \rho_h, V_{pass}, h_g, H) \qquad (3.8)$$

This set of variables takes account of the pressure drop across the slot, the density of each phase, the void fraction and the

passage velocity. Certain fluid properties which may influence the separation of the gas and liquid, notably surface tension and viscosity, were neglected because the flow was assumed to be in a separated flow regime at the slot.

From this set of variables the dimensional analysis produced the following groupings

$$\frac{Q_{slot}}{Q_{total}} = f\left\{\left[\frac{\Delta P}{\rho_h V^2}\right]^n, \left[\frac{h_g}{H}\right]^m\right\} \qquad (3.9)$$

The dimensionless phase height represents the area void fraction of the separated flow in the helical passage and the other group, which will be referrred to as F for convenience, on the RHS of the equation is the ratio of the static pressure drop across the slot to the dynamic head of the mixture in the passage. To investigate the experimental data the LHS of equation 3.9, which is the ratio of the total volume flow rate through the slot to the total volume flow rate through the separator, was plotted against the RHS. The best trend of the results was obtained by setting the indices n = 1 and m = 3, giving

$$N = \left[\frac{\Delta P}{\rho_h V^2}\right]\left[\frac{h_g}{H}\right]^3 \qquad (3.10)$$

The take-off flow ratio decreased from around 0.105 to less than 0.05 as N increased, Fig. 3.41. The trend of this data was

consistent for all the flow conditions which were examined for Slot 1.

The take-off flow quality was plotted against T, which although not a dimensionless grouping has dimensions of time, where

$$T = \frac{\rho_h}{Gh_g} \qquad (3.11)$$

The parameter, T, was taken as a measure of the residence time of the mixture in the separator. The slot take-off quality, x, decreased as T, which is strongly dependent on the mass flux in the separator, was increased, Fig. 3.42, for Slot 1. The trend was consistent at all the flow conditions examined. This showed that the take-off slot quality reduced as the residence time of the mixture in the separator was increased (ie as mixture flow velocity decreased).

The take-off flow ratio for Slot 2 was also plotted against N, Fig. 3.43. A similar curve to that for Slot 1 was found for this data. The decreasing trend was again consistent at all the flow conditions, with the take-off flow ratio reducing as N was increased. Some of the data from Slot 2 was taken with the pressure at the rear of the separator raised above the normal value, this data exhibited similar magnitudes and trends to the data taken with normal back pressure. The take-off quality of the mixture passing through Slot 2, Fig. 3.44, showed a similar trend to that for Slot 1. The quality decreased as T was increased for all the flow conditions, the data taken with raised back pressure at the separator exit was similar to that taken at normal conditions. The data was again consistent at all the flow conditions used in the experiments.

For Slot 3, the take-off flow ratio, Fig. 3.45, followed generally the same trend as that for Slots 1 and 2. The flow ratio through the slot reduced as N was increased. However there was more scatter in the data, due to the lower values of slot flow rate obtained. The take-off quality for Slot 3, Fig. 3.46, followed a similar general trend to that seen for Slots 1 and 2. The quality data from Slot 3 showed greater scatter about the general trend than the data from either Slot 1 or 2.

The results from each slot are compared in Fig. 3.47. The take-off flow ratios given by Slots 1 and 2 were in good agreement and both sets of data adhered to one similar broad curve. The take-off flow ratio for Slot 3 was around 50% lower than those for Slots 1 and 2 at similar values of N. The difference, however, was not caused by the reduced ΔP across Slot 3. The ΔP across Slot 2 was lower than that across Slot 1 by approximately the same factor as the ΔP for Slot 3 was lower than the pressure drop across Slot 2. The take-off flow ratio from Slots 1 and 2 agree closely and the difference in the ΔP across each slot is accounted for in the parameter N. The difference of the data from Slot 3 was thought to be caused by the proximity of the separator exit to the rear of the slot. Azzopardi and Smith (1990) noted that the downstream effect of a bend on a tee piece caused a distinct change in the outlet flow quality from the branch under some two-phase flow conditions.

The take-off quality of the flow from each of the slots is compared in Fig. 3.48. The mixture quality was again plotted against T and it can be seen that each set of data follows a decreasing trend as T increases. The take-off quality was very similar for Slots 1 and 2 for all values of T. The take-off flow quality was higher for Slot 3 than for either of Slots 1 or 2, due to

the proximity of this slot to the separator exit plane. At Slot 3 the flow has passed further down the separator than at Slots 1 and 2, allowing a greater separation of the phases. The lower ΔP across the slot also reduces the liquid draw-off rate. The decrease in quality with increasing residence time was due to the decreasing definition of the phase separation in the helical passages.

The take-off flow ratio from the separator was also measured using the slot Configuration 'b', the results were plotted against the same parameter, N, as for the individual slot positions. The take-off flow ratio, Fig. 3.49, followed a similar reducing trend to that seen for each individual slot position. The take-off flow ratio was slightly higher for Configuration 'b' than for any of the individual slot positions, this was due to the increased slot area available in Configuration 'b' leading to an increased take-off flow rate.

The total flow rates for Configuration 'b' were, however, not as great as the sum of the flow rates from each individual slot position. The performance of each slot in the combination was adversely affected by the presence upstream of another slot. The behaviour of the combination of slots is similar to that of a flow distribution manifold, examined by Collier (1976). As the flow is taken off through a slot there is an associated static pressure rise in the helical passage along the axial length of the slot. This static pressure rise in the helical passage causes an effective reduction in the ΔP across the downstream take-off slot by counteracting the friction pressure losses in the helical passage. This reduction in the ΔP across the take-off slot immediately downstream causes a reduction in the take-off flow from that slot.

The overall effectiveness of the combination of slots is therefore reduced from the sum of the individual slot performances.

The take-off flow quality for Configuration 'b', Fig. 3.50, plotted against the parameter T, showed a decreasing trend as T increased. The quality of the mixture flowing through the slots in Configuration 'b' was around 50% lower than that for Slot 3, which was the highest of the results from the individual slot positions. The Configuration 'b' result was lower than the results from Slot 1, which gave the lowest quality amongst the individual slots.

Azzopardi and Smith (1990) noted the existence of a sudden increase, or jump, in liquid phase height under the branch of a tee in a separated flow, associated with the pressure recovery. This increase in liquid phase depth would cause a decrease in the quality of flow through the next slot downstream as the interface approached the slot. Part of the reason for the increase in liquid phase height is the preferential separation of the gas phase through the branch and another influence appears to be the increase in static pressure in the run.

The above investigation showed that the maximum take-off flow ratio in the separator was at the highest passage velocity. The maximum take-off quality was also obtained at high passage velocity (low residence time). The take-off flow ratio and take-off quality performance of Configuration 'b' was marginally improved from that of Slot 1.

3.7.3 Comparison of Air/Water and Air/Kerosene Separation

The air/kerosene separation results for Configuration 'b' were compared with the air/water data. The gas separation efficiency

in the air/water mixture was clearly higher than for the air/kerosene mixture. The gas separation efficiency in the air/water mixture reduced from around 90% to around 55% across the flow range. In the air/kerosene mixture the gas separation efficiency reduced from around 60% to around 45% across a similar flow range. The measurement uncertainty of the separated gas flow in the air/kerosene experiments was lower than for the equivalent air/water system. For this reason the air/kerosene experimental results were considered more reliable. The liquid draw-off results for the air/water experiments were between 2% and 5% of the total liquid flow rate. The air/kerosene results were between 0.5% and 3.5% liquid draw-off, lower than those for the air/water results. The lowest liquid draw-off rates for the air/water results were given by the highest void fraction flows, where the gas/liquid interface is most distant from the slot entrance.

Visual observations showed that the air/kerosene mixture formed smaller air bubbles in the helical passages than those seen in the air/water flow. These bubbles were then less easily separated from the liquid phase because their smaller diameter determined a lower terminal rise velocity, Bradley (1965). Kerosene also has a higher viscosity than that of water which resulted in a reduction of the rise velocity of the air bubbles toward the helical passage root. Thus a separated continuous gas phase was formed less quickly than in the air/water system and a higher proportion of the air remained dispersed in the kerosene and not free to pass into the take-off slots.

Air is five times more soluble in oil than water, Hayward and Dallas (1965), and up to 10% may have been dissolved into the kerosene making the gas phase less easily separated. There is then a

reduced proportion of the air free to form a separated continuous gas phase, reducing the volume of air available for separation through the take-off slots. The lower gas separation efficiency in the air/kerosene system will also lead to fewer liquid drops being torn off from the liquid interface below the slots, Ishii & Mishima (1982), because the velocity of the air entering the slot will be lower.

These physical phenomena were exacerbated by the lower density of kerosene compared to water. The body forces in the flow which cause the gas/liquid separation were reduced because the difference in density between air and kerosene is around 20% lower than that between air and water.

The secondary flows inherent in flow through helical passages, Dean (1927), also tend to complicate the separation of the gas bubbles from the liquid phase by generating a swirl which causes mixing and counteracts the separation effect to some extent. In the separator passages a single helix secondary flow existed, rather than the double helix flow found in helically coiled tubes. A single vortex explained the observation that the gas phase occupied the centre of the passage (low swirl velocity region) in the initial section of the separator passages before migrating to the passage root. At most flow conditions the gas/liquid interface exhibited a swirl pattern, a further indication of the presence of a single vortex rather than a double recirculation.

The slot flow ratio for the air/water data in Configuration 'b', Fig. 3.51, was plotted against the parameter N. The flow ratio was always higher than for the air/kerosene (see Fig. 3.49), indicating that the difference in the liquid phase properties caused the change in the system behaviour. No trend could be

identified with certainty in the air/water data. The slot quality of the air/water flow in Configuration 'b', Fig. 3.52, was also compared with that seen for the same slot configuration with air/kerosene flow (Fig. 3.50). The air/water data shows large variations in the slot quality at lower values of T. The magnitude of much of the air/water data is comparable with that seen in the air/kerosene system for Configuration 'b'. The data shows a decreasing trend, as the residence time increases, in common with the air/kerosene data.

3.7.4 Review of Separator Experimental Work

The experimental results obtained from the two-phase air/water and air/kerosene flows highlighted several features of the separator performance.

The gas/liquid separator successfully extracted a high proportion of the free gas phase in both air/water and air/kerosene flows. A very low proportion of the available liquid phase was drawn off with the gas phase.

The performance of the separator was better in air/water flow where the gas/liquid density ratio was highest.

Examination of the individual slot performances showed that the most effective slot positions were at locations with the highest ΔP.

The take-off slots were most effective at high passage velocities (low separator residence time).

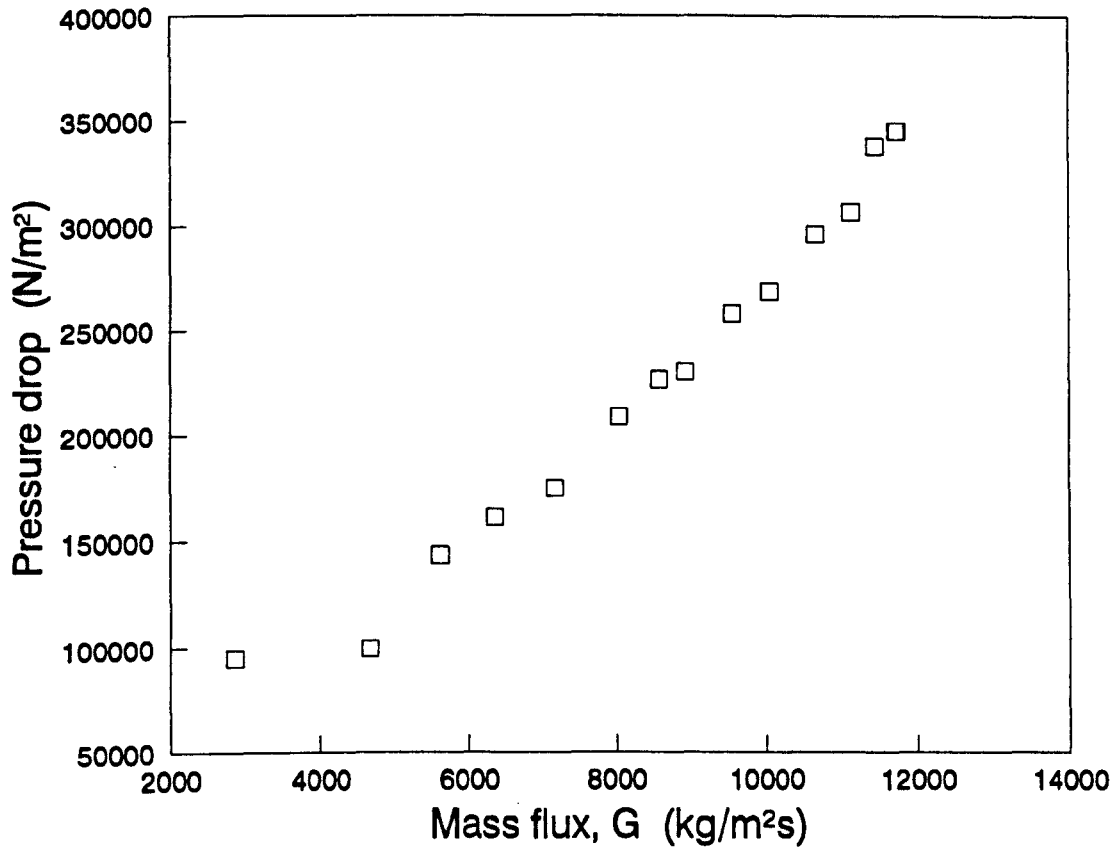

Figure 3.1 Single-phase water pressure drop

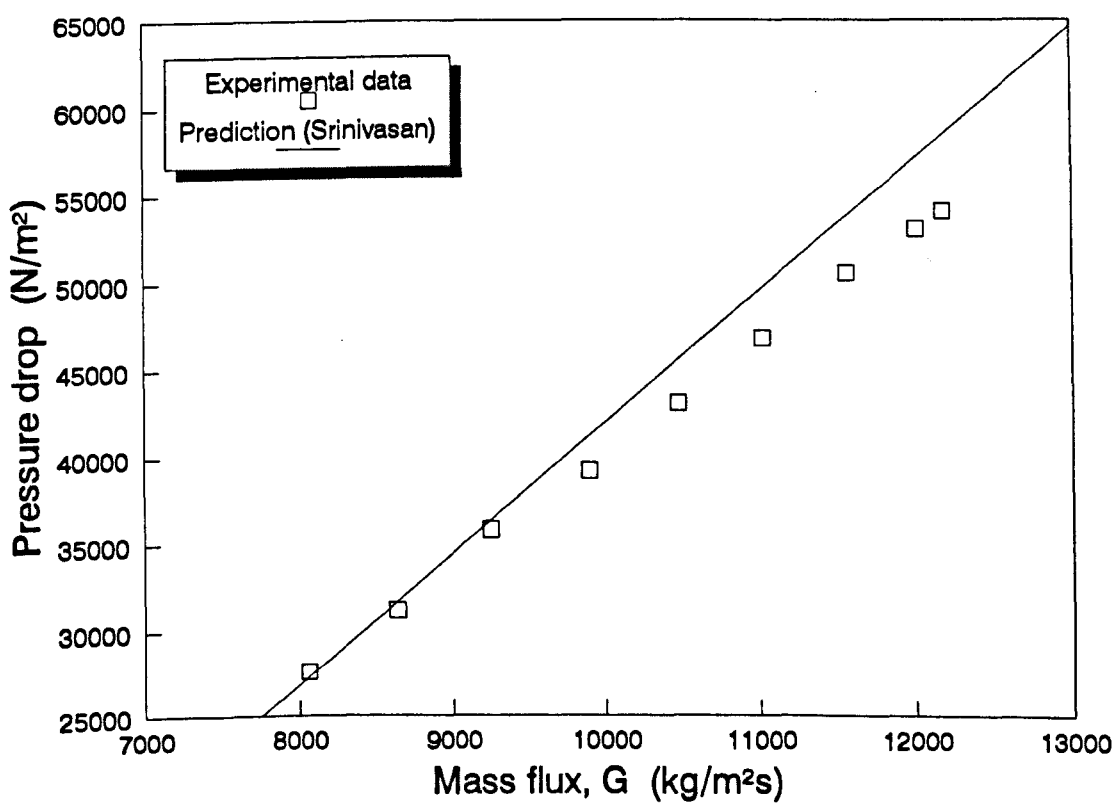

Figure 3.2 Single-phase water friction pressure drop

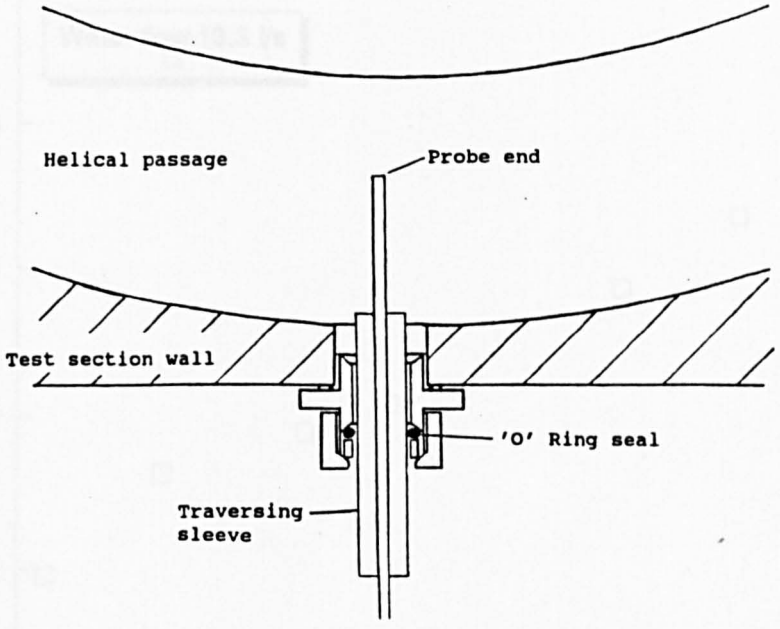

Figure 3.3 Static pressure probe

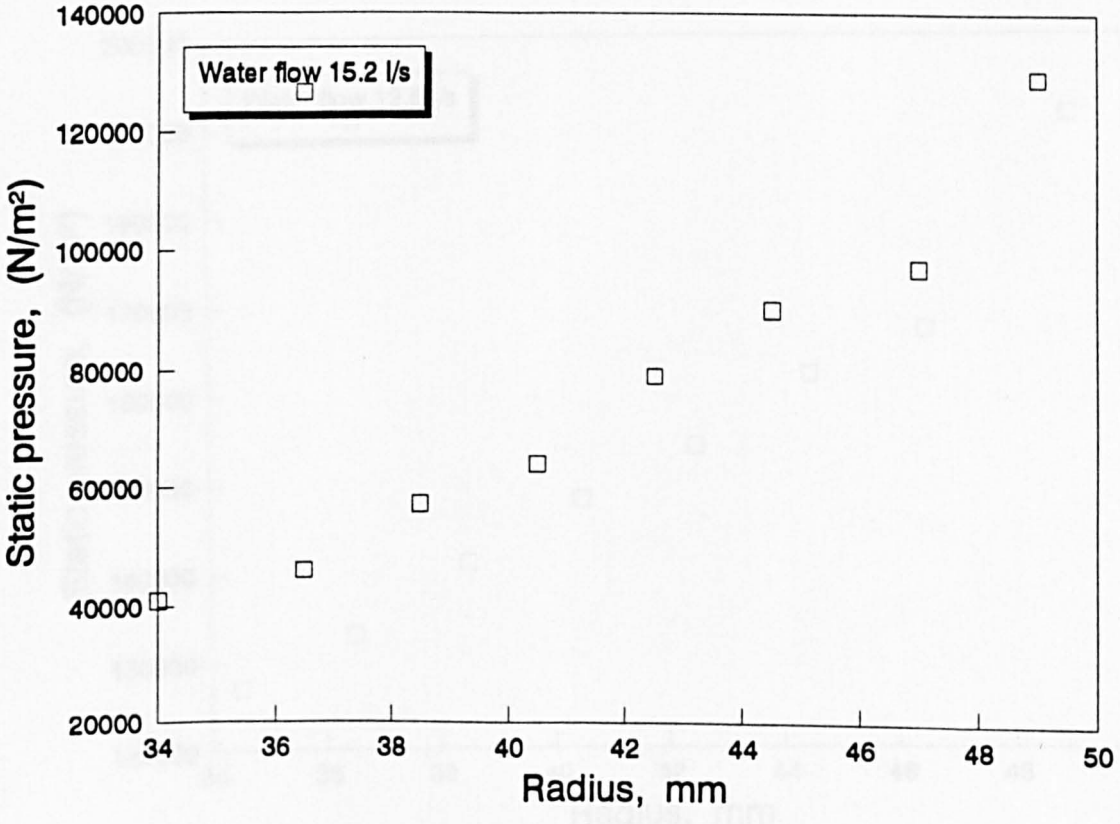

Figure 3.4 Single-phase radial pressure traverse

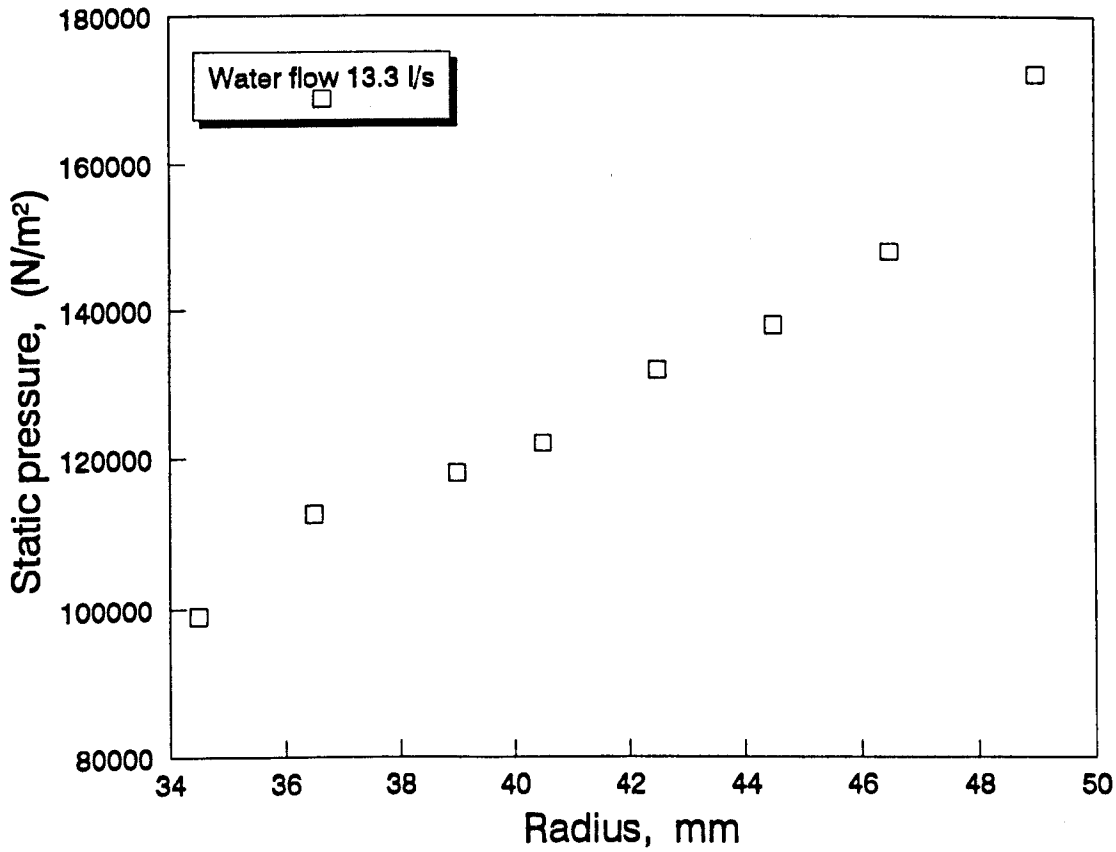

Figure 3.5 Single-phase radial pressure traverse

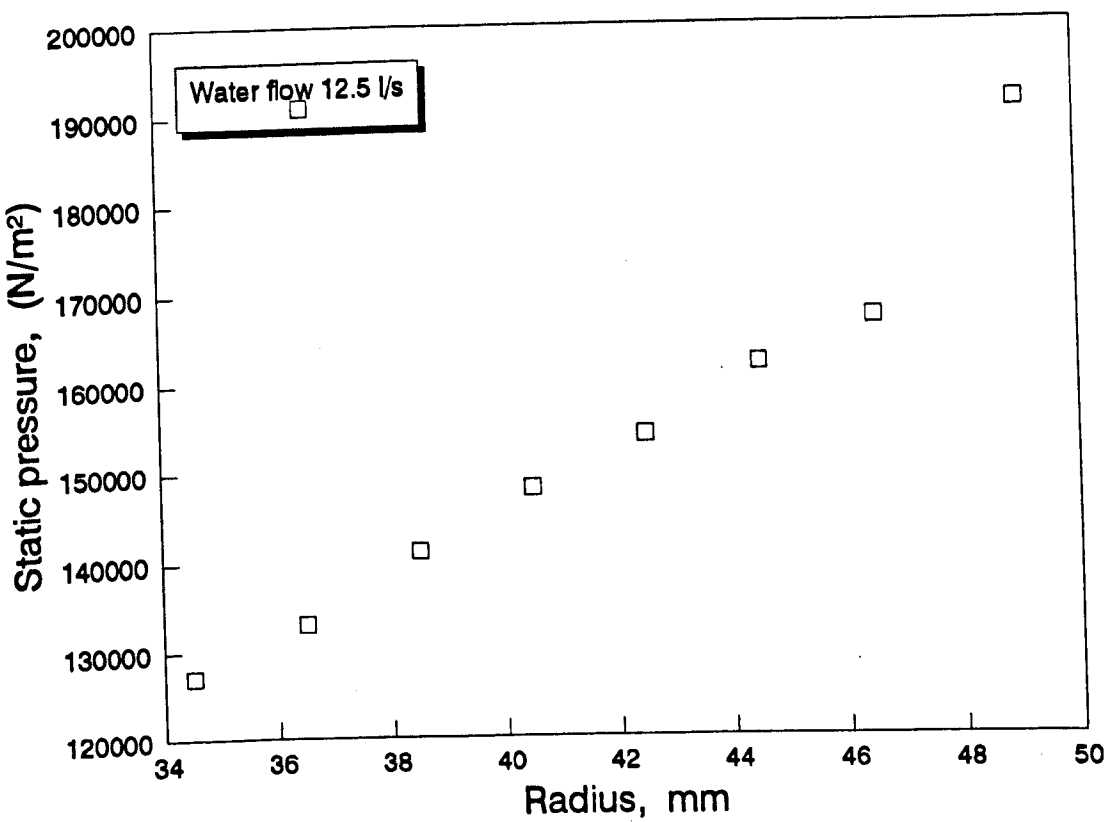

Figure 3.6 Single-phase radial pressure traverse

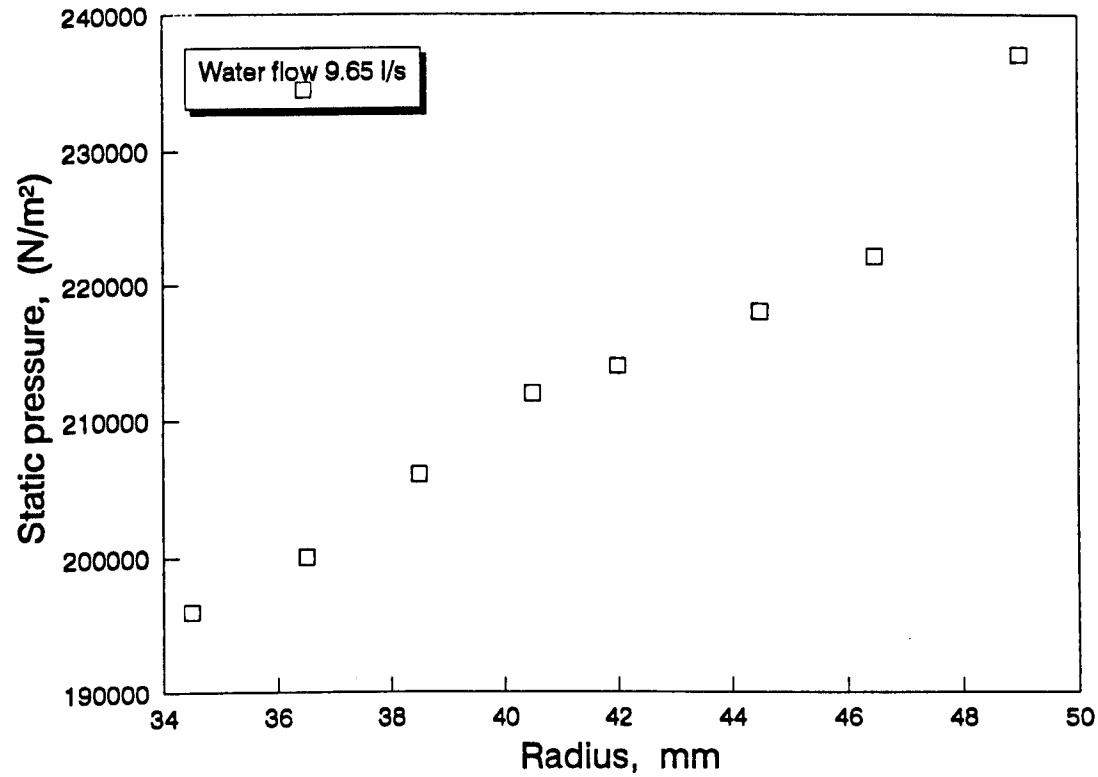

Figure 3.7 Single-phase radial pressure traverse

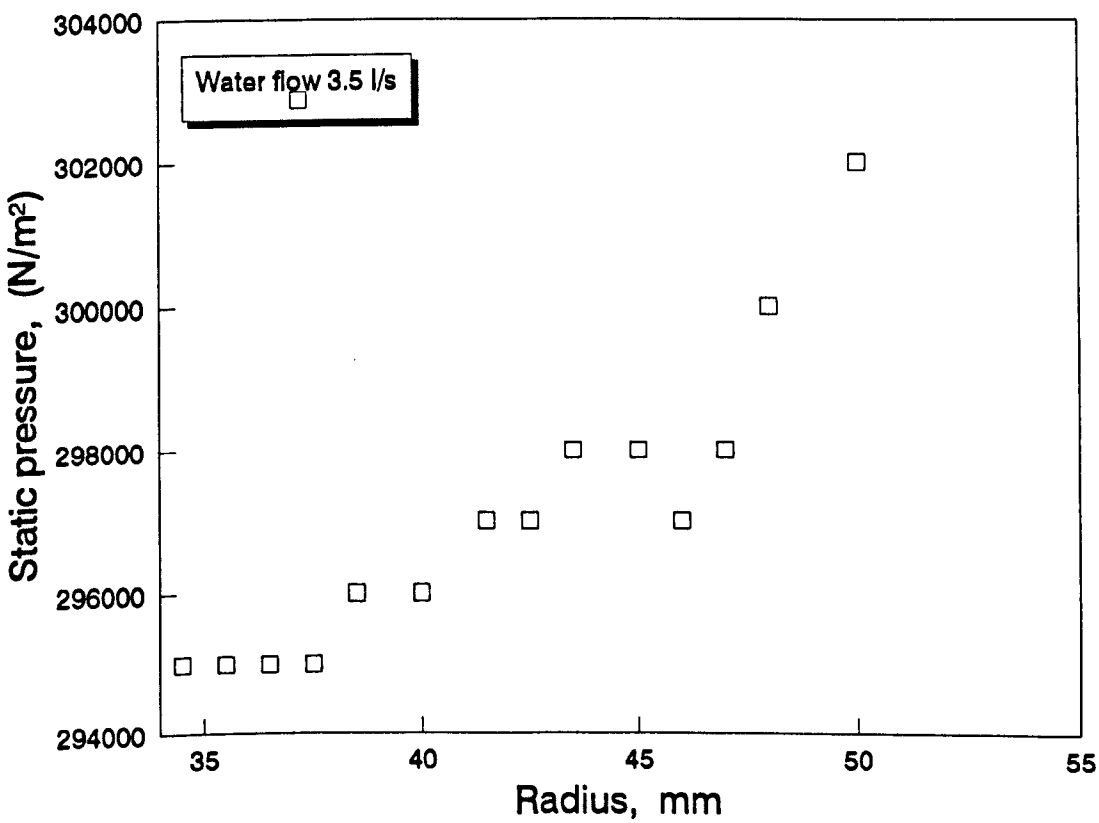

Figure 3.8 Single-phase radial pressure traverse

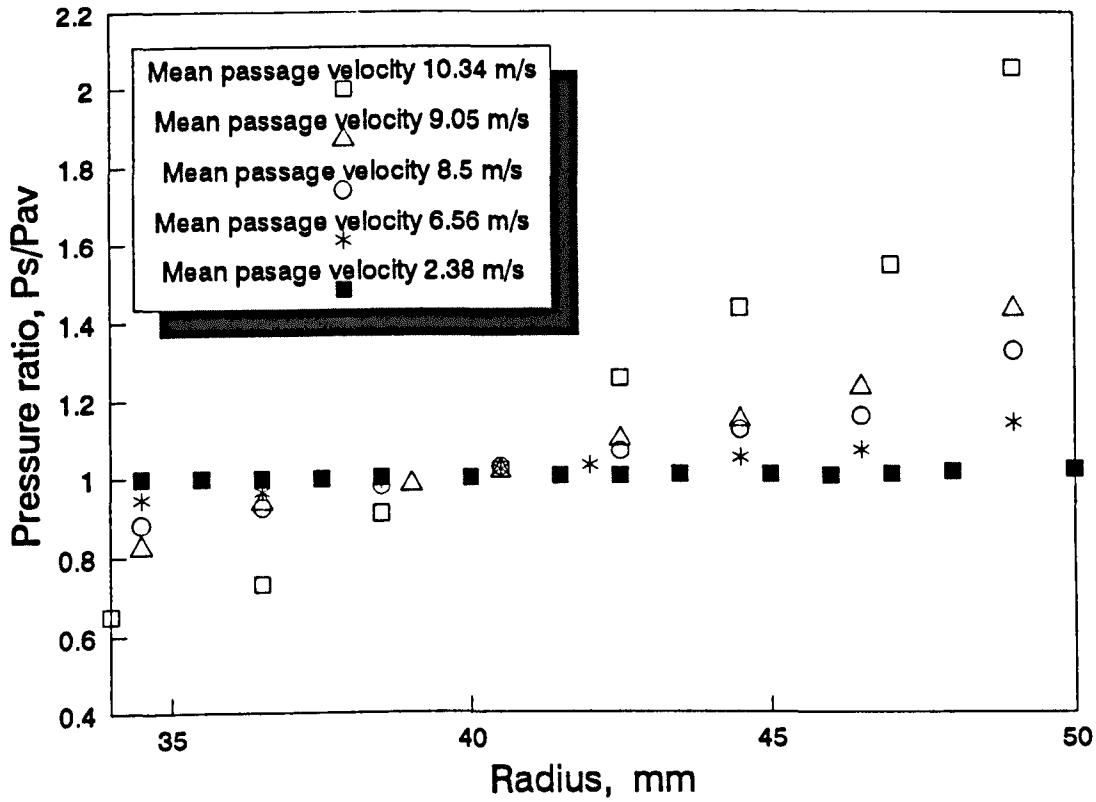

Figure 3.9 Normalised static pressure traverse

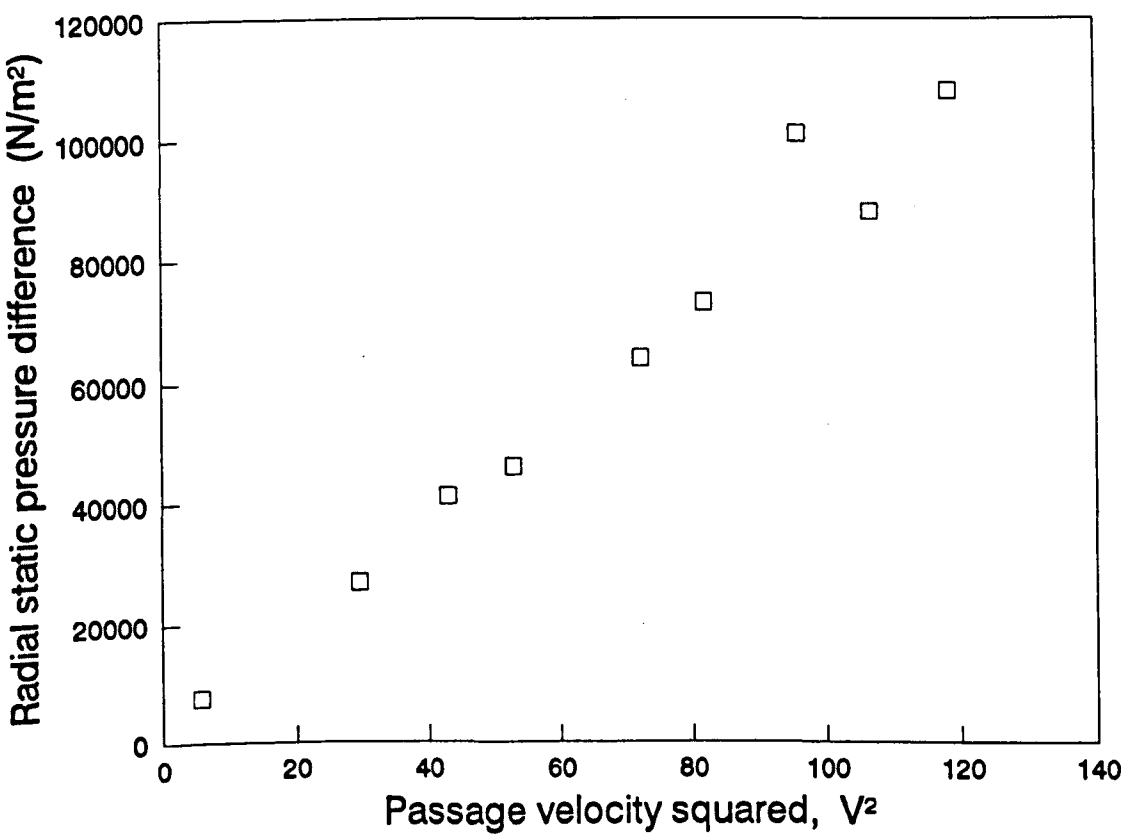

Figure 3.10 Root/wall static pressure difference

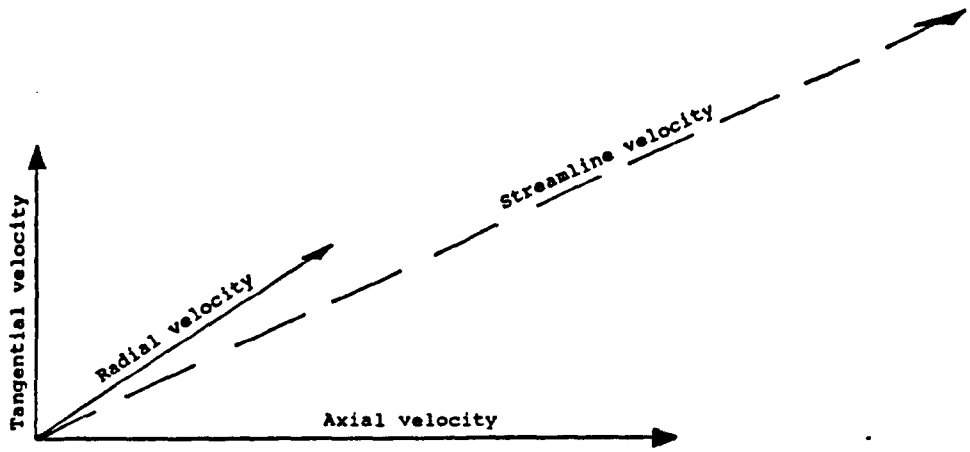

Figure 3.11 Streamline velocity definition

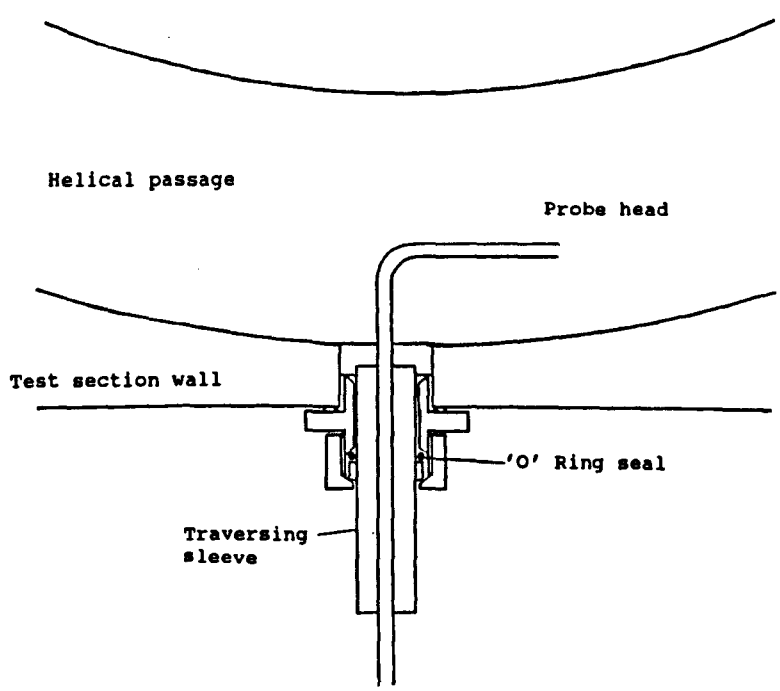

Figure 3.12 Total pressure probe

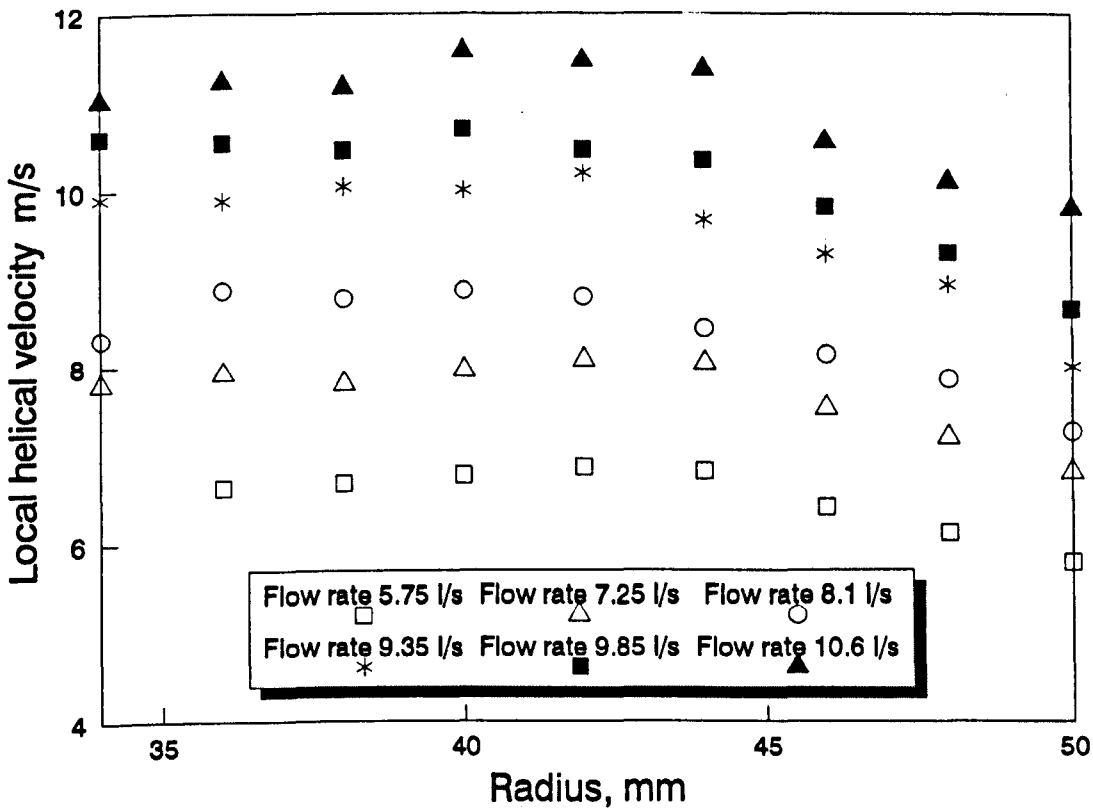

Figure 3.13 Local streamwise velocity

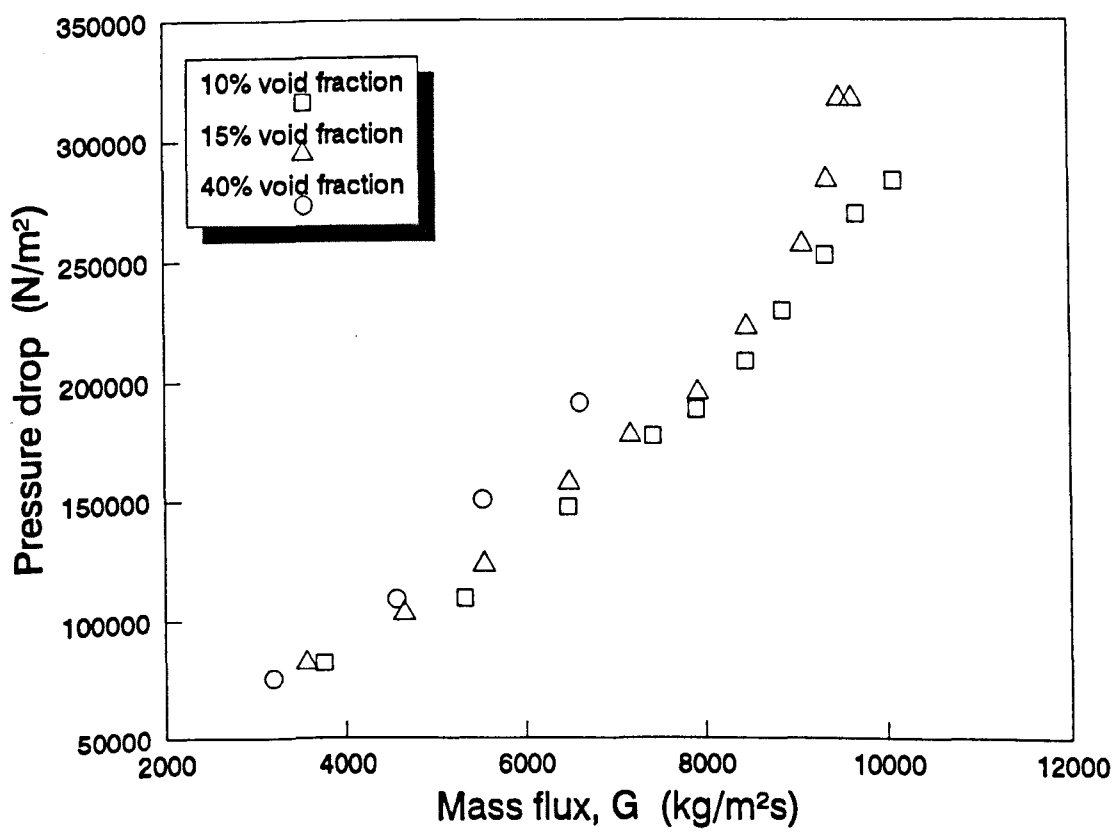

Figure 3.14 Air/water pressure drop

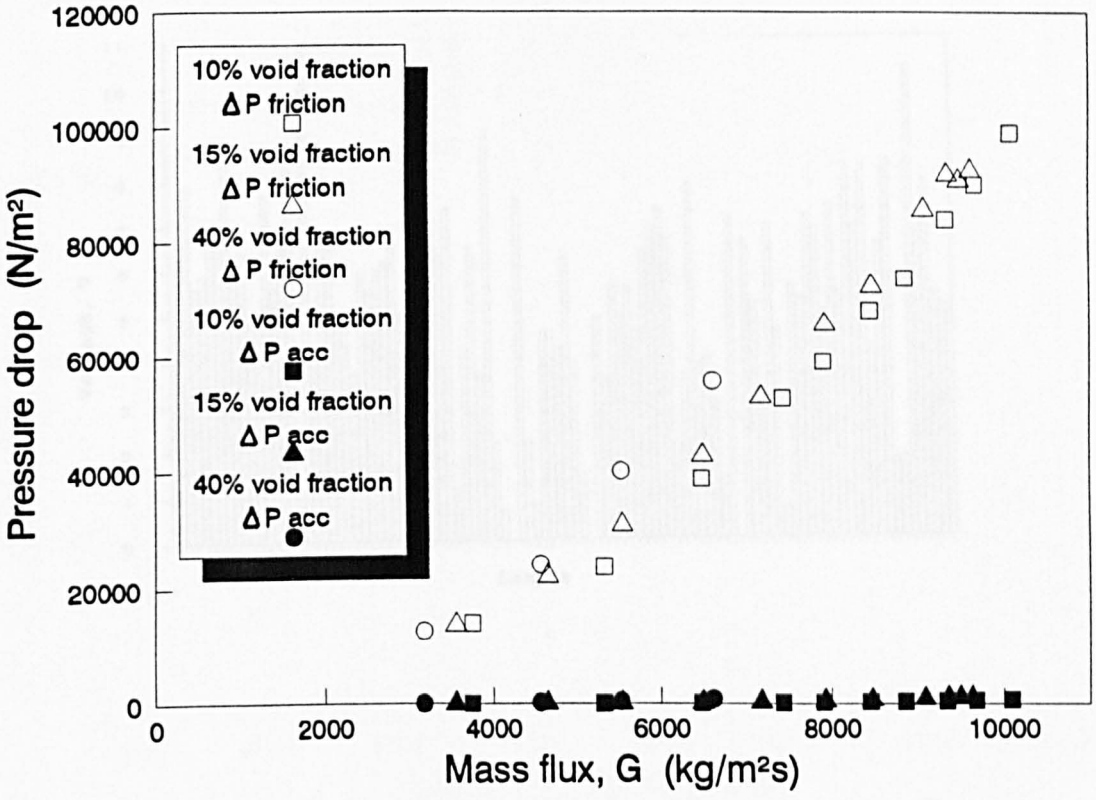

Figure 3.15 Air/water friction pressure drop

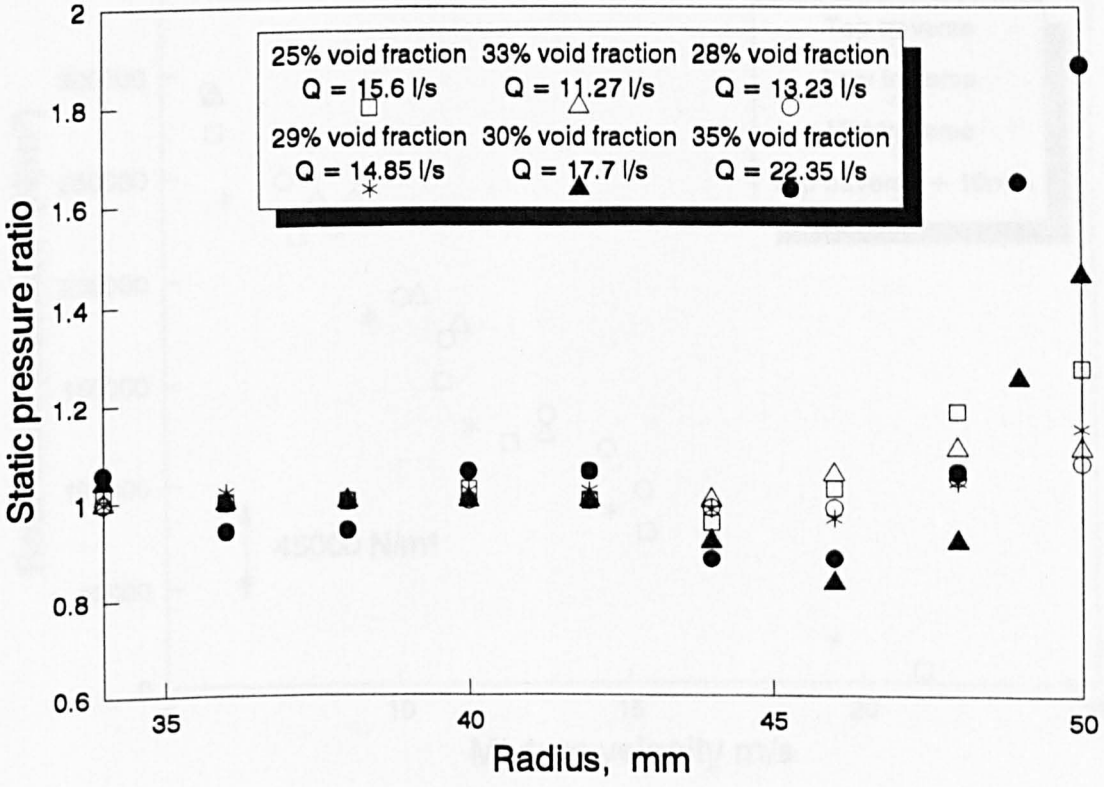

Figure 3.16 Two-phase static pressure traverse

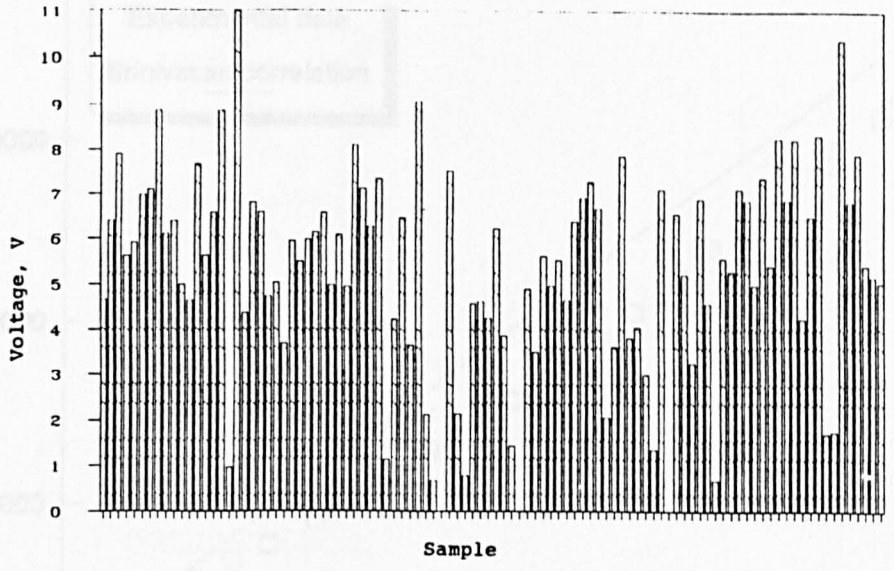

Figure 3.17 Pitot response in two-phase flow

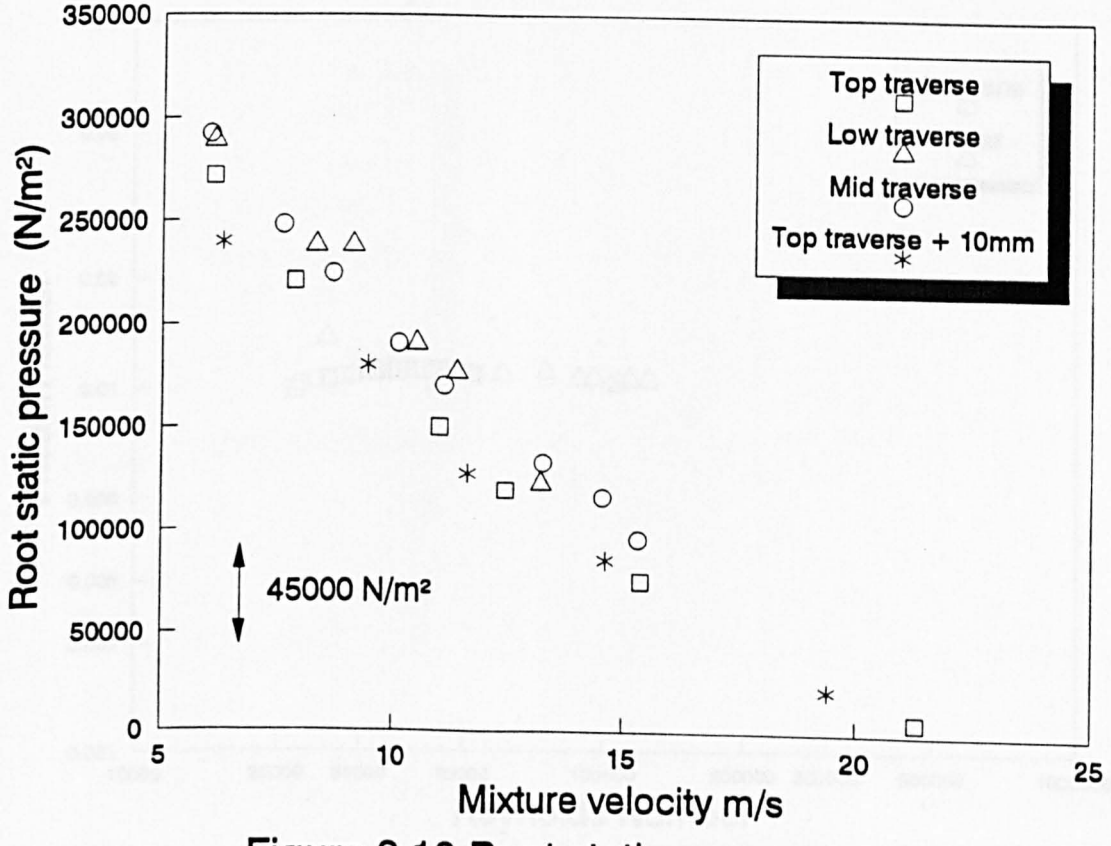

Figure 3.18 Root static pressure survey

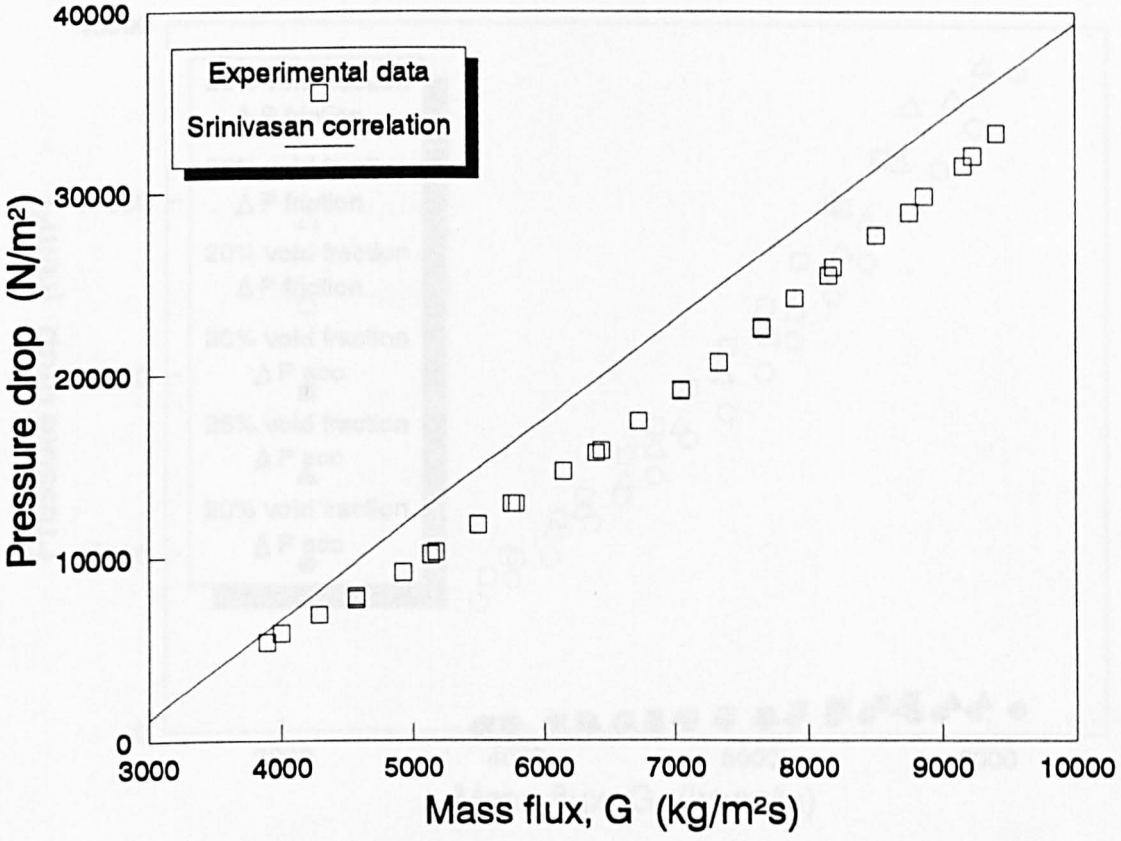

Figure 3.19 Single-phase kerosene friction pressure drop

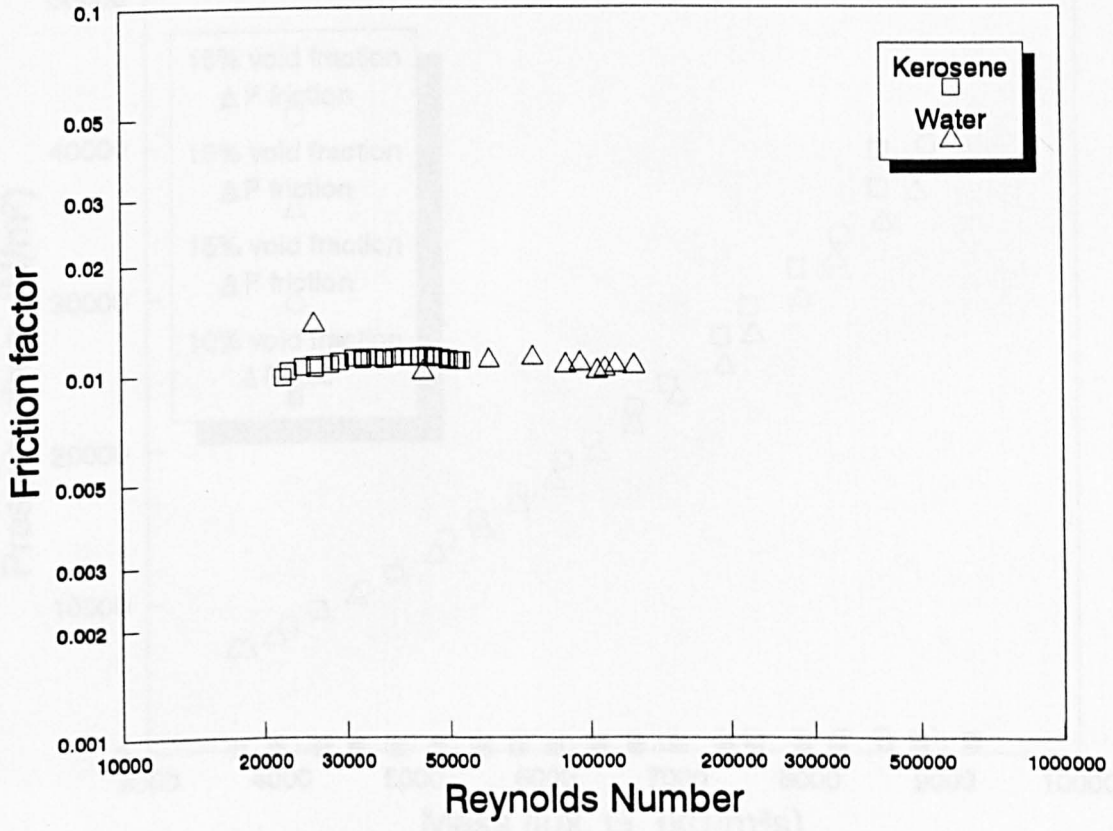

Figure 3.20 Single-phase friction factors

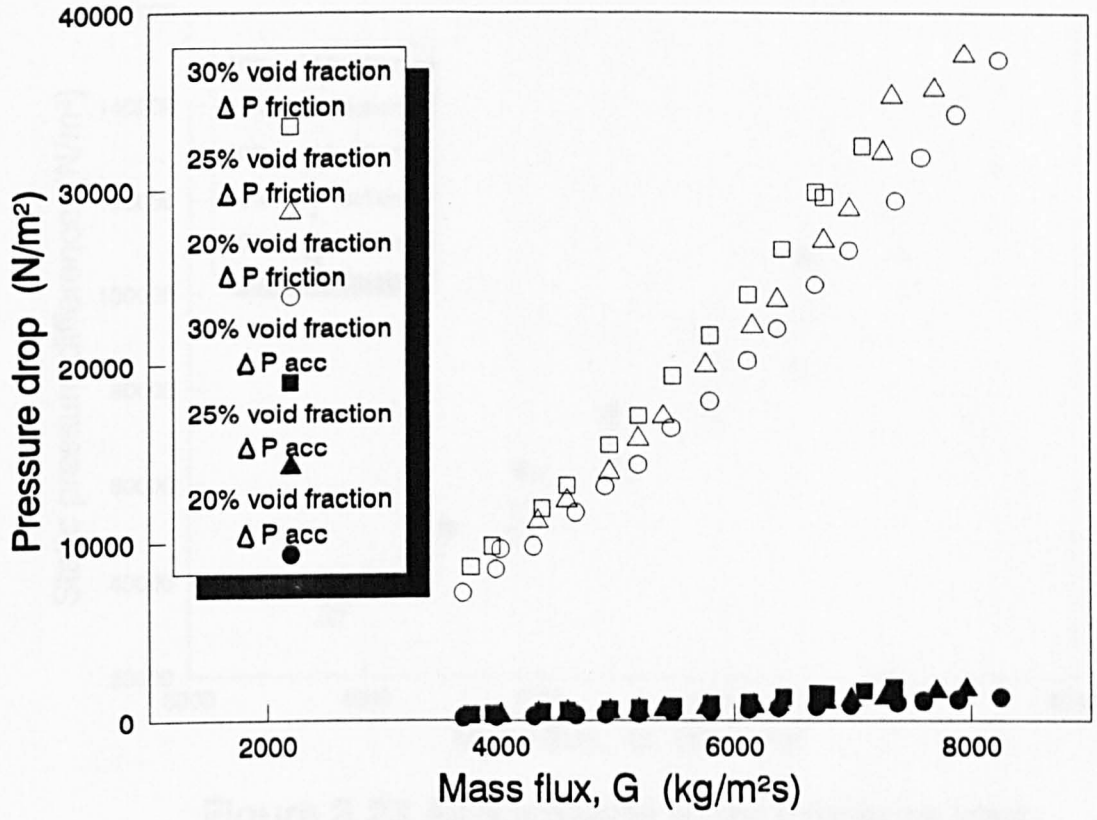

Figure 3.21 Air/kerosene friction pressure drop

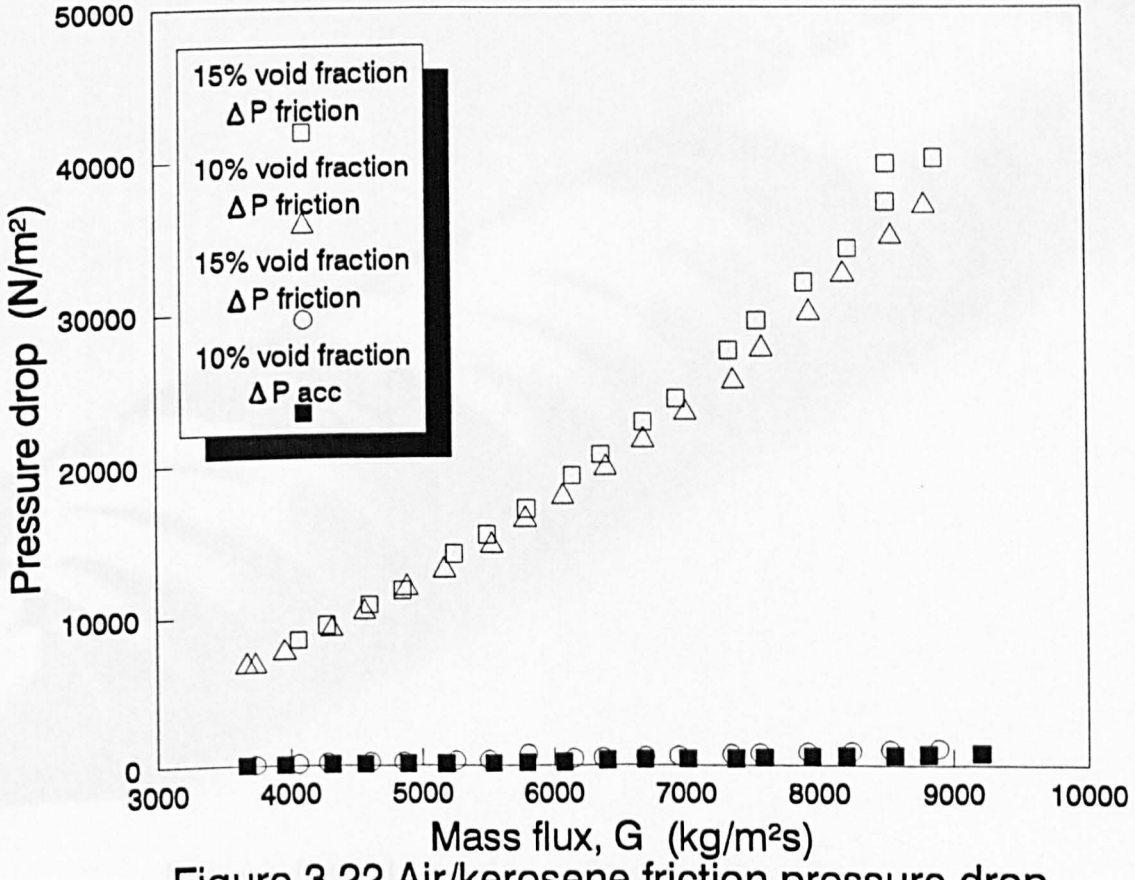

Figure 3.22 Air/kerosene friction pressure drop

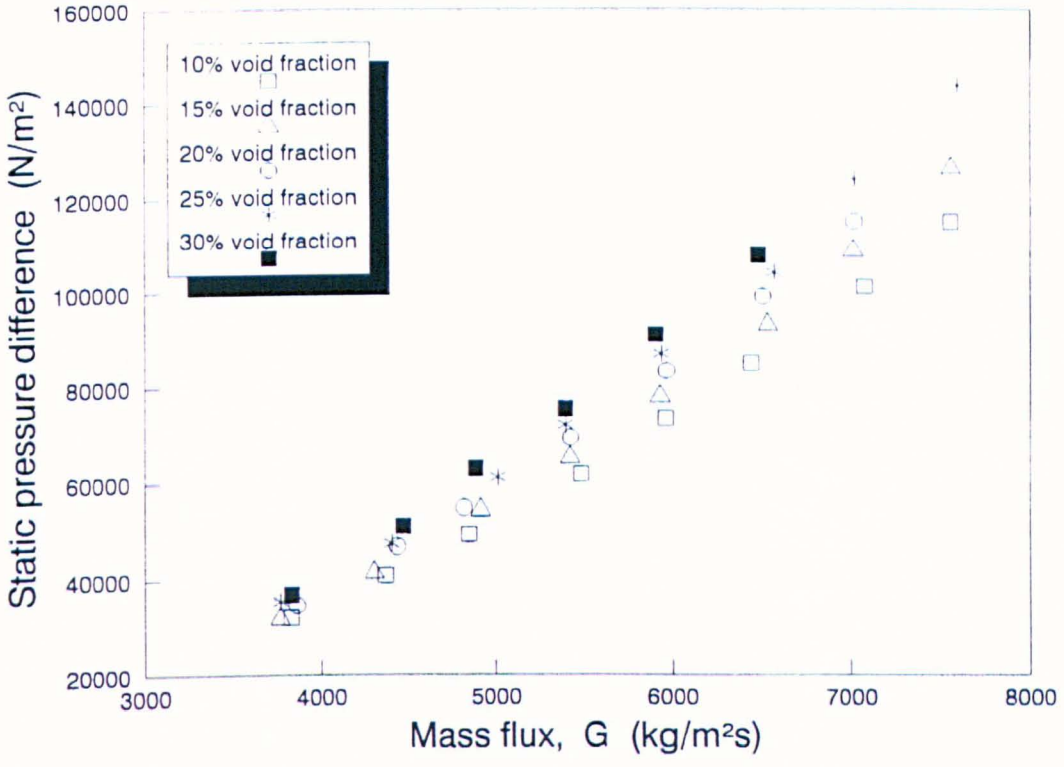

Figure 3.23 Air/kerosene entry pressure loss

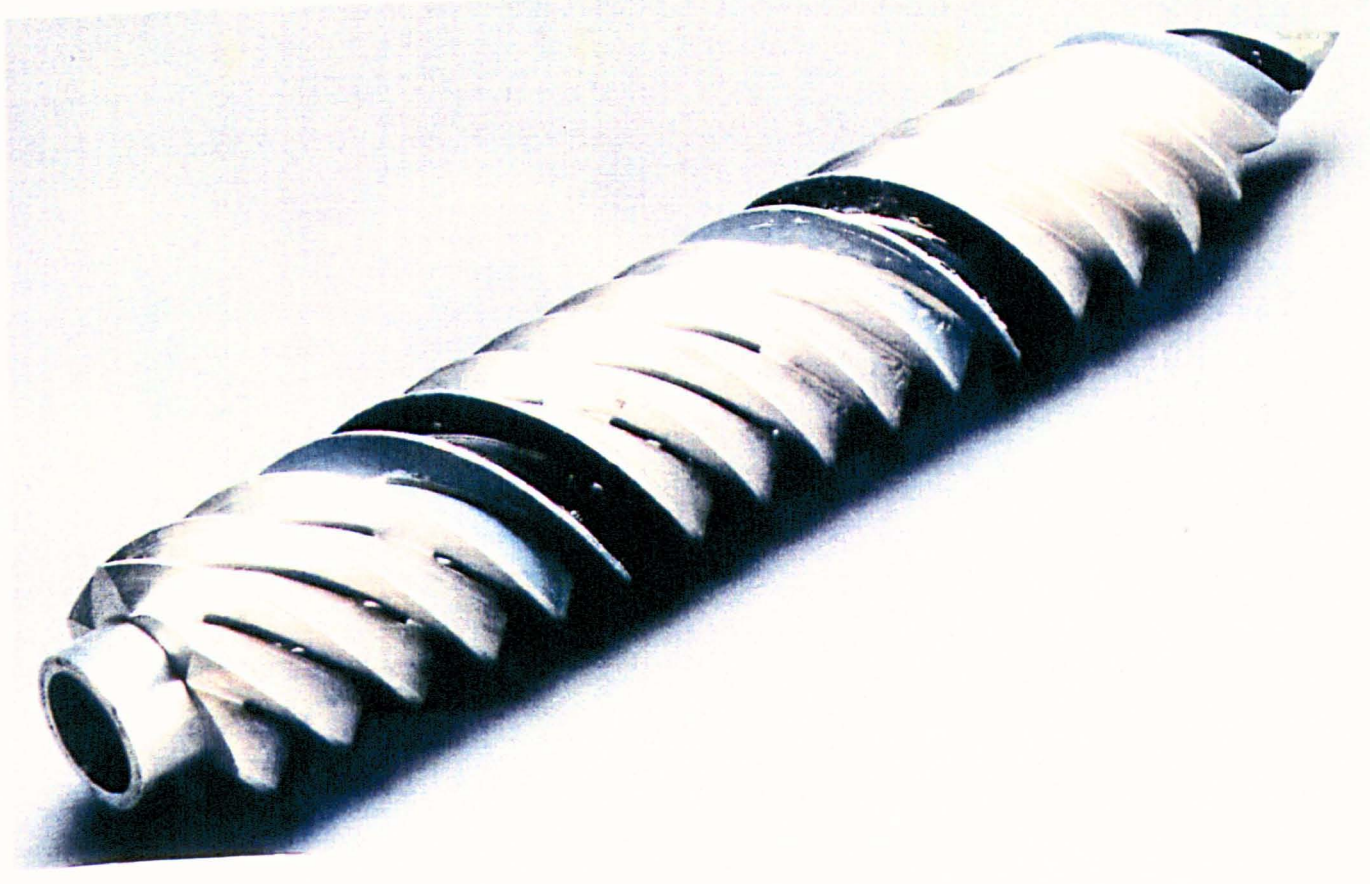

Figure 3.24 Location of take-off slots

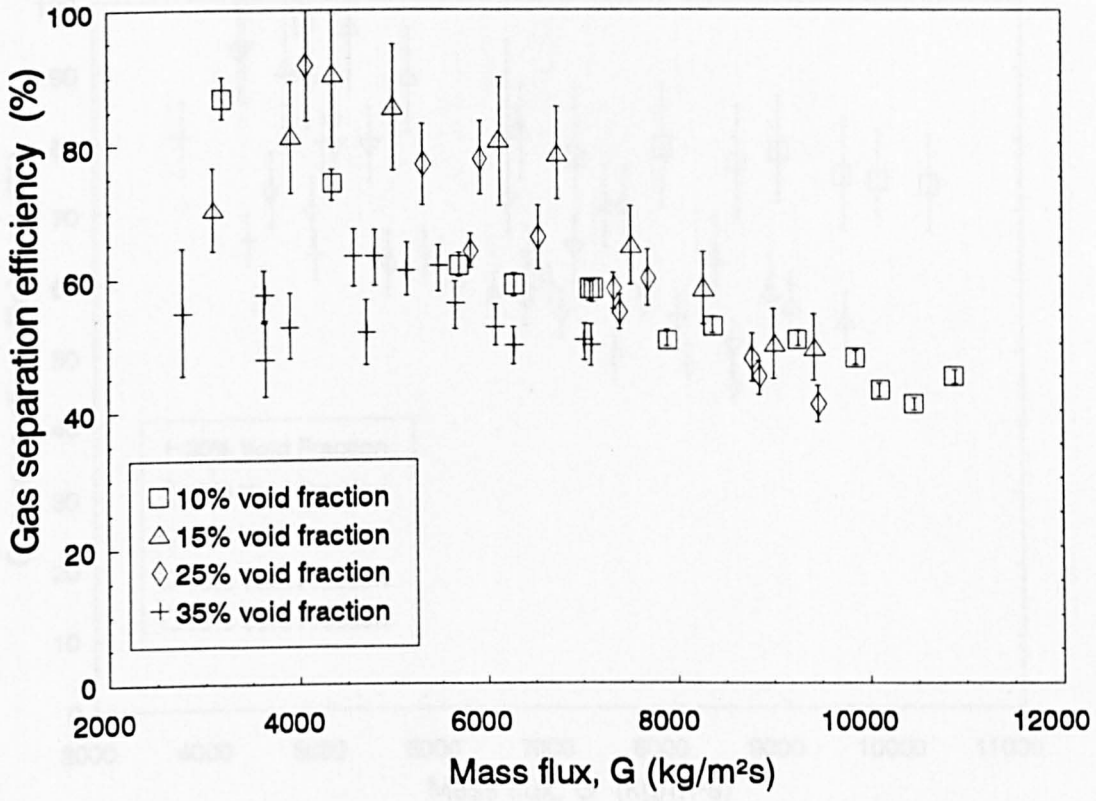

Figure 3.25 Air/water gas separation - configuration a

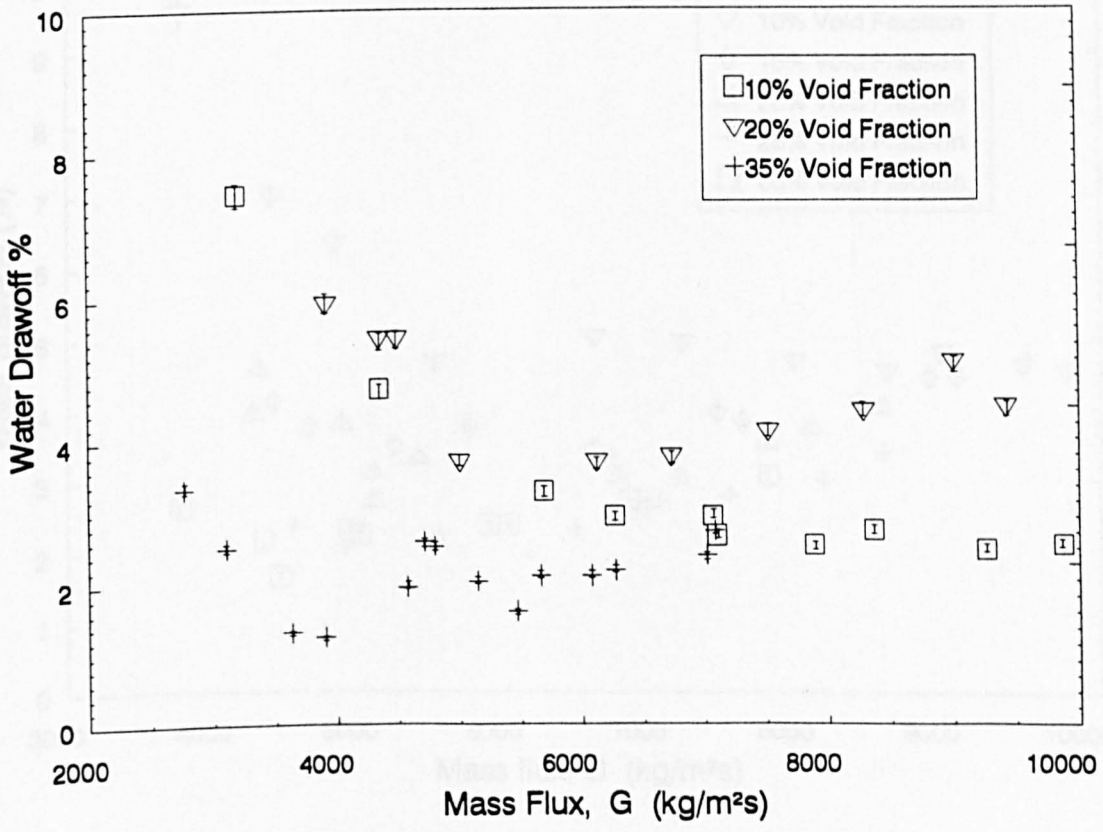

Figure 3.26 Water Draw-off - Configuration a

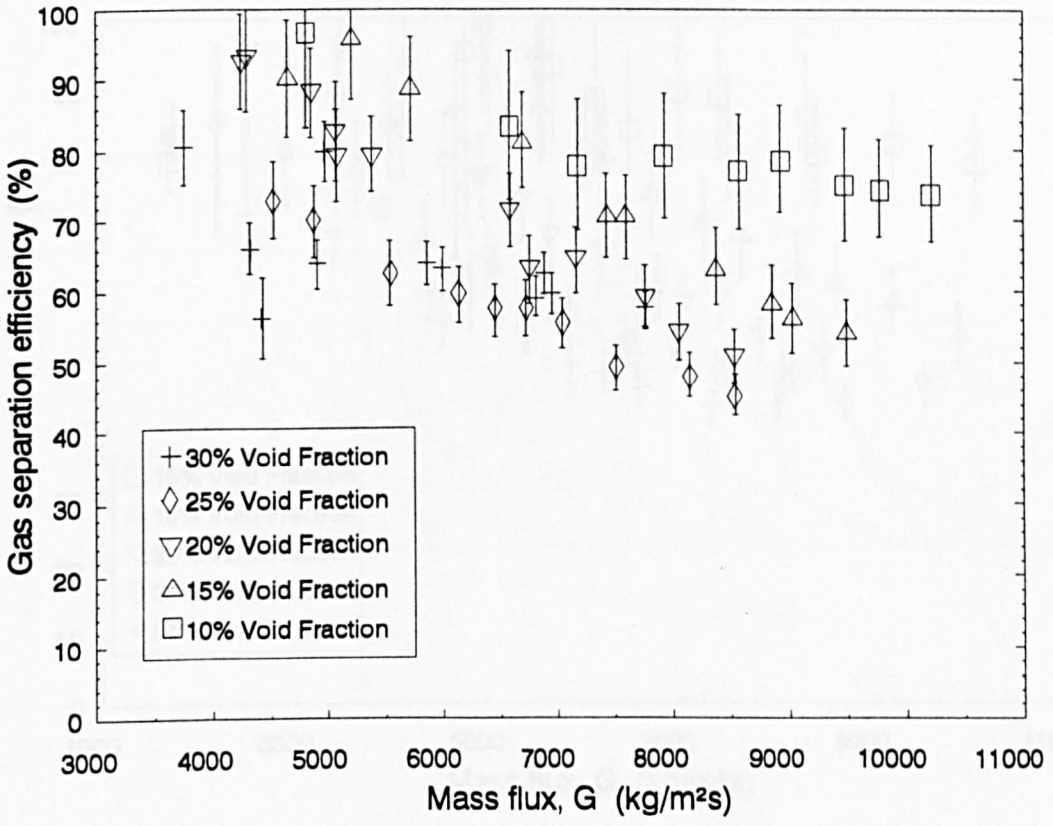

Figure 3.27 Air/water gas separation - configuration b

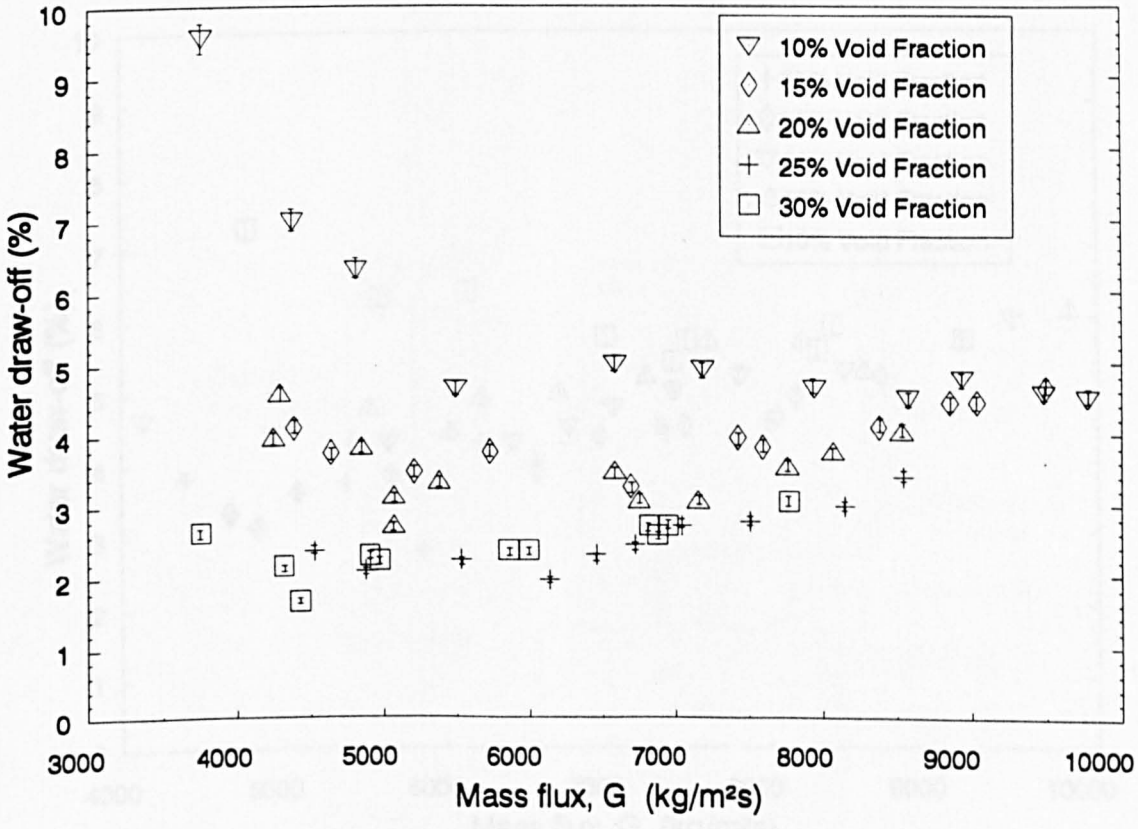

Figure 3.28 Water draw-off - configuration b

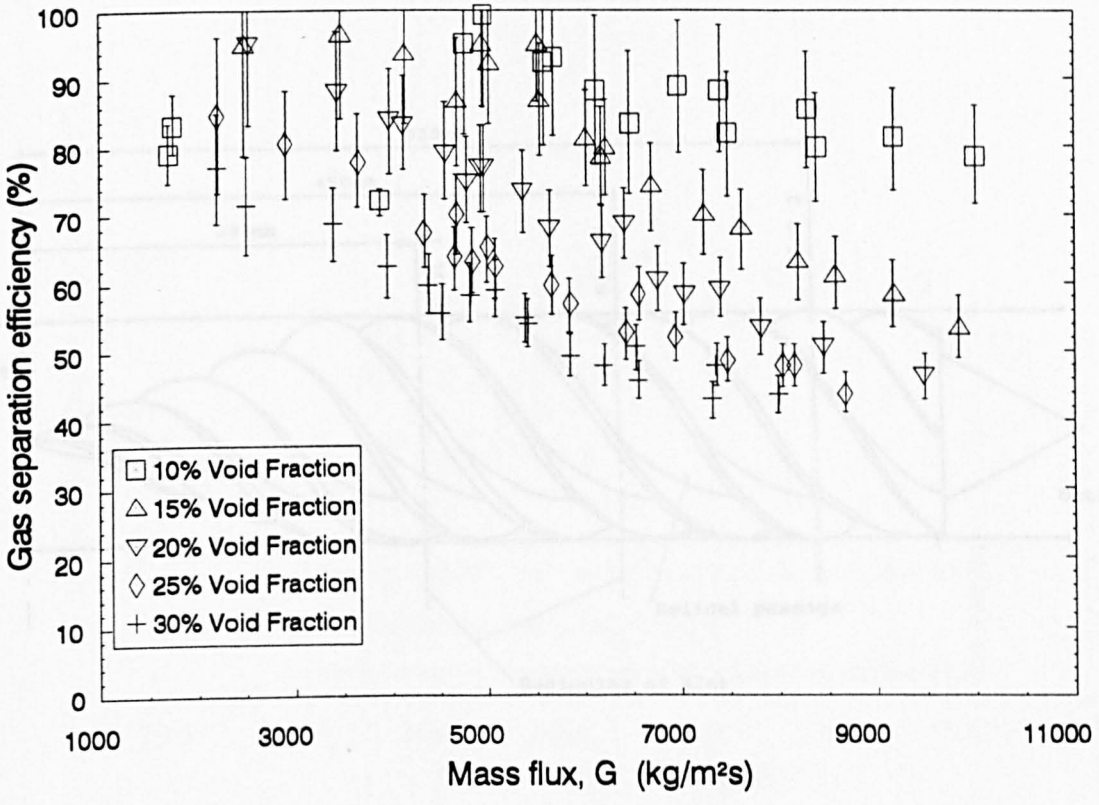

Figure 3.29 Air/water gas separation - configuration c

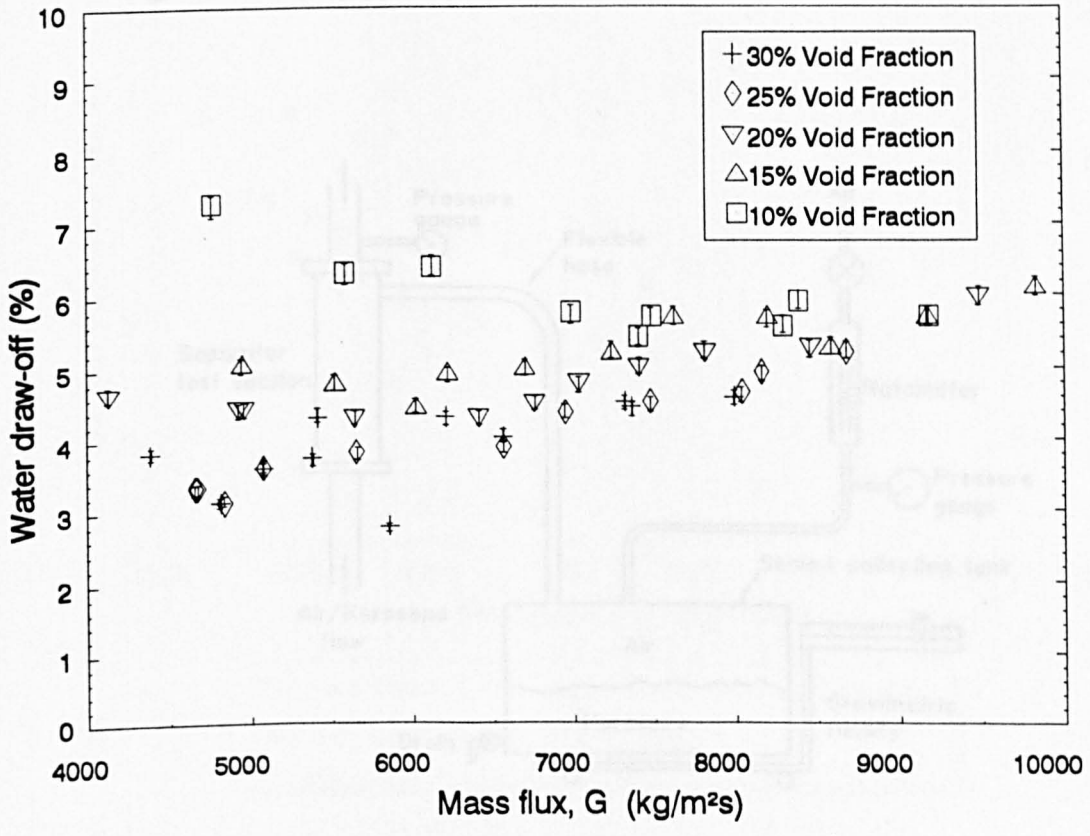

Figure 3.30 Water draw-off - configuration c

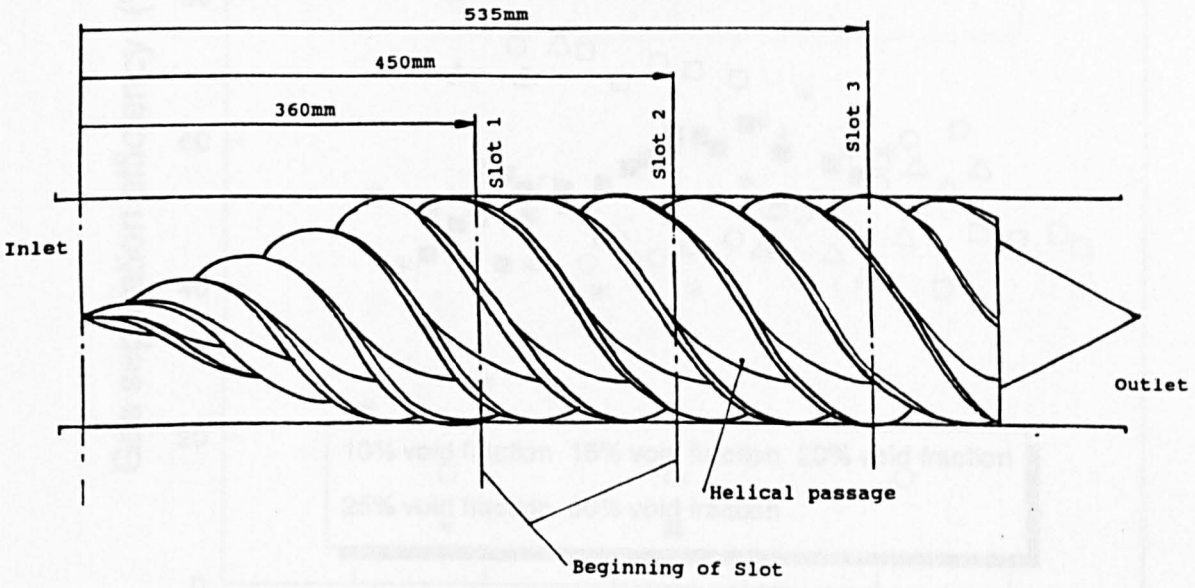

Figure 3.31 Axial location of take-off slots

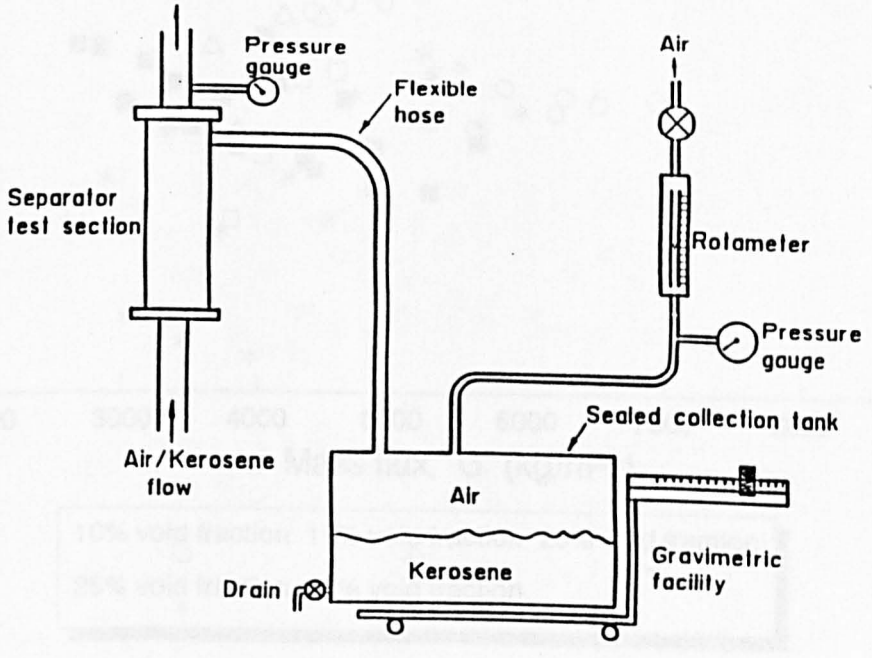

Figure 3.32 Collection and measurement of separated air and kerosene

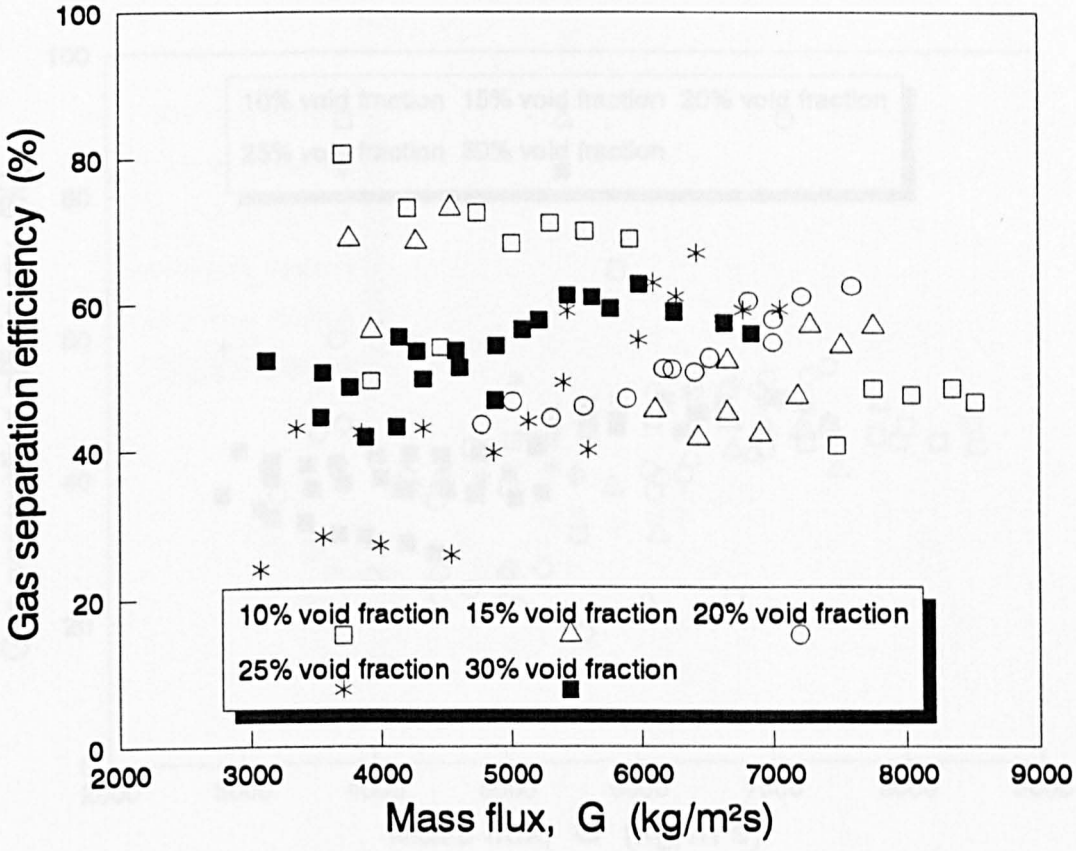

Figure 3.33 Air/kerosene gas separation - slot 1

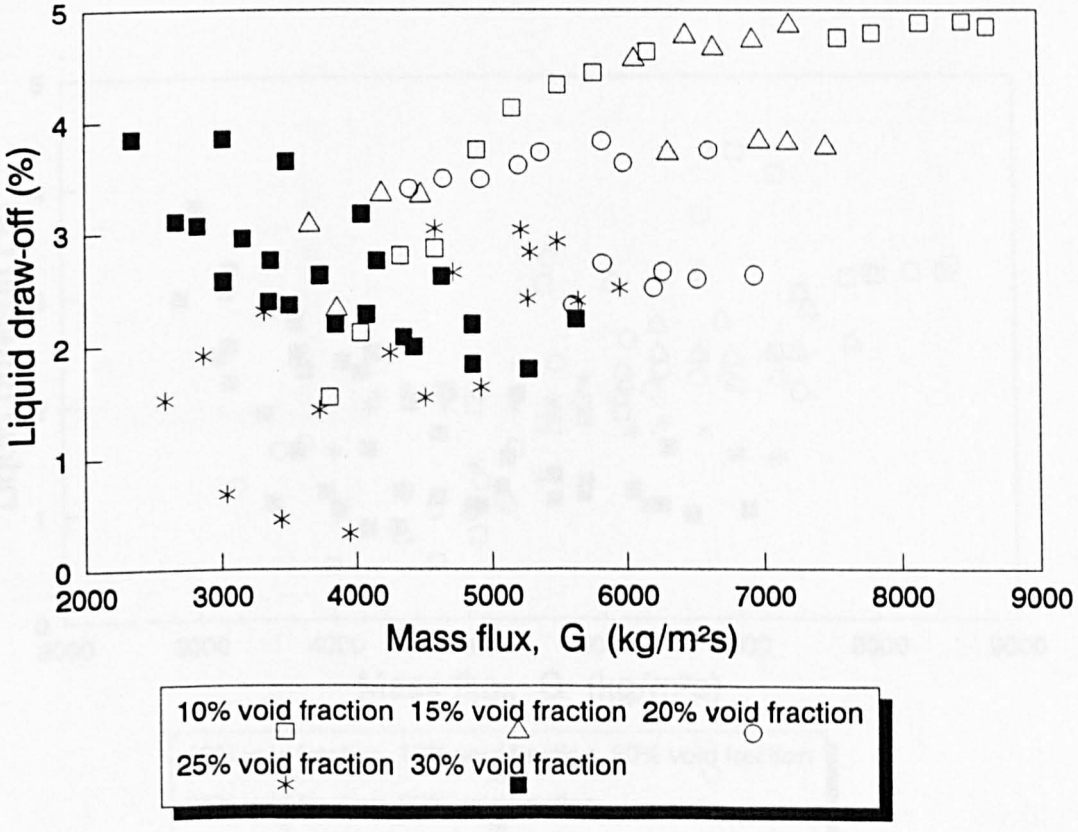

Figure 3.34 Kerosene draw-off - slot 1

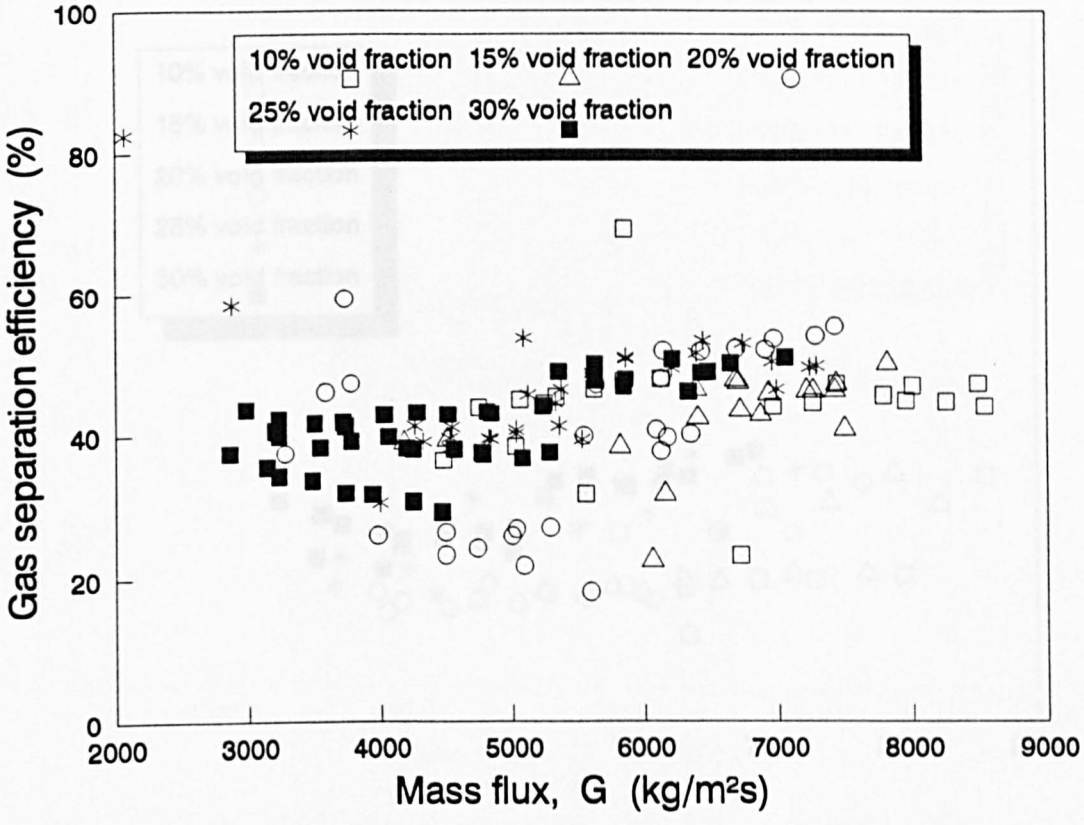

Figure 3.35 Air/kerosene gas separation - slot 2

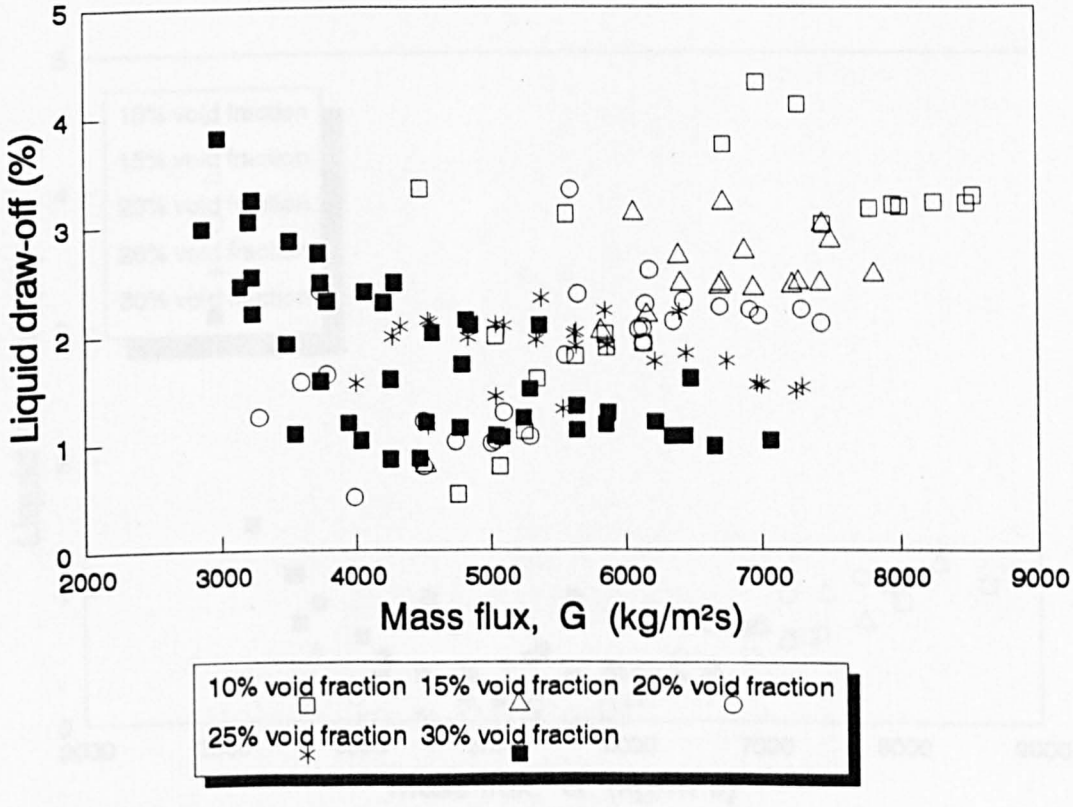

Figure 3.36 Kerosene draw-off - slot 2

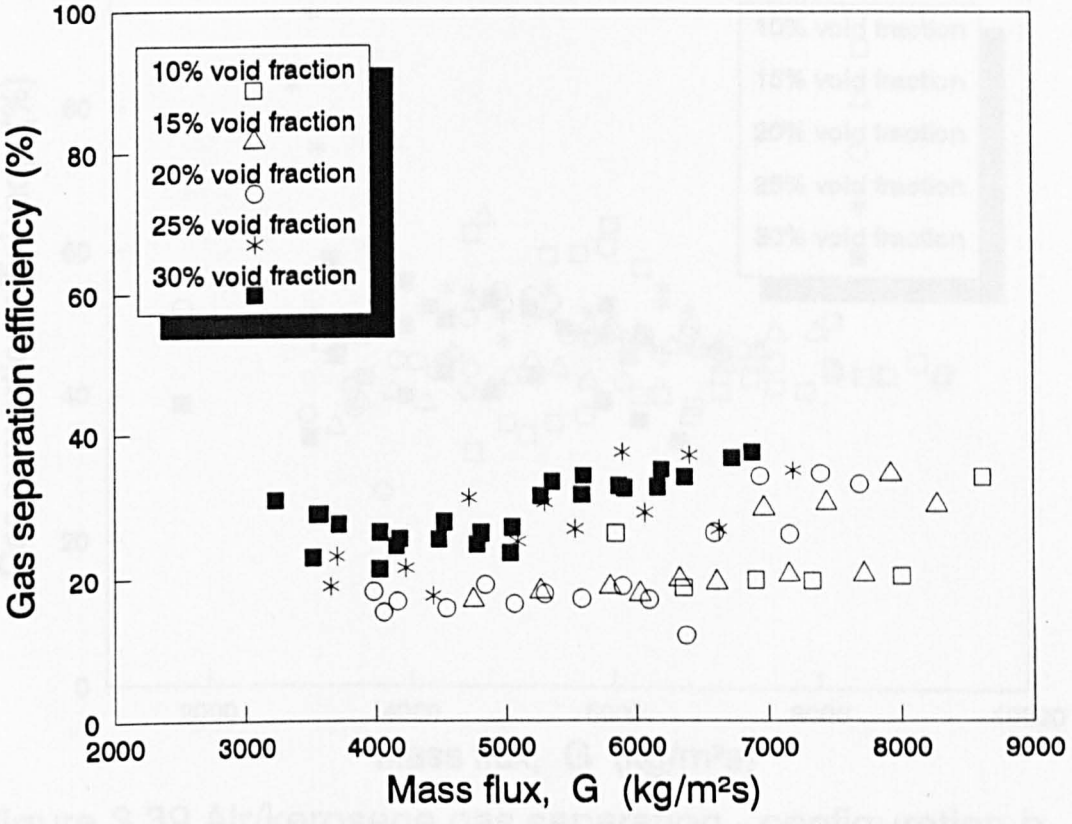

Figure 3.37 Air/kerosene gas separation - slot 3

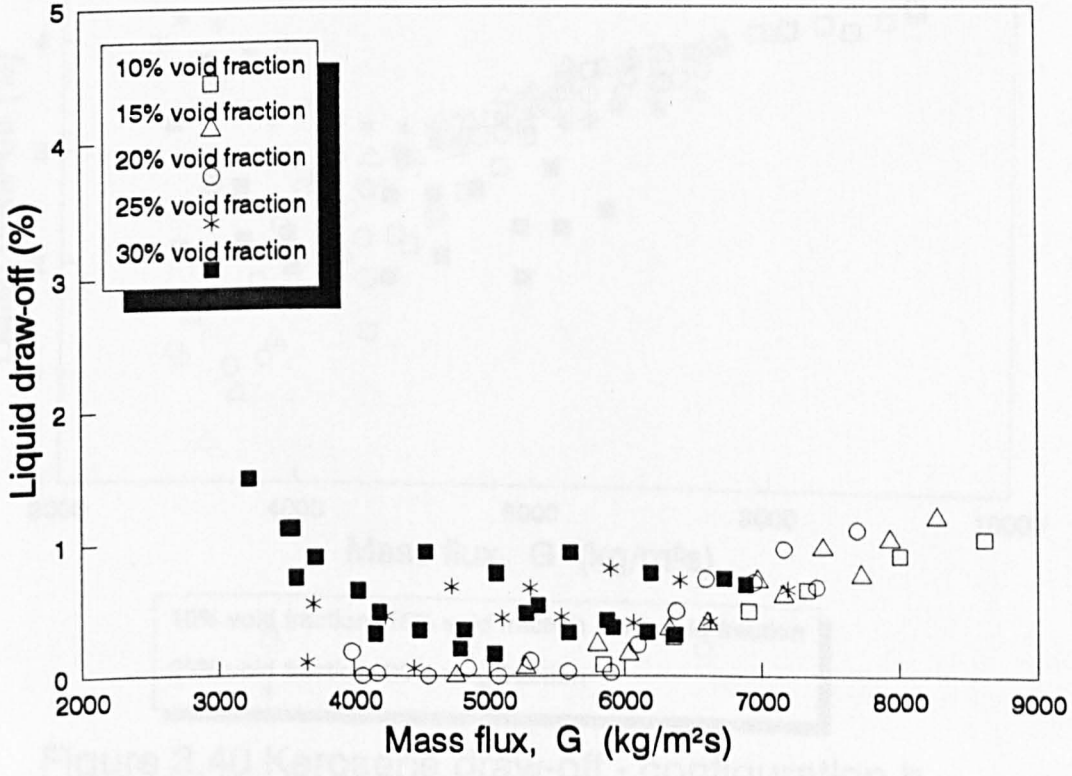

Figure 3.38 Kerosene draw-off - slot 3

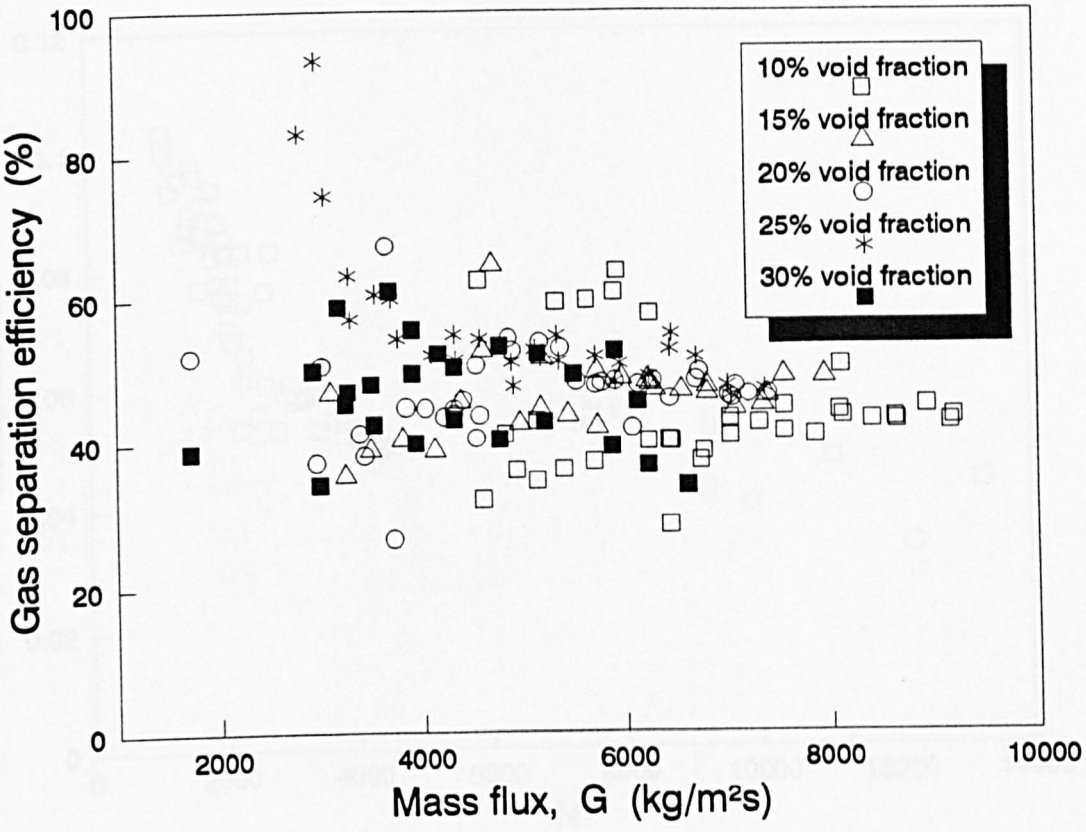

Figure 3.39 Air/kerosene gas separation - configuration b

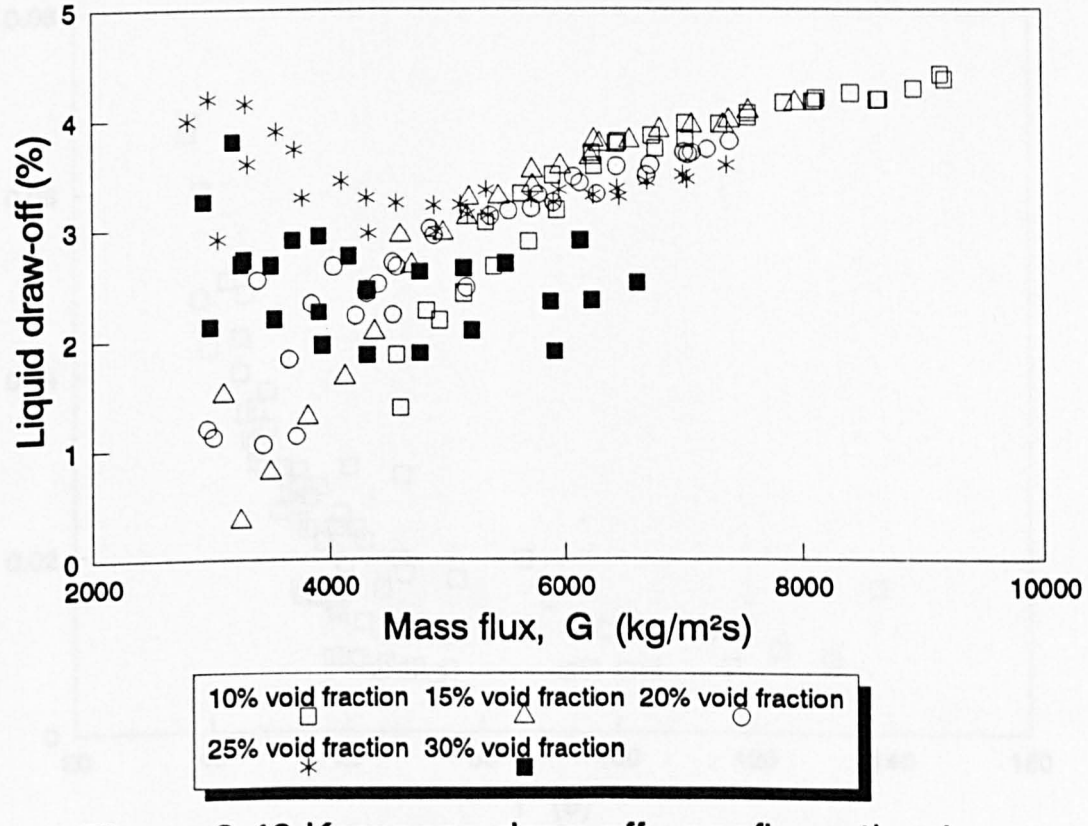

Figure 3.40 Kerosene draw-off - configuration b

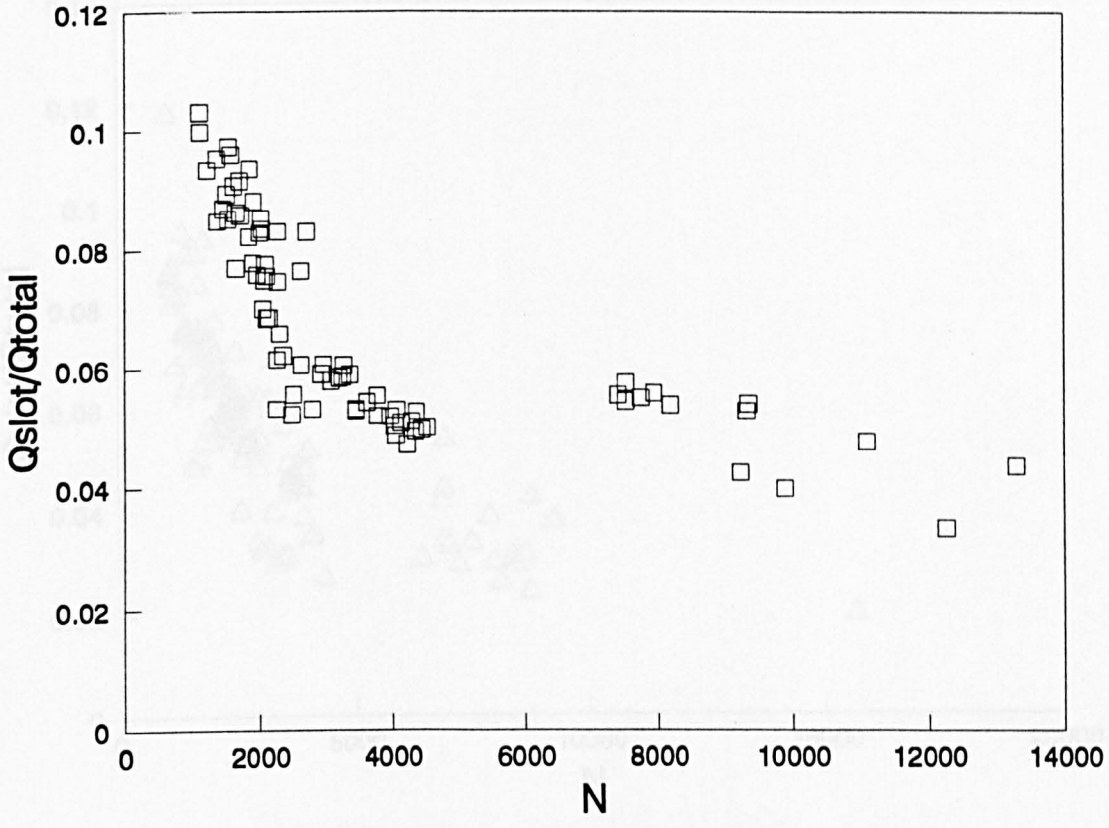

Figure 3.41 Take-off flow ratio - slot 1

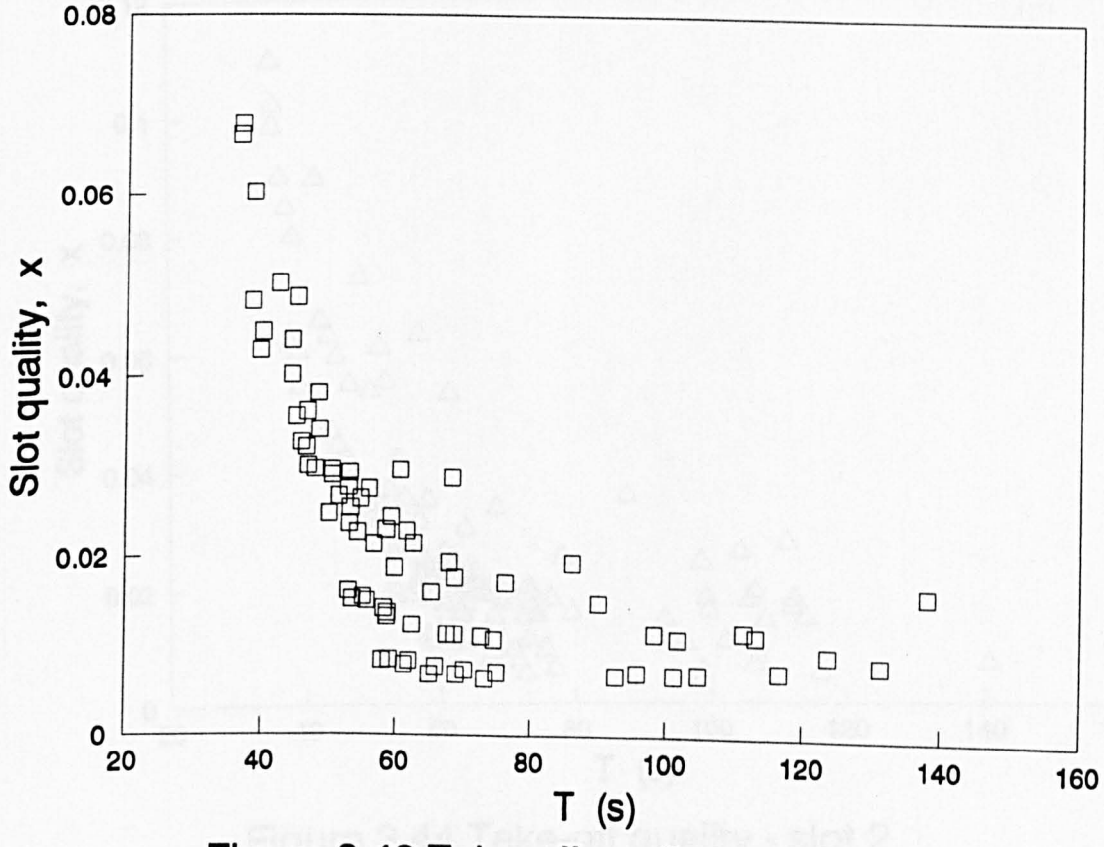

Figure 3.42 Take-off quality - slot 1

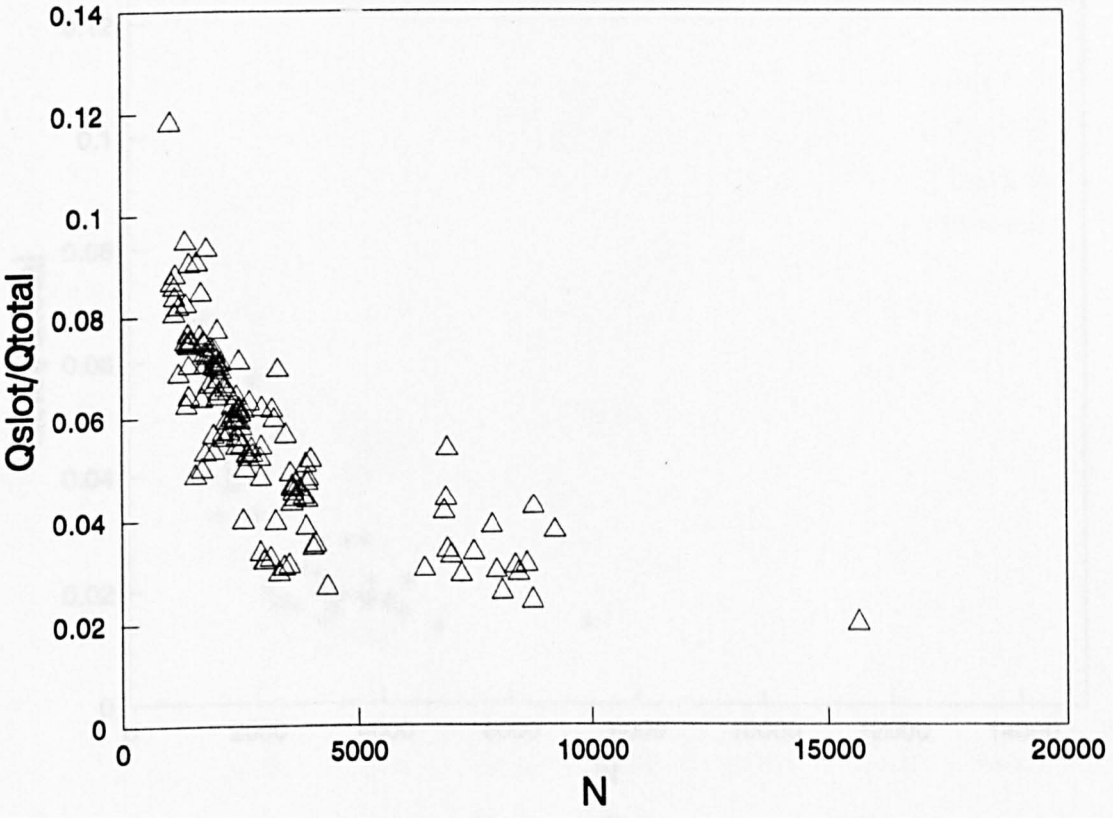

Figure 3.43 Take-off flow ratio - slot 2

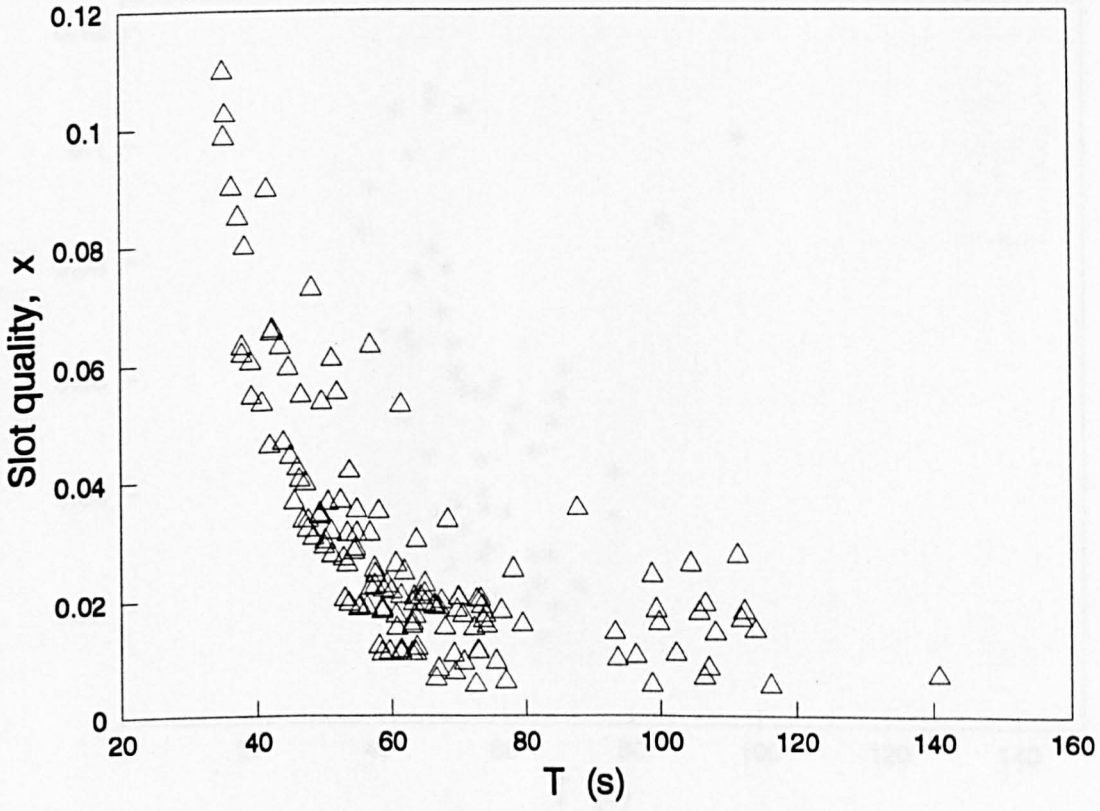

Figure 3.44 Take-off quality - slot 2

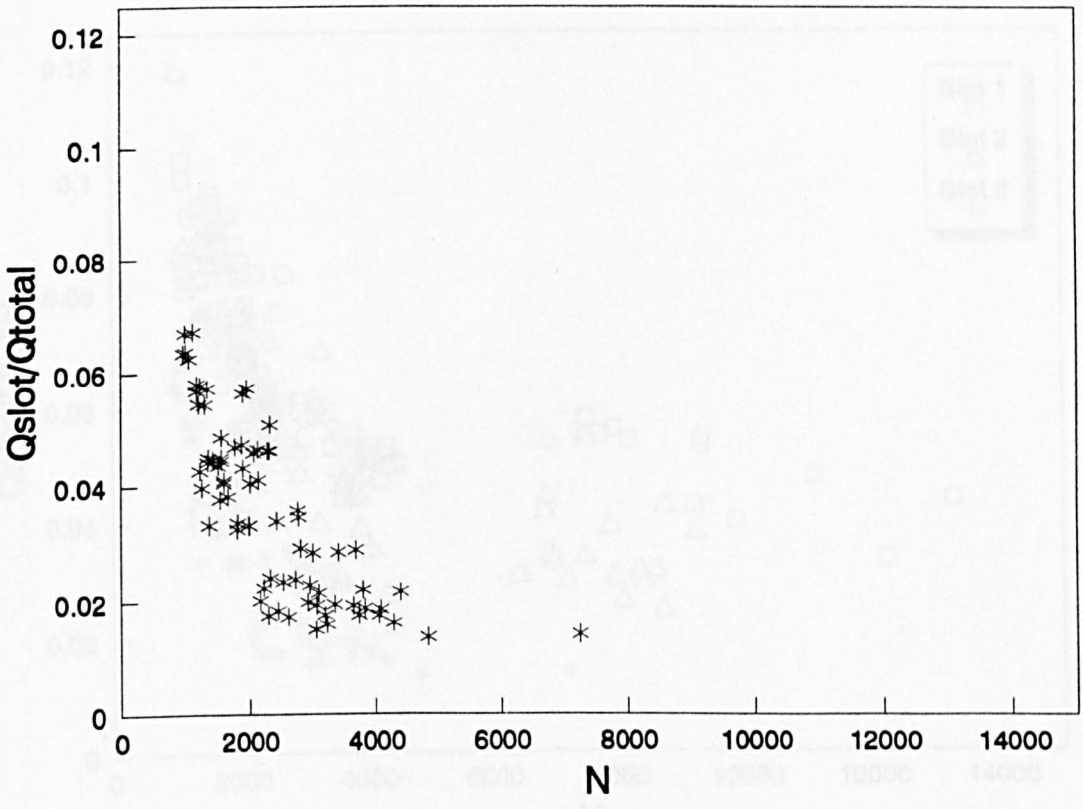

Figure 3.45 Take-off flow ratio - slot 3

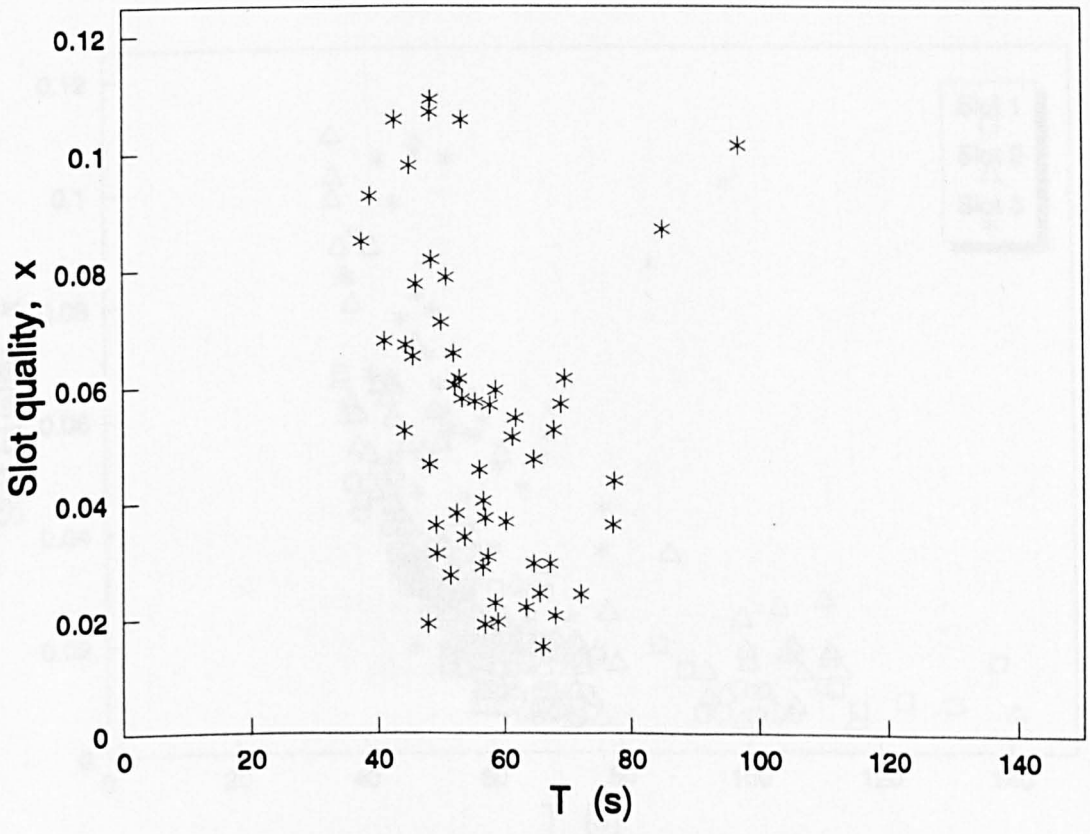

Figure 3.46 Take-off quality - slot 3

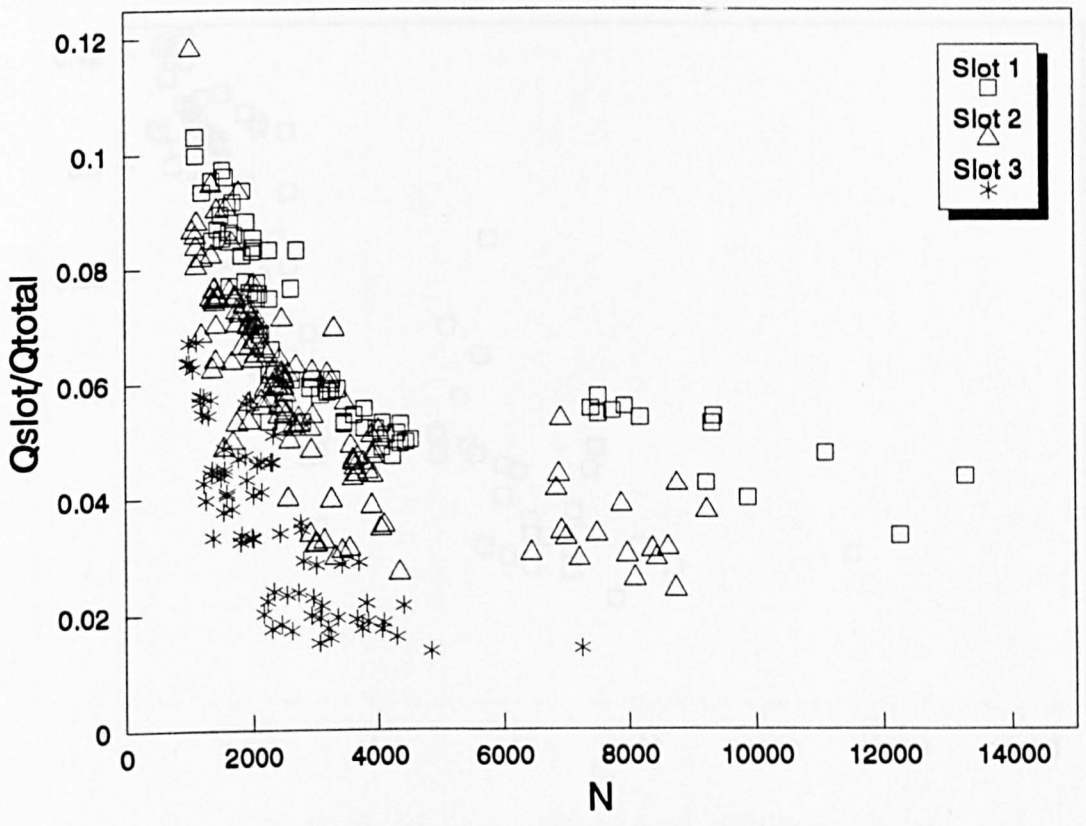

Figure 3.47 Comparison of slot take-off flow ratios

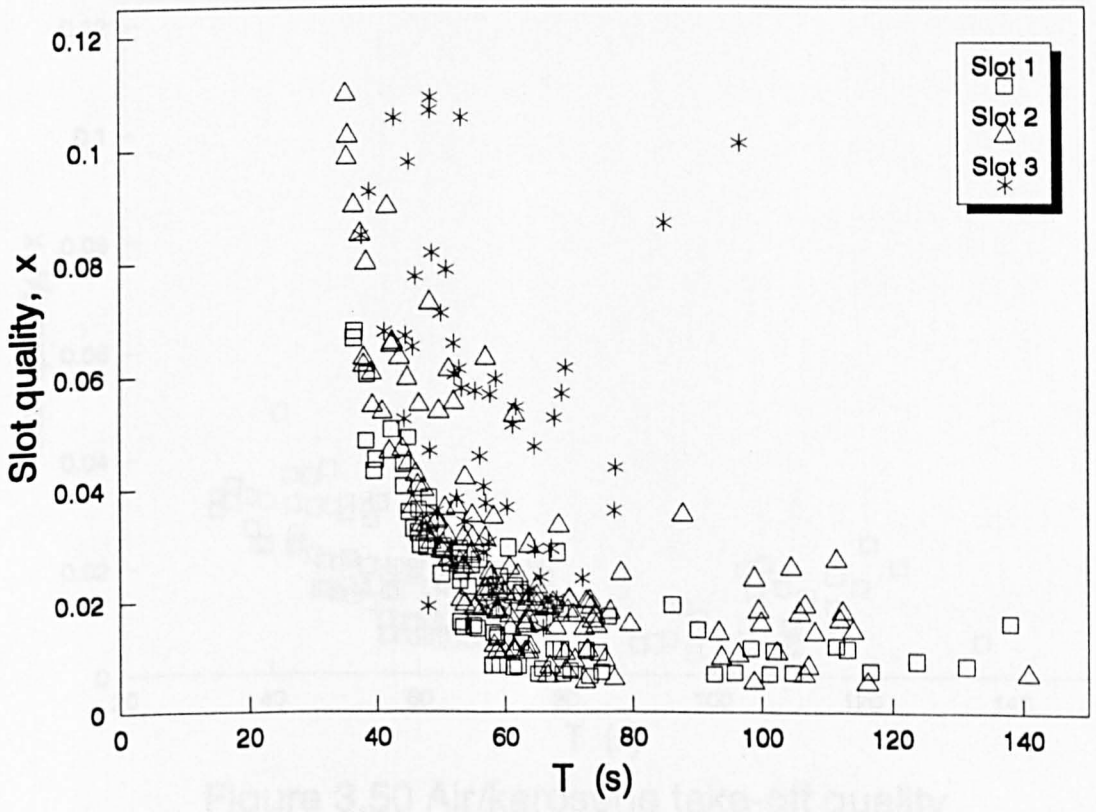

Figure 3.48 Comparison of slot take-off quality

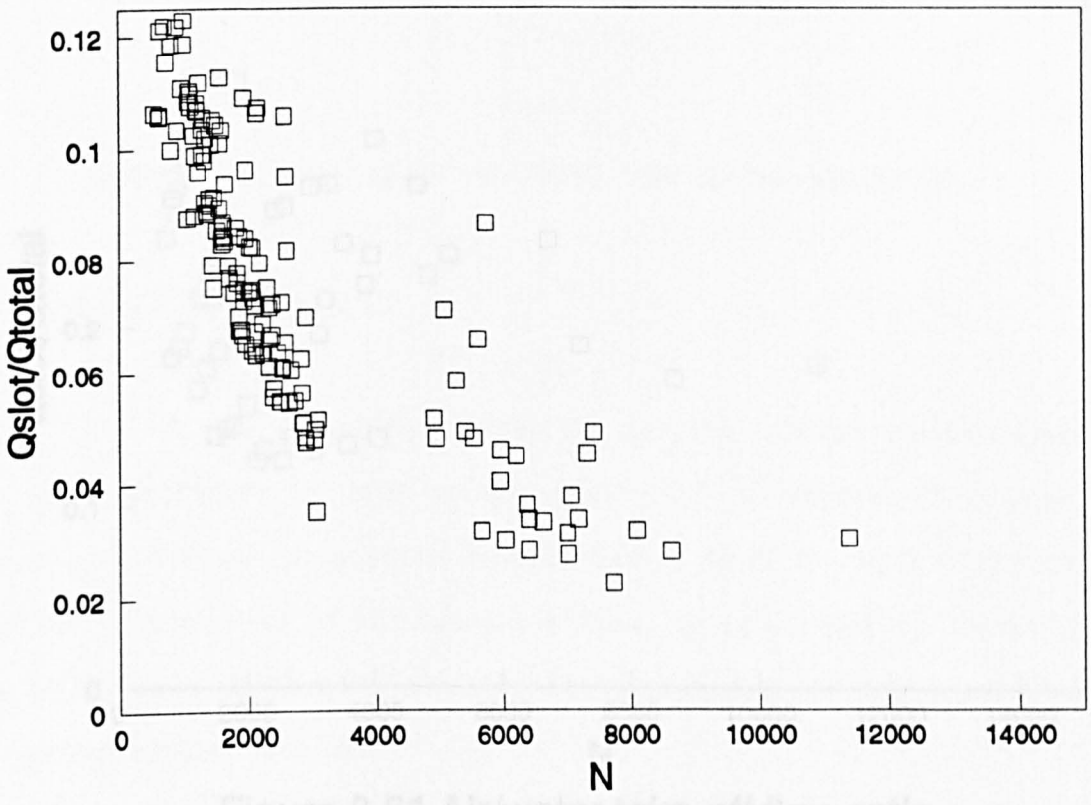

Figure 3.49 Air/kerosene take-off flow ratio
- configuration b

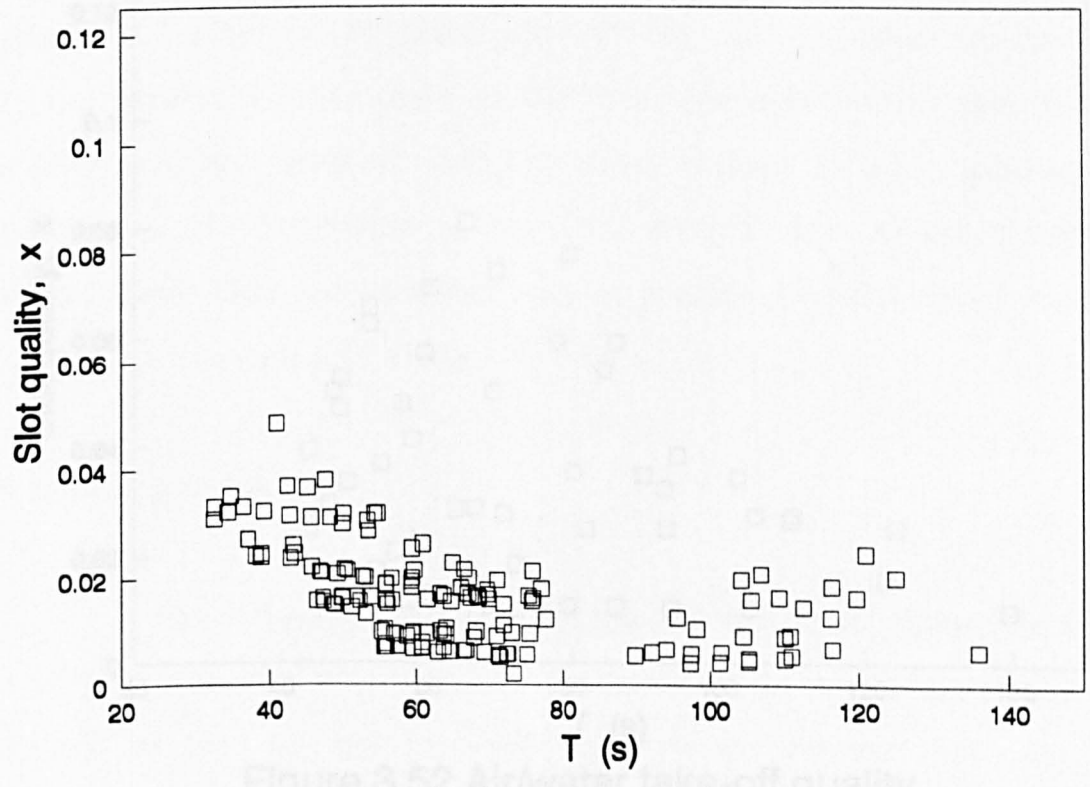

Figure 3.50 Air/kerosene take-off quality
- configuration b

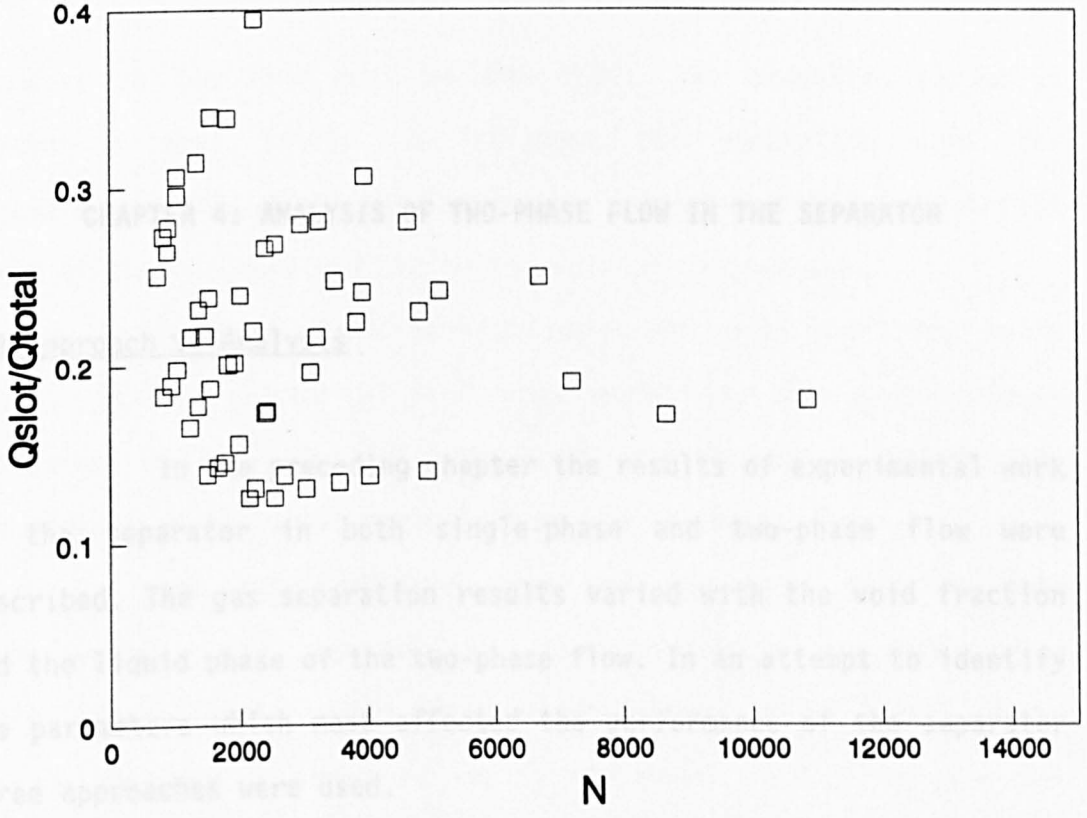

Figure 3.51 Air/water take-off flow ratio - configuration b

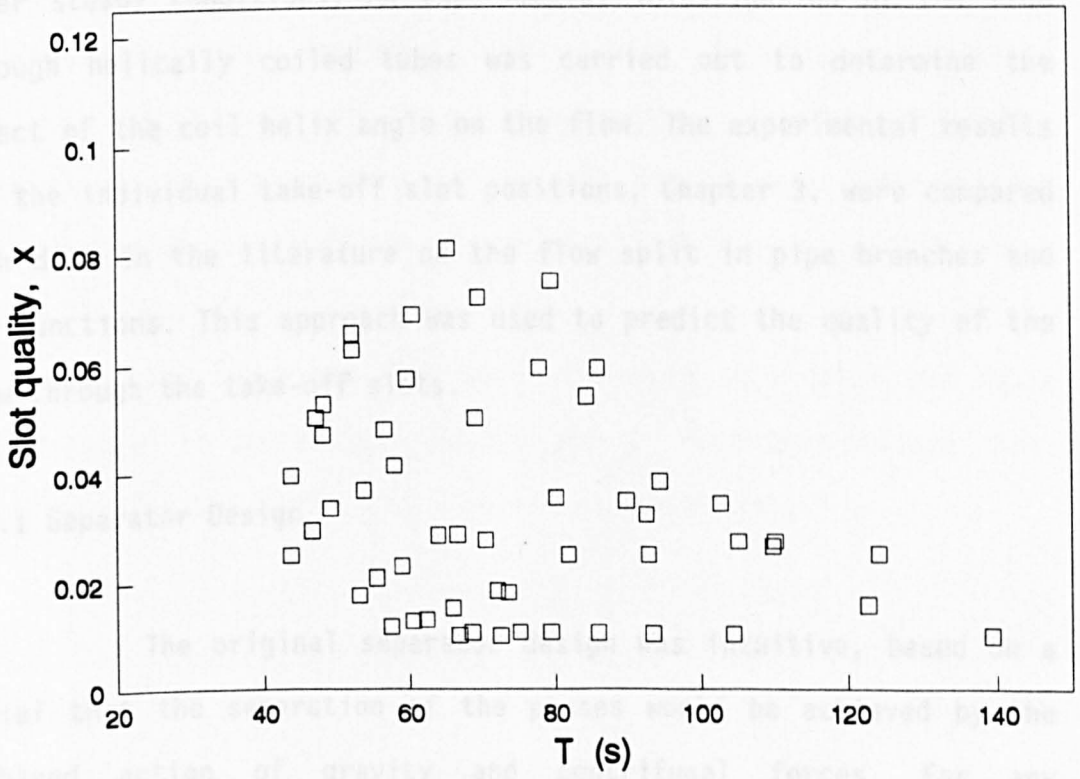

Figure 3.52 Air/water take-off quality - configuration b

CHAPTER 4: ANALYSIS OF TWO-PHASE FLOW IN THE SEPARATOR

4.1 Approach to Analysis

In the preceding chapter the results of experimental work on the separator in both single-phase and two-phase flow were described. The gas separation results varied with the void fraction and the liquid phase of the two-phase flow. In an attempt to identify the parameters which most affected the performance of the separator three approaches were used.

A model of the two-phase flow through a helical duct was developed to predict the area and velocity of each separated phase under steady conditions. An experimental investigation of the flow through helically coiled tubes was carried out to determine the effect of the coil helix angle on the flow. The experimental results for the individual take-off slot positions, Chapter 3, were compared with data in the literature on the flow split in pipe branches and tee junctions. This approach was used to predict the quality of the flow through the take-off slots.

4.1.1 Separator Design

The original separator design was intuitive, based on a belief that the separation of the phases would be achieved by the combined action of gravity and centrifugal forces. For any improvement of the design to be achieved the effects of the separator

geometry on the flow must be understood. The geometric variables considered most likely to influence the separation were the equivalent diameter of the separator passages, the cross-section shape of the passages and the helix angle of the passages.

To manufacture several separators with differing helix angles, passage shapes and flow areas would have been prohibitively expensive. Helically coiled tubes were used instead to investigate the effects of the above parameters on the two-phase flow.

The data gathered from the two-phase pressure drop experiments on the separator was used to verify the model of a helical duct. The two-phase pressure drop along a fixed length of the helical passage was used to verify the model results because the pressure drop was the most easily and accurately measured.

By verifying the pressure drop through the helical passage the prediction of the phase areas and velocities was also verified. The most reliable experimental techniques presently available for direct area fraction measurement involved gamma ray absorption. These techniques involve the use of long time-averages and can be sensitive to the orientation of the instrument, Ince (1990), in relation to the flow regime.

The separated flow model was used to predict the phase area fraction in the helical passage and the separated average phase velocities for the conditions used in the experiments.

4.2 Two-phase Flow Theory

4.2.1 General Equations for Two-phase Flow

The theory of two-phase flow has been developed to the point where the general constitutive equations have been derived, for example Ishii (1975). Unfortunately a general solution to these equations is not available due to their complexity and the large number of variables these contain. The bulk phase conservation equations for mass, momentum and energy have been derived by Agee et al (1978), Banerjee and Chan (1980) and Delhaye (1981). The quantities in these equations are taken to be ensemble averaged quantities, where the bulk phase quantities are averaged in space and time. It is also assumed that the product of the averages is equal to the average of the products for both bulk and interfacial quantities [Agee et al, 1978 and Delhaye, 1981]. These general equations can be applied to most two-fluid problems providing that the type of flow pattern is anticipated. This is because the flow regime and body forces were shown by Boure (1987) to determine the nature of some of the closure relations across the fluid interface. At least one closure relation is required to achieve a specific solution.

Vector notation, as by the above workers, is used to write the general equations in one-dimensional form. The operator $\langle \ldots \rangle$ indicates quantities which have been ensemble averaged. The subscript k refers to the phase of the variable, where k = l for the liquid phase and k = g for the gas phase. Interfacial quantities are indicated by the subscript i.

Mass Conservation

$$\frac{\partial}{\partial t}\alpha_k\langle\rho_k\rangle + \frac{\partial}{\partial z}\alpha_k\langle\rho_k u_k\rangle = -\langle\dot{m}_k\rangle_i \qquad (4.1)$$

Conservation of Momentum

$$\frac{\partial}{\partial t}\alpha_k\langle\rho_k u_k\rangle + \frac{\partial}{\partial z}\alpha_k\langle\rho_k u_k^2\rangle + \alpha_k\frac{\partial\langle p_k\rangle}{\partial z} - \frac{\partial}{\partial z}\alpha_k\langle\tau_{zz,k}\rangle$$

$$- C_k\rho_k u^n\frac{\partial\alpha_k}{\partial z} = \alpha_k\langle\rho_k F_{z,k}\rangle - \langle\dot{m}_k u_k\rangle_i$$

$$+ \langle(\dot{n}_k\cdot\bar{\tau}_z)\rangle_i + \langle(n_{kw}\cdot\bar{\tau}_z)\rangle_w \qquad (4.2)$$

Conservation of Energy

$$\frac{\partial}{\partial t}\alpha_k\langle\rho_k(h_k + \frac{u_k}{2})\rangle + \frac{\partial}{\partial z}\alpha_k\langle\rho_k u_k(h_k + \frac{u_k}{2})\rangle + \langle p_k\rangle\frac{\partial\alpha_k}{\partial t}$$

$$+ C_k\rho_k\delta u^n\frac{\partial}{\partial t}\alpha_k + \frac{\partial}{\partial z}\alpha_k\langle q_{z,k}\rangle - \frac{\partial}{\partial z}\alpha_k\langle\vec{n}_z\cdot(\bar{\tau}_k\vec{v}_k)\rangle$$

$$= -\langle\left[\dot{m}_k(h_k + \frac{u_k^2}{2}) + \vec{n}_k\cdot\vec{q}_k - \vec{n}_k\cdot\vec{v}_k\cdot\tau_k\right]\rangle_i - \langle(n_{kw}\cdot q_k)\rangle_w$$

$$+ \alpha_k\langle(\rho_k\vec{v}_k\cdot\vec{F}_k + Q_k)\rangle \qquad (4.3)$$

This set of equations defines the one-dimensional two-phase flow problem with averaged quantities in the bulk phase conservation equations. The method of ensemble averaging has been used in the above equations, which results in time/space averaged quantities similar to those obtained using practical instrumentation

such as gamma-ray densitometers and pressure transducers. This averaging method simplifies the problem of solving the equation set but leads to detailed information on the phase interface shape and motion becoming lost in the averaging process. To replace some of this information auxiliary relationships must be supplied [see, for example, Boure (1987), Stuhmiller (1977) and Banerjee and Chan (1980)]. These auxilliary relationships, known as 'closure relations', can be determined from the physical nature of the flow. Stuhmiller used the pressure distribution around a bubble and the interphase surface tension in a dispersed flow regime to develop a closure relation for bubbly flow. Banerjee and Chan developed a closure relation using the transverse pressure gradient in a separated flow. This type of closure relation has been used in the present model. The equation of state for the gas phase is also normally used as part of the closure relationship.

Mass Conservation

Considering the general case for the conservation of mass across the interface it is usual to say, following Delhaye (1981), that the mass transfer from phase 1 to phase 2 is equal and opposite to that in the other direction under equilibrium conditions.

$$\langle m_1 \rangle_i = -\langle m_2 \rangle_i \qquad (4.4)$$

The fluids used in the experiments were air/water and air/kerosene mixtures at ambient temperatures and low pressures. The flow thus consisted of two components, neither of which was expected

to undergo a phase change due to evaporation or condensation. We can then say that there will be no interphase mass transfer.

$$0 = -\langle m_k \rangle_i \tag{4.5}$$

The general one-dimensional mass conservation equation (equation 4.1) then reduces to

$$\frac{\partial}{\partial t} \alpha_k \langle \rho_k \rangle + \frac{\partial}{\partial z} \alpha_k \langle \rho_k u_k \rangle = 0 \tag{4.6}$$

Conservation of Momentum

Agee et al (1978) wrote the difference between the bulk phase pressures and interfacial phase pressures as a form drag term;

$$P_{k\,i} - P_k = C_k \rho_k \Delta U^n \tag{4.7}$$

and replaced the form drag term in equation 4.2. The conservation of linear momentum equation may then be written, after Ardron (1980), in terms of the difference between the bulk and interfacial pressures. Taking all quantities to be ensemble averaged the general one-dimensional conservation of momentum equation then becomes

$$\alpha_k \rho_k \frac{\partial u_k}{\partial t} + \frac{\partial}{\partial z}\alpha_k \rho_k u_k^2 + \alpha_k \frac{\partial P_k}{\partial z} + (P_k - P_{ki})\frac{\partial \alpha}{\partial z}$$

$$= \tau_{wk} + \tau_i + \alpha_k \rho_k F_{z,k} \qquad (4.8)$$

where P_k is the bulk phase pressure and P_{ki} is the pressure at the interface in phase k.

Conservation of Energy

The energy equation can be written in a similar form to that for the conservation of linear momentum by using ensemble averaged variables. In the particular case of modelling adiabatic air/water and air/kerosene flows there is negligible heat or energy transfer between the fluid boundaries or across the fluid interface. The energy equation then reduces to the momentum equation.

4.2.2 Equations for Horizontal Stratified Flow

The general one-dimensional equations described above require interfacial balance or 'jump' relations before a solution can be obtained for a particular problem. These jump conditions are often flow regime specific and account for some of the detail lost during the ensemble-averaging process. The flow in a helical passage is assumed to be of a stratified flow pattern from observation and experiment [King and Purfit, 1984]. A typical jump condition used for the separated flow is that of the transverse momentum balance across the fluid interface, Rousseau and Ferch (1979) and Stuhmiller (1977).

Stuhmiller used a balance across a bubble interface taking surface tension into account whereas Rousseau and Ferch used the transverse pressure gradient caused by gravity in a horizontal smooth stratified flow.

In the case of stratified flow the bulk phase and interface pressures are related to the hydrostatic pressure gradient in each phase. The assumption that there is no surface tension, Ardron (1980) and Boure (1987), leads to the phase interface pressures and local interface velocities being equal.

$$P_k = P_{k\,i} \pm \frac{1}{2}\alpha_k \rho_k g H \qquad (4.9)$$

The case of the helical passage was considered, across a small length of the duct with a large radius of curvature, to be analogous to that of a horizontal duct. The centrifugal forces act normal to the duct axis and replace gravity as the major body force acting on the fluids, De Crecy (1986).

To take the effect of viscous forces into account some relationship is also required for the wall and interfacial shear stresses. There is no correlation available for the shear in two-phase flow and so the conventional technique suggested by Taitel and Dukler (1976), which utilises the single-phase value, is adopted

$$\tau = \frac{f_k \rho_k \bar{u}_k^2}{2} \qquad (4.10)$$

This assumption is considered valid for separated flow regimes where there is a continuous flow path and well defined boundary in each phase. In such a case each phase tends to have a continuous contact area with its boundaries, which is generally not the case in dispersed type flow regimes. The boundary shear for each phase in a separated flow regime will then closely resemble that for the single-phase case.

The flow in the helical passage is assumed to be a developed stratified flow regime. The assumption can then be made that the flow is quasi-steady and the area void fraction varies with distance, z, along the duct but not with time, t, at a fixed point. The assumption of separated flow was made due to the effect of the centrifugal forces on the fluid, caused by the helical motion of the flow, which increase the radial pressure gradient in the passage. At the lowest flow rates and void fractions at which the separator was tested (these conditions gave the lowest mean liquid velocity) the centrifugal forces were estimated to be 35 times the force due to gravity. The liquid phase was then forced to the outside of the duct by the centrifugal forces and the gas phase to the inside. If both separated phases are assumed to be continuous in every cross-section then

$$\alpha_g + \alpha_l = 1 \qquad (4.11)$$

and from equation 4.6

$$\frac{\partial}{\partial z}(\alpha_k \rho_k u_k) = 0 \qquad (4.12)$$

and from equation 4.8 we find

$$\alpha_k \rho_k u_k \frac{\partial u_k}{\partial z} + \alpha_k \frac{\partial P_k}{\partial z} + (P_k - P_{ki}) \frac{\partial \alpha}{\partial z} - \frac{f \delta z u_k \rho_k}{2 d_h} = 0 \qquad (4.13)$$

neglecting the influence of gravity.

These equations form a general set of equations which describe the one-dimensional steady adiabatic stratified two-phase flow of a gas/liquid mixture which can be applied to a helical passage where the centrifugal forces dominate gravity. Combined with the equations of state for the gas phase and the assumption of equal interface pressure in each phase a solution is attainable.

4.2.3 Working Equations

For a small distance, dz, along the duct between plane 1 and plane 2, Fig. 4.1, there will exist a small pressure differential ΔP. For a small value of δz, which is a small fraction of dz, it can be assumed that the quantities f_k, ρ_k and Q_k are constant. From equations 4.11 and 4.13 the momentum equation can be re-written in terms of the area occupied by each phase at each cross-section in the duct.

$$P_{k2} = P_{k1} - \rho_k f_k \delta z \frac{Q_{k1}^2}{2d_{hk}} \left\{ \frac{1}{A_{k2}} + \frac{1}{A_{k1}} \right\}^{0.5}$$

$$- Q_{k1}^2 \frac{\rho_k}{2} \left\{ \frac{1}{A_{k2}^2} - \frac{1}{A_{k1}^2} \right\} \pm \frac{1}{2} \rho_k g h_k \qquad (4.14)$$

By use of the assumption that the interfacial pressure, P_{ki}, in each phase is equal and that the initial conditions at plane 1 are known, then the first approximations for the values of ρ_k, u_k and h_k at plane 2 can be found. From these first approximations averaged values between planes 1 and 2 may be used to gain a more accurate estimate of the quantities at plane 2. Because the area of each phase varies with z the relationship between the phase areas, A_k, and phase heights, h_k, at a given cross-section within the duct is required.

For a rectangular duct of unit width, Fig. 4.2a, then equation 4.11 takes the form

$$h_g + h_l = H \qquad (4.15)$$

For a duct of circular cross-section. Fig. 4.2b, the area of the phase occupying the smallest area is given by

$$A_k = r^2(\theta - \frac{1}{2}\sin 2\theta) \qquad (4.16)$$

$$\text{where } \theta = \cos^{-1}(\frac{r - h_k}{r})$$

The separator helical passages have a cross-section which is triangular, Fig. 4.3, and the equation which relates the phase area to the phase height is, assuming that the liquid phase occupies the outer segment of the passage and that the interface is parallel to the outer wall of the passage,

$$A_g = 0.001886h_g + 0.7373h_g^2 \qquad (4.17)$$

In a horizontal duct the influential body force is that of gravity. In the case of flow in a curved or helical duct with sufficiently small radius of curvature then the centrifugal force generated by the motion of the fluid becomes dominant. The flow may then be considered analagous to a one-dimensional horizontal flow with the duct axis as the z-axis.

De Crecy (1986) considered the effects of various forms of body forces operating in two-phase flow through ducts, the body force in a curved duct being that of the centrifugal force generated by the flow. The centrifugal force generated by the fluid motion in a curved path, Fig. 4.4, may cause separated flow to occur which may not have occurred in a straight duct. To account for the centrifugal

force in equation 4.14 the gravity term, g, was replaced with the centripetal acceleration, Acc, given by

$$Acc = \frac{(u_\theta \sin\phi)^2}{(r_o - 0.5h_1)} \qquad (4.18)$$

4.3 Investigation of Flow in Helically Coiled Tubes

A large body of work on single and two-phase flow through helical coils is available in the open literature. Flow through a helically coiled tube is analogous to that through a helical passage in the separator. Using this analogy the flow pattern and pressure losses in the helical coils were examined at the separator helix angles (32°) and at the smaller helix angles of 20° and 5°. Two tubes were used, of 25.4mm and 38.1mm internal diameter. The aim of these experiments was to show whether the tube (passage) area and helix angle would significantly affect the flow pattern, phase distribution and pressure losses in the separator.

4.3.1 Single-Phase Pressure Drops in Helical Coils

The experimental rig used for the helical coil flow experiments was described in section 2.5. To enable analysis of the two-phase results from each coil the single-phase friction coefficient in the coils was required.

Early work on flow in curved pipes was conducted by Dean (1927) who defined a dimensionless ratio of the Reynolds Number

multiplied by the square root of the dimensionless coil diameter ratio. The dimensionless coil diameter is defined as the ratio of the tube bore, d, to the coil diameter, D. The dimensionless ratio, known as the Dean Number (Dn), accounts for the curvature of the pipe and allows the flow in coils of differing curvature ratio to be compared.

$$Dn = \frac{\rho dV}{\mu}\left[\frac{d}{D}\right]^{0.5} \qquad (4.19)$$

Dean also showed that, due to secondary flows, the motion of the fluid within the tube followed that of a double helix, Fig. 4.5. The radial pressure distribution in the tube caused a higher local pressure at the outer wall, providing a pressure gradient across the tube diameter. The pressure gradient caused fluid to flow from the outer wall to the inner wall of the tube at the centreline, with a recirculation around the circumference of the tube.

White (1929) examined the wall friction coefficients for coiled pipes in laminar flow and showed the Dean theory to be correct. Rippel et al (1966) found that the friction coefficients in a coiled tube were in close agreement with the correlation proposed by White in the Reynolds Number range of 1000 to 10 000. Ito (1959) and Srinivasan (1970) conducted further experiments to find the wall friction coefficients for curved tubes and helical coils in turbulent flow. Each defined expressions based on experimental correlations for the single-phase friction factor in terms of the Reynolds Number. Ito defined the friction coefficient for a curved tube in a turbulent flow as

$$f_c = \left\{\frac{r_0}{R}\right\}^{0.5}\left[0.029 + 0.304\left(Re\left\{\frac{r_0}{R}\right\}^2\right)\right]^{-0.25}$$

$$\text{for } 300 \rangle Re\left\{\frac{r_0}{R}\right\}^2 \rangle 0.034 \qquad (4.20)$$

and Srinivasan defined the friction coefficient for helically coiled tubes with turbulent flow as

$$f_c = 0.084/\left[Re\left\{\frac{D}{d_i}\right\}^{0.5}\right]^{0.2} \qquad (4.21)$$

Further work by Anglesea et al (1974) found single-phase friction factors in helical coils that were in close agreement with the correlation proposed by Ito.

4.3.2 Single-phase Friction Factor Experimental Results

The 25.4mm and 38.1mm coils had a nominal diameter ratio of 0.09, compared with an equivalent diameter ratio of 0.12 for the helical passages in the separator. The tube internal walls were taken to be smooth. The friction factor was found from the pressure drop across two pressure tappings in each coil using the Darcy equation (equation 4.22) for smooth pipes.

$$\Delta P = \frac{\rho f \delta l V^2}{2d} \qquad (4.22)$$

The experimental friction factors for each coil at 5°, 20° and 32° helix angles were found for water flow rates between 0.15 l/s and 3.1 l/s. The friction factor in the 25.4mm coil, Fig. 4.6, showed no significant dependence on the helix angle of the coil. For each helix angle the friction factor reduced as the Reynolds Number increased, as would be expected in a straight tube. The friction factor for the 38.1mm coil, Fig. 4.7, was also independent of the helix angle of the coil. The friction factor reduced as the Reynolds Number increased and, for both coils, matched the correlation of Srinivasan more closely than that of Ito. The correlation proposed by Srinivasan (equation 4.21) was based on experiments performed using helically coiled tubes of several diameter ratios and helix angles whereas that of Ito used only a single turn of several diameter ratios, which may not have produced a fully developed flow. Srinivasan had also demonstrated that the helix angle did not significantly influence the single-phase friction factor for small bore tubes (d = 12.7mm). The experiments in the present study have shown that the Srinivasan correlation is equally valid for helically coiled smooth walled tubes of up to 38.1mm diameter.

The small differences between the friction factors obtained in the present experiments and the expression of Srinivasan were attributed to the difficulty of obtaining a completely smooth internal surface in the non-rigid tube. Boyce et al (1969) found that differences between their results and those of previous workers were due to wrinkles on the internal diameter of their coil caused during manufacture.

The out-of-roundness of the tubes used in the present study was measured after they had been wound, as any alteration of the cross-section area could affect the data reduction. The cross-

section area of the 38.1 mm tube decreased by 3.4% after winding, caused by a measured tube eccentricity of 1.22. This area reduction led to a corresponding increase of the mean velocity in the coil. The increase in the mean flow velocity was accounted for in equation 4.22 by using the equivalent tube diameter and the increased mean velocity calculated from the reference flow rate using the reduced area of the tube.

Srinivasan (1970) gave an expression for predicting the critical Reynolds Number for the flow.

$$Rn_{crit} = 2100\left[1 + 12\left[\frac{d}{D}\right]^{0.5}\right] \qquad (4.23)$$

The transition between laminar and turbulent flow regimes was taken as that point at which the gradient of the friction factor curve decreased. The critical Reynolds Number at this point is greater than that found in straight tubes, as is the magnitude of the friction factor. The increase in the critical Reynolds Number is due to the increase in the friction in a coiled tube from that in a straight tube, Rippel et al (1966), which allows laminar flow to be maintained to higher Reynolds Number. The transition is noted to occur at the point at which the friction factor curve undergoes a change in gradient rather than the discontinuity which is typically found in straight tubes. The expression matched the experimental data well, with the transition occurring at around Rn = 10 000 in both coils (see Fig. 4.6 and 4.7).

4.3.3 Two-phase Flow Pattern in Helical Coils

The separator had already been tested with a vertical axis and shown to produce a separated flow in the helical passages. The helical coils were set with a horizontal axis, which gave an alternating up and down flow. The flow components were air and water. The water flow rate was varied between 0.3 and 3.0 l/s. The air flow rate was between 0.2 and 1.7 l/s, which gave void fractions between 10% and 50% at the maximum flow rate.

A survey of previous work found conflicting evidence on the flow patterns in up and down inclined tubes under natural gravity. The present experiments, which included the effect of centrifugal forces, were used to show whether separated flow could be achieved with a horizontal axis. Barnea et al (1985) examined flow in upward inclined straight tubes under natural gravity and found that for large inclinations from the horizontal the stratified flow pattern did not occur and was replaced by intermittent flow, although Gardner and Kubie (1976) found stratification between alcohol and water flowing in straight tubes of up to 60° inclination. For the case of downward inclined flow Barnea et al (1982) found that the stratified wavy region was greatly extended over that for a horizontal tube. Usui et al (1983) noted that the flow regimes in an inverted U-bend were modified from those in a horizontal tube by the combined action of the gravitational force and centrifugal forces. Usui also found annular flow at lower velocities than would be expected in horizontal or vertical tubes. The balance of the centrifugal and gravity forces, Fig. 4.8, on the liquid phase in a helical coil can be given as

$$\frac{\rho_l U_l^2}{r_l} d = \rho_l g(r_l - R) \qquad (4.24)$$

Whalley (1980) analysed the forces acting on a separated liquid film in a coil, giving comparable results to those of Banerjee (1967) who originally noted the phenomena of inverted ribbon flow in a vertical axis helical coil. Whalley showed that due to the balance of gravity and centrifugal forces the liquid phase could run on the inner wall of the tube when the gas velocity was much greater than the liquid velocity. Whalley also demonstrated that the circumferential position of the liquid ribbon varied with the magnitude of the centrifugal forces acting on the gas phase. Hart et al (1988) noted the existence of pressure differentials between the inner and outer walls of a coiled tube, proportional to the square of the flow velocity. Similar pressure differentials were measured in the separator helical passages and were also proportional to the square of the flow velocity.

The flow pattern prevailing during the experiments on helically coiled tubes was identified visually as a wavy stratified flow. The flow pattern in the separator helical passages had also been stratified flow. The flow pattern at very low flow rates in the 38.1mm tube was identified as intermittent flow. At these low flow rates the centrifugal forces were small compared with gravity, due to the low mean flow velocity, and less likely to affect the flow structure than at the higher flow rates. At some of the flow conditions there were occasional, infrequent, plugs of liquid which

bridged the tube, but these were not considered to be of a frequency to class the flow as a plug flow.

Kaji et al (1984) examined the flow structure in a single turn of helix angle 8° using visual and conductance probe techniques. They noted the extension of the region in which stratified wavy flow might be expected, although the flow in the helical coil experiments was predicted as slug flow by their modified map. Chen and Zhang (1984) noted similar transition boundaries to those of Kaji and found that the stratified region of the map diminished as the helix angle of the coil was increased. Kaji used 10mm diameter tubes, with a larger diameter ratio than that of the helical coils used in the present experiments, to attain the data on which the flow map was based and the differences between the flow patterns observed may be attributed to the physical differences between the experimental apparatus. Watanabe et al (1986) noted that at low flow rates the stratified flow regime was present at the conditions used by Kaji and Usui.

4.3.4 Two-phase Pressure Losses

Development lengths for two-phase flows are not well understood and developed velocity profiles do not occur in some flow patterns. Sim and Lahey (1985) noted development lengths of 20 diameters in triangular conduits and Akagawa et al (1971) found development lengths of around 50 diameters in helically coiled tubes with similar tube/coil diameters ratio to those used in the present study. To ensure fully developed flow the first pressure tapping was situated 70 diameters after the coil entrance, with a further 30 diameters to the second tapping.

The two-phase pressure losses determined by experiment in the 25.4mm and 38.1mm helical coils increased as the mass flux increased, see Fig. 4.9 and 4.10. The two-phase pressure losses increase with void fraction at constant mass flux because the mean flow velocity increases to compensate for the reduction in mean density.

The two-phase pressure losses in each of the coils were analysed in terms of the square root of the two-phase multiplier, ϕ_{lo}, and the Lockhart-Martinelli parameter, X, defined by Lockhart and Martinelli (1948).

$$\phi_{lo} = \left[\frac{\Delta P_{tp}}{\Delta P_{lo}}\right]^{0.5} \qquad (4.25)$$

$$X^2 = \frac{\Delta P_l}{\Delta P_g} \qquad (4.26)$$

The results from the 25.4mm coil, Fig. 4.11, show that ϕ_{lo} reduced as X was increased for all the coil helix angles. Kubie and Gardner (1977) obtained a similar trend for higher values of X. The results from the 38.1mm coil for all the helix angles appear confused and scattered with no clear trend when plotted together, Fig. 4.12, although there appear to be differences between the values of ϕ_{lo} for each helix angle/void fraction at similar values of X. A clearer picture is given by examining the data at each helix angle independently. Taking a single helix angle (5°) of the 38.1mm coil, Fig. 4.13, shows that for each void fraction there is a distinct

relationship between ϕ_{lo} and X. The same trend was seen in the 25.4mm coil, Fig. 4.14, although the change of ϕ_{lo} with the void fraction was not so marked as in the 38.1mm coil.

The influence of the coil helix angle on the flow was ascertained by plotting ϕ_{lo} against X for the same void fraction condition. The coils exhibited differences in the values of ϕ_{lo} between the differing helix angles. For a given value of X the magnitude of ϕ_{lo} increased slightly as the helix angle of the 25.4mm coil increased, Fig. 4.15. The differences between the values of ϕ_{lo} were less than in the 38.1mm coil, Fig. 4.16, where the magnitude of ϕ_{lo} for the 5° coil was much reduced from that for the 20° and 32° helix angles. The helix angle of the coil clearly has an influence on the pressure losses in a two-phase flow. The two-phase pressure losses in the separator helical passages will, therefore, be influenced by the helix angle of the passage.

The helix angle governs the magnitude of the tangential velocity of the flow. The tangential velocity determines the magnitude of the centripetal acceleration causing the separation of the two phases.

$$\text{Acc.} = \frac{(U.\cos\phi)^2}{r} \qquad (4.27)$$

At a constant velocity, U, and radius, r, the centripetal acceleration in a helical passage will decrease as the passage helix angle, ϕ, increases. In the present experiments the 5° coil produced

the largest centripetal acceleration in the flow whilst the 32° coil produced an acceleration 28% lower in magnitude.

The lower value of ϕ_{lo} in the 5° helix angle coils was caused by the large centrifugal force which produces a more stable stratified flow than for the same flow rate in coils of 20° and 32° helix angle, where the smaller centrifugal force gradient would allow larger surface waves to develop. The effect of the helix angle on the magnitude of ϕ_{lo} can be taken into account by using the mean tangential velocity of the flow as the main parameter. For a given void fraction, Fig. 4.17, the value of ϕ_{lo} lay along the same line for the 25.4mm coil at each of the helix angles used. The data for each of the helix angles also collapsed to one curve for the 38.1mm coil, Fig. 4.18, although there was greater scatter in the data at low flow rates.

The value of ϕ_{lo} increased at lower values of mass flux in the 25.4mm coil and 38.1mm coil, see Fig. 4.19 and Fig. 4.20. The increase at low mass flux was due to the reduced flow velocity which caused a reduction in the centrifugal forces acting on the flow. As a result the stratified flow pattern was unstable at low flow velocity, giving rise to intermittent flow and higher irreversible pressure losses.

The flow velocities in the separator helical passages were large enough to maintain stratified flow at all conditions however, any increase in flow area of the helical passages may reduce the flow velocity sufficiently to allow the development of intermittent flow.

The 5° coils produced the most stable stratified flow pattern and reducing the separator helix angle to this order would improve the separation in the helical passages. The tube cross-

section area clearly affected the stability of the stratified flow because of its effect on the mean flow velocity.

4.3.5 Prediction of Wave Growth Criteria

Taitel and Dukler (1976) described the transition from stratified to intermittent flow in terms of the amplitude of interfacial waves postulating that an unstable wave will grow to form a plug bridging the tube. Taitel and Dukler described the criteria for the formation of interfacial waves as:

$$(U_g - c)^2 c \rangle \frac{4\nu_l g(\rho_l - \rho_g)}{s\rho_g} \qquad (4.28)$$

where c = wave propagation velocity

and s = sheltering coefficient = 0.01

Taitel and Dukler used the approximation of $c = U_l$. For the case of the helical coils the acceleration due to gravity term (g) may be replaced with a term for the centrifugal force acting on the liquid phase.

$$\frac{(U_g - U_l)^2}{U_l} \rangle \frac{4\nu_l(\rho_l - \rho_g)}{Rs\rho_g} \qquad (4.29)$$

Due to the low viscosity of the liquid phase in an air/water or air/kerosene system this criterion is fulfilled and surface waves are predicted on the interface, as was observed during the experiments.

The stability criterion (Kelvin-Helmholtz theory) is that surface waves will grow in a horizontal duct if:

$$U_g > \left\{ \frac{g(\rho_l - \rho_g)h_g}{\rho_g} \right\}^{0.5} \qquad (4.30)$$

In the case of the helical coils the acceleration due to gravity (g) was replaced by the centripetal acceleration due to the motion of the fluid. If the centripetal acceleration, equation 4.27, is substituted into equation 4.30 in terms of the liquid velocity then the criterion for the growth of surface waves becomes

$$U_g > \left\{ \frac{U_l^2 \cos^2\phi \ (\rho_l - \rho_g)h_g}{r\rho_g} \right\}^{0.5} \qquad (4.31)$$

Thus the instability of any surface disturbance will decrease as the mean liquid flow velocity increases for a given interface level in the helical duct. At higher flows the stratified flow will be more stable than at low flow rates, as seen in the experiments. At a constant radius, R, as U_l increases then the magnitude of the gas velocity U_g required before the wave can grow to form a slug must also increase. Once the centripetal acceleration is greater than gravity then the gas velocity required for a small wave to become unstable is greater than that required in a horizontal tube.

The results from the model gave values for the mean stable interface heights and the mean phase velocities in the helical

coils. These values can only give an indication of the likely physical conditions in the helical tubes. The data can be used to give an indication of whether or not the wave growth criteria will be met. Fig. 4.21 shows the slip ratio, calculated from equation 4.29, required at a given interface height for wave growth to occur. This is compared with the slip ratio predicted by the separated flow model. The slip ratio predicted by the model was sufficiently high for wave growth to be predicted in the helical coils by the theory of Taitel and Dukler for all the interface height conditions. This, however, did not agree with the experimental observations which recorded only occasional plugs of liquid in the coils, superimposed on a stratified wavy flow.

The model does not take account of the secondary flows in the coil. These were noted by Koutsky and Adler (1964) to act to entrain gas into the liquid phase and may also suppress growth of interfacial waves. The entrainment of significant proportions of the gas phase will tend to reduce the slip ratio between the phases and so reduce the potential for wave growth according to equation 4.29. The mean flow velocity in the separator helical passages was much greater than that in the helical coils, resulting in a much greater centrifugal force on the mixture which suppressed the growth of interfacial waves.

4.3.6 The Influence of Coil Helix Angle and Tube Diameter

The increase in the magnitude of ϕ_{lo} at low mass flux was more pronounced in the 38.1mm coil than the 25.4mm coil, due to the lower mean velocities in the 38.1mm coil. The lower velocity in the 38.1mm tube resulted in reduced centrifugal forces being

generated. The stratified flow regime in the 38.1 mm tube was therefore less stable and so an intermittent flow regime predominated at low mass flux. The intermittent flow regime in the 38.1mm tube caused increased irreversible pressure losses, which gave higher values of ϕ_{lo} than in the 25.4mm tube for the same mass flux.

The helical coil experiments were performed to investigate the effect of the helix angle on the flow of a two-phase gas/liquid mixture. The results have shown that the single-phase friction factor can be satisfactorily represented by the correlation of Srinivasan (1970) for tube diameters up to 38.1mm with helix angles of up to 32°.

In two-phase flow the flow regime was separated flow, similar to that in the separator helical passages. The liquid phase occupied the outer part of the tube and the gas phase occupied the region closest to the coil axis. At low mass flux the flow pattern in the 38.1mm tube remained un-modified by the centrifugal forces acting on the flow.

The two-phase pressure losses in the coils were not affected directly by the helix angle of the coils. However, the helix angle of the coils dictated the magnitude of the centrifugal forces acting on the fluid mixture. The magnitude of the centrifugal forces influenced the flow pattern in the tube by suppressing the growth of interfacial waves. The flow regime in the coils did affect the pressure loss, with the intermittent flow regime giving rise to pressure losses higher than those found in the separated flow regime. A reduction in the separator helix angle would yield a slightly lower pressure loss and improve the gas/liquid phase separation.

4.4 Verification of the Separated Flow Model

The separated flow model was validated using the two-phase air/kerosene pressure loss data taken during the separator experiments (Chapter 3). The model yielded information on the radial location of the phase interface in the helical passages, which was of use when considering the flow through the take-off slots.

4.4.1 Initial Conditions

The separated flow model required information on the initial phase flow rates, phase pressures and the fluid properties. The model was tested with flow conditions prevailing at the time the experimental data was collected. The initial conditions were set as separated flow with zero slip between the phases. Each of the phases was assumed to be continuous with the liquid phase occupying the outer sector in the passage. The centrifugal force acting on each phase in the flow was related to the mean velocity of that phase. The initial pressure at the gas/liquid interface was set to the pressure measured at the test section entrance during the experiments.

The single-phase friction factor was used in the two-phase separated flow model. The correlation of Srinivasan (1970), which had previously been found adequate to describe the friction factor in helical coils, was used to predict the single-phase pressure loss in the helical passages. The predicted pressure loss was then compared with that measured during the single-phase kerosene experiments, Fig. 4.22. The correlation proposed by Srinivasan for turbulent flow fitted the experimental data well. The transition Reynolds Number of the flow was given as around 10 000 by the

prediction of Srinivasan which indicated that the flow in the separator helical passages should be laminar, as the passage Reynolds Number was between 2320 and 5225. The conclusion must be drawn that the triangular cross-section of the separator passages caused laminar-turbulent flow transition at a lower Reynolds Number than in a helically coiled tube.

The difference in the transition number may be explained by the apparent difference in the internal flow structure (see Chapter 3). The secondary flow in a helically coiled tube will cause greater turbulence than the single vortex thought to occur in the helical passages of the separator, and suppress the transition until at higher Reynolds Number.

The length of the helical passage over which the model calculated the pressure losses was 1000mm whereas the experimental pressure loss was measured across 172mm. The model was split into 20 cells of equal length, Fig. 4.23, which were used to calculate the flow parameters at the exit from each cell, given those at the cell entrance. The model calculated the area, average velocity and pressure loss for each phase across each cell using iteration techniques to balance the pressure losses in each phase across the interface. After around 5 cells the phase area for each phase did not change significantly from one cell to the next; at this point the model was considered to represent developed flow in the helical passage. With no significant change in the phase area across each cell the pressure loss across each cell was also constant. The pressure drop across a single cell, corrected to the equivalent length used in the experiments, was then compared with the experimental pressure loss.

4.4.2 Comparison of Separator Experimental Results - Separated Flow Model Results

The pressure losses measured during the air/kerosene separator experiments were used to validate the separated flow model. The separated flow model results were also compared with the pressure loss predictions given by the homogeneous model, as this model [Whalley, 1987] is considered to give satisfactory pressure drop predictions for mass flux over 2000 kg/m^2s. The experimental pressure drops were measured at five different mean void fractions in the range $10\% < \alpha < 30\%$.

The experimental data is compared with the two-phase pressure drops predicted by the separated flow model and homogeneous model in Figs. 4.24 - 4.28. The homogeneous model predicted higher pressure losses than those found experimentally at all the flow conditions. The separated flow model gave a closer prediction of the experimental data than the homogeneous model, over-predicting slightly at the 10% and 15% void fraction conditions and under-predicting the data at the 30% void fraction.

For all the above comparisons the separated flow model gave an error in the predicted pressure loss of less than ± 15% and was close to the experimental values at the majority of the flow conditions. The precision with which the separated flow model predicted the two-phase pressure losses found by experiment gave confidence in the values predicted by the model for the interface height and phase velocities. The predicted gas interface heights are given in Fig. 4.29 against the mean void fraction of the air/kerosene flow.

The model can also provide other data describing the motion of the two phases through a helical duct. The model predicted that for all the initial conditions there is a length of the duct along which the area of each phase varies. After this length the phase area of each phase remains near constant. At this point the model corresponds to fully developed steady stratified two-phase flow. Other information can also be extracted from the model, such as the mean phase velocities and densities, which can be useful in determining the influence of these properties on the behaviour of the flow. If the rate of gas and liquid extraction from a particular take-off slot were known then the phase depths can also be predicted at the next slot downstream, providing that the slot is sufficiently distant that the flow has time to re-establish a stable flow pattern.

4.5 Flow Through Take-Off Slots

4.5.1 Basis of Slot Flow

The centrifugal force generated by the fluid motion in the helical passages of the separator caused the gas phase to separate to the passage root and the liquid phase to occupy the outer sector of the passage. The separated gas then flowed through the take-off slots cut in the root of the helical passages. This was due to the pressure difference between the helical passages and the central gallery, see Fig. 4.30. The central gallery, which is open to the flow at the separator exit, is at a lower pressure than the helical passages in the vicinity of the take-off slots. The resulting pressure difference across the slots was caused by the friction pressure losses in the helical passages.

There has been relatively little work on the problem of flow past a slot with its longitudinal axis parallel to the direction of the flow. Madden and St. Pierre (1970) examined the flow through this type of slot in a slot distributor. They found that the flow rate through the slot could be calculated using the standard orifice equation and employed discharge coefficients which were dependent upon the ratio of the cross-flow to mainstream velocities. This ratio was equivalent to the ratio of the pressure drops in the cross-flow and main run. These discharge coefficients were then used to predict the slot flow rate in bubbly flow. The gas phase and the liquid phase slot flow rates could then be found if the average void fraction of the flow were known.

The experimental examination of the gas separation efficiency indicated that although the volume of gas take-off through the slots increased as the mass flux through the separator increased, the proportion of the gas flow rate through the take-off slots to that in the separator did not. A possible explanation for this may be that the take-off slots were close to choking. It is well known, Wallis (1969), that two-phase choking may occur at a considerably lower velocity than that for either of the two components flowing alone as a single phase.

To determine the theoretical choking condition for the slots the homogeneous frozen flow model, Whalley (1987), may be used. The quality of the flow is assumed not to change in the slot as the flow through the take-off slot is adiabatic. The raised local flow velocity of the two-phase mixture through the slot is assumed to lead to an approximately homogeneous flow pattern. The critical mass flux through the slot is given by:

$$G_c^2 = \frac{x\nu_{g0}P_0\gamma}{\nu^2}\left\{\frac{2}{\gamma+1}\right\} \qquad (4.32)$$

where

$$\nu = (1 - x)\nu_{10} + x\nu_{g0}\left\{\frac{2}{\gamma+1}\right\}^{\frac{1}{1-\gamma}}$$

and γ = gas property index

The stagnation conditions, subscript 0, were taken as those in the helical passage gas phase, which is the continuous phase at the slot entrance. The critical mass flux given by the analysis, Fig. 4.31, was at least 10 times greater than the mass flux found during the air/kerosene experiments for the individual slot positions. The take-off slots were therefore unlikely to be choked and did not limit the volume flow rate of the mixture which passed through the slots to the central gallery.

The limiting parameter for the slot flow rate will be the driving pressure drop across the slots. The total volume flow rate is given by the standard orifice equation

$$Q = CdA_1\left\{\frac{2\Delta P}{\rho}\right\}^{0.5} \qquad (4.33)$$

The pressure drop, ΔP, across the take-off slots was governed by the velocity of the flow in the helical passages. The driving pressure drop across the slots was approximately equal to the two-phase pressure loss in the passages between the slot position and

the exit plane of the separator, assuming that the pressure loss in the central gallery was negligible.

From this it can be seen that the further upstream the slot is from the exit plane then the greater the pressure drop across that slot will be. The flow rate through a slot, for a given passage flow rate, will be highest for the slots furthest upstream from the exit which have the greatest pressure differential (see section 3.3.4), providing that the separated flow pattern has become established at the slot.

The slot total volume flow rate, Fig. 4.32, was found to increase with the pressure differential across the slot for all the void fractions used in the main separator flow. The slot volume flow rate also increased with the void fraction of the flow in the helical passages.

To find a discharge coefficient for the take-off slots, equation 4.33 was used to predict the total volume flow rate through the slots. To obtain a value of Cd which was applicable across the range of flow conditions in the helical passage the homogeneous mixture density of the test section flow was used. The values of discharge coefficient obtained from dividing the total measured volume flow through the slot by that predicted using equation 4.33 lay on a single curve, Fig. 4.33. The data for each flow condition lay on the same curve and the discharge coefficient increased as the flow through the slot was increased. The discharge coefficients for each slot position lay on the same curve.

By analysis of a small volume of fluid travelling along a curved streamline in the helical passage, Fig. 4.34, the influence of the pressure gradient at the slot and the centrifugal force on the

fluid can be seen. The balance of forces across the element can be expressed as:

$$R\delta P\delta\theta = \rho U^2 \delta R\delta\theta \qquad (4.34)$$

Clearly for the fluid to remain on a streamline parallel to the duct wall the centrifugal force and radial pressure gradient must be balanced. For fluid to move toward the slot the radial pressure gradient must have a greater influence than the centrifugal force. For a given pressure gradient the gas phase will move to the slot more quickly than the liquid phase due to its lower density. The gas phase will then be preferentially separated through the slots to the central gallery.

4.5.2 Flow Through Tee Junctions

The flow of a fluid through a slot with the entry at 90° to the main direction of the flow is analagous to the flow through the run and branch of a 90° tee junction, Fig. 4.35, with a horizontal run and a vertical branch. The main flow through the helical passages in the separator is representative of the flow in the horizontal run. The flow through the take-off slot is analagous to that which passes to the upward branch of the tee junction. Azzopardi and Whalley (1982) have shown that the flow split between the run and branch of a tee junction is difficult to predict in two-phase flows. Either the gas or liquid phase may be preferentially separated to the run or the branch.

The flow split between the run and branch of a tee in two-phase flow was shown by Azzopardi and Whalley to depend, to some extent, upon the flow pattern before the junction. The liquid phase was found to preferentially enter the branch when annular and churn flows regimes existed in the run. The gas phase preferentially entered the branch with a bubbly flow regime in the run.

The difference in separation behaviour between the two flow regimes can be explained in terms of the momentum of each individual phase. In the case of annular flow the liquid film has relatively low velocity and momentum whereas the gas phase has high velocity and similar momentum to the liquid phase. The liquid phase is then preferentially separated into the branch because it tends to flow on or near to the pipe wall and so is close to the branch entrance. For the case of bubbly flow, where the phase velocities are similar, the gas phase has lower momentum than the liquid phase and is then preferentially separated through the branch. Clearly the orientation of a tee junction can also have a great effect upon the flow split at the junction, Zuber (1980), as can the presence of upstream and downstream disturbances, Collier (1976). Azzopardi (1990) also noted that the downstream geometry may affect the flow split at the junction if there is stratified flow entering the junction.

The fraction of the gas and liquid phases taken off in the separator slots was similar to that found for a wavy-stratified flow regime, see Fig. 4.36, by Azzopardi (1990) using air/water flows in a horizontal tee junction with a vertically upward branch. The data of Azzopardi for the annular flow regime shows higher fractions of liquid take-off than for the wavy-stratified flow regime, which has similar values to the separator data.

Azzopardi also noted the existence of a sudden increase in the stratified flow interface height after the vertical branch. The phenomenon is akin to that of 'film stop' recorded by Azzopardi (1988) for annular flow at a tee junction which also appeared to be related to a hydraulic jump. The reduced gas flow rate resulting from the preferential gas phase take-off through the branch allows the flow area for the liquid to increase. The increase in the gas/liquid interface height is aided by the pressure recovery, noted by Collier (1976), which occurs across a tee junction.

Smoglie (1984) examined the flow split between a large diameter tube (run) and a much smaller diameter branch. The main tube was horizontal and the branch was positioned in vertically upward, vertically downward and horizontal positions. Smoglie used branch-to-run diameter ratio's of between 0.029 and 0.1. The equivalent diameter for a long thin slot, such as the separator take-off slots, is 2 × slot width which gives an equivalent diameter ratio for the slot/passage of 0.313. The flow regime investigated by Smoglie was smooth stratified flow and the flow split was found to depend on the orientation of the branch and the ratio of the phase heights in the main tube.

McCreery and Banerjee (1990) showed clearly the flow paths in a square edged tee junction using mist and rivulet flows. Recirculation zones were shown to exist just inside the branch at the upstream edge and in the run on the wall opposite the branch, starting near the junction centreline. The recirculation zone in the run is in the same region as the film stop/hydraulic jump phenomena noted by Azzopardi. The recirculation in the run will probably affect the performance of the next slot immediately downstream in the separator by contibuting to the local raising of the interface level.

The experimental work in the air/kerosene flow showed that the sum of the individual separation performances of the slots was greater than the separation performance of the combined slot configuration. Thus the preceding slots must affect the performance of those further downstream, the problem was exacerbated by the small distance (15mm) between each take-off slot.

The flow regime in the separator was separated flow, with the centrifugal force being analagous to the gravity force in a horizontal duct. The slot entrance was 'vertically' above the fluid interface as the branch would be in a stratified flow through a horizontal tee with a vertical branch. The slot cross-section used in the separator had a large l/d ratio (l/d = 50) unlike the branch in a tee junction (l/d = 1). Azzopardi (1984) showed that increasing the diameter ratio between the branch and the run increases the proportion of the liquid entering the branch. In the separator the width of the slots was physically constrained by the passage cross-section and so the slot length had to be large to increase the flow area of the slot. The disadvantage of the long slot is that, as with a large diameter ratio branch, the entrainment of liquid may be increased.

4.5.3 Theoretical Approach to Flow Split

Zuber (1980) considered the problem of the flow split in small breaks in large pipes in an attempt to predict the proportion of liquid phase which would escape from a break in a pipe during a loss of coolant accident (LOCA) in a pressurised water reactor. Zuber concluded that with a break located above the interface of a stratified flow some of the liquid phase could be entrained as drops

in the escaping gas flow due to the Bernoulli effect, Fig. 4.37, locally decreasing pressure at the branch entrance and raising the fluid interface under the branch. Drops could then be torn off the locally raised liquid surface by the escaping gas which would then carry the entrained drops through the branch. Rouse (1956) showed that liquid could be drawn into a tube vertically above a surface by the flow of gas into the tube. The liquid flow rate was governed by the density difference between the gas and liquid, the tube diameter and the distance from the surface to the mouth of the tube. This mechanism for liquid entrainment was observed for tee junctions in experiments conducted by Schrock et al (1986).

Work on the modelling of the flow split in a tee junction has concentrated on the idea that the branch has a zone of influence from which fluid is drawn off from the run. Azzopardi and Whalley (1982) proposed a geometric model based on experiments with annular and churn flows in a vertical tee junction where the fluid drawn into the horizontal branch was from a zone close to the branch entrance. The proportion of each phase which was taken off into the branch of the junction was determined by the momentum of each phase. The phase with the lowest momentum will be preferentially separated into the branch because of the greater ease with which this fluid can turn the corner.

A similar concept to the geometric zone of influence is that, for each phase, there exists a dividing streamline in the main flow. All the fluid to one side of this streamline flows to the branch and all that on the other side continues in the run. Given the equation of the dividing streamline, the equation of motion for a small volume of fluid can be calculated [Shoham et al, 1987] and the fraction of each phase passing to the branch and the run may then be

calculated. This technique yields the flow split for each phase between the run and the branch and appears to give reasonable results for the case of a tee junction where the run and branch are both horizontal. Hwang et al (1988) also considered the problem of flow split in a tee junction using dividing streamlines for each phase. Although the analysis of both Shoham and Hwang appear to offer the advantage of some theoretical basis in predicting the flow split in horizontal tee junctions there are some problems when applying these models to a horizontal tee junction with a vertically orientated branch. Unless the liquid phase has a much lower velocity than the gas phase and hence a similar momentum then the gas phase will always be preferentially extracted through the branch. For a stratified flow with the interface vertically below the branch entry no liquid entrainment would be predicted by either of the above models.

Smoglie (1984) examined flow through tees using high quality flows at all the experimental conditions and found that the branch quality obtained was also very high at over 95%. The branch quality was found to be proportional to the ratio of the liquid phase depth to the distance of the interface below the branch entrance. Smoglie and Reimann (1986) also noted that this ratio (h/h_b) had critical values for differing orientations of the branch at which the second phase became entrained in the continuous phase in the branch. Smoglie and Reimann proposed an empirical correlation based on their data to predict the branch quality and mass flux from h/h_b which proved quite accurate. Maciaszek and Micaelli (1988) also used an empirical correlation, based on the data of Smoglie, to predict the phase split under LOCA conditions in the CATHARE reactor safety model.

Schrock et al (1986) produced a complementary correlation to that of Smoglie and Reimann which included data with the interface much closer to the branch entrance, as is the case in the separator passages. Schrock noted that as the interface approached the branch entrance the liquid entrainment increased considerably. Schrock also found that for a wavy interface the entrainment was unstable, coming from waves passing under the break entrance.

This flow pattern was noted in the separator passing the slot entrance, illustrating one mechanism by which liquid entrainment could occur in the take-off slots in the separator. The entrainment mechanism observed by Schrock and by Smoglie for liquid entrainment in an upward branch involved a locally raised liquid interface below the branch entrance from which droplets are torn off by the swirling gas flow entering the branch. This mechanism is similar to that noted for vapour or gas pull-through in a downward orientated branch or plug hole where a gas core is created. Once the entrainment became established the continuous two-phase entrainment flow was vortex free. Gardner (1990) examined flow through a plughole with air entrained in the off-take. Theory indicated that a correlation based on the light and heavy phase Froude Numbers would prove useful. Gardner plotted these criteria for various circulation angles in the liquid phase and found reasonable agreement with the experimental data when using quiescent liquid above the plughole. The correlation of Gardner showed agreement with some of the data of Smoglie and of Schrock, despite the crossflow across the off-take in the latter two data sets. The work of Gardner offers further confirmation that the quality of the take-off flow is dependent on the depth of the phase adjacent to the off-take.

4.5.4 Comparison with Experimental Data

The slot quality data from the air/kerosene separation experiments was compared with the predictions of the Smoglie and the Schrock theories and correlations. For a junction with a horizontal run and a vertical branch (analogous to the take-off slots in the separator) the geometric model and the zone of influence/dividing streamline models are unsuitable: these models predict that only gas will be removed by the branch for stratified flows in the run [this limitation was also noted by Azzopardi, 1990].

The correlations of both Schrock and Smoglie require information on the heights of the gas and liquid phases. The level of the liquid interface in the helical passage, which was difficult to measure under experimental conditions, was predicted using the stratified flow model, developed in section 4.2, at the flow conditions used in the take-off slot experiments. The levels were found to be outside the range of the experiments conducted by Smoglie and so this correlation was of little value and predicted branch qualities of around 100%. The correlation arrived at by Schrock was determined for similar values of flow quality to those used in the separator experiments, although Schrock used air/steam and air/water rather than air/kerosene. This correlation proved to be the most suitable because of the close approximation of the experimental conditions to those of the data for which the correlation was established.

The correlation of Schrock et al (1986) predicted the air/kerosene data from the separator experiments well, Fig. 4.38 (the Smoglie correlation predicted much greater branch qualities), showing the same trend as the data and similar values of branch quality to

those found experimentally. Schrock gave the correlation in terms of the dimensionless distance of the gas/liquid interface from the branch entrance:

$$x = \left[\frac{h}{h_b} \right]^{3.25(1-h/h_b)^2} \qquad (4.35)$$

The experimental data was plotted using the phase depth results from the separated flow model at the experimental initial conditions. The data is shown at the five void fractions which pertain to the experimental conditions in the helical passages.

The experimental data for the higher void fractions used, 20% and over, agree very well with the Schrock correlation. At the lower values of void fraction used, the experimental data from the take-off slot shows higher quality than that predicted by the Schrock correlation. The divergence at these lower values of h/h_b is understandable because these data are outside the range used by Schrock to fit the correlation. The only data given by Schrock in this region was in good agreement with the experimental data from the take-off slot.

The agreement of the data from the take-off slot experiments with the Schrock correlation shows that the entrainment of the liquid phase into the slot takes place via a similar mechanism to that observed by both Schrock and Smoglie. That is, that a local deformation of the gas/liquid interface occurs below the slot due to the movement of gas from the passage into the slot. Once the interface has been sufficiently raised below the slot entrance the

local decrease in pressure caused by the increase in the local gas velocity at the slot entrance is sufficient to entrain liquid droplets in the gas flow. These droplets are then carried into the take-off slot by the gas take-off flow.

The closeness of the agreement of the take-off slot data with the Schrock correlation was surprising given the differences in the geometry between the two sections. The centrifugal forces in the separator were much greater than natural gravity and would thus have acted to reduce the liquid entrainment into the take-off slots. The quality of the take-off slot flow would be expected to be greater than that for a similar flow under natural gravity. However, the length of the slots will lead to a greater liquid entrainment than that for a circular cross-section branch of similar area.

4.6 Predictions of Two-phase Gas/liquid Behaviour in the Separator Helical Passages

4.6.1 Performance of Two-phase Separated Flow Model

The two-phase separated flow model was used to predict the individual phase areas occupied by the gas and liquid phases in a helical duct. The model was verified by using the pressure drops found in the separator air/kerosene experiments. The gas and liquid phase areas achieved stable values after a short development length when under the influence of the centrifugal force caused by the helical motion of the fluid. The model predicted the experimental pressure drops well at all the flow conditions, giving confidence in the phase area and velocity predictions. The magnitude of the phase area predicted for the helical ducts was dependent on the void

fraction of the flow. In contrast, the model was run using gravity to simulate a horizontal duct. No stable solution could be obtained under these conditions which indicated an intermittent flow.

4.6.2 Experimental Investigation of Helically Coiled Tubes

The experimental work carried out on air/water flow in helical coils showed that the helix angle of the tubes had no direct effect on the pressure losses in the tubes. The helix angle did affect the magnitude of the centrifugal force generated in the coils. The magnitude of the centrifugal force influenced the flow pattern in the coils, particularly at low mass flux. The flow pattern had some influence on the two-phase pressure drop in the coils. As the centrifugal forces were increased the separation of the phases increased and produced a more defined separated flow pattern. As the separation became better defined the two-phase pressure losses reduced, for a given mass flux and void fraction. The separation of the phases was improved at the smallest helix angle, indicating that at lower passage velocity the gas/oil separator performance may be improved by a smaller helix angle.

4.6.3 Prediction of Take-off Slot Quality

The experimental data from the individual slot investigations were compared with theories developed to predict the two-phase flow split in pipe branches and tee junctions. Some experimental data reported in the literature for tee junctions with vertical branches were found to be in close agreement with the data from the separator take-off slots. The quality of the take-off flow

through the slots was shown to be related to the dimensionless distance of the gas/liquid interface from the slot entrance. The closer the interface was to the slot entrance the greater was the proportion of the liquid phase which was drawn through the take-off slot and thus the lower the quality of the take-off slot flow. Thus the separation quality will be highest at the highest void fractions.

4.6.4 Overall Performance Prediction

The performance of the separator may be predicted using a combination of the models described above in conjunction with some of the empirical correlations confirmed earlier by experiment, providing that the inlet conditions to the separator are known. The separated two-phase flow model provided information on the gas and liquid phase areas at a given point in the helical passages. The slot flow model can then be used to predict the quality of the flow through the slot and the flow rate through the slot. From this information the quality of the internal gallery flow and the flow exiting from the helical passages can be deduced.

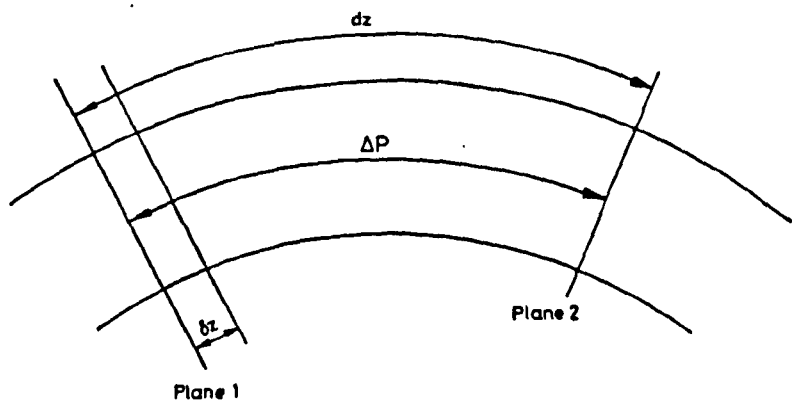

Figure 4.1 Helical duct

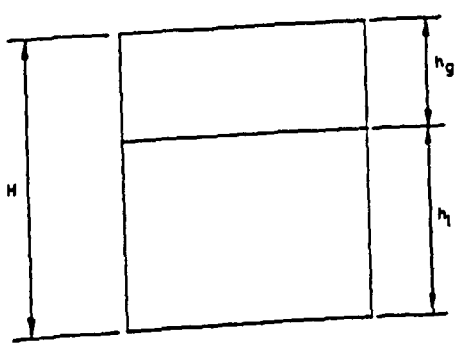

Fig. 4.2a Rectangular Cross-Section

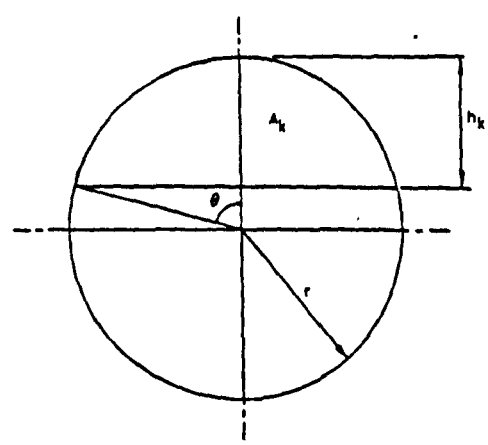

Fig. 4.2b Circular Cross-Section

Figure 4.2 Rectangular and circular cross-section ducts

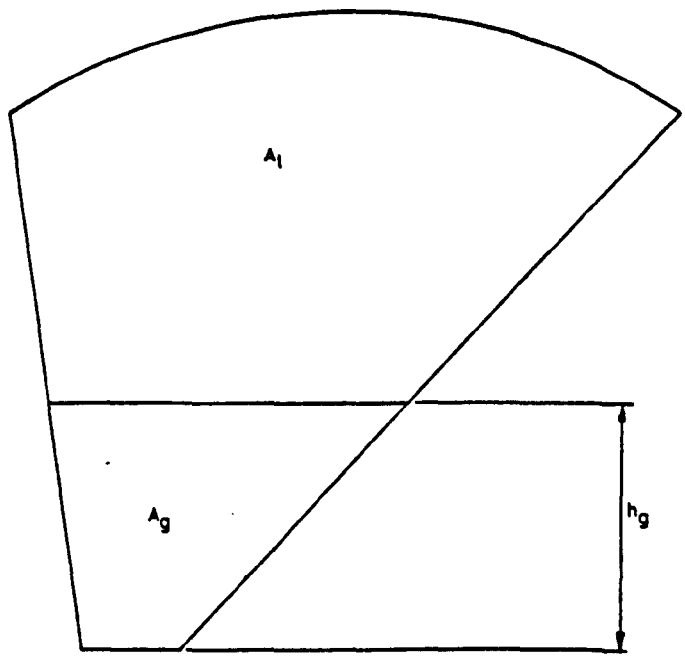

Figure 4.3 Triangular cross-section duct

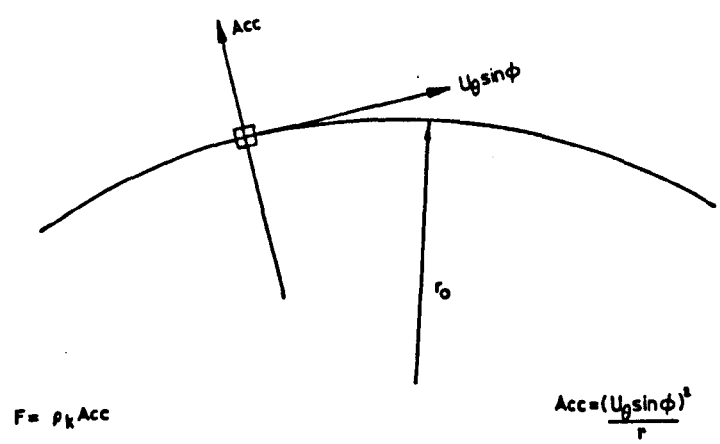

Figure 4.4 Forces generated by curved path of fluid

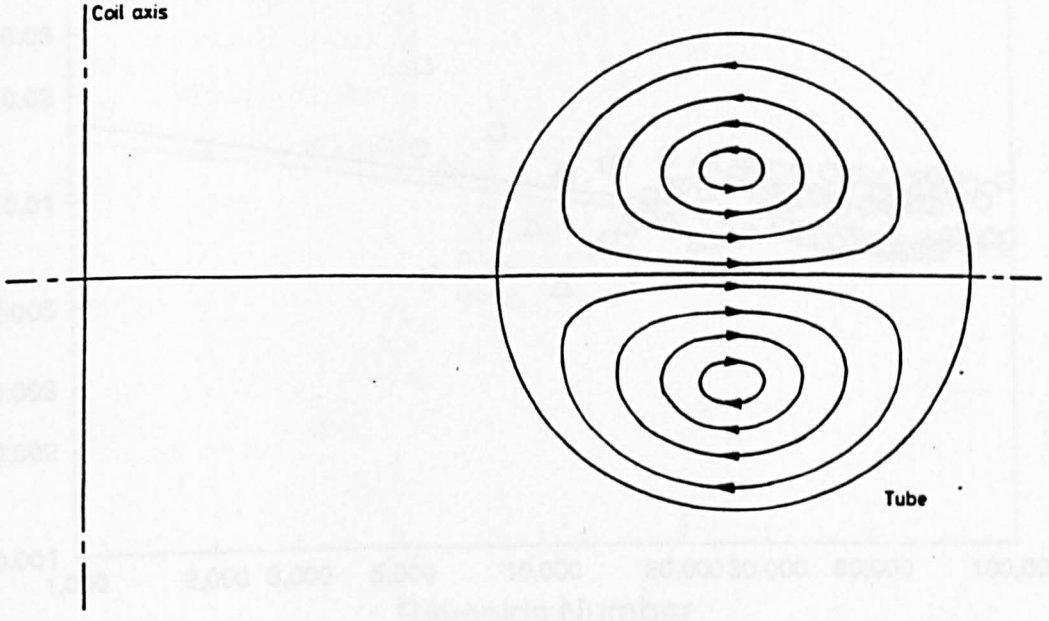

Figure 4.5 Secondary flow in coiled tube

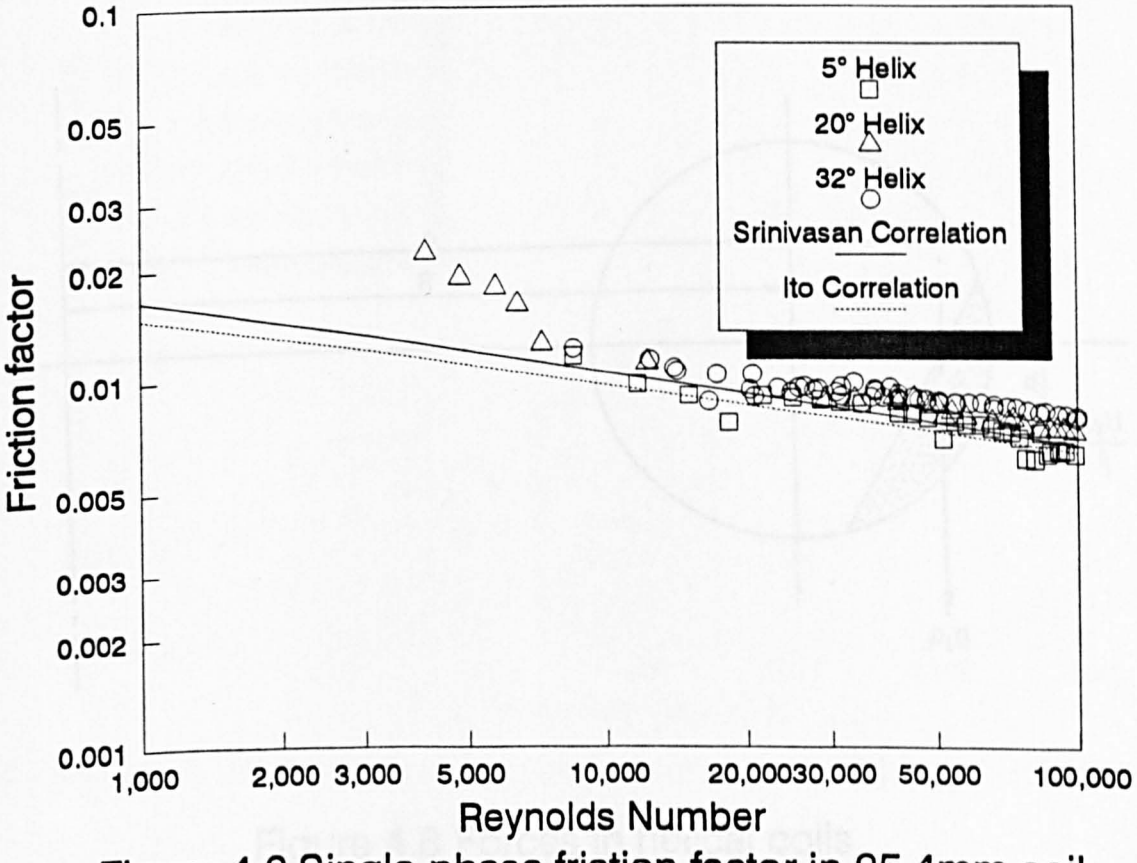

Figure 4.6 Single-phase friction factor in 25.4mm coil

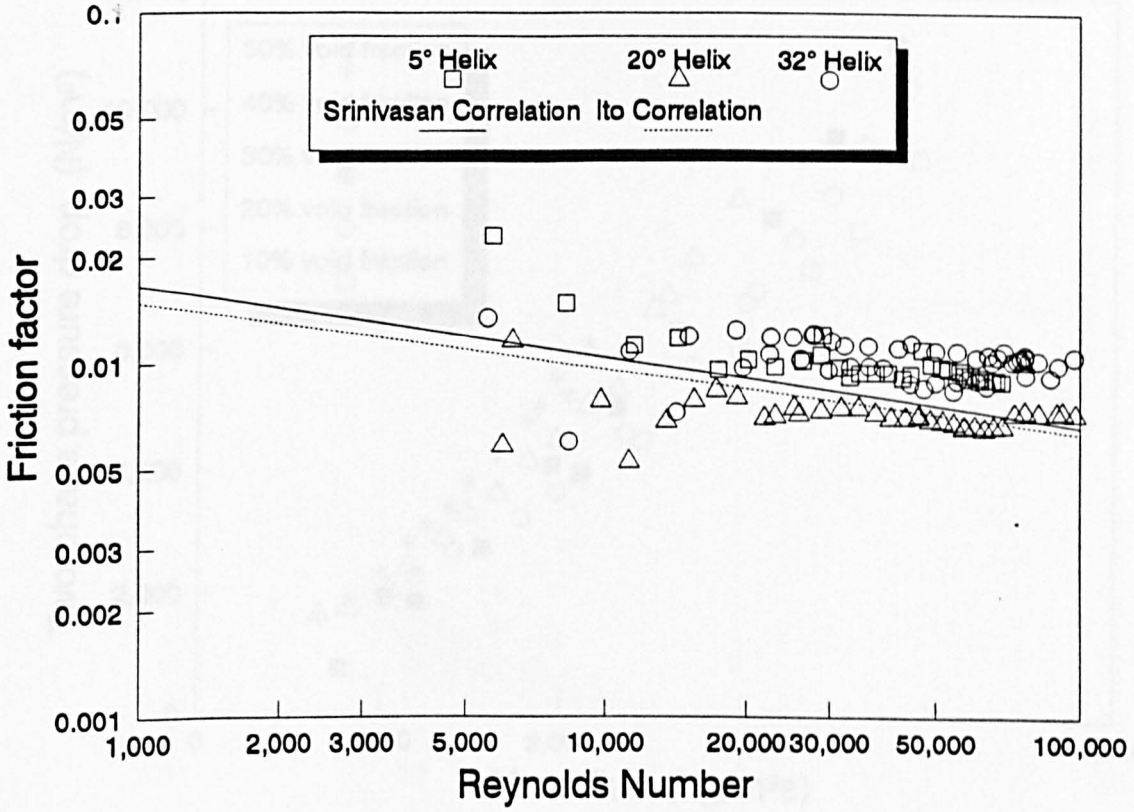

Figure 4.7 Single-phase friction factor in 38.1mm coil

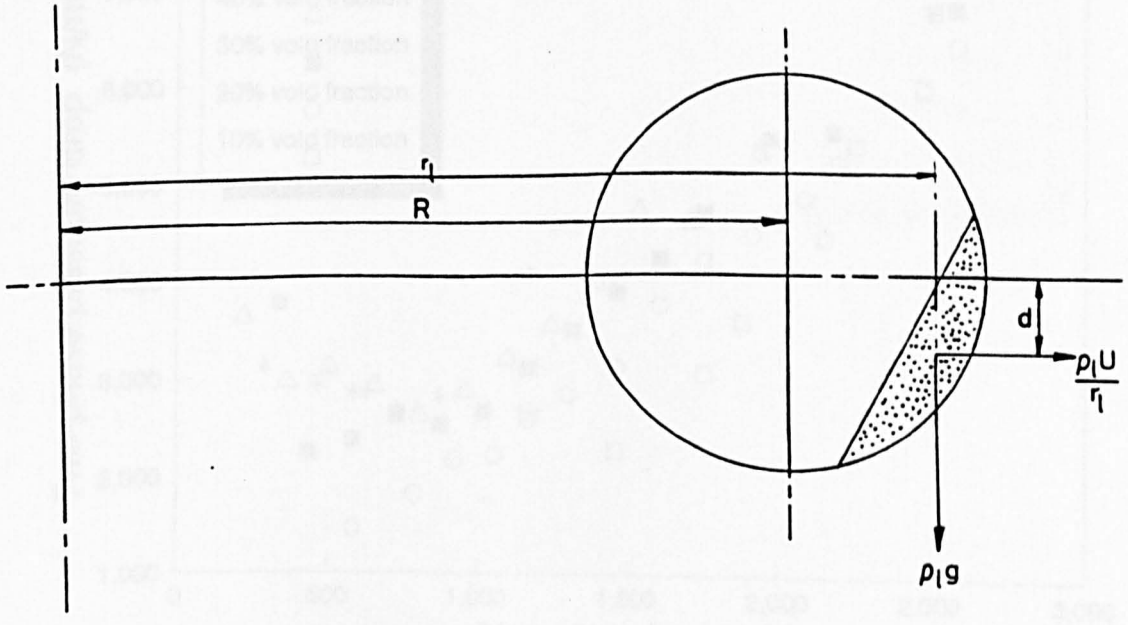

Figure 4.8 Forces in helical coils

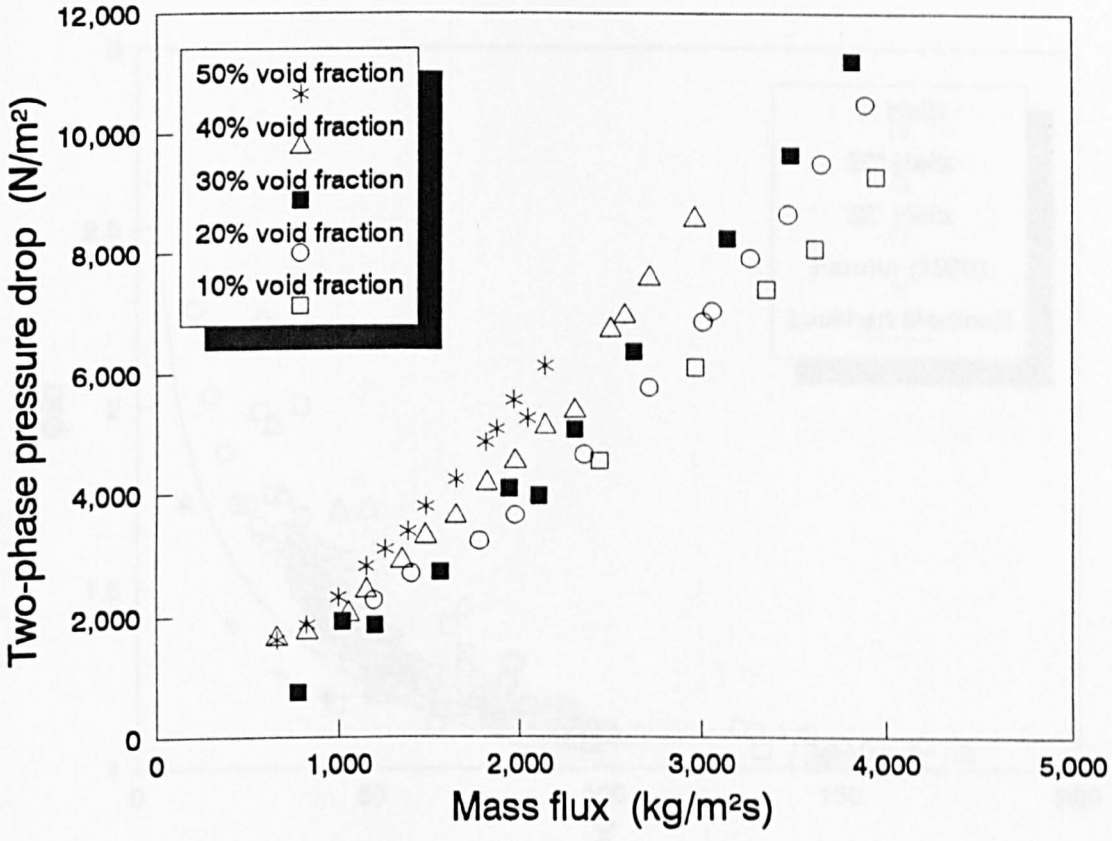

Figure 4.9 Two-phase pressure losses in 25.4mm coil at 5° helix angle

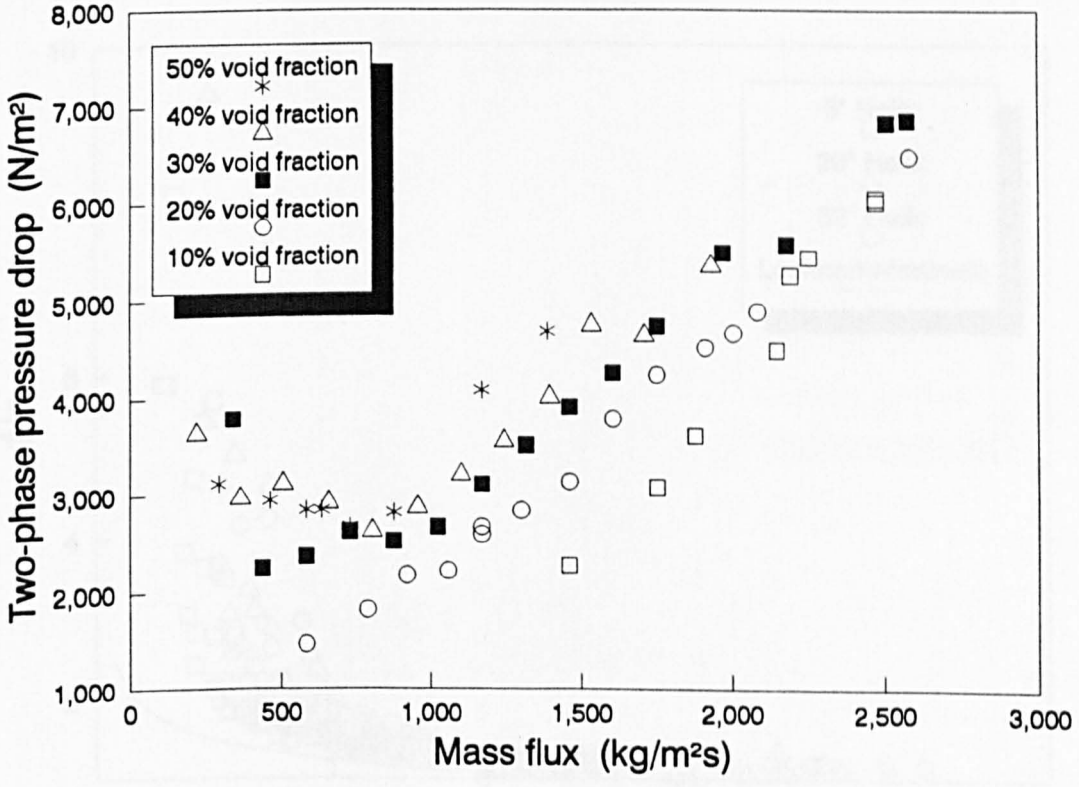

Figure 4.10 Two-phase pressure losses in 38.1mm coil at 5° helix angle

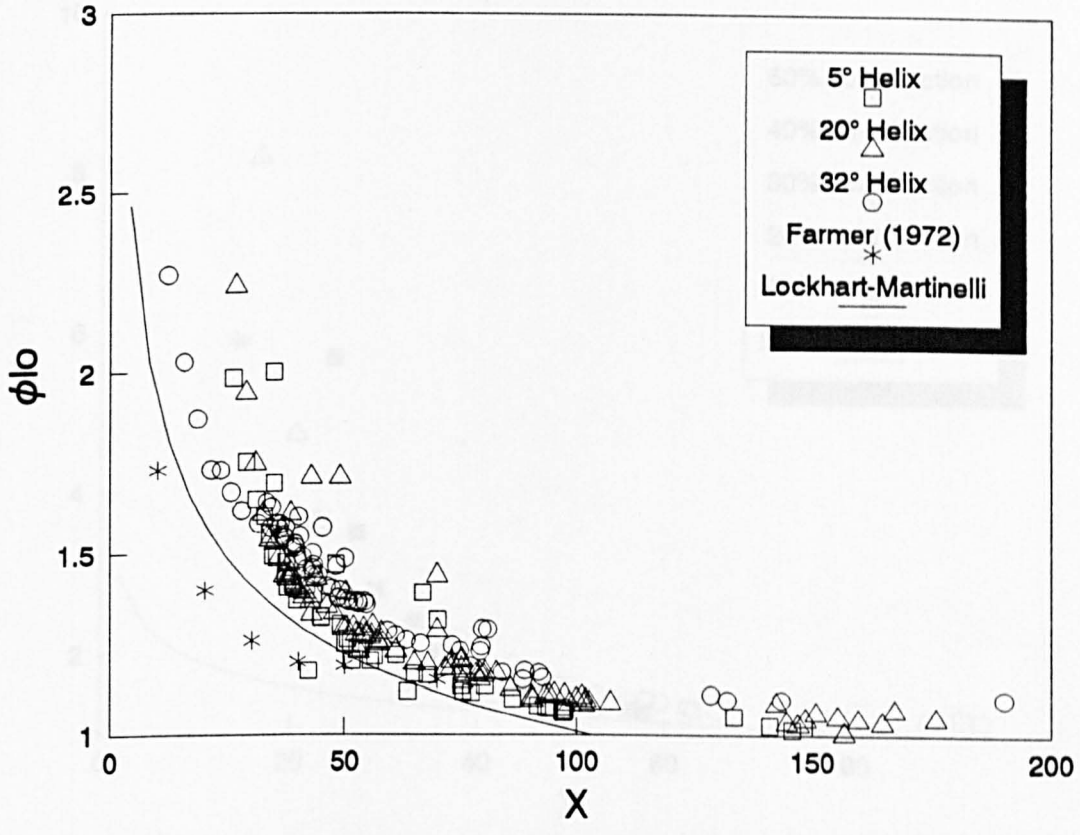

Figure 4.11 ϕlo in 25.4mm coil

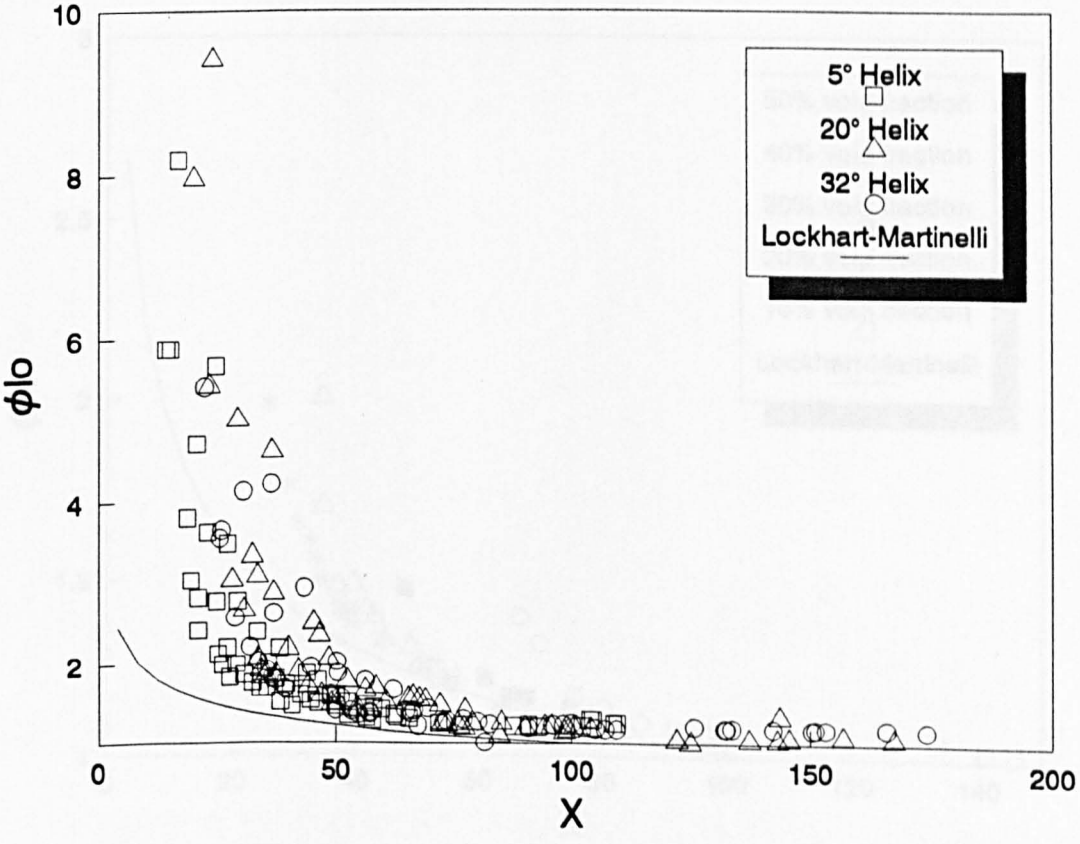

Figure 4.12 ϕlo in 38.1mm coil

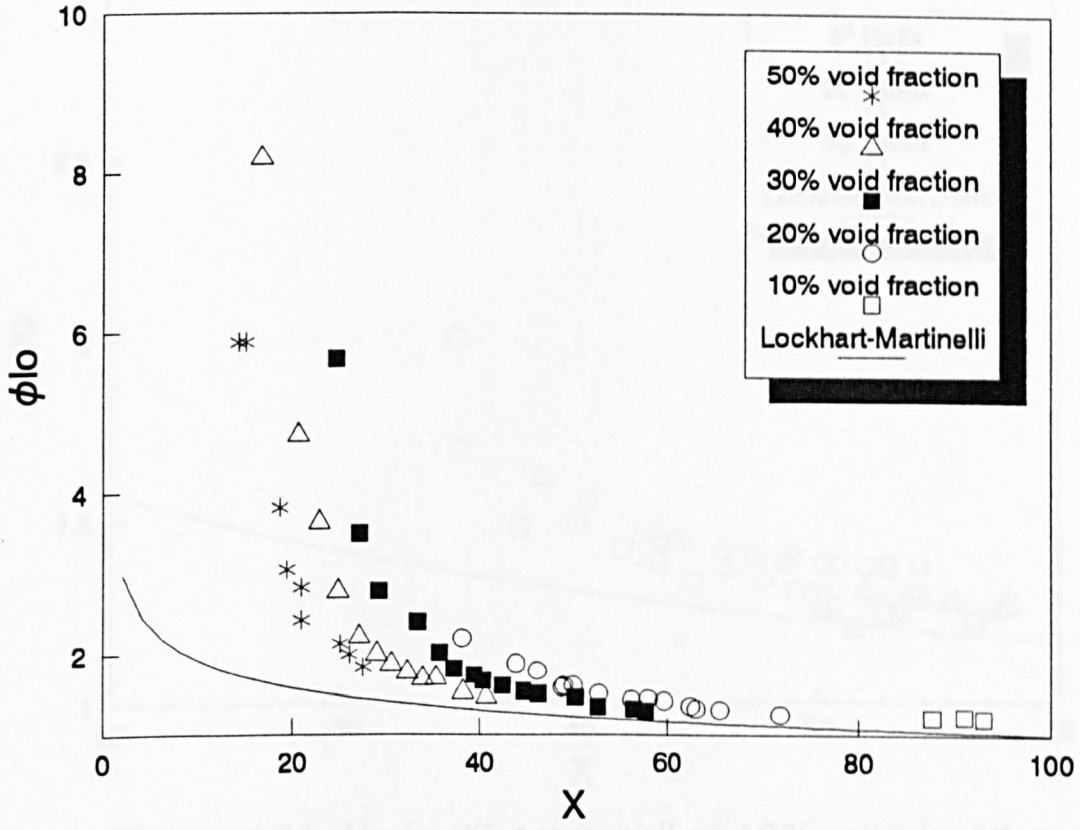

Figure 4.13 ϕlo in 38.1mm coil at 5° helix angle

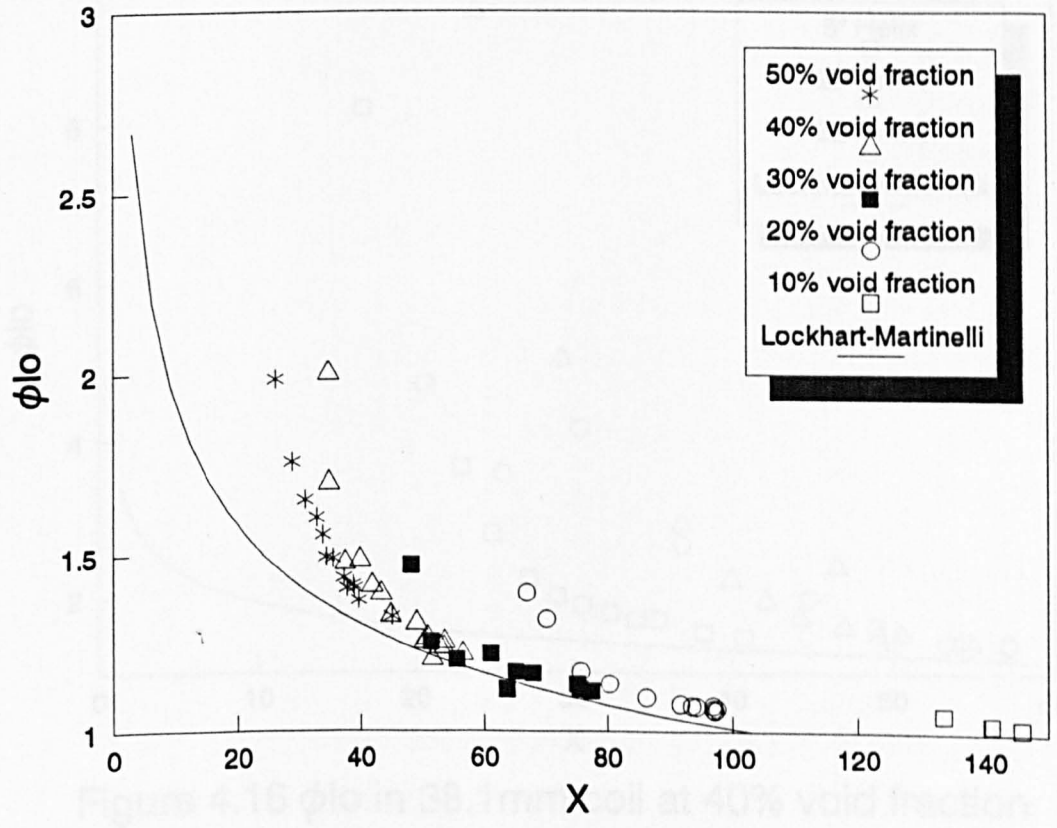

Figure 4.14 ϕlo in 25.4mm coil at 5° helix angle

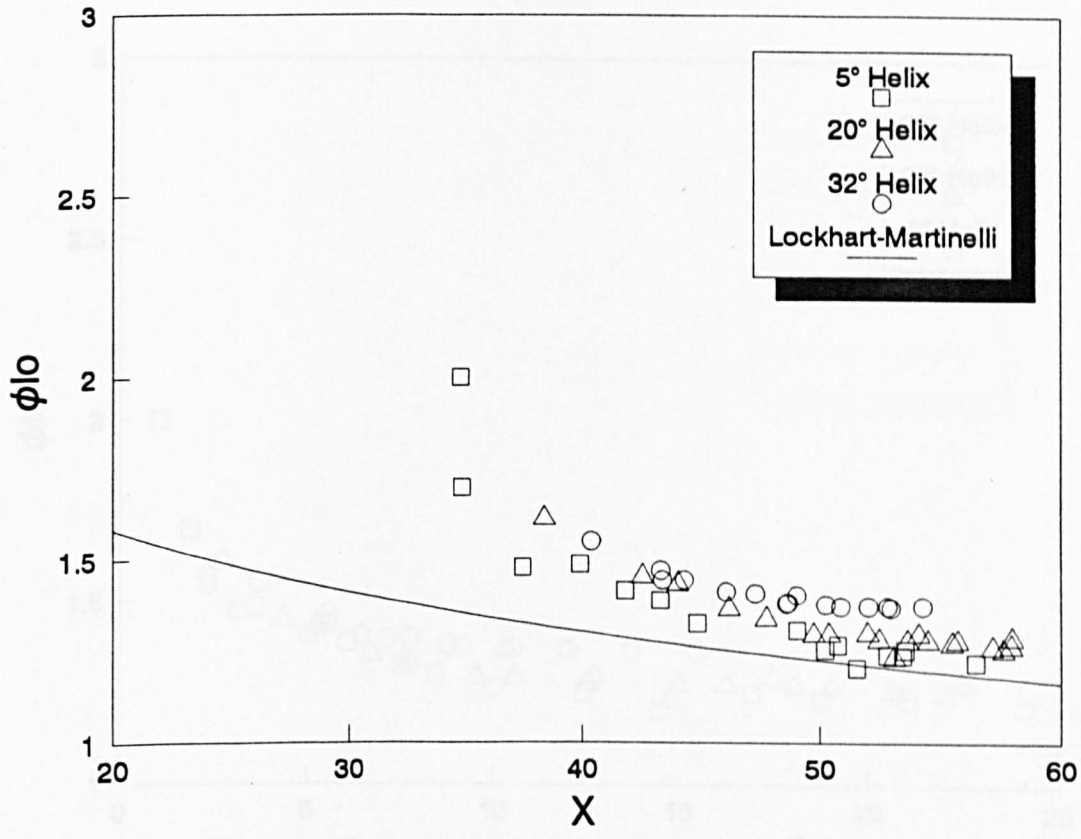

Figure 4.15 ϕlo in 25.4mm coil at 40% void fraction

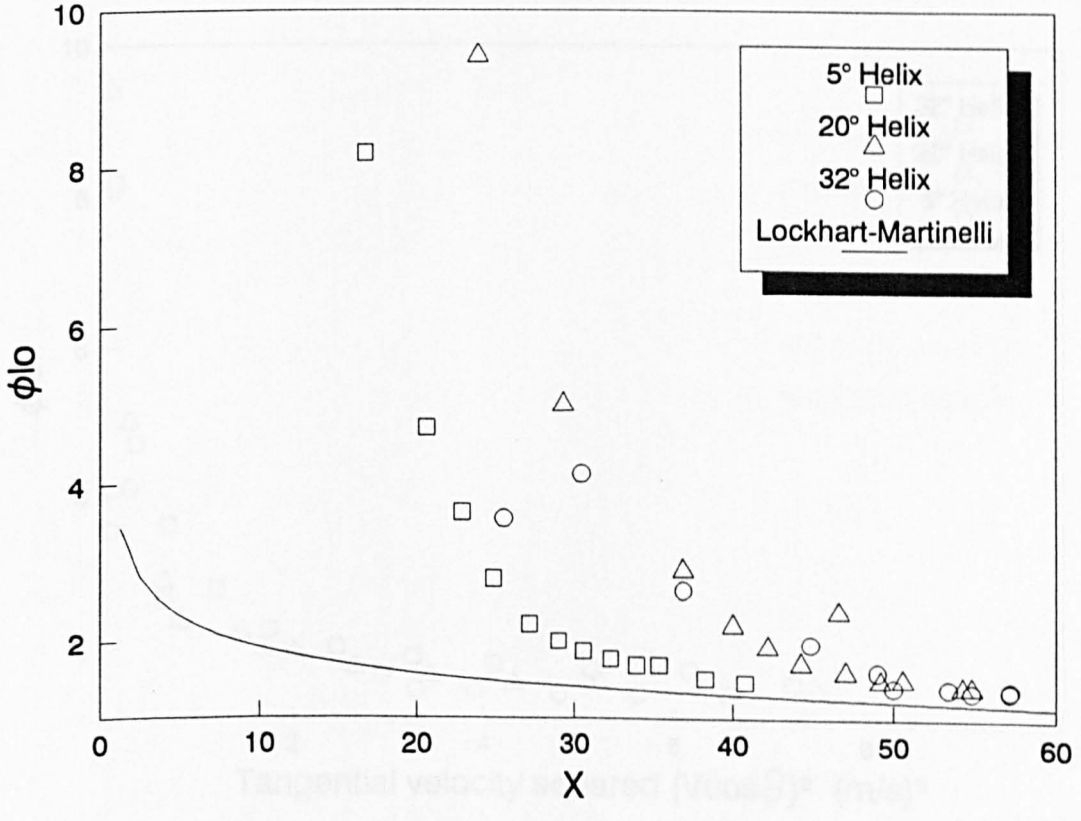

Figure 4.16 ϕlo in 38.1mm coil at 40% void fraction

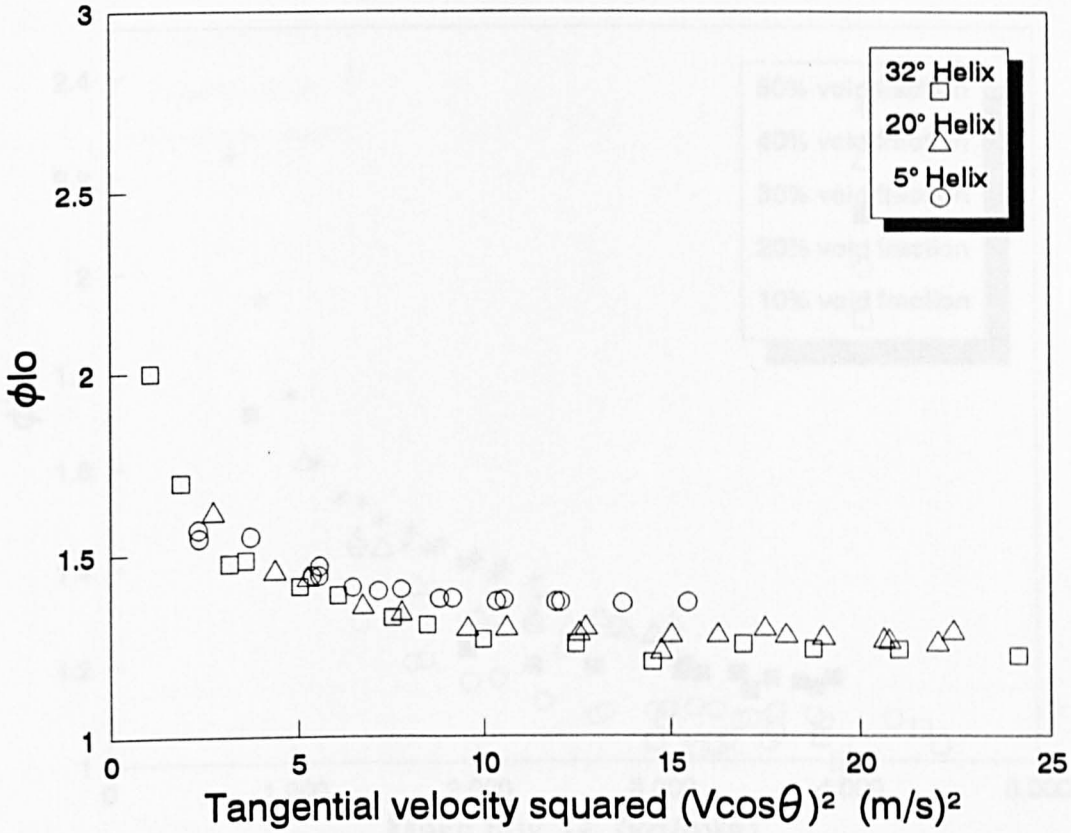

Figure 4.17 ϕlo vs. velocity squared in 25.4mm coil at 40% void fraction

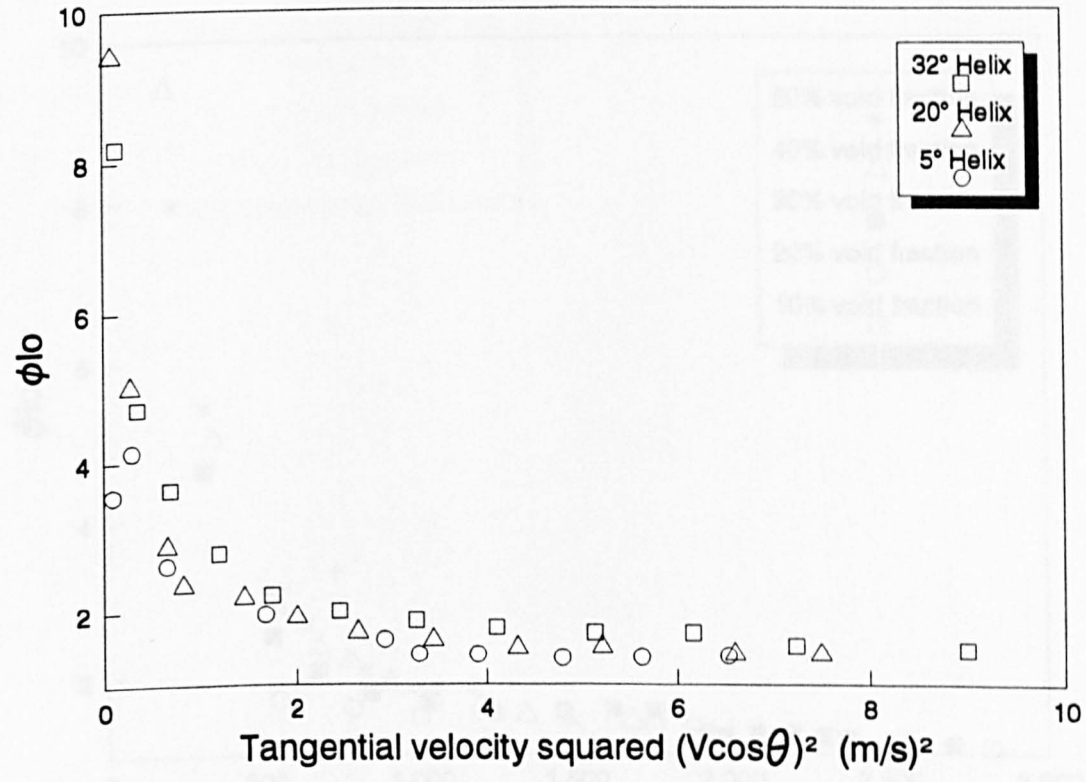

Figure 4.18 ϕlo vs. velocity squared in 38.1mm coil at 40% void fraction

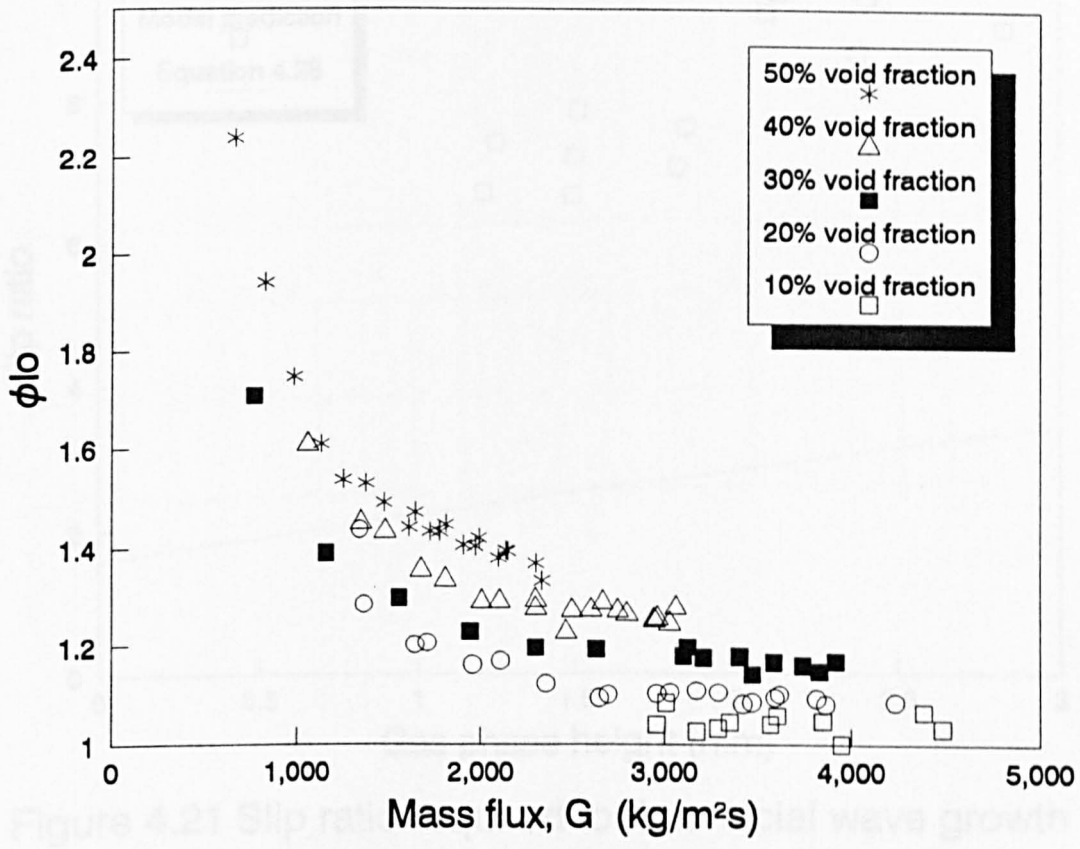

Figure 4.19 ϕlo in 25.4mm coil at 5° helix angle

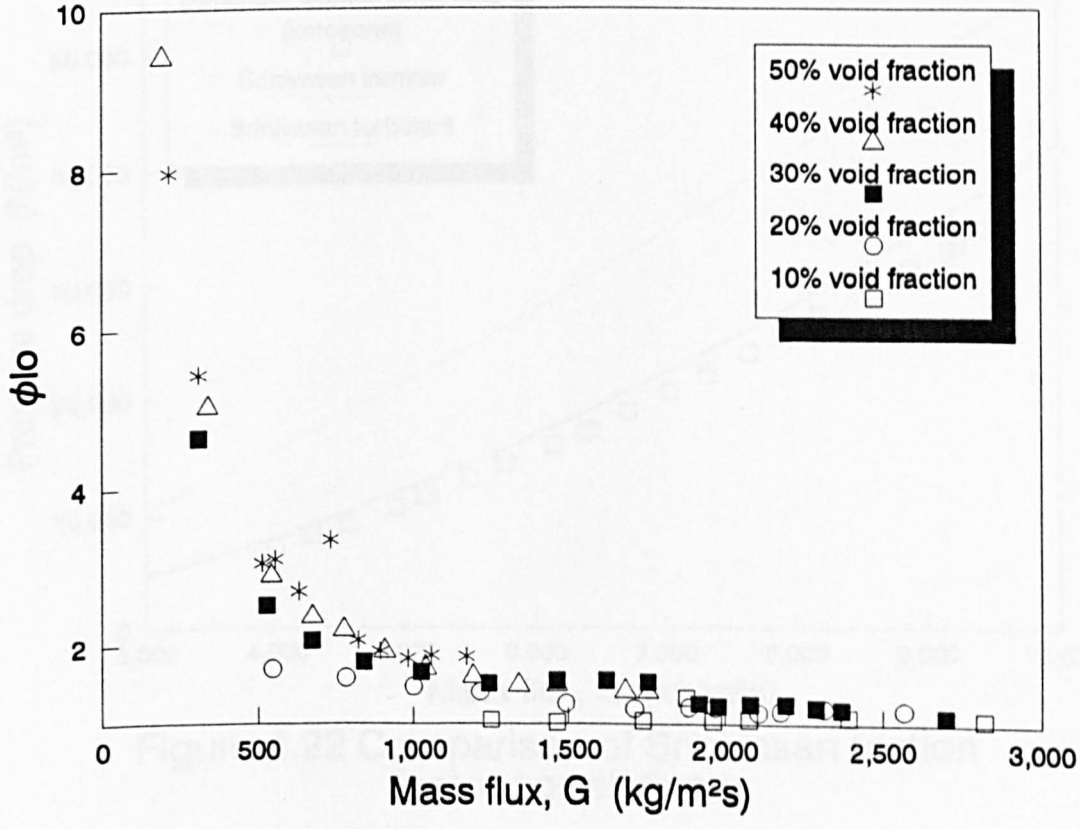

Figure 4.20 ϕlo in 38.1mm coil at 5° helix angle

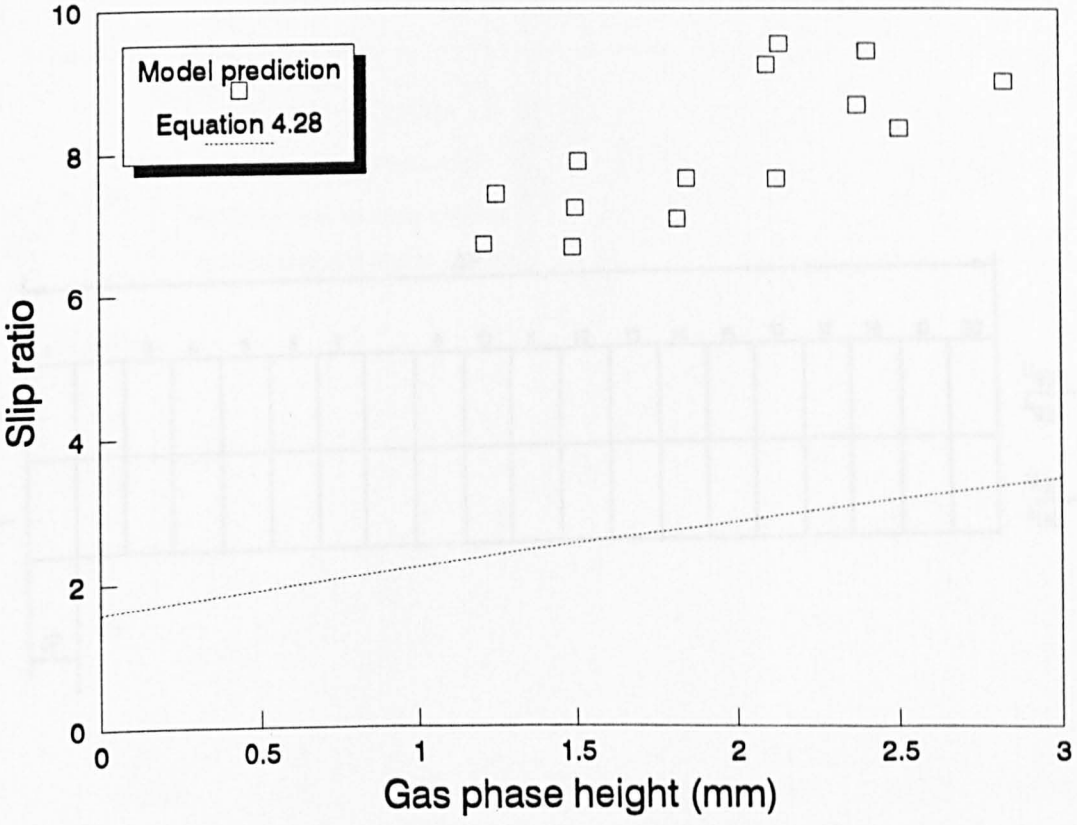

Figure 4.21 Slip ratio required for interfacial wave growth

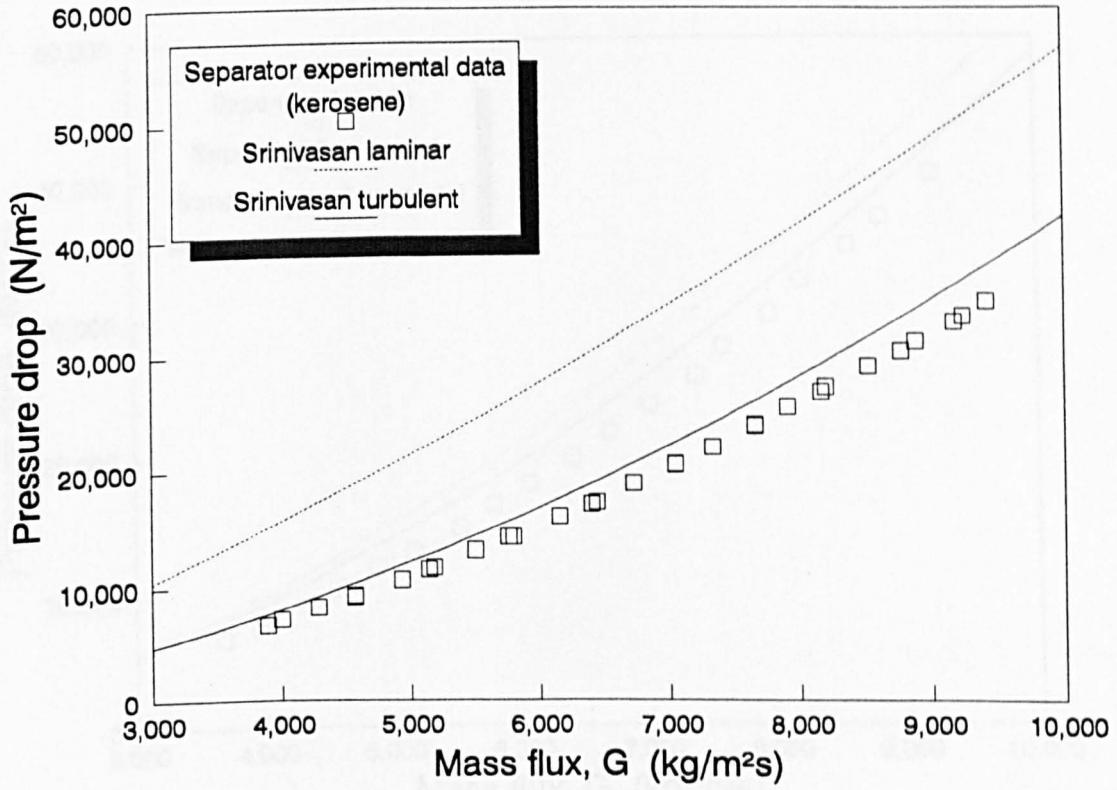

Figure 4.22 Comparison of Srinivasan friction factor correlations

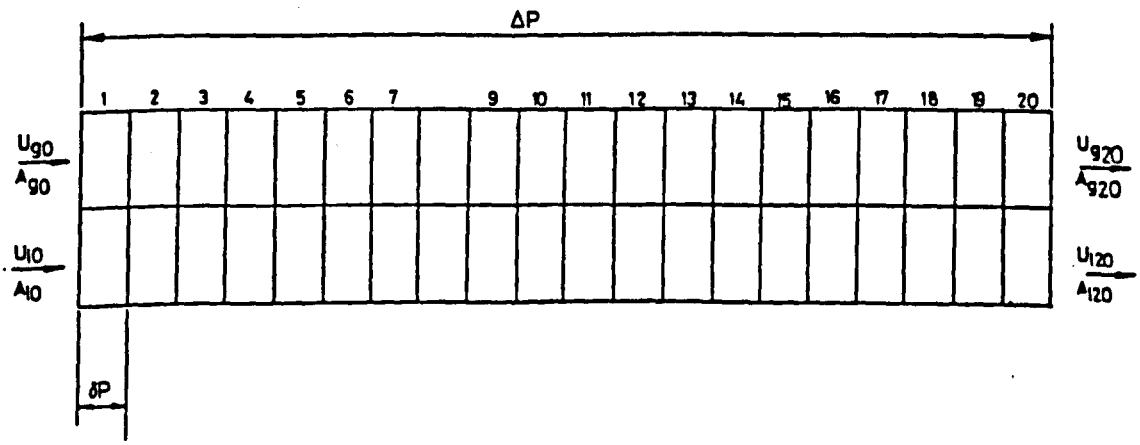

Figure 4.23 20 cell model of helical duct

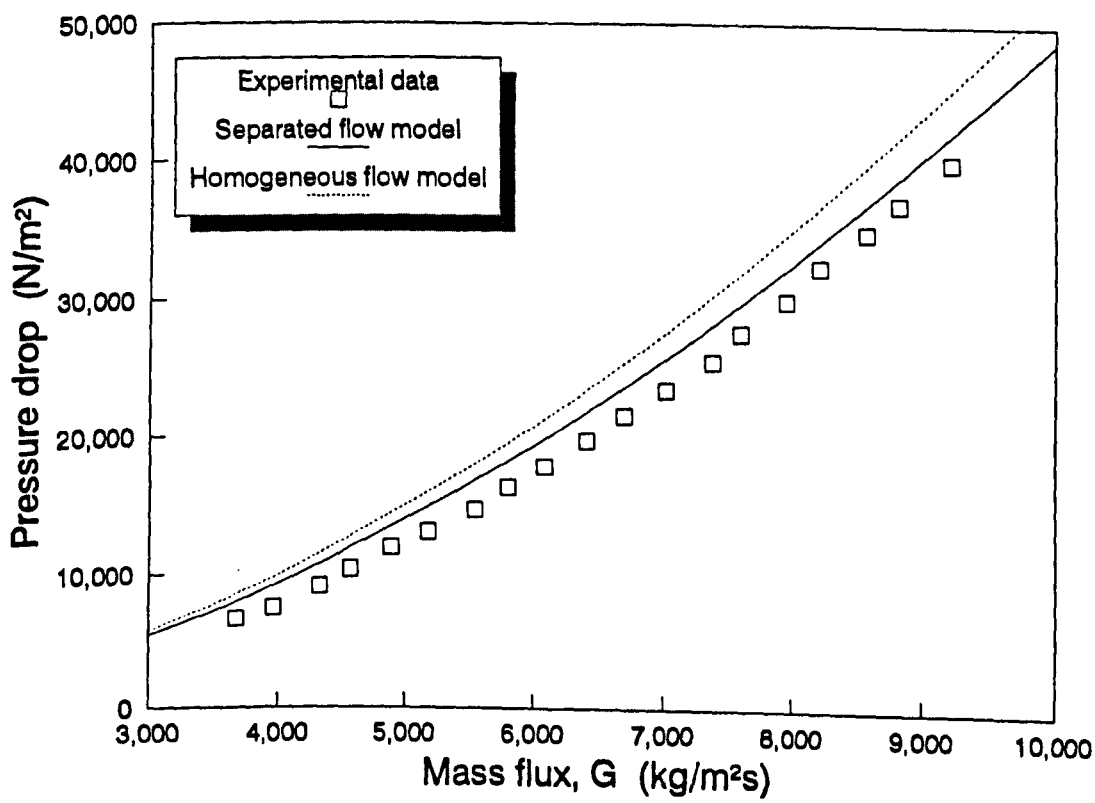

Figure 4.24 Experimental data for model results at 10% void fraction

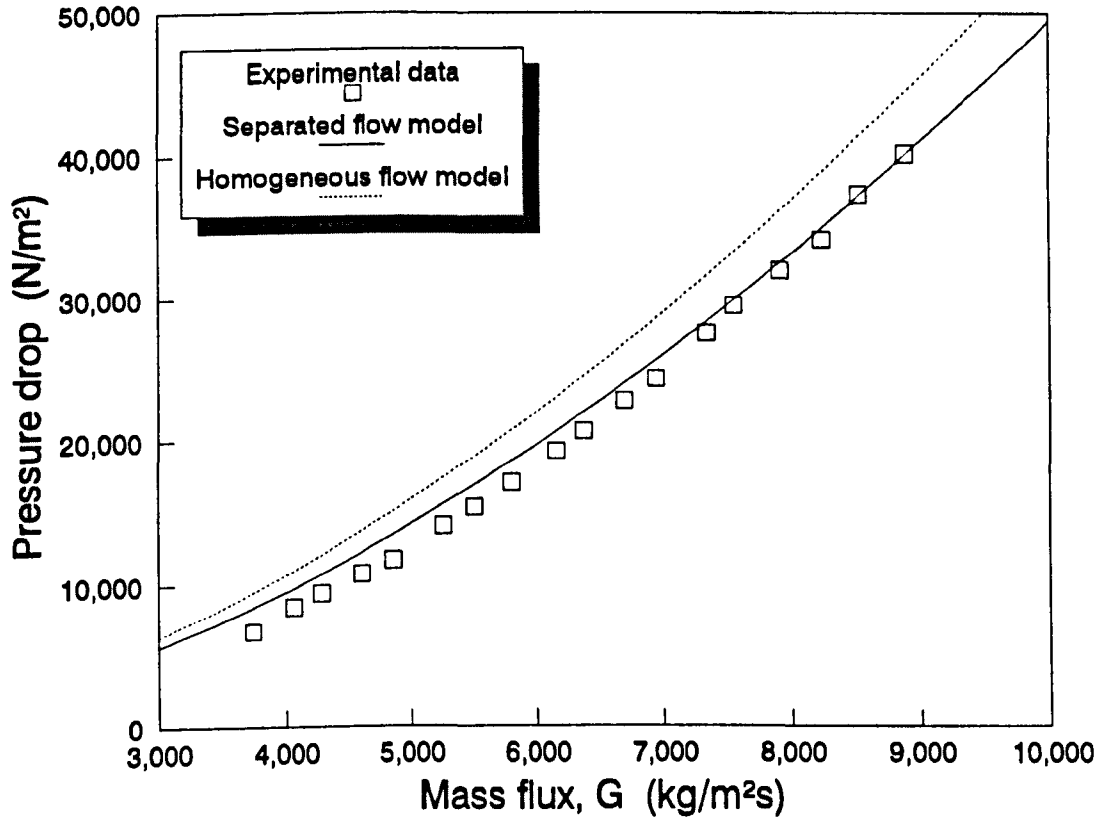

Figure 4.25 Experimental data for model results at 15% void fraction

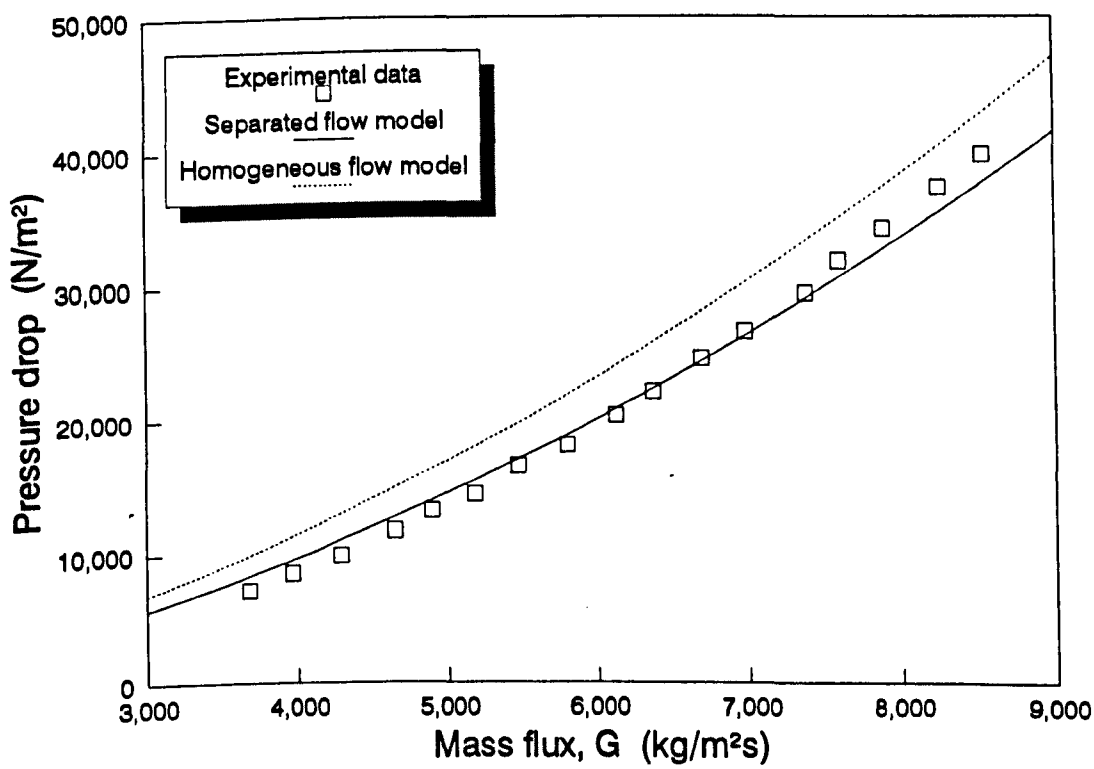

Figure 4.26 Experimental data for model results at 20% void fraction

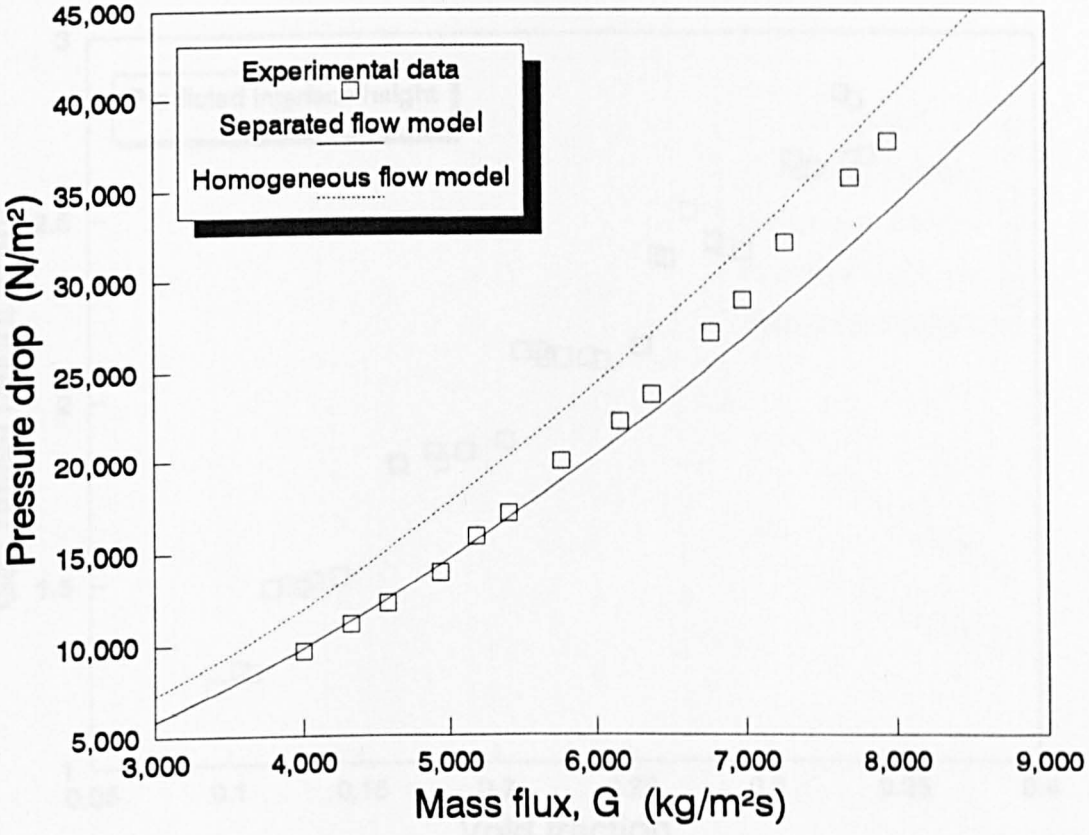

Figure 4.27 Experimental data for model results at 25% void fraction

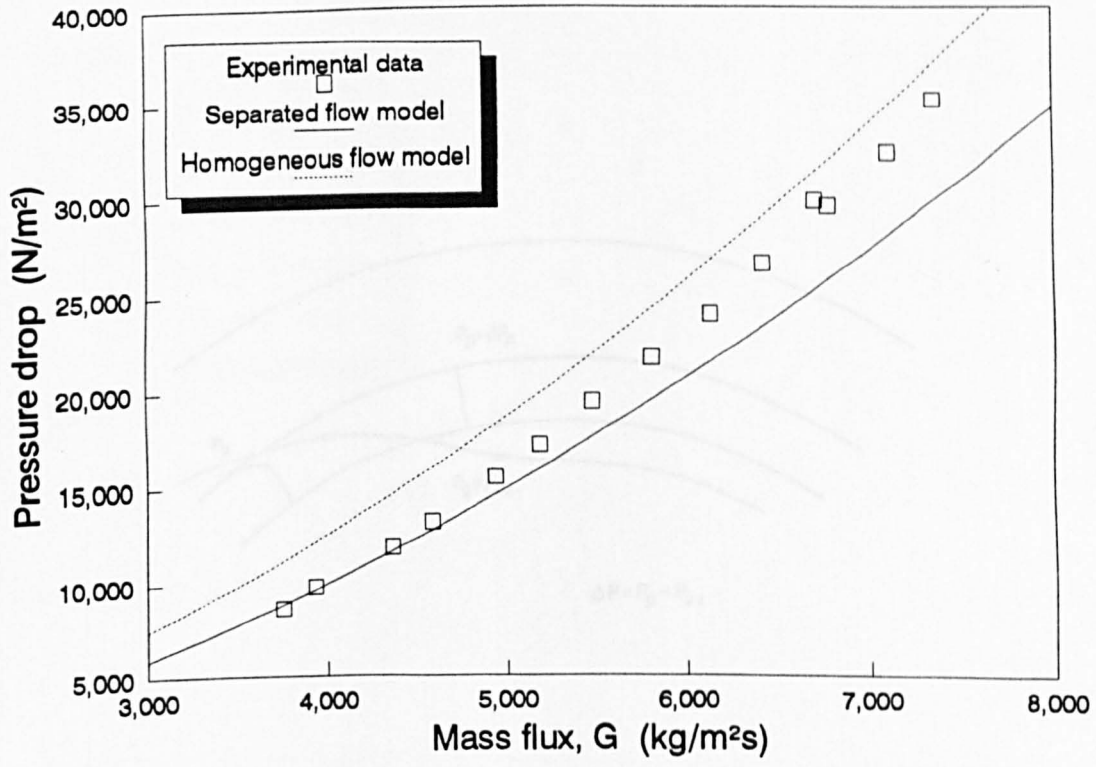

Figure 4.28 Experimental data for model results at 30% void fraction

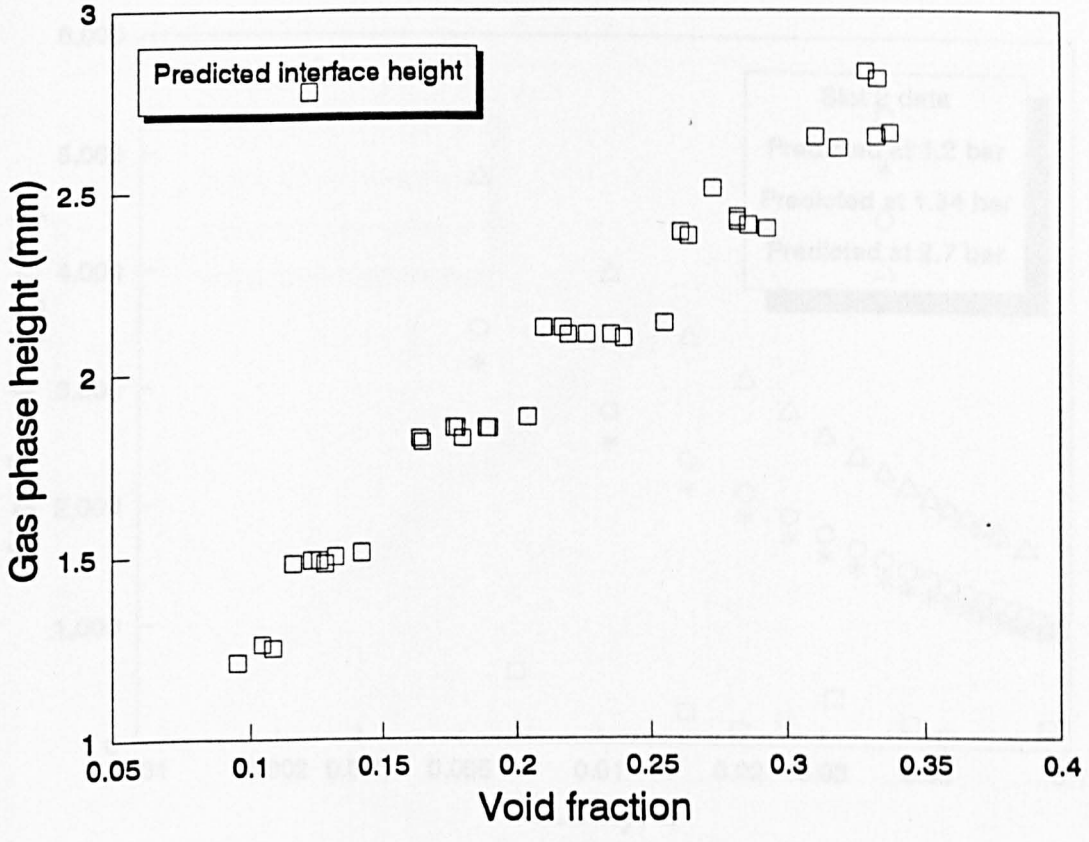

Figure 4.29 Separated flow model interface height prediction

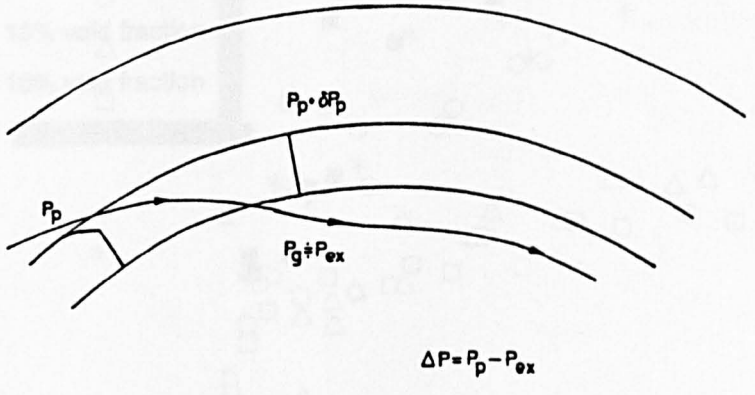

Figure 4.30 Flow through take-off slot

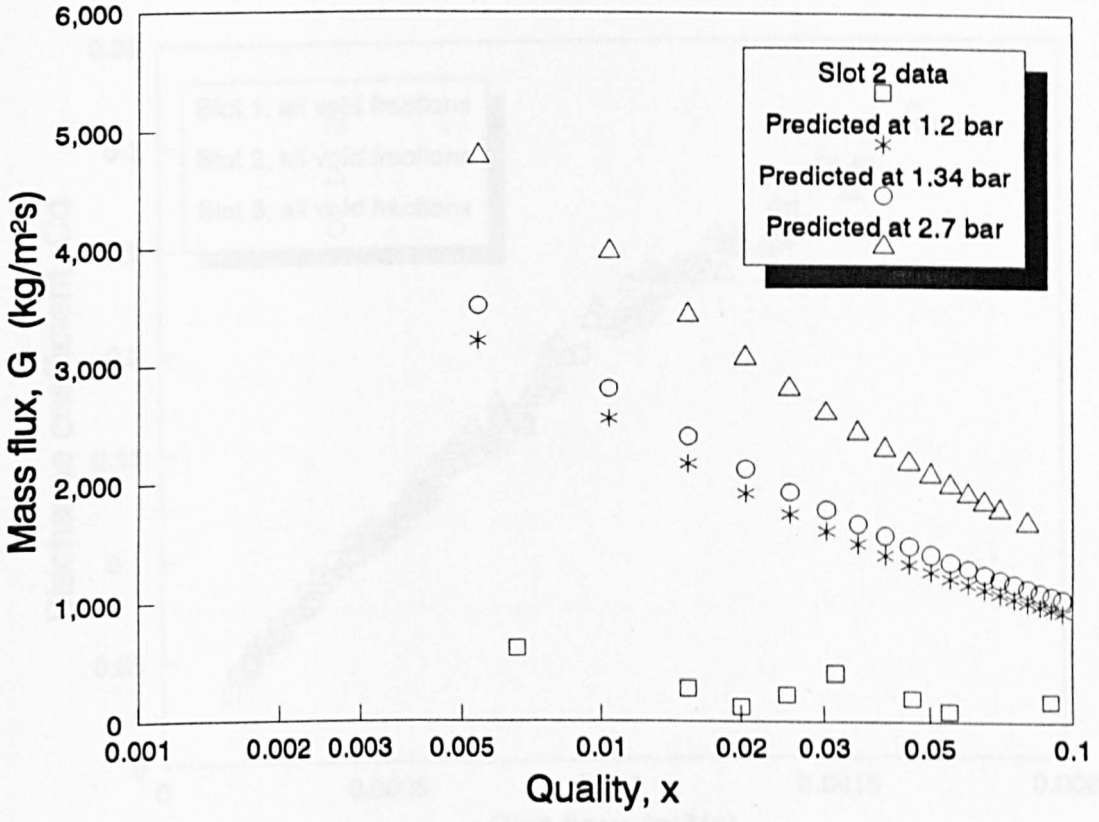

Figure 4.31 Choking condition at slot 2

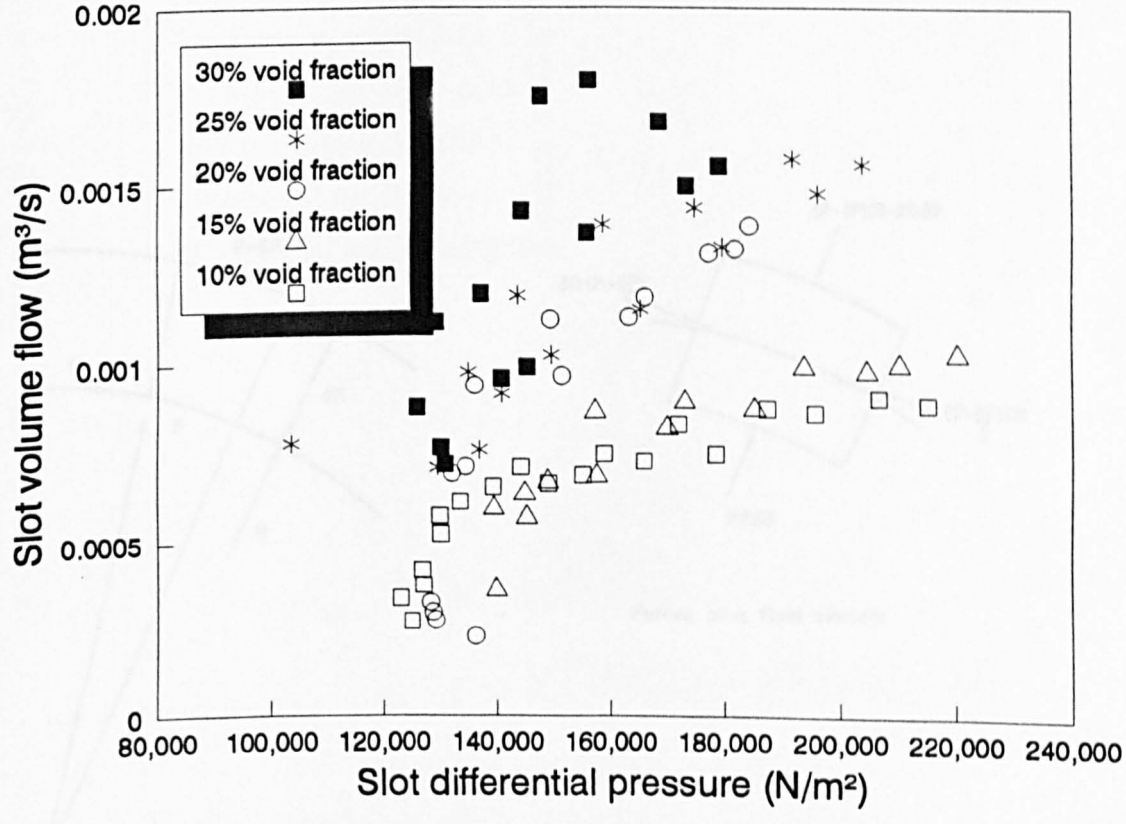

Figure 4.32 Total slot flow for Slot 1 in air/kerosene flow

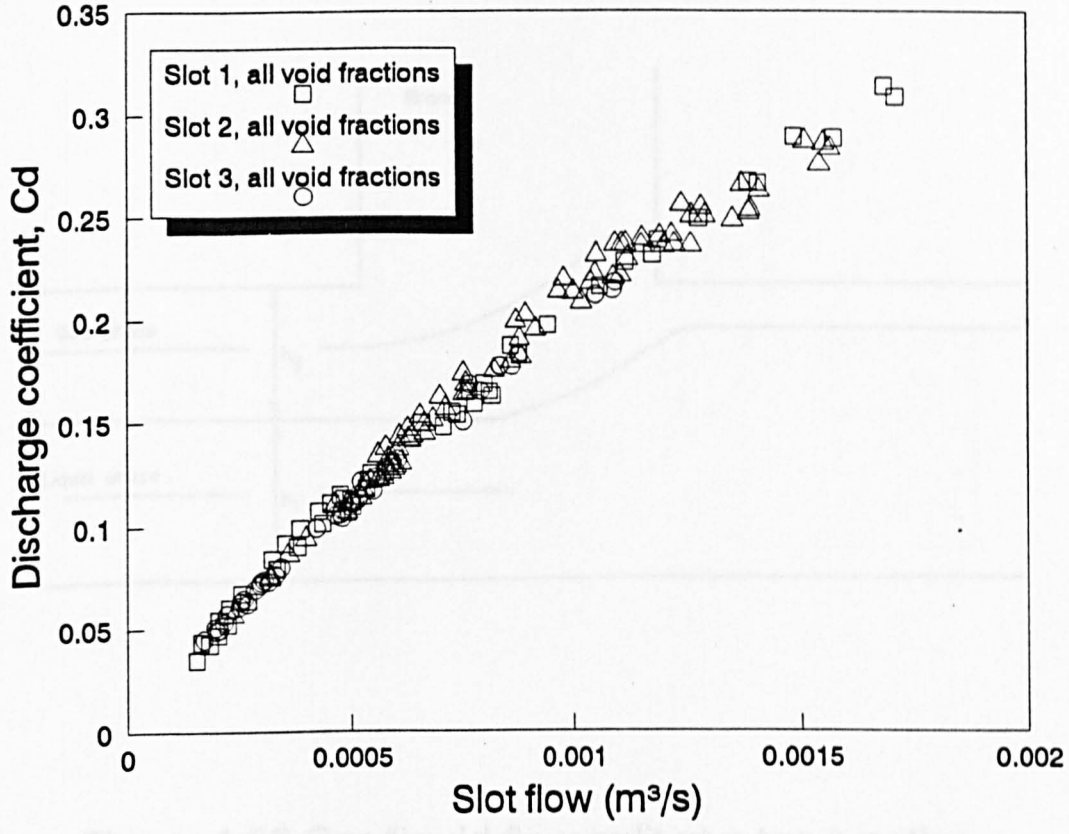

Figure 4.33 Take-off slot discharge coefficients

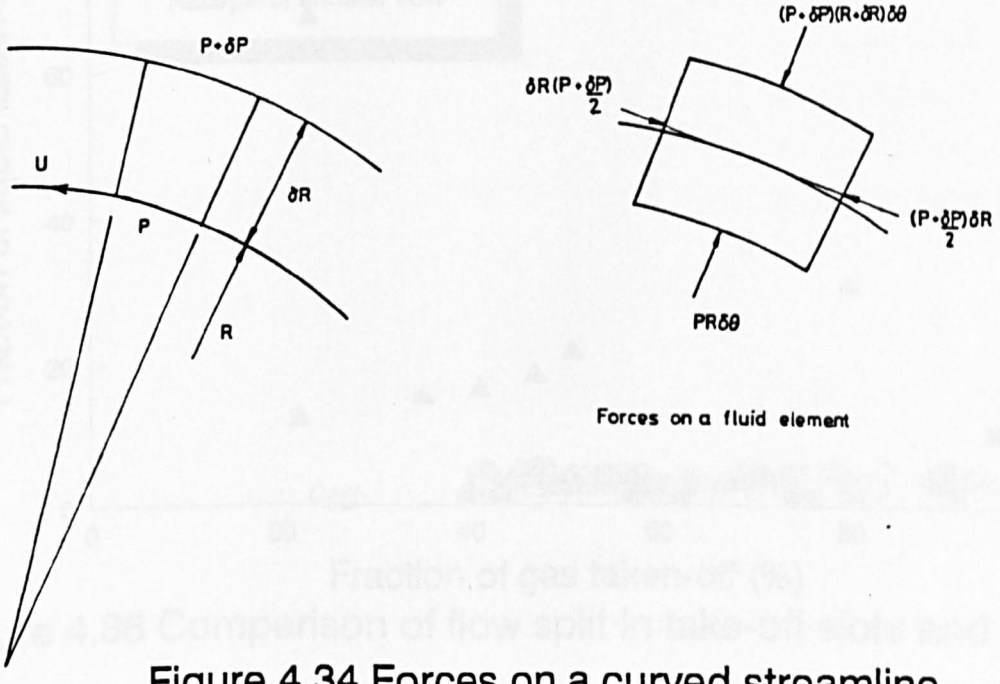

Figure 4.34 Forces on a curved streamline

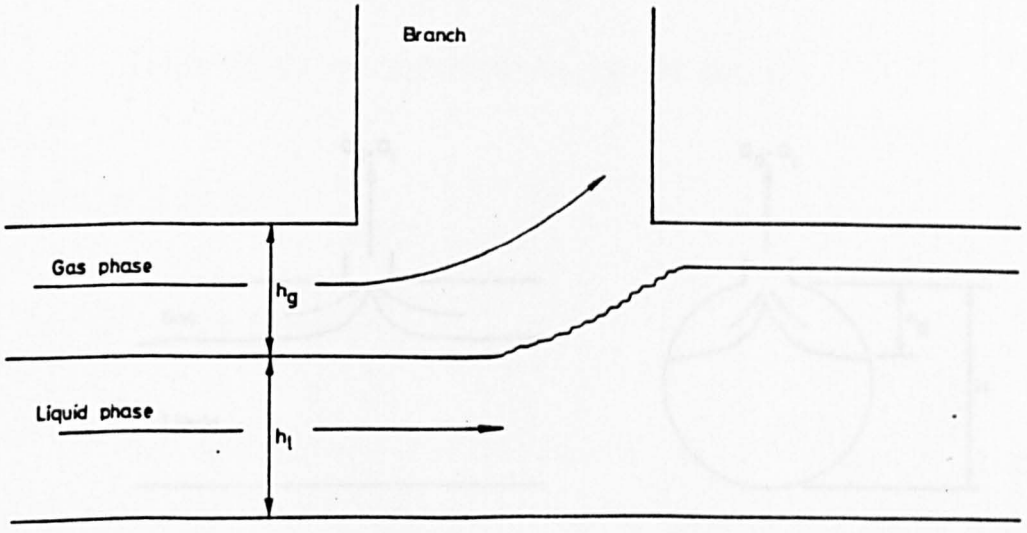

Figure 4.35 Gas/liquid flow split at a tee junction

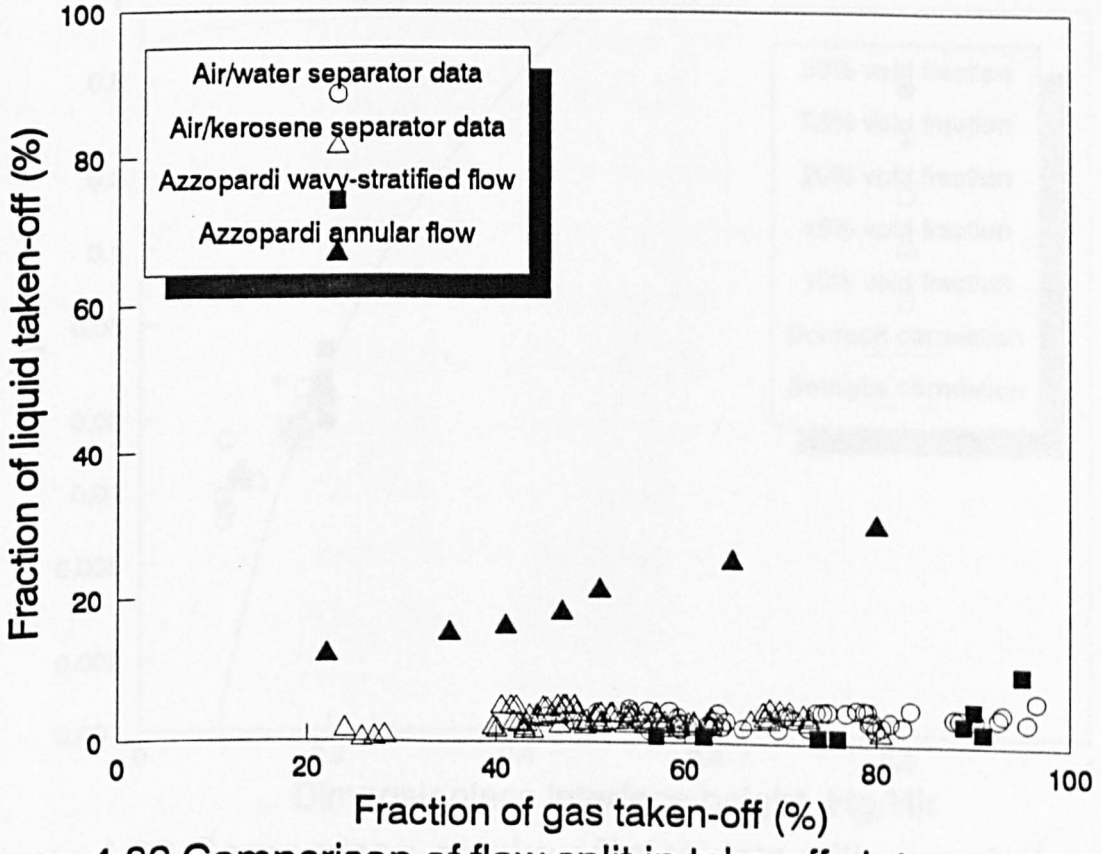

Figure 4.36 Comparison of flow split in take-off slots and tees

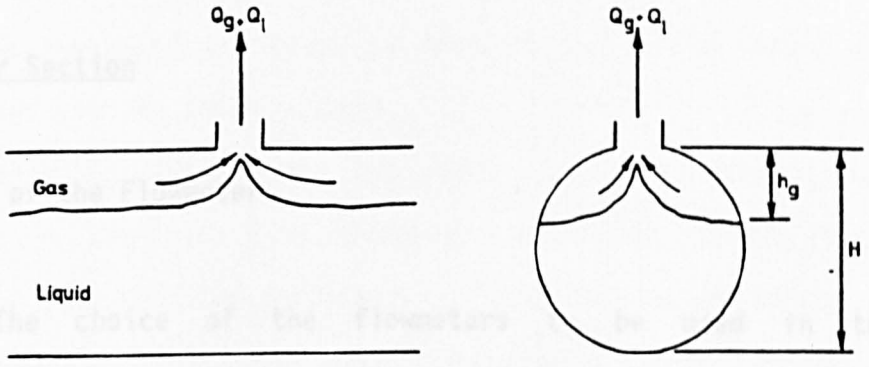

Figure 4.37 Entrainment of liquid into gas offtake

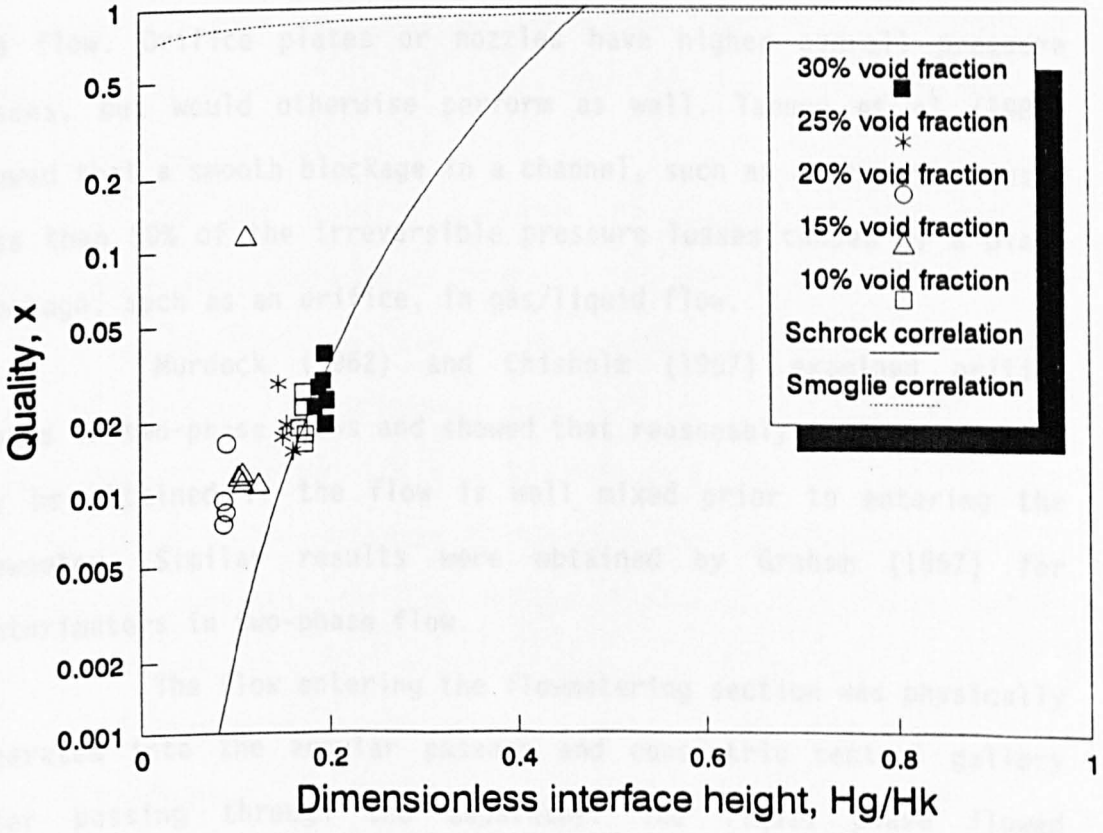

Figure 4.38 Comparison of take-off slot data with correlations

CHAPTER 5: THE SEPARATOR/FLOWMETER PACKAGE

5.1 Flowmeter Section

5.1.1 Design of the Flowmeter

The choice of the flowmeters to be used in the measurement section of the separator/flowmeter package was based upon the pressure losses which would be incurred by the flowmeters and the likely reliability of the devices. Differential pressure flowmeters were chosen because the pressure transducer output signal is relatively simple to measure and interpret. Venturimeters were chosen because of their low overall pressure loss and minimal disturbance to the flow. Orifice plates or nozzles have higher overall pressure losses, but would otherwise perform as well. Tapucu et al (1989) showed that a smooth blockage in a channel, such as a venturi, caused less than 50% of the irreversible pressure losses caused by a plate blockage, such as an orifice, in gas/liquid flow.

Murdock (1962) and Chisholm (1967) examined orifice plates in two-phase flows and showed that reasonably accurate results may be obtained if the flow is well mixed prior to entering the flowmeter. Similar results were obtained by Graham (1967) for venturimeters in two-phase flow.

The flow entering the flowmetering section was physically separated into the annular passage and concentric central gallery after passing through the separator. The liquid phase flowed

predominantly in the outer, annular, passage and the gas phase predominantly in the inner gallery. To measure the flow rate of each of the separated phases two venturimeters were required, mounted concentrically after the separator. This arrangement facilitated the supply of the separated air phase to the internal venturimeter and the liquid phase to the outer venturi.

Although much work has been done on conventional venturimeters in two-phase flow, Azzopardi and Govan (1985), there was a lack of data for the performance of annular venturimeters in both single-phase and two-phase gas/liquid flows. Harris and Shires (1973) found that venturimeters could be used to measure steam quality after individual calibration. Crowe (1982) found that the perfomance of an annular venturimeter in gas/solid flow was comparable with that of a standard venturimeter and was less sensitive to upstream installation effects than the conventional venturimeter. Some experimental work was therefore required to quantify the suitability of this type of flowmeter for use in gas/liquid applications.

In the annular passage the throat of the annular venturimeter was formed by a change in section of the core diameter to ease the manufacturing and assembly tasks. The pressure tappings for the annular venturimeter were set in the tube wall for convenience of manufacture and to ease the run of the pressure sensing lines to the pressure measurement instrumentation. There is no standard available for the design of annular type venturimeters and so the B.S.1042 (1981) guide-lines were used where applicable.

The annular venturimeter test section was formed by a centrebody mounted concentrically inside a plain acrylic tube, Fig. 5.1. The centrebody was formed by a cylinder of aluminium alloy which

was machined to give an annulus at the entrance to the test section. The annulus was followed by a contraction and a throat, after the throat the flow was passed through an annular diffuser before returning to an annulus of similar dimensions to that preceding the throat. The venturi was designed with an area ratio of 0.78, equivalent to a classical venturimeter of β ratio 0.88. Similar entrance and diffuser included angles to those recommended in BS. 1042 (1981), for a classical venturimeter, were used in the annular venturimeter. After the annular diffuser a short length of annulus was formed by the centre body before the end of the test section. To measure the differential pressure across the annular venturimeter the test section was fitted with two rings of static pressure tappings, one was at the inlet to the meter and the other at the throat. The inlet tappings were situated upstream of the throat by an axial distance equal to one half of the annular throat equivalent diameter, d_{ea}, where

$$d_{ea} = \frac{4A_t}{s_c + s_t} \qquad (5.1)$$

and s_c = Core perimeter, s_t = Tube perimeter

The throat tappings were situated at the throat mid-section.

5.1.2 Role of the venturi

The annular venturimeter will measure the flow rate of the separated liquid phase, the internal (classical) venturimeter will measure the separated gas flow rate. The annular venturimeter is

likely to have a gas/liquid mixture passing through it. This is because the separator cannot realistically be expected to remove all the separated gas phase from the two-phase mixture. A proportion of the gas phase will therefore be carried over into the flow entering the annular venturimeter. If the effect of the reduced proportion of gas phase on the annular venturimeter performance were to be quantified then the readings from the flowmeter in two-phase flow would be more reliable. Residual swirl may persist in the flow after the exit from the separator and so the effects of swirl on the performance of the flowmeter were investigated.

Due to space limitations in the main experimental rig the annular venturimeter was tested in a horizontal test section (described in section 2.4) for both single-phase and two-phase flow. The initial experiments in two-phase flow showed that a consistent flow pattern could not be achieved throughout the annular venturimeter in the horizontal test section. To remedy this problem a plate type mixer was fitted immediately upstream of the test section. The mixer consisted of a plate covering the full flow area of the pipe. The plate had 40 holes of 8mm diameter drilled through it. The result was a homogeneous flow pattern throughout the annular venturimeter at all the flow conditions, although the maximum attainable flow rate was reduced by the mixer pressure loss to around 40 l/s.

5.2 Single-phase Results

5.2.1 Single-phase Water Calibration

Before assessing the annular venturimeter in air/water flows the performance of the flowmeter in single-phase water flow was examined. The flow rate of the liquid passing through the venturimeter was inferred from the pressure drop across the throat in the same way as that for the classical venturimeter where

$$Q = CdA_1\left\{\frac{2\Delta P}{\rho\left[\left\{\frac{A_1}{A_t}\right\}^2 - 1\right]}\right\}^{0.5} \qquad (5.2)$$

where A_t = Throat Area, A_1 = Annulus Area

The pressure drop was measured using a water manometer at low flow rates and a mercury manometer for higher flow rates, where the differential pressure was greater. The experiments were carried out using water at ambient temperatures.

The flow rate derived using the pressure differential measured experimentally and equation 5.2 was greater than that given by the reference turbine meter and gravimetric facility. The ratio between the actual and inferred flow rates, known as the coefficient of discharge of the meter (Cd), is defined by equation 5.2. The coefficient of discharge would normally be defined using the geometry of the venturimeter. For the annular venturimeter this was not possible and so the discharge coefficient was found by experiment.

The water flow rate was varied to give a Reynolds Number between 10 000 and 300 000, with the characteristic diameter taken as the equivalent diameter of the annulus upstream of the throat. The discharge coefficient for this data, see Fig. 5.2, was found to be constant at Cd = 0.975 between 60 000 < Rn < 300 000 with a standard deviation of 6.05×10^{-3}. This discharge coefficient is greater than that predicted for a classical venturimeter of similar area ratio by BS. 1042 (1981), which is Cd = 0.924 indicating lower losses. For a Reynolds Number lower than 60 000 the discharge coefficient reduced markedly to around 0.8 and there was increased scatter in the data. Some of the scatter in the data at the low flow rates was due to the increased reading error for small differences in the manometer column heights. This led to a similar increase in the uncertainty in the pressure drop across the throat and thus in the flow rate predicted by the annular venturimeter (see Appendix 1). The reduction in the discharge coefficient at very low flows is also characteristic of that given for classical venturimeters by BS. 1042.

5.2.2 Single-phase Swirling Flow

Experiments were conducted to find the effect of a swirling flow on the uncertainty of the annular venturimeter measurement. A swirl generator of the same helix angle as the separator was placed in the flow path immediately upstream of the annular venturimeter, Fig. 5.3. This device induced a swirling flow throughout the venturimeter of the same angle as that produced by the separator. The pressure drop was measured across the throat again using the water and mercury manometers. The flow rate was inferred in the same way as that for the case of no swirl using equation 5.2. The

discharge coefficient, Fig. 5.4, was found to be 0.882 with a standard deviation of 0.01085 for a Reynolds Number, defined as for the previous experiments, between 50 000 and 164 000. Reynolds Numbers greater than 164 000 could not be obtained because of the increased pressure losses caused by the swirl generator. Below a Reynolds Number of 60 000 the discharge coefficient reduced gradually as in the case of no swirl. The reduction of the discharge coefficient due to swirl caused by installation effects was noted by Lugt (1961) and Hobbs (1990) for orifice plates. The effect of the swirl in these experiments was to cause a reduction of 9.5% in the discharge coefficient of the annular venturimeter, thus, providing that the presence and swirl angle of swirling flow is known and the discharge coefficient is modified accordingly then the annular venturimeter will still function effectivly.

5.3 Two-phase Results

5.3.1 Two-phase Air/Water Calibration

The two phases used in these experiments were compressed air and water. The void fractions used for the investigations were between 5% and 30%. The water flow rate was set using the reference turbine meter and the air flow was added through a mixing tee until the desired void fraction and mass flux had been achieved. The mixer plate ensured that at all conditions the flow pattern throughout the annular venturimeter was homogeneous. The homogeneous flow theory may be used to find the mean density of the flow

$$\rho_h = \alpha\rho_g + (1-\alpha)\rho_l \qquad (5.3)$$

The homogeneous density was then substituted in equation 5.2 to find the inferred flow rate from the measured pressure drop across the venturimeter throat. The two-phase discharge coefficient was defined in the same way as that for the single-phase flow, the ratio of the actual volume flow rate to the inferred volume flow rate from the annular venturimeter. The pressure differential across the throat was measured using water and mercury manometers. Due to the unsteady nature of the flow some column oscillations were present in the manometers and the head difference had to be averaged by eye. The error involved in this process is difficult to evaluate but is clearly greater than the error for a similar measurement in single-phase flow.

5.3.2 Two-phase Air/Water Discharge Coefficient

The two-phase discharge coefficient for the air/water mixture, found from equations 5.2 and 5.3, did not vary significantly with the void fraction of the flow, Fig. 5.5. The data at each void fraction decreased slightly as the flow rate increased, the magnitude of the discharge coefficient did not vary with the void fraction. Previous work on two-phase flow through orifice plates by Chisholm (1967) and Smith et al (1977) has shown that the void fraction of the flow has no significant effect on the discharge coefficient of this type of differential pressure flowmeter. The two-phase Reynolds Number was defined, in terms of the mass flux and homogeneous viscosity, as

$$Rn_{tp} = \frac{Gd}{\mu_h} \qquad (5.4)$$

where $$\frac{1}{\mu_h} = \frac{x}{\mu_g} + \frac{1-x}{\mu_l}$$

The above definition of the homogeneous viscosity has no real theoretical basis. Reasonable results are obtained when applied to pressure gradients, Whalley (1987), which gives confidence that it is a reasonable approximation when applied across a differential pressure flowmeter.

Between a two-phase Reynolds Number of 100 000 and 260 000 the two-phase discharge coefficient, Cd_{tp} has a mean value of 0.9304, the decreasing trend can be accounted for by fitting a curve to all the data giving the expression

$$Cd_{tp} = 0.998 - 0.4054 \times 10^{-6} Rn_{tp} \qquad (5.5)$$

The convergent section and throat of the venturi form a contraction in the flow path through the annular venturimeter. As the fluid mixture passes through this contraction it undergoes an acceleration to increased velocity. The gas phase has a lower density than the liquid phase and so accelerates more quickly and to a higher velocity. This relative acceleration between the phases leads to a velocity slip between the gas and liquid and consequently an increase in interfacial friction. The phenomenon is complicated by the presence of the gas phase as dispersed bubbles in the continuous

liquid phase. The inertia of the gas phase is increased by the virtual mass effect noted by Hinze (1962). Cook and Harlow (1984) demonstrated the existence of a 'tail' of liquid which is drawn in the bubble wake as it travels through the liquid, increasing the equivalent density of the bubble. Kowe et al (1988) showed that this effect will reduce the relative acceleration between the gas and liquid phases. The effect on the flow mixture in a venturi will be to produce a relative velocity between the phases at the throat. Thang and Davis (1979) found slip ratios of up to 1.7 at the throat of venturis in bubbly flow with void fractions of between 20% and 60%.

There will also be a small decrease in the gas density at the throat due to the friction and momentum pressure loss between the annulus and the throat of the venturi. The decrease in gas density will cause a small increase in the void fraction of the flow, as the gas will occupy a larger volume. The homogeneous flow model used in the analysis, however, makes no provision for such an increase in the void fraction (decrease in mixture density) or inter-phase slip. The increase in void fraction at the throat will become more marked as the pressure drop increases. This leads to an increasing over-prediction of the total volume flow rate by the annular venturimeter. This effect is manifest as the decrease of the two-phase discharge coefficient with increasing two-phase Reynolds Number.

The total volume flow rate predicted by the annular venturimeter was compared with the reference total volume flow rate, Fig. 5.6. The predicted flow rate was calculated from the two-phase pressure drop measured across the throat of the flowmeter. The homogeneous density of the fluid mixture, found from the reference flow rates, was also used and the appropriate value of the two-phase discharge coefficient for the flow through the meter was taken. The

predicted flow rate agreed closely with the reference flow rate, although the deviation from the actual flow rate increased slightly as the total volume flow rate was increased. The percentage error of the annular venturimeter against the mass flux through the meter is shown in Fig. 5.7. The percentage error is somewhat greater at the lower end of the flow range, below 6000 kg/m^2s, than at higher mass flux because the uncertainty in the differential pressure reading is greater in this region. At the low mass flux the error is between ± 10% of total volume flow and decreases to between ± 5% at over 6000 kg/m^2s.

5.3.3 Two-phase Swirling Flow

The annular venturimeter was also examined to find the effect of the presence of a gas phase on the single-phase swirling flow calibration. The same swirl device used in the single-phase flow investigation was added immediately before the annular venturimeter. The plate mixer was situated upstream of the swirl device to ensure a well mixed flow. For air/water flows with void fractions as low as 4% the pressure drop across the annular venturimeter throat was lower than in the single-phase flow. The swirl in the flow was observed to separate the gas phase to the inner diameter of the annulus and the liquid phase to the outer diameter. As the contraction of the flow area is formed by the change in section of the inner diameter of the annulus only the gas phase underwent a significant increase in velocity. Due to the low density of the air the associated momentum pressure drop at the throat was not significant in comparison with the increased friction pressure losses in the liquid phase. Increased friction losses were noted by Gambill et al (1961) for liquid flow

through twisted tape swirl generators. Jensen et al (1985) also found increased friction losses in swirling annular flow compared with normal annular flow. The pressure losses in the separated swirling liquid phase are attributable to wall shear which is increased above the normal due to the increased local velocity of the fluid at the wall. Although the friction pressure losses are increased, the liquid phase undergoes little momentum change because there is no significant change of liquid phase flow area as it passes through the throat. The result is that the annular venturimeter underestimates the total volume flow rate under swirling two-phase flow conditions.

The annular venturimeter clearly cannot tolerate the swirling two-phase flow which would exit from the separator. The flow must be straightened and re-mixed to approximate to a bubbly/homogeneous type of flow pattern before the annular venturimeter will function effectively.

5.4 Annular Flowmeter

5.4.1 Design of Annular Venturimeter

The initial air/water experiments on an annular venturimeter had shown that this type of differential pressure flowmeter was suitable for use with two-phase mixtures. Good results were obtained, providing that the mean density of the fluid mixture was known and that the flow was well mixed. The annular venturimeter which had been used in the air/water experiments could not be used in conjunction with the separator due to a mismatch between the design flow range of the annular venturimeter and the flow range over which the separator operated.

In addition to this problem the previous investigations with swirling two-phase flow entering the annular venturimeter had indicated that the gas phase was concentrated near the inner wall of the meter and the liquid phase near the outer wall. This non-uniform void concentration profile modified the flow through the meter and led to the flowmeter underestimating the total volume flow rate.

A flow straightener was designed in order to remove the swirl and reduce the non-uniformity of the void concentration profile before the entrance to the flowmeter. The flow straightener was downstream of the separator exit and upstream of the entrance plane of the annular venturimeter, Fig. 5.8. The flow straightener was formed by a set of eleven equispaced radial vanes around a centrebody of the same diameter as the separator helical passage root diameter. These vanes intersected the annular space to create eleven passages. Spark erosion techniques were used in conjunction with conventional machining techniques to form the aluminium flow straightener piece, Fig. 5.9. The flow straightener was preceded by a short dump type diffuser situated immediately after the separator exit plane. On entering the diffuser the deceleration of the flow caused mixing of the separated phases prior to the entrance to the straightening section. To break up the six vortices formed in the separator passages the straightener was formed with eleven passages of length-to-equivalent diameter ratio of 8. This length to diameter ratio is smaller than that for a tube bundle straightener but greater than that for an Etoile type straightener, see ISO/DIS 5167-1 (1989) and Bosch and Hebrard (1984).

After the straightening section the flow passed through a settling length of 10 times the passage equivalent diameter before entering the annular venturimeter. The geometry of the annular

venturimeter was designed for a mixture flow range of 5 - 20 l/s. This flow range corresponded to the flow range which could be accurately measured and passed through the separator in the air/kerosene test rig. The annulus inner diameter was 60mm and the throat diameter was 95.1mm in a 102mm diameter bore perspex section, Fig. 5.10. The relatively low area ratio of 0.2, which was equivalent to a β ratio of 0.45, was dictated by the availability of a 0 - 136 kN/m^2 differential pressure transducer. A second venturimeter, which will be described later, was manufactured concentrically inside the flow straightener to measure the flow rate of the separated mixture flowing in the central gallery.

5.4.2 Single-Phase Kerosene Flow

The assembled separator, flow straightener and venturimeters were tested in the air/kerosene flow facility which had previously been used for the separator experiments (Section 2.3). The assembly was fitted in a vertical test section similar to that used in the previous separator experiments.

For these experiments the central gallery and internal venturi in the separator/flowmeter package were blocked at the exit plane of the test section, preventing any kerosene from passing through the central gallery of the separator. All the liquid entering the test section was forced to exit via the annular venturimeter in the outer passage. The calibration of the annular venturimeter was thus established with all the upstream and downstream installation effects of the separator and test section accounted for.

Four equispaced pressure tappings were used at the plane of each of the upstream and throat stations to measure the static

pressure. Each set of tappings was inter-connected so that any circumferential pressure variations were averaged out. The differential pressure across the venturi throat was measured using a 0 - 136 kN/m^2 differential pressure transducer. The signal from the transducer was converted from 4 - 20 mA to 0 - 1 V and was read through an ADC on to a computer, then averaged over 100 readings. The mean of each data set was used to calculate the predicted flow rate using equation 5.2. A discharge coefficient for the meter was then calculated from the ratio of the reference and predicted flow rates.

The flow rates used in the experiments were between 5 l/s and 17.5 l/s. These were the minimum available which could be accurately measured and the maximum flow rate which could be passed through the separator. The discharge coefficient for the meter was found to average approximately 0.9, increasing from 0.87 at a mass flux around 2500 kg/m^2s to around 0.92 at around 9500 kg/m^2s, Fig. 5.11.

The discharge coefficient was lower than for the annular venturimeter tested in water flow, where the discharge coefficient (Cd) was around 0.975. The magnitude of the discharge coefficient decreases with β ratio, BS. 1042 (1981), however the discrepancy was higher than predicted and was probably due to installation effects. Lugt (1961) found reductions of up to 19% in the discharge coefficients of orifice plates with various swirl generators installed upstream. This indicated that the flow straightener may not have completely removed the residual swirl from the flow exiting the separator helical passages.

5.4.3 Two-phase Air/Kerosene Flow

After the single-phase discharge coefficient had been established, the performance of the annular venturimeter in two-phase air/kerosene flow was investigated. The same experimental rig and test section were used as had been used for the single-phase experiments. Compressed air was used as the gas phase and was injected through a tee piece in the vertical test loop 20 diameters before the test section. The flow rate and pressure of the air at the injection point were measured using Rotameters and pressure gauges. As the test section pressure was known, the volume flow rate of the gas phase at this point could be calculated. The mean void fraction of the flow entering the test section was then calculated from the known air and kerosene flow rates, assuming no slip. The internal venturimeter and central gallery remained blocked so that all the flow which entered the test section then passed through the annular venturimeter.

Visual observation showed that the flow was well mixed at the entrance to the venturimeter, but contained some residual swirl from the separator. The flow exiting from the rear of the separator consisted of six vortices issuing from the passages. These vortices were not broken down entirely by the dump diffuser and flow straightener, tending to form new vortices inside the straightener passages. Regardless of the presence of these regions of localised swirl the flow through the annular venturimeter appeared to be well mixed. Visual assessment showed that the air/kerosene mixture appeared to have a consistent concentration profile throughout the annular space downstream of the flow straightener. The flow through the annular space upstream of the original annular venturimeter with

swirling air/water flow had shown a marked separation of the mixture with the water at the outer wall and air at the inner wall (section 5.3.3). The vertical orientation of the test section for the air/kerosene experiments also assisted mixing by removing gravitational distribution effects. The pressure differential across the throat of the annular venturi was measured using the same differential pressure transducer and analysis method as for the single-phase kerosene experiments. The static pressure lines from the tappings to the transducer were observed during the experiments to ensure that no air was ingested from the flow and, if necessary, flushed between each experimental condition.

The voltage signal from the transducer was averaged over 100 readings to produce an average which varied by less than ± 0.5% between individual data sets taken at the same nominal flow rate. The standard deviation of the transducer signal in the two-phase flow, for example 21.16 at 500mV, was 4.5 times greater than that for the single-phase flow, which was 4.5 at 500mV. The increase in the standard deviation of the signal was expected given the more unpredictable and turbulent nature of the gas/liquid flow.

The void fraction of the flow, which was calculated from the known reference flow rates of each phase, enabled calculation of the fluid mean density using equation 5.3. The total volume flow rate through the meter was predicted from the differential pressure measured across the annular venturimeter throat, using equation 5.2. The actual volume flow rates of the air and kerosene were given by the reference flow meters and the test section pressure. The two-phase coefficient of discharge for the annular venturimeter was then calculated from the ratio of the actual to predicted flow rates.

As in the case of the air/water tests on the first annular venturimeter the two-phase discharge coefficient for air/kerosene, Fig. 5.12, decreased slightly as the mass flux increased. The discharge coefficient reduced from around 0.9 at low mass flux to around 0.85 at higher mass flux. The void fraction of the air/kerosene flow through the annular venturimeter, between 5% and 30%, had no clear influence upon the discharge coefficient as the flow rate increases. The decrease in the magnitude of the discharge coefficient was due to the method of calculation of the predicted flow rate (see section 5.3.2). The mixture density was assumed to be the homogeneous density throughout the flowmeter although at the throat there was a small decrease in the mixture density due to the reduced pressure at this point. The reduction in throat pressure, left uncorrected, gives an artificially high prediction of the total volume flow rate through the flowmeter and so leads to a reduction in the discharge coefficient. The gas phase, in the form of small bubbles, will have a relative velocity with respect to the liquid due to the acceleration through the convergent section of the venturi, as shown by Kuo and Wallis (1988). As the flow through the venturimeter was increased so was the magnitude of the pressure drop at the throat which exacerbated the reduction in the discharge coefficient.

5.5 Internal Flowmeter

5.5.1 Internal Venturimeter

The internal venturimeter was designed to measure the flow rate of the gas phase separated into the central gallery of the separator/flowmeter. The design was based on that of a classical

venturimeter in accordance with BS. 1042 (1981). The inlet diameter was nominally 20mm with a throat diameter of 8.92mm, giving a diameter ratio of β = 0.45. The pressure tappings were at D and D/2 before the inlet and at the throat respectively, Fig. 5.13. At both the inlet and the throat there were 6 separate static pressure tappings connected with a piezometer ring to average any circumferential pressure variations. The venturi was situated internally in the flow straightener piece with the pressure tappings passing through the flow straightener vanes to the outside of the test section and the pressure transducer connections.

5.5.2 Single-phase Air Flow

From the two-phase separator experimental results, section 3.5.3, the continuous phase in the central gallery was expected to be the gas phase. The single-phase calibration of the internal venturimeter was therefore carried out using compressed air. When installed in the separator/flowmeter the internal venturimeter was placed immediately downstream of an expansion and so could not be expected to have a fully developed velocity profile at the inlet section.

The reference air flow rate was given by the Rotameters which had been calibrated against traceable turbine meters. The pressure drop across the throat of the internal venturimeter was measured using a differential pressure transducer and ADC. The density of the air at the venturimeter entry plane was found using the equation of state with the static pressure and the reference flow rate was corrected accordingly. The discharge coefficient for the venturimeter was then found in the usual way (see section 5.2.1) from

the reference flow rate and the flow rate measured by the internal venturimeter. The discharge coefficient was found to decrease gradually, Fig. 5.14, as the Reynolds Number of the inlet flow was increased. At Reynolds Number of around 10 000 the discharge coefficient was around 0.81. The discharge coefficient then decreased to around 0.65 at Reynolds Number of 35 000. The discharge coefficient given by BS. 1042 for a classical venturimeter of this β ratio is around 0.98. The lower discharge coefficient found in these experiments was probably due to the installation of the flowmeter.

5.5.3 Two-phase Air/Kerosene Flow

At all conditions the separation process allowed a small proportion of the liquid phase to be carried into the central gallery. The internal venturimeter was therefore required to measure a two-phase mixture of air and kerosene when forming part of the flowmeter package. From the experimental data on the separation efficiency (Chapter 3) the approximate liquid phase content of the flow through the central gallery was predicted. The calculated void fraction of the internal gallery flow is shown in Fig. 5.15. The void fraction varied between around 92% and 95% and did not show any dependence upon the void fraction of the main flow passing through the separator. With such a high void fraction the internal flow pattern was likely to be a mist or churn flow pattern. The variation in the central gallery void fraction is small and so, therefore, is the variation in the mixture density in the central gallery.

5.5.4 Flow Regime Prediction

As the internal venturimeter will experience gas/liquid flow when used as part of the two-phase flowmeter package it would be useful to predict the type of flow regimes which are likely to occur in the central gallery. Taitel et al (1980) produced a model for predicting flow regime transitions in vertical tubes. The transitions between these flow regimes are based on the physical mechanisms thought to be responsible. The (flooding) condition given for annular flow to exist is for the minimum superficial gas velocity to support a liquid droplet of maximum stable size in the flow:

$$\frac{U_{GS}\rho_g^{0.5}}{[\sigma_g(\rho_l-\rho_g)]^{0.25}} = 3.1 \qquad (5.6)$$

which for air/kerosene flow at the conditions anticipated in the internal venturi gave a minimum condition of $U_g = 6.9\ ms^{-1}$. The gas flow expected in the internal gallery at the maximum gas separation conditions had a superficial velocity of around 5.9 ms^{-1}. Annular flow was therefore not anticipated at the majority of the test conditions.

The criteria given for a bubbly flow to exist is that

$$U_{gs} + U_{ls} = 4.0\left[\frac{D^{0.429}(\sigma/\rho_l)^{0.089}}{\nu_l^{0.072}}\left\{\frac{g(\rho_l-\rho_g)}{\rho_l}\right\}^{0.446}\right] \qquad (5.7)$$

This criteria was met by the flow at the majority of the flow conditions predicted in the internal gallery. However, the system is of small diameter and the liquid superficial velocity was insufficient to sustain a bubbly flow. In this case, according to Taitel, a slug/churn flow may be expected.

The transition from a bubbly to a churn flow is governed by the void fraction of the fluid. As the void fraction is increased the frequency of the coalescence of the small bubbles is increased until a churn flow regime is formed. Taitel et al give the lower limit for the existence of churn flow as

$$\frac{U_{gs}}{U_{gs}+U_{ls}} > 0.52 \qquad (5.8)$$

For all the flow conditions through the internal venturimeter the void fraction of the flow is greater than this, typically around 0.92. The flow regime was predicted to be churn flow throughout the operating region of the flowmeter with annular flow possible only at the highest gas flow conditions.

McQuillan and Whalley (1985) developed the transition criteria proposed by Taitel and compared their modified transition boundaries with an empirical database using data from tube diameters between 10mm and 105mm diameter with several two-phase mixtures. The generally good agreement obtained gave confidence to the prediction of churn flow in the internal gallery. The prediction of churn flow was in agreement, at some conditions, with the experimental observation of foaming/churning flows leaving the separator central gallery. The prediction of churn flow indicated that at the wall of the internal venturimeter there may exist conditions for a falling

liquid film. The occurence of these conditions may affect the repeatability of some of the differential pressure measurements and showed the need for time-averaged measurements.

5.5.5 Internal Venturimeter Calibration in Two-phase Flow

The two-phase flow conditions for the calibration of the internal venturimeter were matched as closely as possible to those expected in the internal gallery during the operation of the separator/flowmeter package. The void fraction, calculated using the homogeneous approximation, of the flow through the rig was varied between 0.96 and 0.975 between a mass flux of 40 kg/m^2s and 160 kg/m^2s. The required void fraction was achieved by setting the kerosene mass flow rate and then by adding the air flow required. The density of the fluid passing through the internal venturimeter, for calculation purposes, was taken as the homogeneous density for the flow. The discharge coefficient for the venturimeter was then calculated, using the method of section 5.2.1, from the reference flow rate through the test section and the flow rate predicted using the measured pressure drop across the internal venturimeter.

The discharge coefficient for the venturi in two-phase flow varied between 0.6 and 0.95 across the flow range used, Fig. 5.16. The mean value across the range of 40 to 160 kg/m^2s was 0.864 with a standard deviation of 0.045. The large deviation of some of the data from the mean value was caused by fluctuating ΔP due to the intermittent flow pattern in the test section during some experiments. The flow pattern at the rig exit was noted to be of a slug type for some of the experimental points. The uncertainty in the readings of the Rotameters, which were used in a bank of up to four

simultaneously, was ± 2% of the full scale reading. The weighbridge which was used to collect 10kg of kerosene for each point had an uncertainty of ± 1.2%. The slugs of liquid, which were encountered at some experimental conditions, caused fluctuations in these readings despite the long period used for time-averaging in the weigh-tank. The experimental data exhibited no particular trend with mass flux except below a mass flux of 60 kg/m^2s where the discharge coefficient decreased.

5.6 Separator/Flowmeter Performance

5.6.1 Combination of Separator/Flowmeter Package

After the calibration for the internal venturimeter had been established for both single-phase air and two-phase air/kerosene flow the combined separator/flowmeter package was assembled (Fig. 5.8). In the vertical orientation used in the test section the annular venturimeter was situated axially above the separator and flow straightener. The mixture separated through the separator slots thus passed into the internal gallery and then vertically upward through the internal venturi. The remainder of the total flow, including the greater proportion of the kerosene, continued in the helical passages to the separator exit. The main flow then passed through the flow straightener and the annular venturimeter. After passing through the internal venturimeter the separated mixture was re-combined with the main flow at the annular venturimeter exit plane.

5.6.2 Indication of Flow Void Fraction

The results from the experiments carried out to determine the gas separation efficiency (see Chapter 3) and the liquid draw-off of the separator enabled the void fraction of the flow in the internal passage to be found. The internal passage void fraction was near constant at between 92% and 95%. The near constant void fraction was due to the small percentage volume of kerosene carried through the take-off slots into the central gallery with the separated gas phase. The void fraction of the flow passing through the outer annulus was also predicted from the results of earlier experiments. The annulus void fraction was around 45% lower than the test section void fraction at the majority of the flow conditions. The annular void fraction predicted from the measured separator performance is shown in Fig. 5.17.

The flow through the separator/flowmeter can be split into two components: the flow passing through the annular venturimeter, Q_a, and the flow passing through the internal venturimeter, Q_i. These two components are each made up of gas and liquid flows;

$$Q_a = Q_{ga} + Q_{la} \qquad (5.9)$$

$$Q_i = Q_{gi} + Q_{li} \qquad (5.10)$$

Each of these flows contains a proportion of each phase and so has an associated void fraction, α. The flow through each venturi was taken to be well mixed and was assumed to approximate to

a homogeneous flow with no slip between the phases. This approximation will lead to errors, particularly in the internal venturimeter, but the proportion of the mass flux passing through it is small compared to that which passes through the annular venturimeter. This will result in a relatively small error in the total mass flux. The void fraction may then be taken as

$$\alpha_n = \frac{Q_{gn}}{Q_{gn}+Q_{ln}} \qquad (5.11)$$

where n = a (annular) or i (internal)

The volume flow rate, Q, through each venturi is given by the standard venturi equation, with the fluid density calculated using the homogeneous approximation, equation 5.3.

$$Q = k\left[\frac{\Delta P}{\rho_h}\right]^{0.5} \qquad (5.12)$$

$$\text{where} \quad k = CdA_1\left[\frac{2}{\left\{\frac{A_1}{A_2}\right\}^2 - 1}\right]^{0.5}$$

By inspection of the homogeneous density equation (equation 5.3) it can be seen that at a low ambient pressure in a system with a high liquid phase density and a low gas phase density, such as that for air/kerosene or air/water, the homogeneous density is only weakly dependent on the gas phase fraction. This is the case even for void fractions as great as 90% where the gas phase contributes less than 3% of a mixture density of around 82 kg/m^3.

The mixture density can thus be approximated, in terms of the liquid density, as:

$$\rho_h = (1-\alpha)\rho_l \qquad (5.13)$$

The approximate mixture density, equation 5.13, can then be substituted into equation 5.12 to give

$$Q = \frac{k}{\sqrt{\rho_l}} \left[\frac{\Delta P}{1-\alpha} \right]^{0.5} \qquad (5.14)$$

The total volume flow rates predicted by the measured pressure drop across each of the two venturi meters can then be divided:

$$\left[\frac{\Delta P_a}{\Delta P_i}\right]^{0.5} = \frac{Q_a}{Q_i} k_r \left[\frac{1-\alpha_a}{1-\alpha_i}\right]^{0.5} \qquad (5.15)$$

Substituting into equation 5.15 from equation 5.9 and 5.10 for Q_a and Q_i we get:

$$\left[\frac{\Delta P_a}{\Delta P_i}\right]^{0.5} = k_r \frac{\alpha_i}{\alpha_a} \left[\frac{1-\alpha_a}{1-\alpha_i}\right]^{0.5} \qquad (5.16)$$

From the separation experiments performed on the separator it is known that the void fraction in the internal gallery, α_i, is near constant at a value of between 92% and 95% (Fig. 5.15). By assuming a constant value of $\alpha_i = 0.94$ the internal void fraction

can be eliminated from equation 5.16. The void fraction in the annular venturimeter, α_a, is a function of the void fraction of the flow entering the separator, α (see Fig. 5.17). The ratio of the pressure differentials in the venturis can be related to the separator (test section) void fraction, α, by:

$$\left[\frac{\Delta P_a}{\Delta P_i}\right]^{0.5} = k_1 \left[\frac{1-\alpha_a}{\alpha_a^2}\right]^{0.5} \qquad (5.17)$$

$$\text{where } \alpha_a = f_n[\alpha]$$

5.6.3 Void Fraction Measurement

The flowmeter/separator package was installed in the vertical test section of the air/kerosene test rig (Section 2.3). The separator/flowmeter package was tested over a range of mass flux from 3300 kg/m^{2}s to 7500 kg/m^{2}s with test section void fractions in the range 10% < α < 30%. The differential pressures across each venturi throat were measured simultaneously using separate differential pressure transducers, each time-averaging over 100 readings. The voltages from the pressure transducers were read onto a microcomputer using an ADC and voltmeter.

To prove the relationship in equation 5.17 the pressure drop across the internal venturimeter was plotted against that across the annular venturimeter, Fig. 5.18, for the same flow conditions. A distinct relationship between the ratio of the pressure losses and the void fraction of the two-phase flow at the test section entrance can be seen. The pressure drop ratio follows discrete lines for each of the void fractions examined. At the lower void fractions, 10% < α

< 15%, there was only a small difference between the trends. At higher void fractions the differences between the trends for each of the void fractions tested were more marked. These differences increased as magnitude of the pressure losses across the venturimeters increased, except at higher pressure differences for the 25% and 30% void fraction conditions.

The convergence of the trends at the 25% and 30% void fraction conditions can be explained after close examination of Fig. 3.40 and 3.41. At the highest mass flux conditions the gas separation efficiency and liquid draw-off at the 25% condition increase slightly. At similar mass flux the gas separation efficiency and liquid draw-off at the 30% void fraction condition decrease slightly. The resulting effect on the flow split will be a slightly higher proportion of the flow passing through the internal venturi at the high mass flux for the 25% void fraction flow, leading to a slightly larger internal venturi pressure difference. This reduces the difference between the trends at mass flux over 6000 kg/m^2s.

As each void fraction showed a discrete trend for the ratio of the differential pressures between the annular and internal venturimeters this pressure ratio can be used to indicate the void fraction of the flow through the separator. The ratio of the pressure drops across the venturi throats was plotted against the annular venturi differential pressure, Fig. 5.19. A line was then fitted to each curve of constant void fraction. These empirically established lines have now been defined and linear interpolation can be used to find the void fraction for the flows which lie between these contours on the pressure ratio map. Due to the nature of the curves used to fit the experimental data any extrapolation beyond the extents of the experimental data was unreliable.

The blurring of these boundaries at the lowest void fractions, 10% and 15%, was caused by the decrease in the quality of the mixture drawn into the separation slots at these flow conditions. The greater liquid content of the flow into the internal gallery at these conditions caused an increase in the mass flux through the internal venturimeter and an associated increase in the pressure drop across the throat of the meter. This increase in pressure drop caused spuriously high predictions of the separator void fraction from the pressure ratio map (Fig. 5.19).

The performance of the separator/flowmeter in predicting the void fraction of the flow using the ratio of the pressure drops through the venturis is shown in Fig. 5.20. The predicted void fraction is generally good in the regions away from the experiemntal boundaries. At the lowest and highest void fractions the empirical boundaries, which are imposed by the prediction method and were also limited by the capabilities of the experimental rig, do not allow interpolation beyond these extents. The predicted void fraction then reaches a plateau at these extreme constraints. The percentage error in the prediction of the void fraction is shown in Fig. 5.21. The error in the predicted void fraction is shown against the reference void fraction in the test section. The void fraction error was defined as

$$e(\alpha) = \frac{\alpha_{pred} - \alpha_{ref}}{\alpha_{ref}} \qquad (5.18)$$

where α_{ref} (test section void fraction) is known from the test section pressure and the reference flow rates. The

percentage errors are greatest at low void fraction, below α = 20%, where the error is magnified by the low void fraction. Above this value the prediction is generally within around + 25 % and - 30% of the reference void fraction. Other methods of obtaining the void fraction, such as attenuation techniques, are described by Snoek (1988) and by Jones and Delhaye (1976). These techniques can offer absolute errors of the order of ± 5%, but require mixing to achieve this. Even with mixers larger errors can occur when there is a high gas content and a low flow velocity, Millington (1990).

5.6.4 Flow Rate Measurement

The volume flow rate of the mixture passing through the separator/flowmeter can be determined by use of the standard venturi equation, equation 5.2, once the void fraction of the mixture passing through each venturimeter has been determined. The void fraction of the two-phase flow at each venturimeter can be determined from the empirical results obtained during the separator experiments. The void fraction of the internal venturimeter is known to be near constant, section 5.6.2. The mean mixture density and hence the total volume flow rate and individual phase volume flow rates through the internal venturi meter can then be found. The flow split between the annular and internal venturimeters was approximated at 50% for all the gas phase flow conditions (see Chapter 3). The void fraction at the annular venturimeter can then be found from the predicted test section void fraction (Fig. 5.17), gained from the ratio of the differential pressures across the flowmeters (section 5.6.3), and the gas separation efficiency of the separator.

The predicted void fraction can then be used to find the mean density of the flow passing through the annular venturi and thus the total volume flow rate passing through this meter. The total volume flow rate passing through the combined separator/flowmeter package was the sum of the volume flow rates from each venturimeter. The individual phase flow rates through the separator/flowmeter package can then be found from the total volume flow rate and the predicted test section void fraction where

$$Q_g = \alpha Q_{tot} \tag{5.19}$$

and

$$Q_l = (1-\alpha)Q_{tot} \tag{5.20}$$

The total volume flow rate predicted by the separator/flowmeter for two-phase air/kerosene flows, Fig. 5.22, was in very close agreement with the reference flow passing through the test section. The errors varied a little with the void fraction of the flow entering the test section but were within ± 10% of the total volume flow rate. The percentage error in the flow rate was defined as

$$e(Q) = \frac{Q_{pred} - Q_{ref}}{Q_{ref}} \tag{5.21}$$

The largest errors were found to occur at the lowest mass flux used, Fig. 5.23. At mass flux over 4000 kg/m^{2}s the errors were

within + 10% and - 5% of the reference flow. The increase in errors at the extremes of void fraction was due to the problem of extrapolation beyond the empirically defined boundaries on the pressure ratio map causing poor estimates of the test section void fraction at the lowest and highest void fractions tested.

The separator/flowmeter package gave good predictions of the total volume flow rate of the air/kerosene flow through the test section using the method described above. The difference between the reference flow rate in the test section and that predicted by the separator/flowmeter was within ± 10% of the total volume flow at all the flow conditions.

To find the individual phase flow rates through the separator/flowmeter the void fraction of the test section flow was required. By combining the void fraction and total volume flow rates, predicted using the differential pressure measurements from the venturimeters (equations 5.19 and 5.20), the uncertainties associated with the individual phase flow rate measurements were increased and thus the percentage errors increased. This can be seen from the larger errors in the gas phase flow rates, Fig. 5.24, where the error in the gas phase flow rate varied from between - 25% and + 70% of the reference flow rate, depending on the test section void fraction. The errors were highest at the lowest void fraction (α = 10%) and lowest at the highest void fraction (α = 30%). The errors were generally underestimates of less than - 20% with the exception of the flow at 10% void fraction. This is due to the nature of percentage uncertainties where an error is magnified by the low value of the quantity.

The separator/flowmeter gave an excellent prediction of the liquid flow rate, Fig. 5.25. The errors varied between -3% and

+10% across the range of mass flux used in the experiments. The lower error in the liquid flow rate measurement was due to the majority of the liquid passing through the annular venturimeter which gave a more repeatable measurement than the internal venturimeter.

5.6.5 The Separator/Flowmeter as a Two-phase Flowmeter

Differential pressure flowmeters were selected as the most suitable for making effective measurements in two-phase mixtures. For the present application a classical and an annular venturimeter were required. The venturimeters were shown to give an accurate measurement of total volume flow rate providing that the void fraction of the two-phase flow was known. The flowmeters were calibrated in two-phase air/water and air/kerosene mixtures, giving errors of less than ± 10%.

The two venturimeters were then combined with the separator. The ratio of the pressure drops across the annular and internal venturimeters was found to be proportional to the test section void fraction at the separator entrance. The void fraction at each of the venturimeters was predicted from the gas separation efficiency and liquid draw-off of the separator found in previous experiments (see Chapter 3). Using the predicted void fraction at each venturimeter the total volume flow rate through each flowmeter was found and summed to give the total volume flow rate through the two-phase flowmeter.

Close prediction of the total volume flow rate, within ± 10% of the reference value, was achieved. The individual phase flow rates were found from the total volume flow rate and the predicted test section void fraction. The error in the gas phase flow rate was

generally between 0 and - 20%, with the exception of the lowest void fractions. The liquid phase flow rate was predicted very closely, to between -3% and +10% for all the flow conditions.

The magnitude of the errors in the individual phase flow rates reflects the compounding of the errors caused by combining two measurements to give a single result and, in the case of the gas phase, this is magnified by the gas phase forming a relatively small proportion of the total flow.

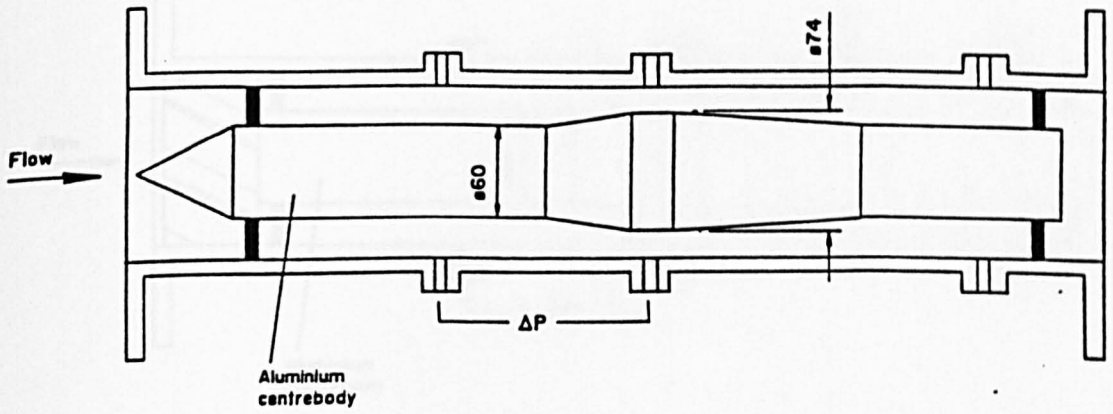

Figure 5.1 Annular venturimeter test section

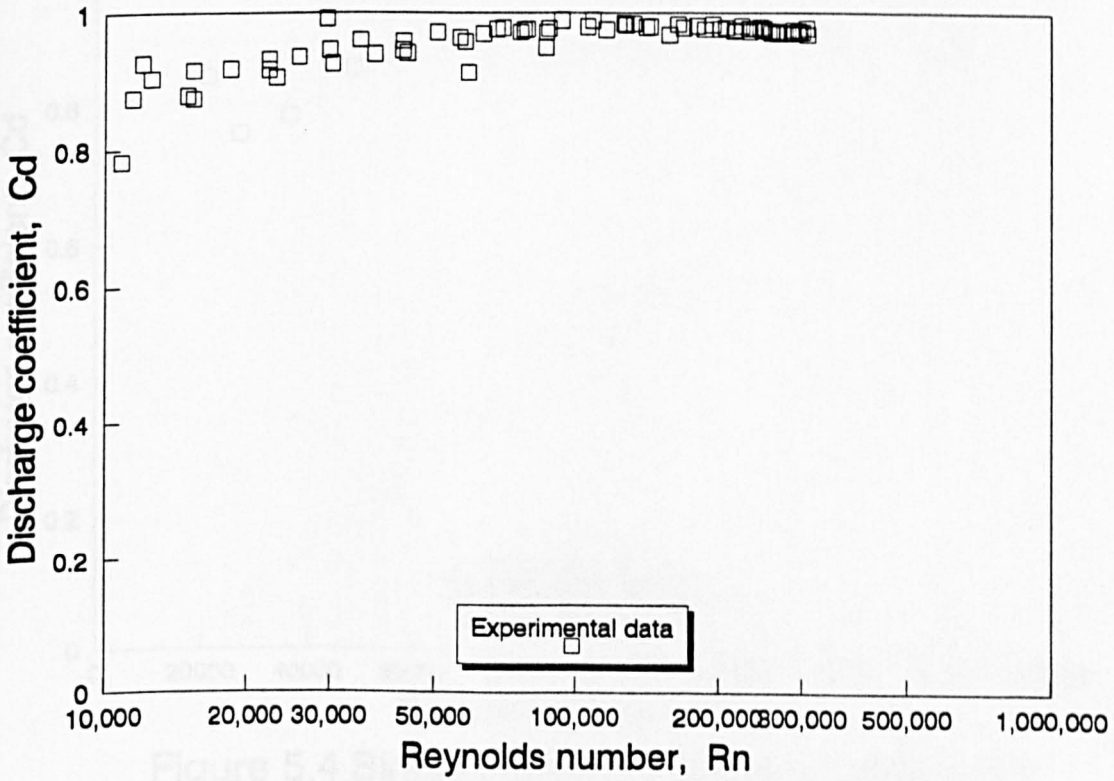

Figure 5.2 Single-phase discharge coefficient for annular venturi

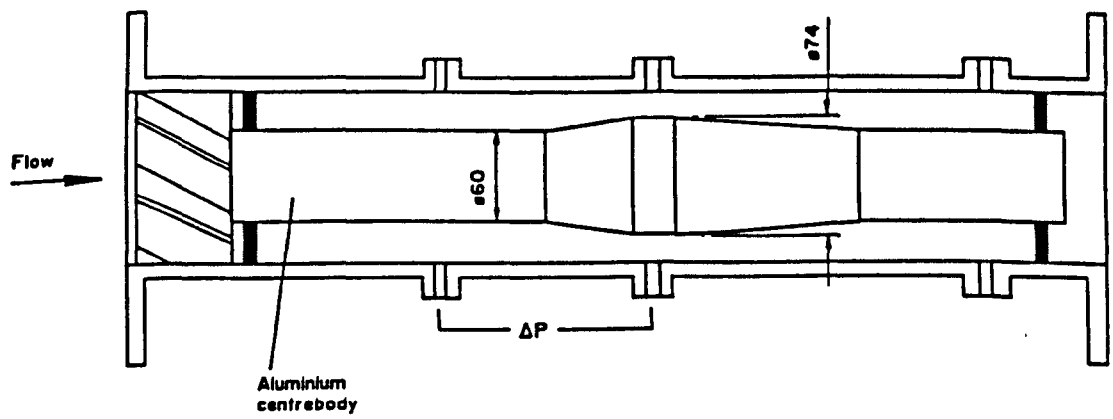

Figure 5.3 Annular venturimeter with swirl generator

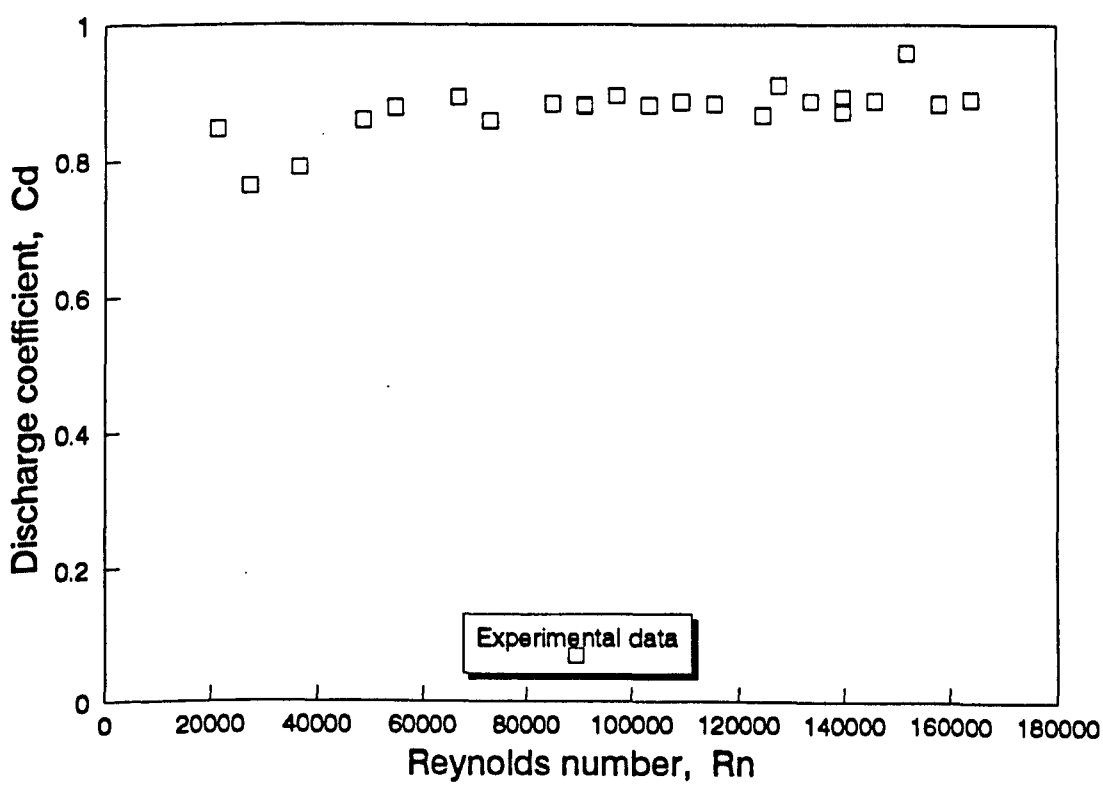

Figure 5.4 Single-phase discharge coefficient in swirling flow

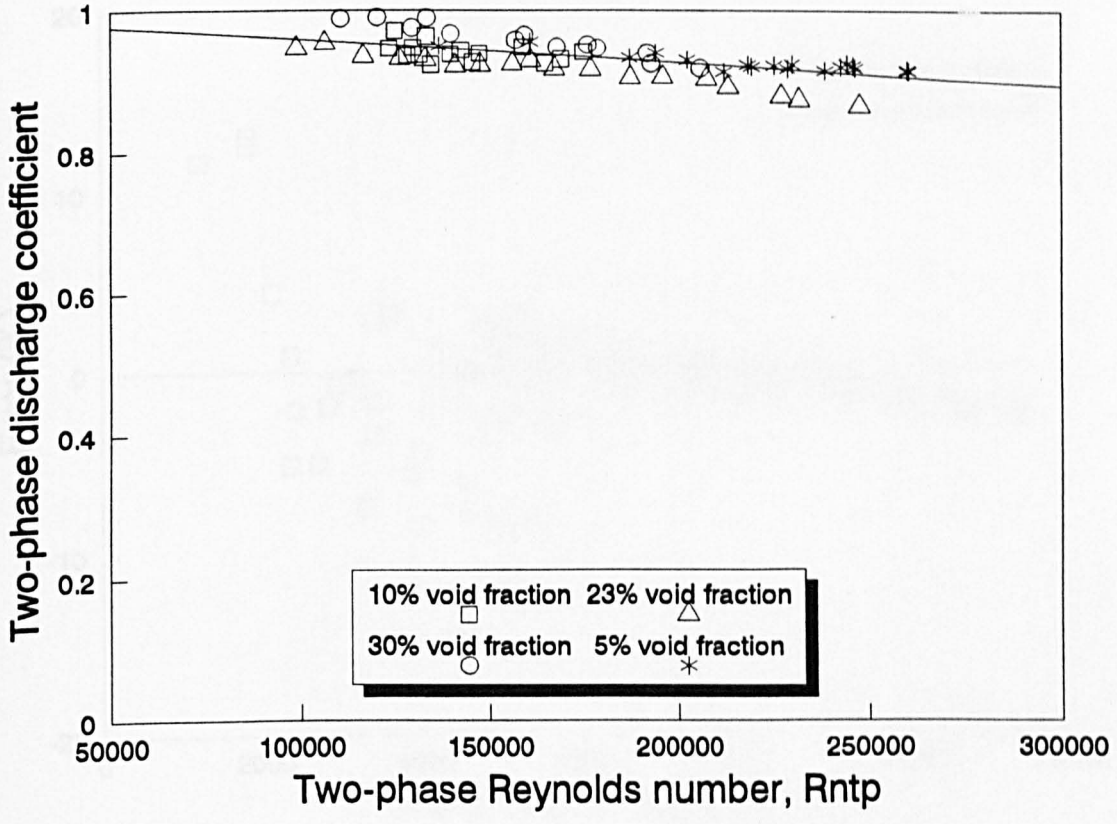

Figure 5.5 Two-phase air/water discharge coefficient

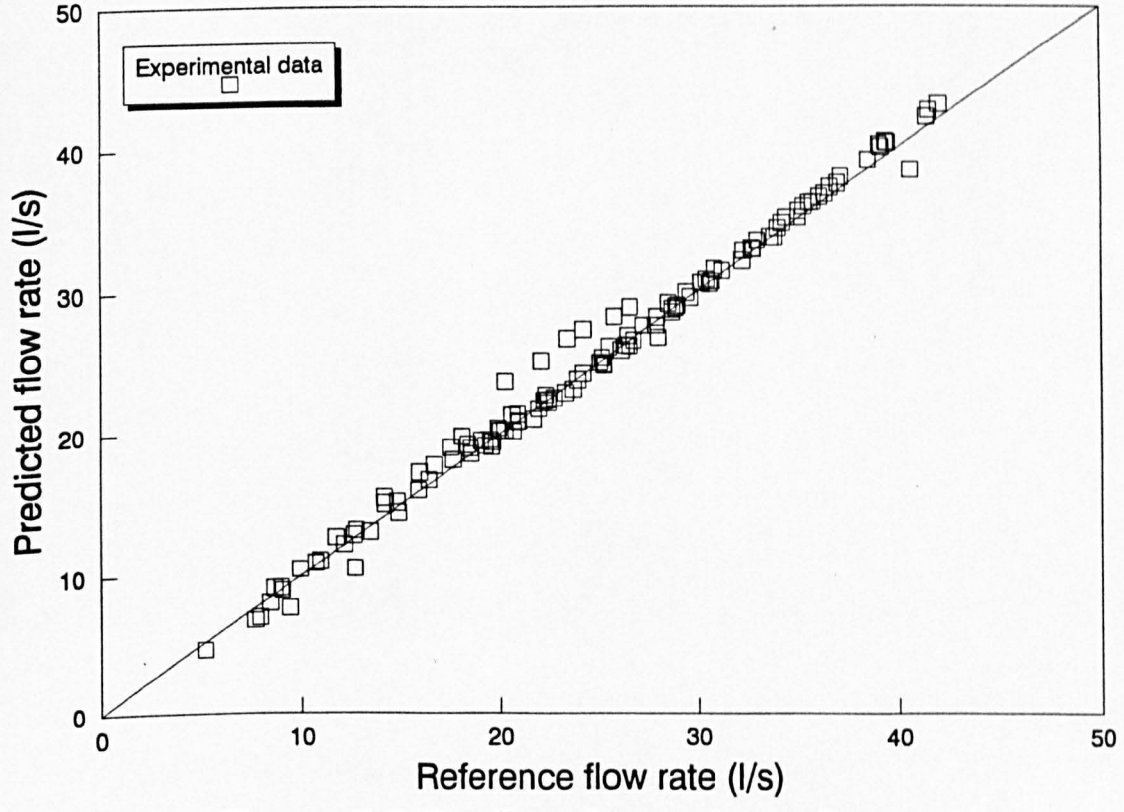

Figure 5.6 Predicted two-phase flow rate

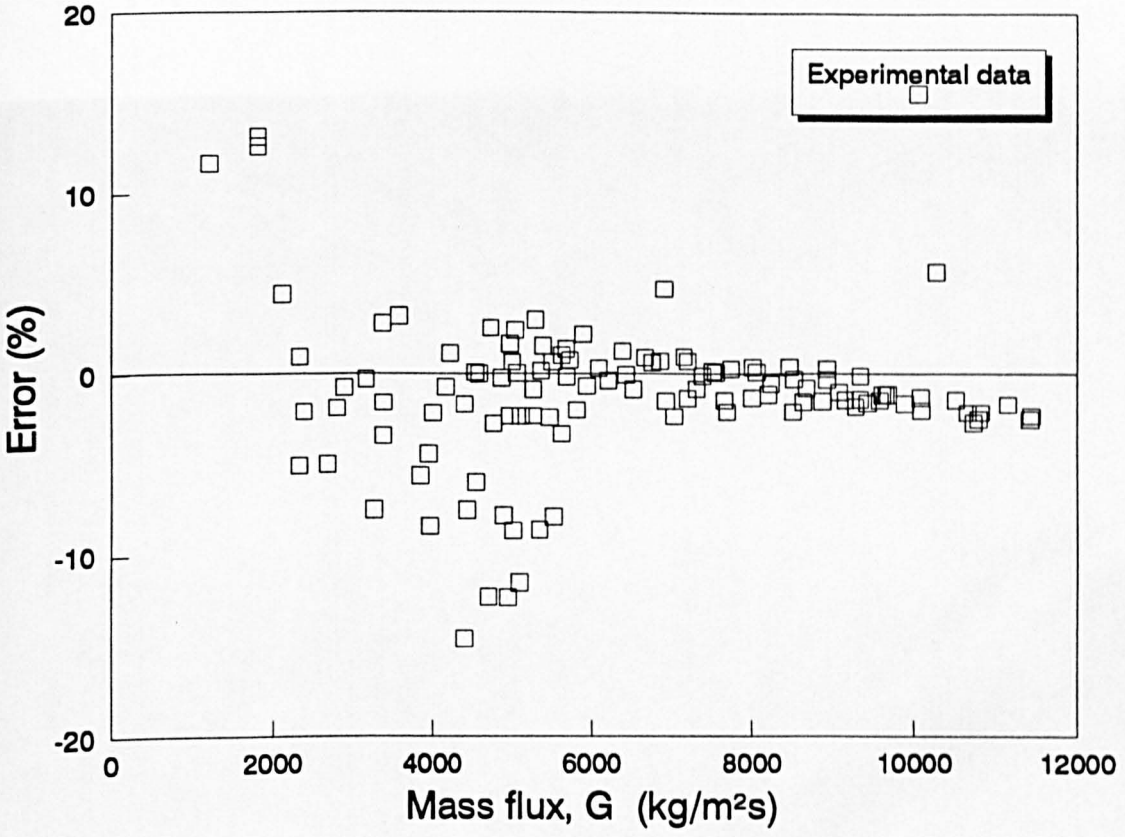

Figure 5.7 Error in predicted flow rate

Figure 5.8 Separator/flowmeter assembly

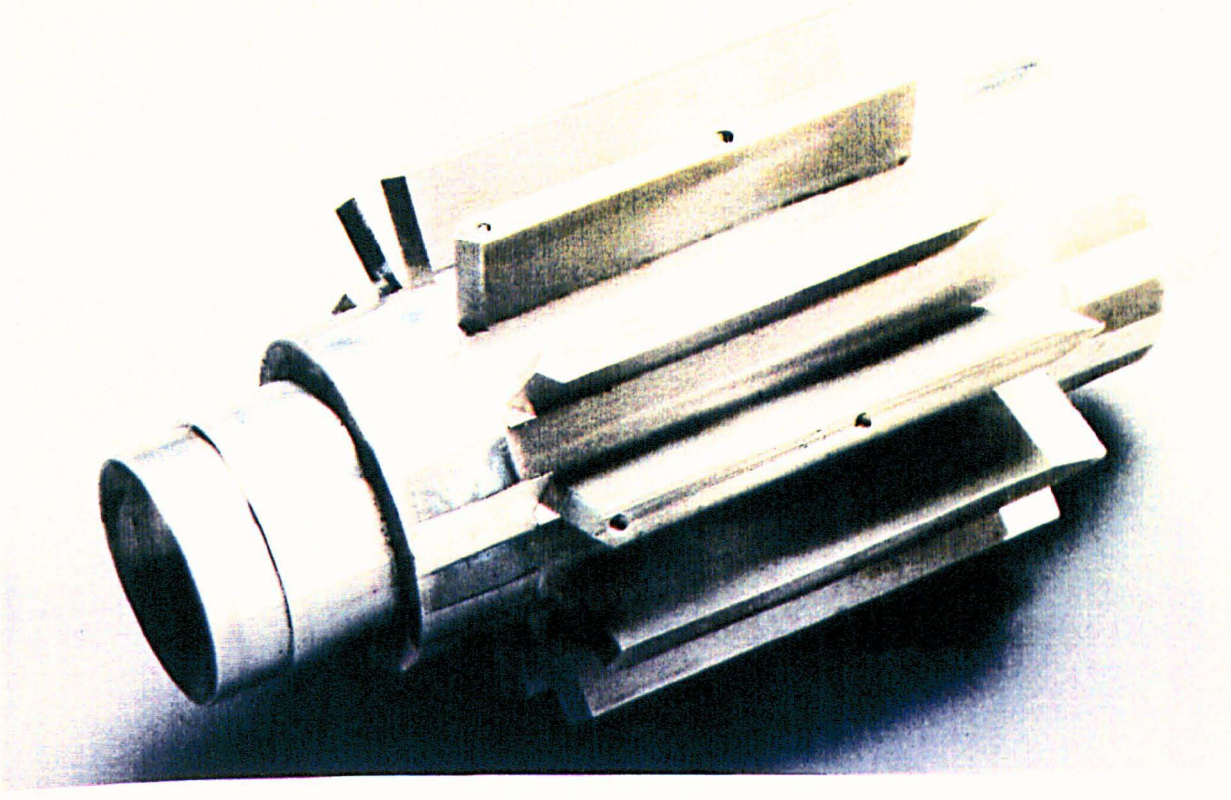

Figure 5.9 Flow straightener

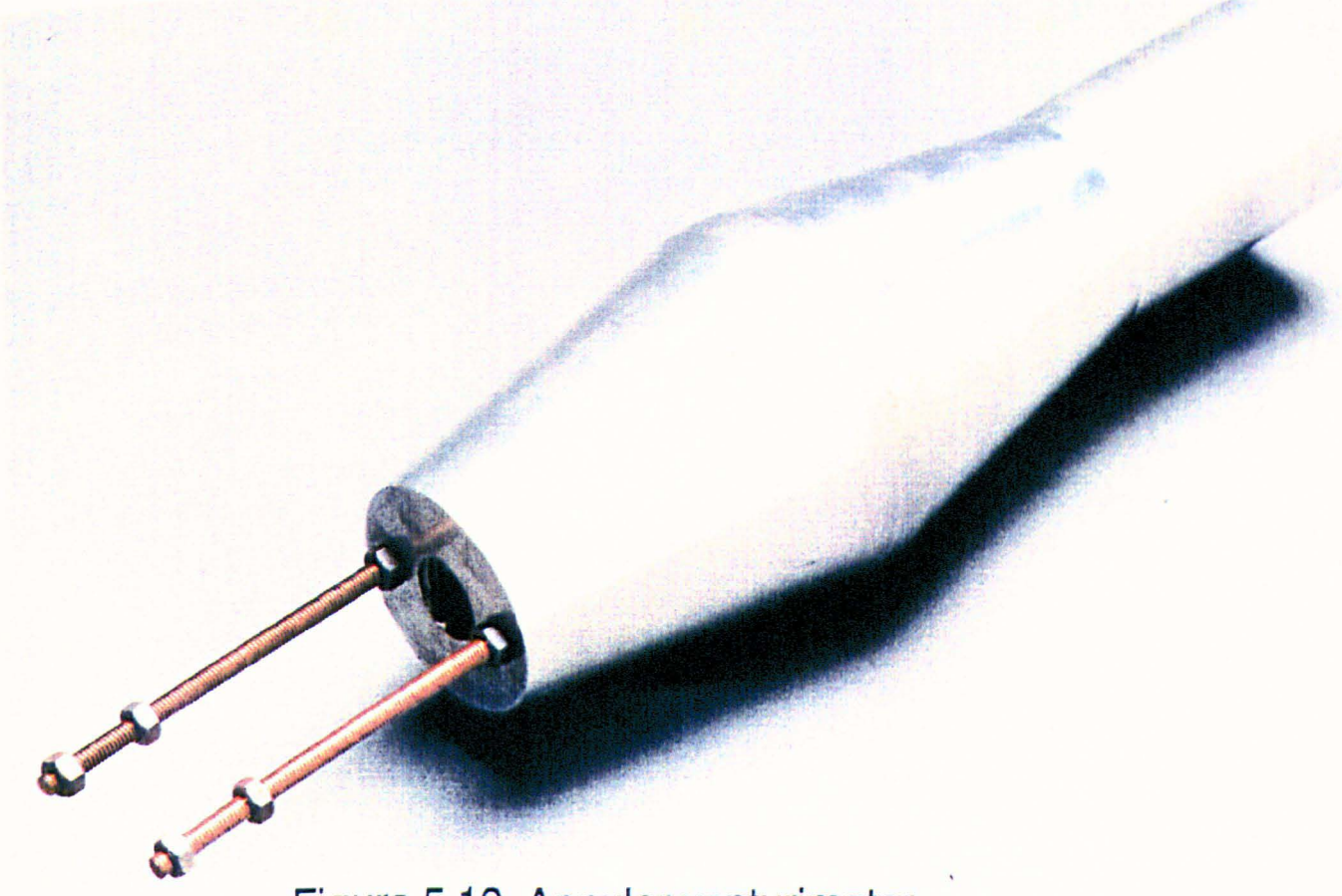

Figure 5.10 Annular venturimeter

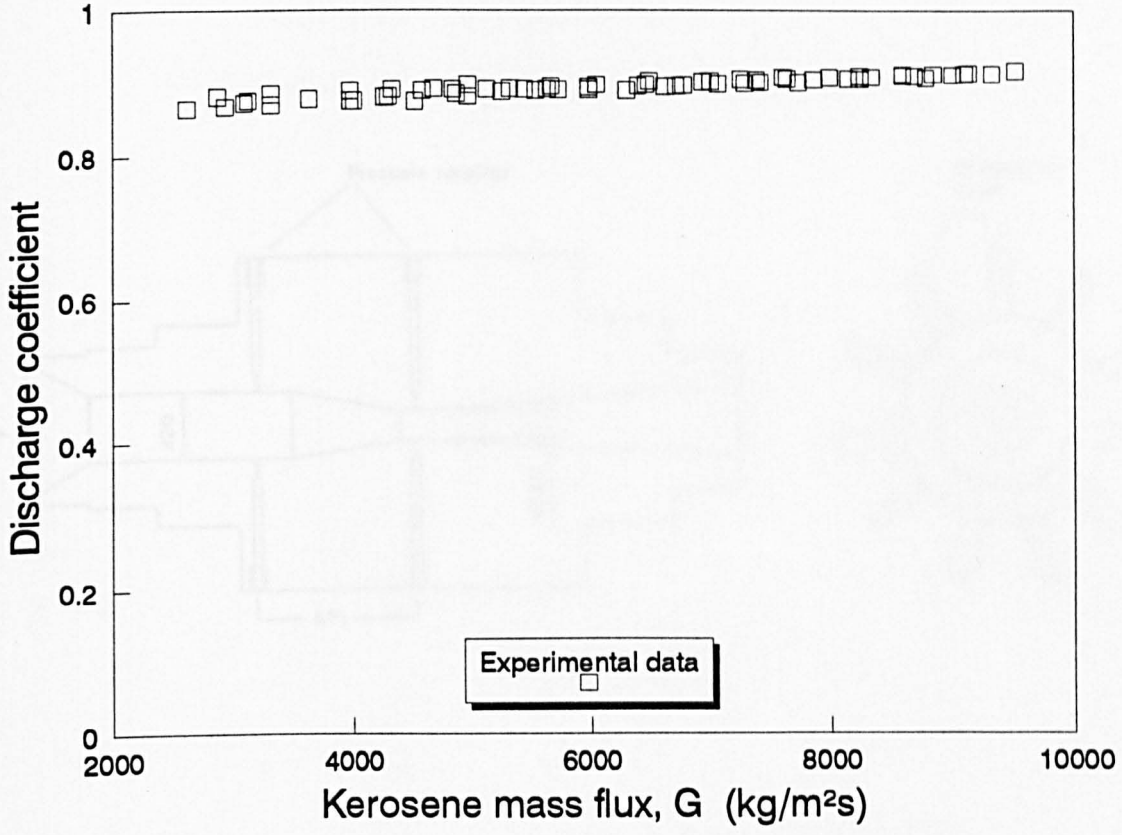

Figure 5.11 Single-phase discharge coefficient (annular venturimeter)

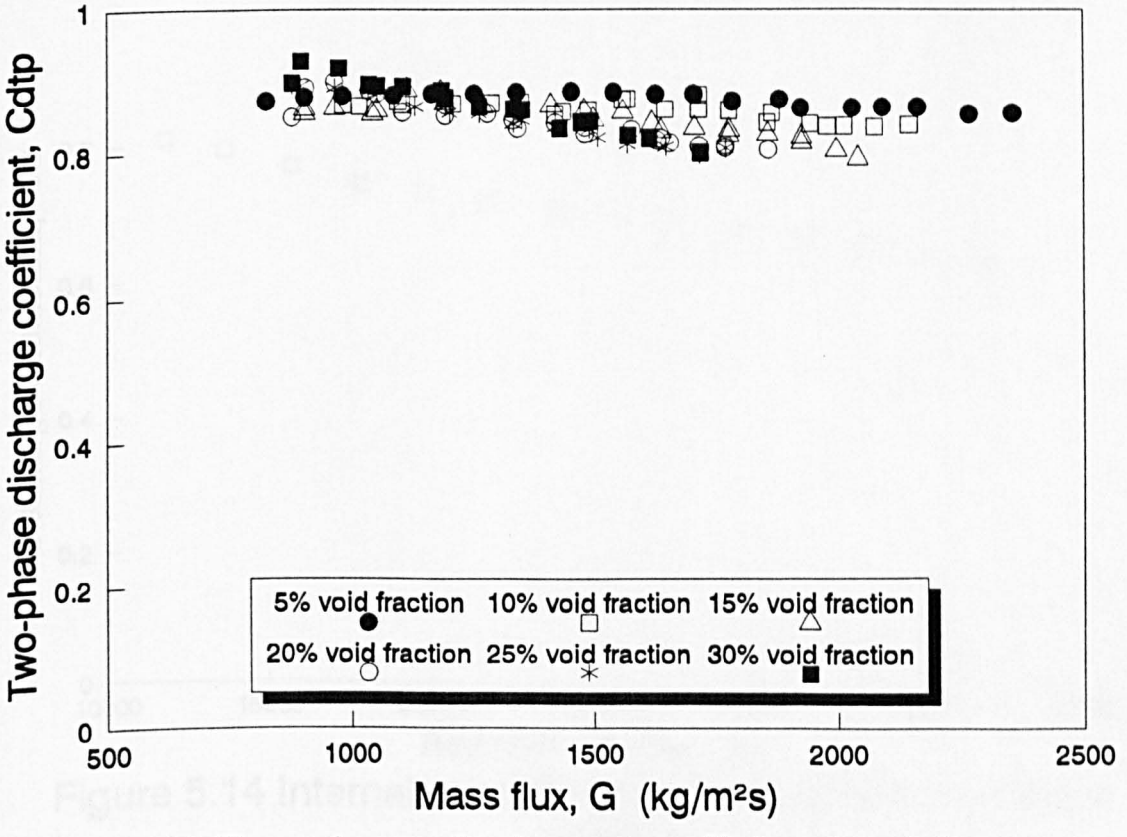

Figure 5.12 Two-phase discharge coefficient in air/kerosene

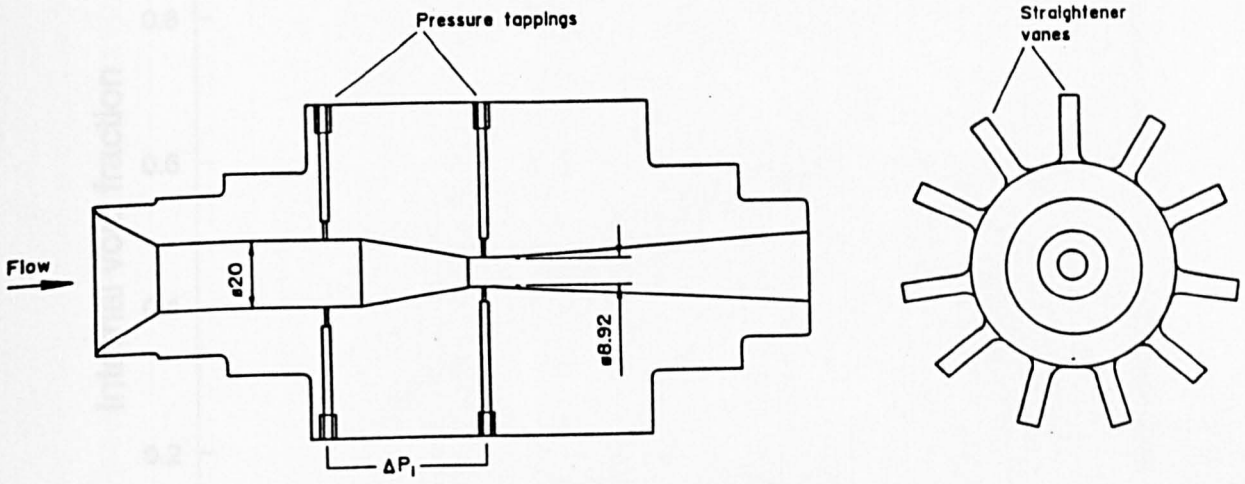

Figure 5.13 Internal venturimeter

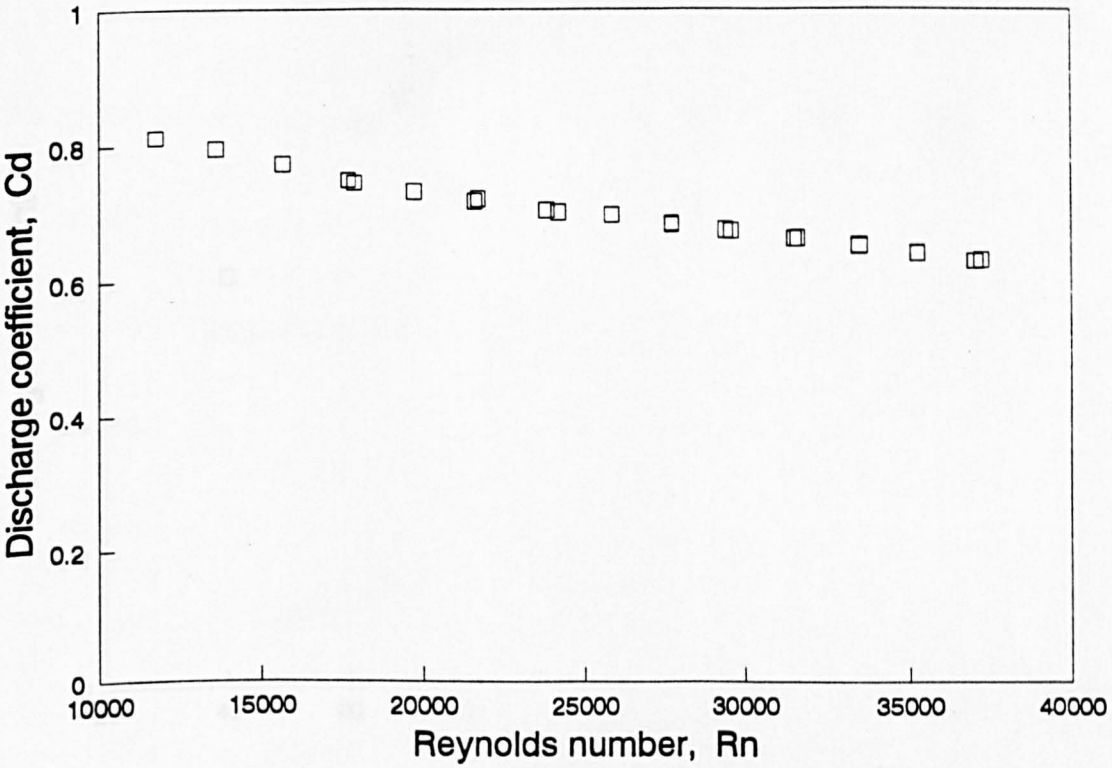

Figure 5.14 Internal venturimeter single-phase discharge coefficient

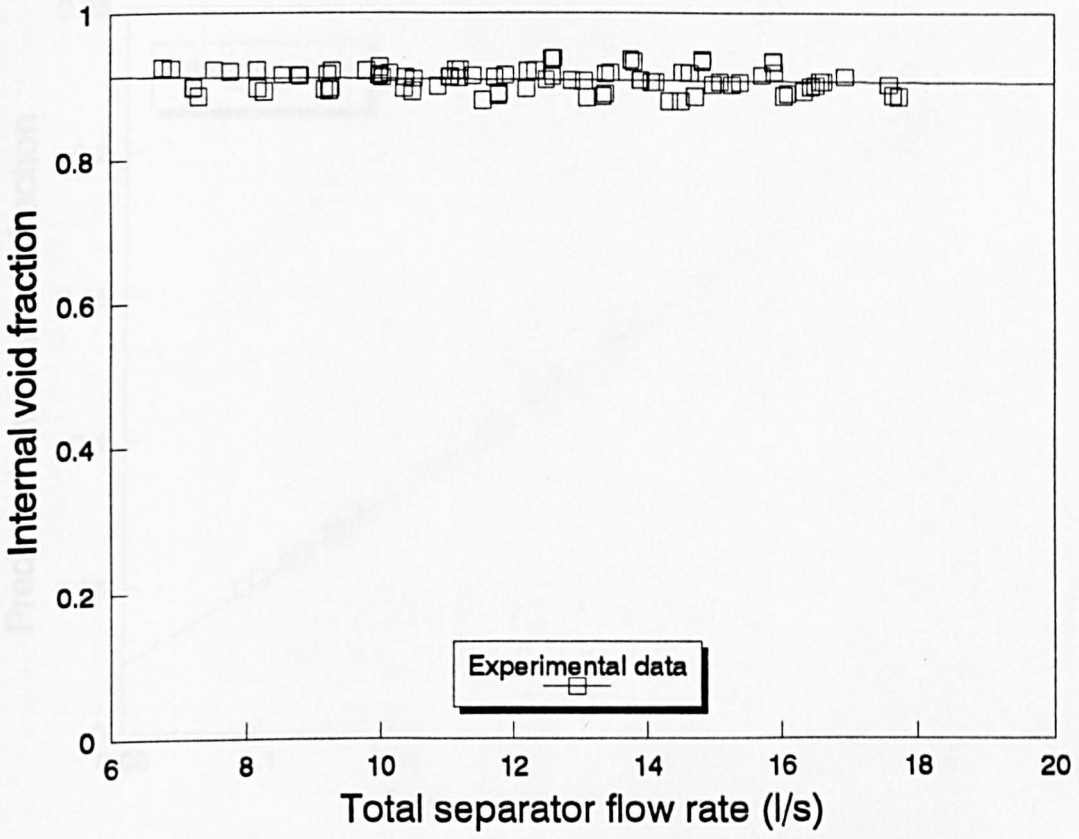

Figure 5.15 Internal gallery void fraction

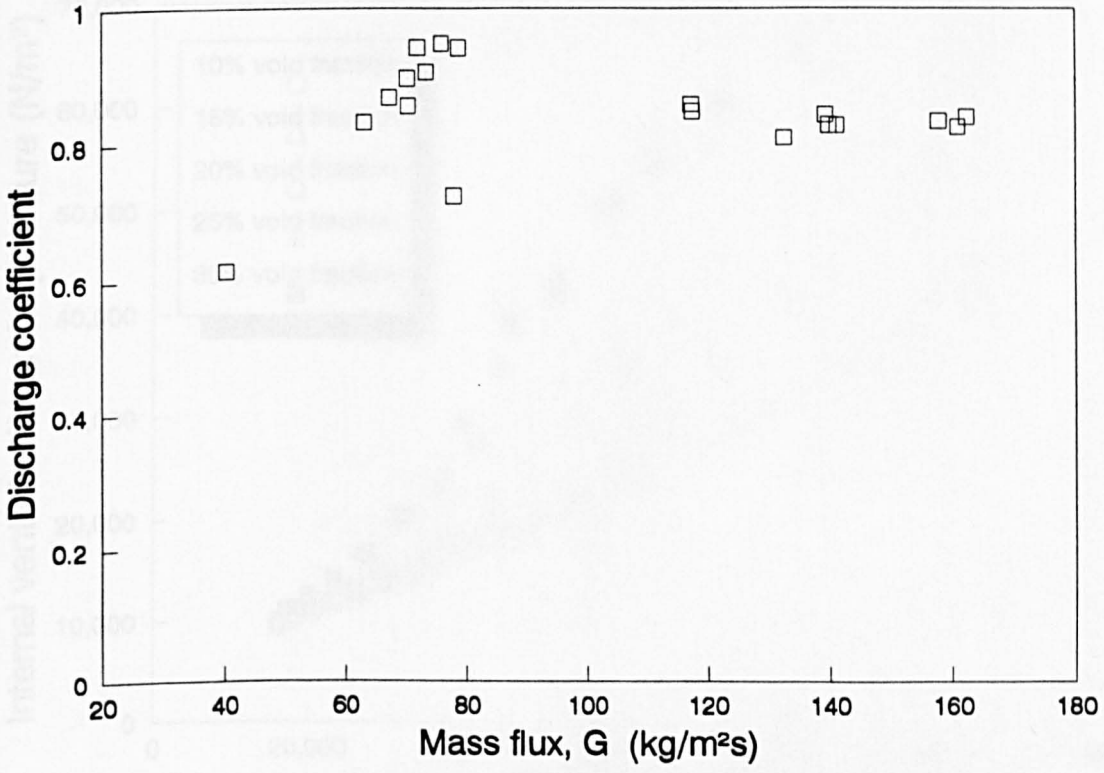

Figure 5.16 Internal venturimeter - two-phase discharge coefficient

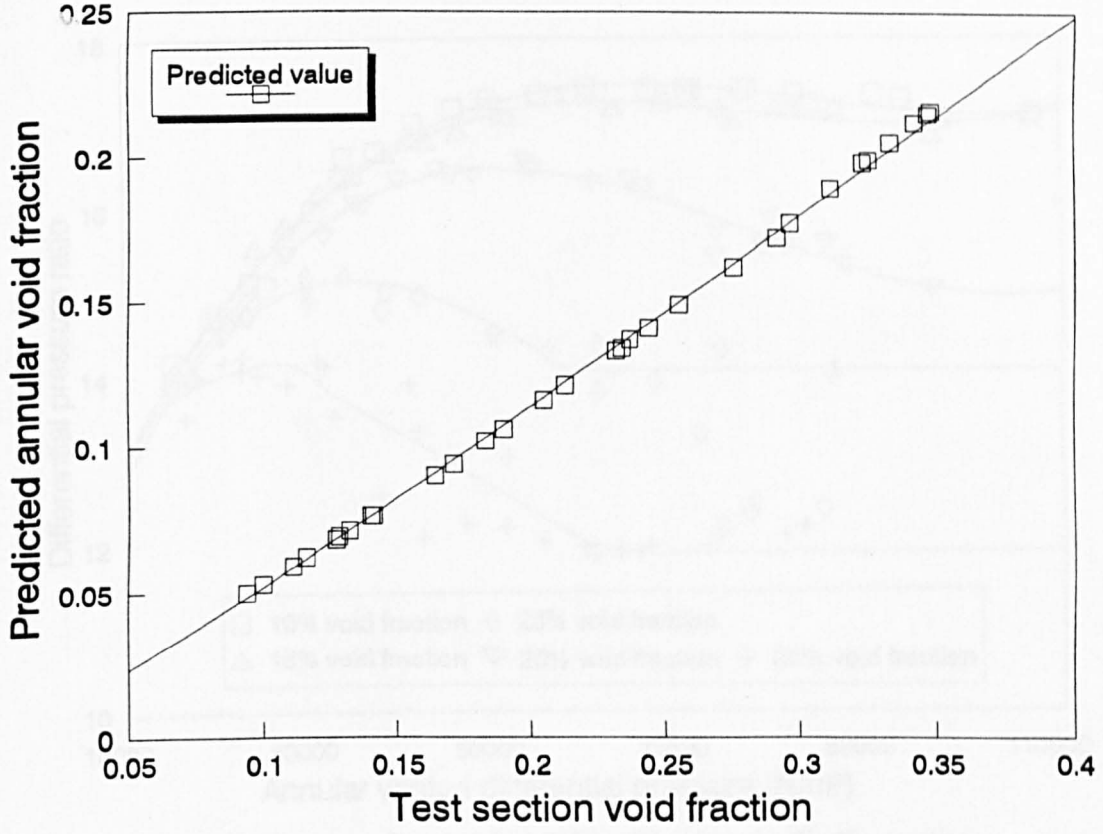

Figure 5.17 Predicted annular void fraction

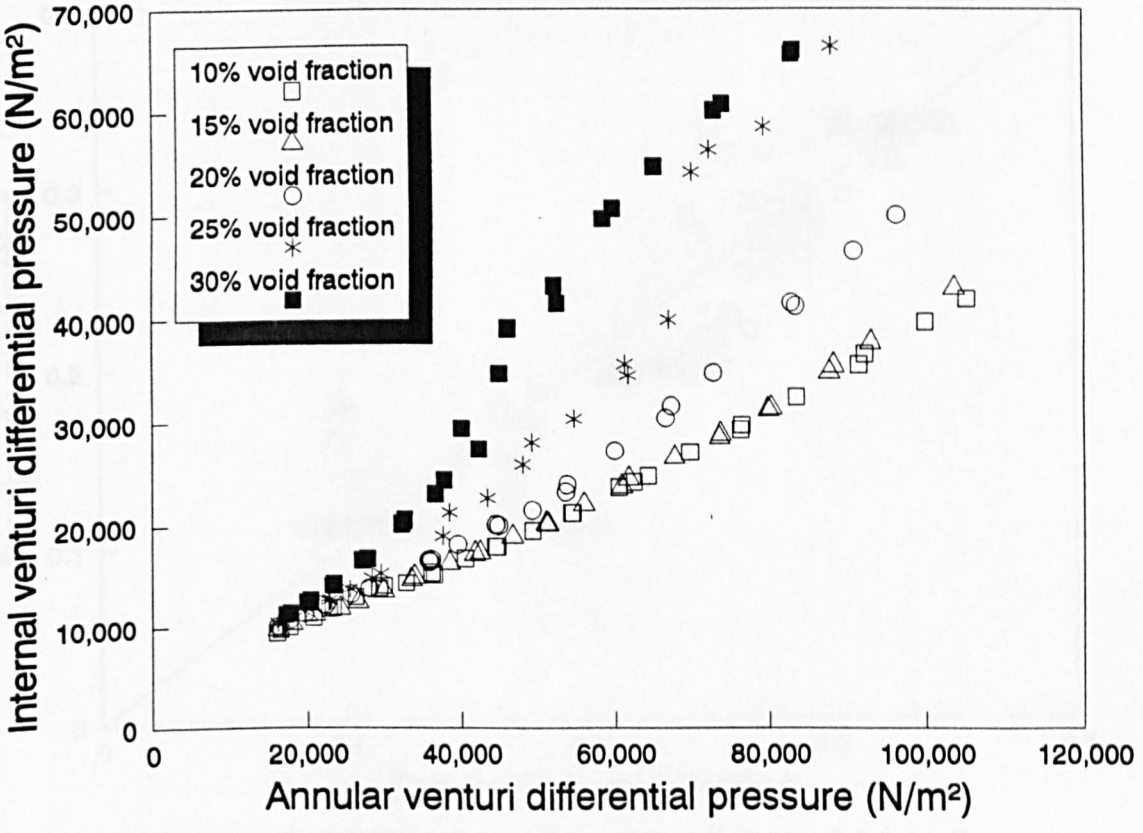

Figure 5.18 Relationship of venturi differential pressures

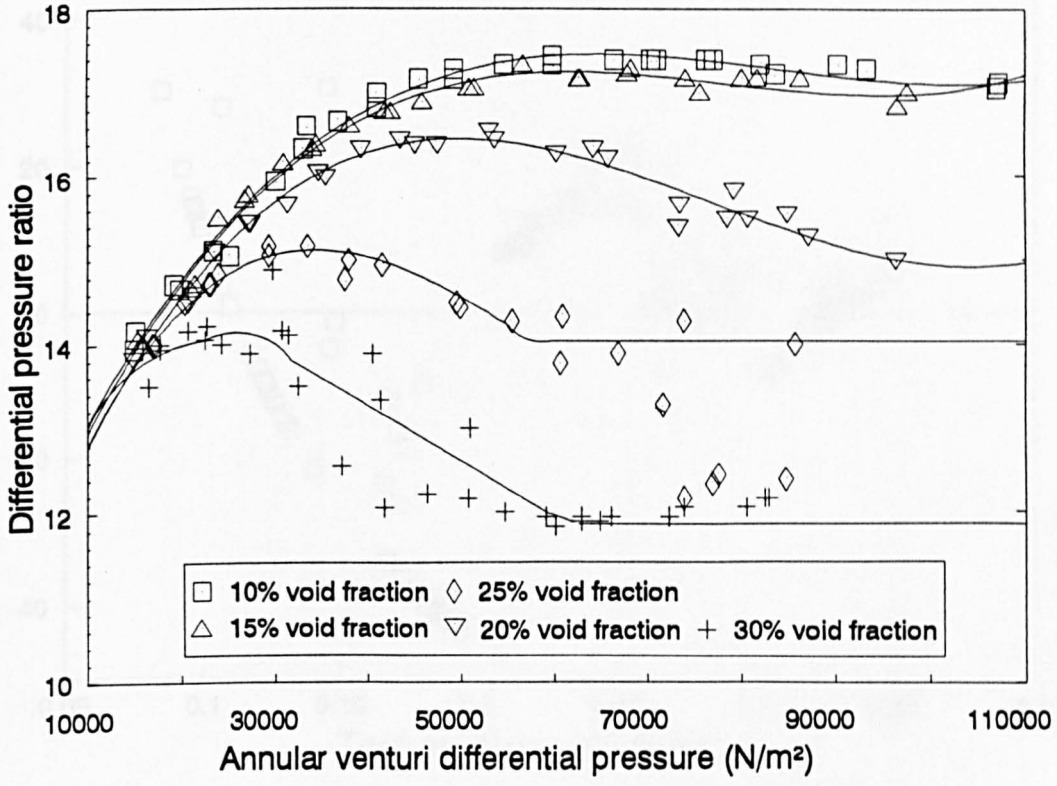

Figure 5.19 Void fraction prediction map

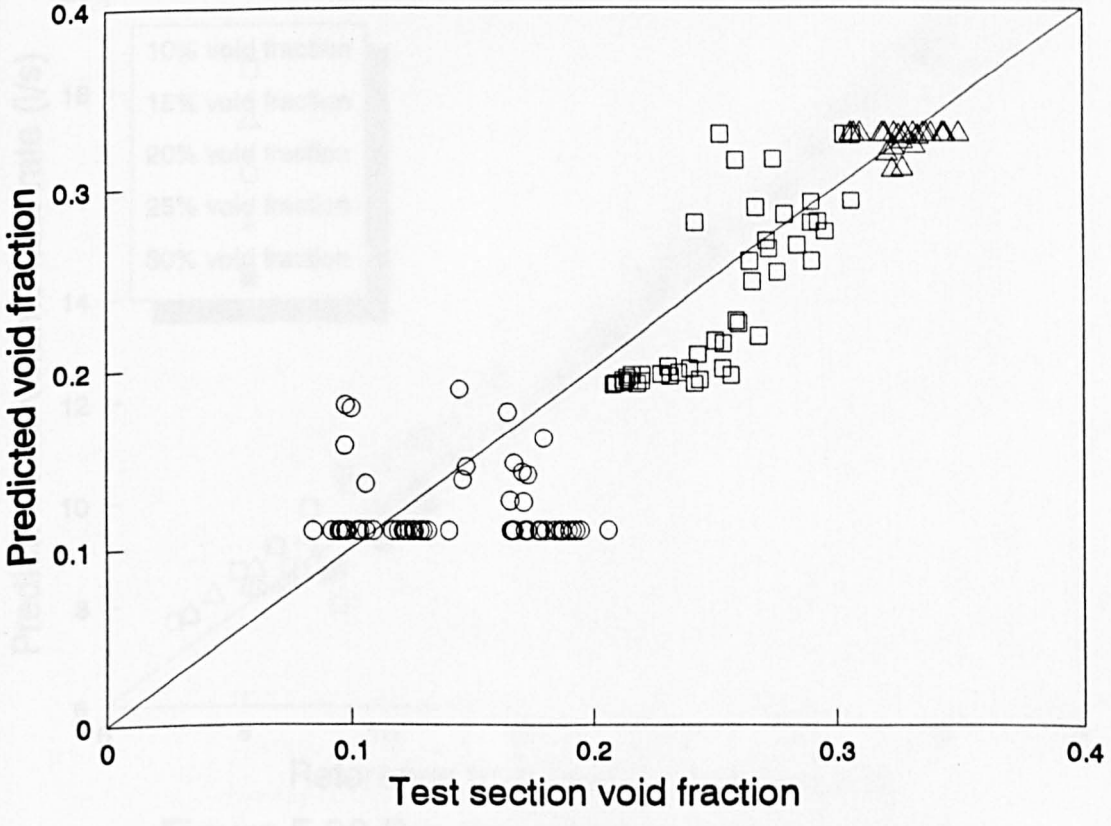

Figure 5.20 Predicted test section void fraction

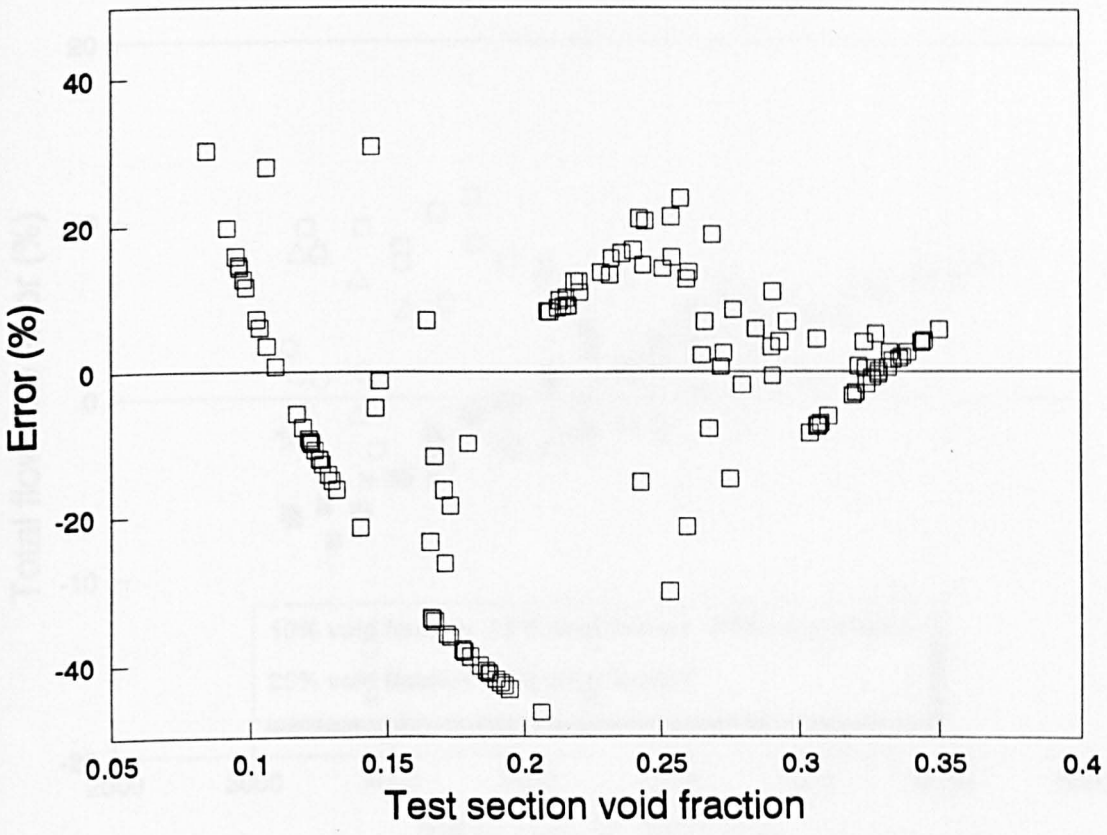

Figure 5.21 Error in predicted void fraction

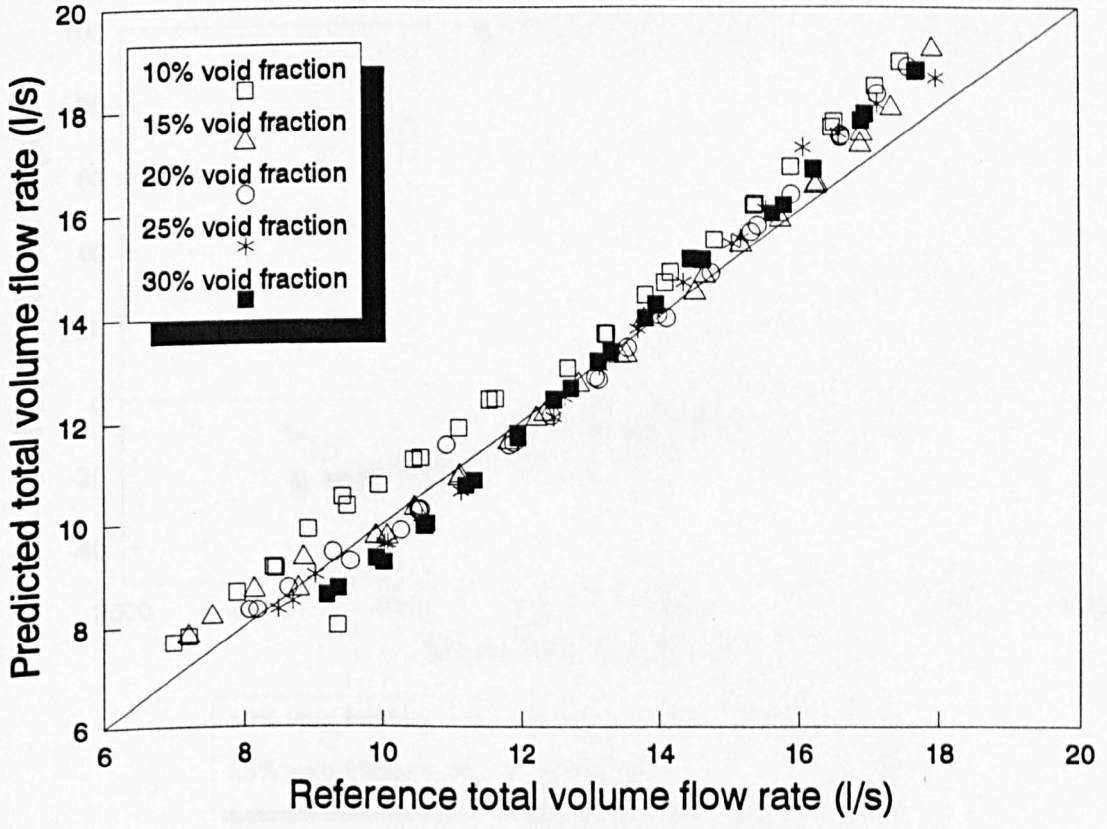

Figure 5.22 Predicted total volume flow rate

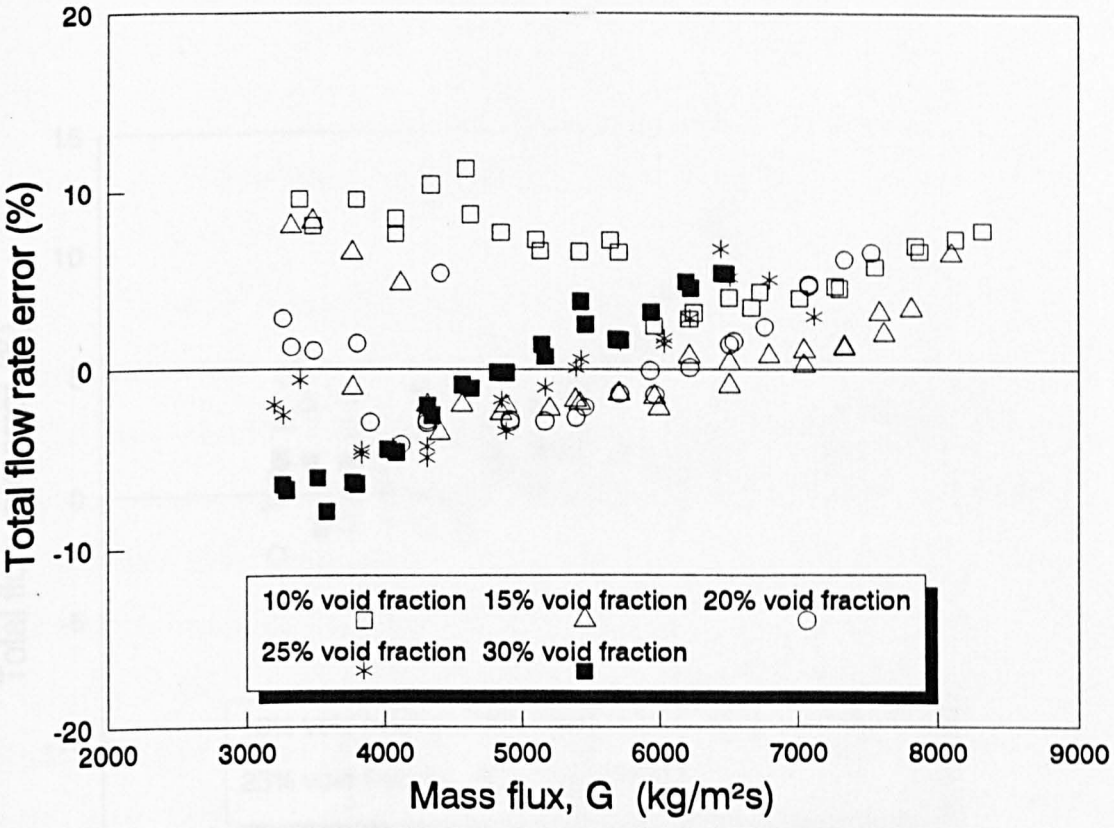

Figure 5.23 Error in total volume flow rate

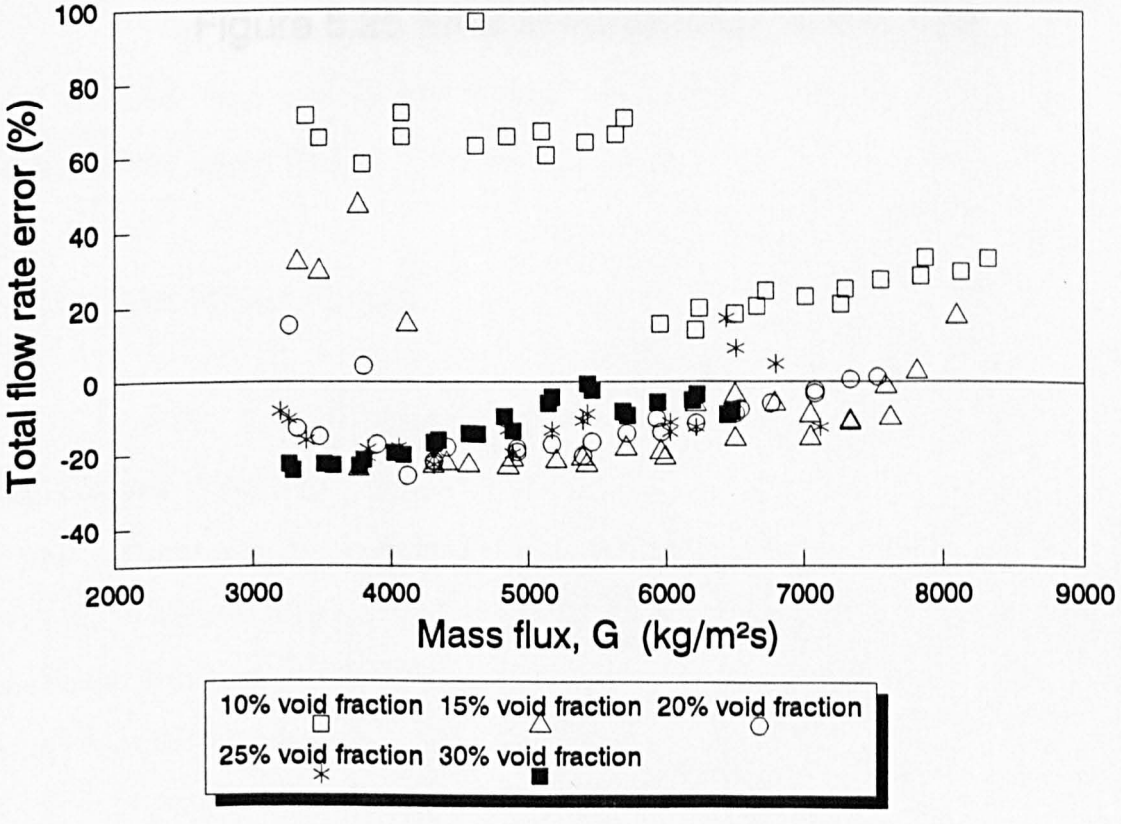

Figure 5.24 Error in gas volume flow rate

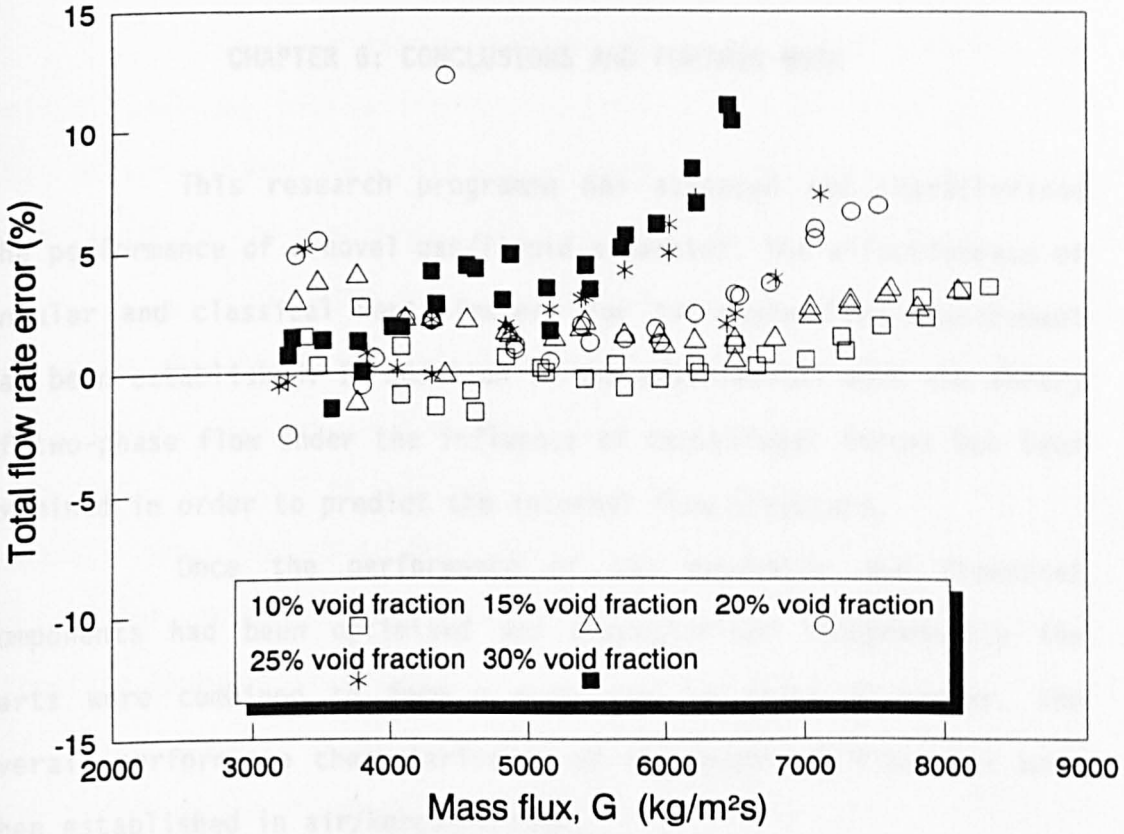

Figure 5.25 Error in liquid volume flow rate

CHAPTER 6: CONCLUSIONS AND FURTHER WORK

This research programme has assessed and characterised the performance of a novel gas/liquid separator. The effectiveness of annular and classical venturimeters for two-phase flow measurement has been established. In addition to the experimental work the theory of two-phase flow under the influence of centrifugal forces has been examined in order to predict the internal flow structure.

Once the performance of the separator and flowmeter components had been optimised and characterised independently the parts were combined to form a prototype two-phase flowmeter. The overall performance characteristics of the prototype flowmeter were then established in air/kerosene flow.

In the main body of the thesis the investigations have been divided into three main areas. The conclusions from each of these can be summarised as follows.

6.1 The Gas/Liquid Separator

The initial experimental investigations showed that the single-phase frictional pressure losses through the helical passages of the separator were around 30% higher than would be expected in a straight smooth tube of similar equivalent diameter. The experimentally determined values of friction factor were similar to those found in turbulent flow through helically coiled tubes. The

increased pressure losses reduced the overall length of the separator, an important feature for a practical device.

A radial pressure gradient was found to exist across the helical passages with a higher pressure at the outer passage wall than at the passage root. The radial pressure gradient was caused by centrifugal forces generated by the helical motion of the flow.

The profile of the radial pressure gradient and that of the streamwise local velocity indicated the presence of a vortex in the helical passages. Similar flow structures had been seen previously in work on helical coils. The secondary flow in the separator was thought to be a single vortex akin to those seen in rectangular cross-section bends rather than the double helix structure found in coiled tubes.

Under air/water two-phase flows the gas and liquid phases were successfully separated in the helical passages. The liquid phase occupied the outer region of the passage and the gas phase occupied the sector close to the passage root. A similar vortex existed in the liquid phase to that found in the single-phase flow and from visual observation there appeared to be a second vortex in the gas phase.

The radial pressure gradient in the separated liquid phase was similar to that found in the single-phase liquid flow. The radial pressure gradient in the separated gas phase was found to be much smaller than that in the liquid phase.

Experiments to find the frictional pressure losses in the separator showed that the gas/liquid frictional pressure losses were greater than in single-phase liquid flow. The accelerational pressure losses were shown to be negligible in the air/water flow. Because of the high frictional pressure losses the static pressure in the

passage root was significantly lower at the separator exit than at the mid-point of the separator. Sufficient pressure differential existed to drive the gas phase through the take-off slots to the internal gallery.

Take-off slots cut into the passage root at several locations were observed to remove a large proportion of the gas phase in the flow. An optimised configuration, which removed the highest proportion of separated gas with the lowest proportion of liquid phase, was identified quantitatively.

Examination of the data from the investigations of the individual slots showed that the quality of the separated flow stream was dependent on the residence time of the main flow through the separator; at low residence time (high velocity) there was high quality flow through the take-off slots. To maximise the separation high velocity should be maintained. The volume flow rate through the take-off slots was dependent on the pressure differential across the slot and the ratio of the gas phase height to the liquid phase height (area void fraction).

The performance of individual slots depended on their axial location. The performance of slots 1 and 2 was better than slot 3. The improved performance was caused by the distance from the separator exit of Slot 1 and 2, reducing exit effects. The gas separation efficiency of the take-off slots was between 40% and 50%. At some of the experimental conditions the gas separation efficiency was higher, between 70% and 80%.

The results were compared with the performance of the complete configuration of three slots per passage. The gas separation of the complete configuration was lower than the sum of the

individual slot performances. This indicated that upstream and downstream disturbances affected the performance of individual slots and showed the need for greater axial distances between take-off slots.

The gas separation efficiency in the air/kerosene flow was lower than that in the air/water flow. The reduction in the performance was attributed to the lower density ratio of the air/kerosene mixture compared with that of air/water. The performance reduction may be combated by increasing the separator length.

6.2 Analysis of Separator Flow

The general three-dimensional equations for two-phase flow were modified for the case of a one-dimensional adiabatic gas/liquid flow through a closed duct. Further modifications to the theory were made to include the effect of centrifugal forces on the flow. A closure relationship was introduced in the form of a radial pressure gradient with equal interfacial pressures in each phase. The equations were solved for the specific case of adiabatic gas/liquid flow through a helical duct. The model gave a good agreement with the experimentally measured air/kerosene pressure losses in the separator passages. The accurate prediction of the pressure losses gave confidence in the other parameters, such as the area void fraction, predicted using the two-phase flow model.

The effects of the changes in diameter and helix angle of a helical passage were investigated using coiled tubes. In single-phase flow the experimentally derived friction factor agreed well with those found by previous workers. Under two-phase air/water flow

a distinct stratification of the flow, similar to that in the separator, was observed at most conditions although at low mass flux the flow pattern was intermittent. The water occupied the outer sector of the coiled tube with the air at the inner wall.

The two-phase pressure losses through the tubes were dependent on the mean streamwise velocity and the helix angle of the coil. The flow velocity and the helix angle of the coil govern the magnitude of the centrifugal forces acting on the flow. The flow pattern in the coil was strongly influenced by the centrifugal forces which modified the phase distribution in the tube, especially at high mass flux. The two-phase pressure losses were dependent on the flow pattern in the coil.

The single-phase pressure losses in the separator helical passages were adequately predicted using the correlations of Srinivasan (1970) for turbulent flow in coiled tubes. However, the work of Srinivasan predicted a laminar flow in the separator under these conditions. This indicated that the characteristic double helix internal flow found in a coiled tube was not present in the separator. The structure of the internal flow in a triangular cross-section was therefore different to that in a coiled tube of similar flow area and helix angle, causing the transition Reynolds Number to occur at a lower value than for a tube. From experimental investigations, and the results of other workers, the helical passages were thought to have a single vortex secondary flow.

The mechanism by which the gas phase flowed preferentially through the take-off slots was also examined. The take-off slot was treated as an orifice. This resulted in a discharge coefficient curve which was common to each of the take-off slots.

Using this curve the volume flow rate through the slot could be predicted.

An analogy was also made with the flow split in a tee branch under two-phase flow conditions. The experimental results for flow split through the take-off slots were in close agreement with those in the literature, under similar conditions, for tee junctions. The take-off slot experimental results were compared with correlations in the literature for flow split in tee branches. One such correlation [Schrock et al, 1986], based on the ratio of the gas phase height to the liquid phase height, was found to be in good agreement with the experimental data.

By use of the two-phase flow model, the slot discharge coefficients and the Schrock correlation the volume flow rate and quality of the flow through the take-off slots can be predicted. The theories in the literature showed that as the liquid surface approaches the branch entrance the flow quality in the branch decreases. This was also found to be the case in the slot flow experiments.

6.3 Separator/Flowmeter Combination

Venturimeters were selected as the differential pressure flowmeters with the lowest pressure loss. When presented with well mixed gas/liquid flows both annular and classical designs were found to give good results. The indicated total volume flow rate was within ± 10% of the reference value, providing that the mean density of the flowing mixture was known.

Combined together with the separator the ratio of the pressure drops through the internal and annular venturimeters was found to be proportional to the test section void fraction, providing a means of predicting the void fraction of the mixture passing through the separator/flowmeter without recourse to further instrumentation. The void fraction of the flow passing through each venturimeter was then predicted using the known gas separation efficiency and liquid draw-off. The volume flow rates measured through each venturimeter were combined to give the total volume flow rate through the separator/flowmeter with an error of less than ± 10% at all the test conditions. The phase flow rates, derived from the predicted void fraction and the total volume flow rate, were within the range 0 to - 20% of the reference gas phase flow rate for void fractions between 15 and 30%. The liquid phase flow rate error was between - 1% and + 8% of the reference in all the tests. The gas flow rate (percentage) error was magnified due to the relatively low mass flow rate of the gas phase.

In general the overall uncertainty target of ± 10% was met by the separator/flowmeter for the total volume flow rate and the liquid phase flow rate for void fractions in the range 10% to 30%. The error in the gas phase flow measurement would be acceptable in many practical applications, where the process fluid of most interest is the liquid phase. The errors found in the two-phase flowmeter are larger than required for use as a fiscal flowmeter. The two-phase flowmeter would provide adequate measurements for use as part of a reservoir management system.

6.4 Further Work

The research described in this report was concerned with a specific method of measuring two-phase flow parameters. This method has been developed into a prototype device. Presently there are no commercially available devices which can perform this complex task. Those devices which are under development concurrently are unlikely to achieve significantly better performance. The present two-phase flowmeter has exhibited good performance in gas/liquid mixtures with a high density ratio. The performance is acceptable for applications such as reservoir management. At some flow conditions up to 80% of the gas phase was removed and with further development these flow conditions could be further extended. To find a wider application for the two-phase separator/flowmeter a similar level of performance in flows of lower density ratio must be demonstrated.

1. It is anticipated that a gas/liquid mixture of lower density ratio will require a longer residence time in the separator to achieve the same degree of separation demonstrated by this work. To achieve the same gas separation efficiency with a mixture containing a high density gas will also require higher pressure differentials across the take-off slots.

2. Many practical problems involve the presence of a second liquid phase, such as water in the production stream of an oil well. Given the turbulent nature of the internal flow structure of the separated liquid phase in the helical passages it is unlikely that two liquid phases of similar density will be separated. However it may be possible, using capacitance or radiation attenuation techniques, to determine the water cut in the separated liquid phase.

This would then enable the flow rate of each liquid phase to be measured.

3. Work on downward flow of gas/liquid mixtures in pipes [see Barnea et al, 1985] has shown that the liquid phase is distributed to the outer wall of the tube, with gas 'coring' in the centre. This phase distribution may be advantageous to the performance of the separator, allowing the use of a shorter unit with a lower overall pressure loss.

4. Further experimental work with fluid mixtures of different density ratios to those used in the present study is required. This may allow the requirement for the separator performance to be characterised in each fluid combination to be relaxed.

5. The present study did not investigate the performance of the separator/flowmeter in mixtures with void fractions of greater than 30%. It is necessary to expand the void fraction envelope to seek wider application for the device. The typical phase distribution and high gas fraction found in annular flow, for example, may enhance the performance of the device.

6. The take-off slots were shown to interact, causing a higher than expected liquid draw-off. Increasing the axial separation of these slots may improve their performance.

REFERENCES

Agee LJ, Banerjee C, Duffey RB, Hughes ED (1978) Some Aspects of Two-fluid Models for Two-phase Flow and their Numerical Solution. 2nd OECD//NEA Specialists Meeting on Transient Two-phase Flow, Paris, June 1978.

Akagawa K , Sakaguchi T and Ueda M. (1971) Study on Gas-Liquid Two-Phase Flow in Helically Coiled Tubes. Bull of JSME. 14, 564-571.

Anglesea W.T, Chambers D.J.B and Jeffrey R.C. (1974) Measurement of Water/Steam Pressure Drop in Helical Coils at 179 bar. Conf Multiphase Flow Systems I Mech E. 11,i2, 1-37.

Ardron K.H. (1980) One-Dimensional Two-Fluid Equations for Horizontal Stratified Two-Phase Flow. Int J of Multiphase Flow. 6, 295-304.

Azzopardi B.J. (1988) An Additional Mechanism in the Flow Split of High Quality Gas-Liquid Flows at a T Junction. AERE-R 13058. 385-404.

Azzopardi B.J. (1984) The Effect of the Side Arm Diameter on the Two-Phase Flow Split at a T Junction. Int. J. Multiphase Flow. 10, n4, pp509-512

Azzopardi B.J and Whalley P.B. (1982) The Effect of Flow Patterns on Two-Phase Flow in a Tee Junction. Int J Multiphase Flow. 8, 491-507.

Azzopardi B.J and Govan A.H. (1985) Annular Two-Phase Flow in Venturis. European Two-Phase Flow Group Meeting , Marchwood Eng. Lab., 4-7 June 1985.

Azzopardi B.J and Memory S.B. (1989) The Split of Two-Phase Flow at a Horizontal T-Annular and Stratified Flow. AERE R13473 (1989 HTFS report). 71-87.

Azzopardi B.J and Smith P.A. (1990) Two-Phase Flow Split at T Junctions with Horizontal and Vertical Side-Arms. Int. Conf. on Basic Principles & Industrial Applications of Multiphase Flow. 24-25 Apr 1990 London.

Baker O (1954) Simultaneous Flow of Oil and Gas. Oil and Gas Journal. v53 n12 pp185-195

Banerjee S and Chan A.M.C. (1980) Separated Flow Models-1 Analysis of the Averaged and Local Instantaneous Formulations. Int J Multiphase Flow. 6, pp1-24.

Banerjee S, Rhodes E and Scott D.S. (1967) Film Inversion of Cocurrent Two-Phase flow in Helical Coils. A.I.Ch.E. Journal. 13, 189-191.

Barnea D, Shoham O and Taitel Y. (1982) Flow Pattern Transition for Downward Inclined Two-Phase Flow; Horizontal to Vertical. Chem. Eng. Sci. v37 n5, pp735-740

Barnea D, Shoham O and Taitel Y.(1985) Gas-Liquid Flow in Inclined Tubes: Flow Pattern Transitions for Upward Flow. Chem. Eng. Sci. v40 n1, pp131-136

Baroczy C.J. (1966) A Systematic Correlation for Two-Phase Pressure Drop. Chem Engng Prog Symp Series. 62, pp232-249.

Bosch M and Hebrard P (1984) Experimental and Theoretical Studies of a New Flow Conditioner. Int. Conf. on Metering of Natural Gas and Liquefied Hydrocarbon Gases. London 1-2 Feb 1984

Boure J.A. (1987) Two-Phase Flow Models: The Closure Issue. in Multiphase Science and Technology 3. ed. Hewitt, Delhaye and Zuber, Hemisphere.

Boyce B.E, Collier J.G and Levy J. (1969) Hold-up and Pressure Drop Measurements in the Two-Phase Flow of Air-Water Mixtures in Helical Coils. Proc Int Symp on Research in Concurrent Gas-Liquid Flow . Univ Waterloo Sept 18-19 1968. 203-255.

Bradley D. (1965) The Hydrocyclone. pub Pergamon Press.

BS.1042 (1981) Methods of Measurement of Fluid Flow in Closed Conduits: Section 1.1 Orifice Plates, Nozzles and Venturi Tubes Inserted in Circular Cross-Section Conduits Running Full. London BSI

Chen X and Zhang M. (1984) An Investigation on Flow Pattern Transitions for Gas-Liquid Two-Phase Flow in Helical Coils. Multi-Phase Flow and Heat Transfer 3 part a: Fundamentals ed. Veziroglu and Bergles. 185-201.

Chisholm D. (1967) Flow of Incompressible Two-Phase Mixtures through Sharp-Edged Orifices. J Mech Eng Sci. 9, 72-78.

Collier J.G. (1976) Single-Phase and Two-Phase Flow Behaviour in Primary Circuit Components. Proc. Advanced Study Institution Two-Phase Fflows and Heat Transfer. Istanbul; August 1976. 313-355.

Cook T.L and Harlow F.H. (1984) Virtual Mass in Multiphase Flow. Int J Multiphase Flow. 10, 691-696.

Crowe C.T. (1982) Venturi Design for Metering Solids Flow in Gas-Liquid Suspensions-Final Report. Washington State Uni DOE Grant DE-FG22-80pc30212.

Davis M.R. (1980) Response of Small Pitot Tubes in Gas-Liquid Flows. Int J Multiphase Flows. 6, 369-373.

Dean W.R. (1927) Note on the Motion of Fluid in a Curved Pipe. Phil Mag (Series 7). 4, 208-223.

De Crecy F. (1986) Modelling of Stratified Two-Phase Flow in Pipes, Pumps and other Devices. Int J of Multiphase Flow. 12, 307-323.

Delhaye J.M. (1981) Local Instantaneous Equations: Instantaneous Space Averaged Equations; Local Time Averaged Equations; Composite Averaged Equations. in Thermohydraluics of Two-Phase Systems for Industrial Design and Nuclear Engineering ed Delhaye, Giot and Riethmuller, McGraw-Hill

Farmer P.R. (1972) Air-Water Mixtures Flowing in Helices. part 2: Pressure Drop Measurements. CEGB rd/l/n 156/72.

Gambill W.R, Bundy R.D and Wansborough R.W. (1961) Heat Transfer, Burnout and Pressure Drop for Water in Swirl through Tubes with Internal Twisted Tapes. Chem Eng Prog Symp Ser 57. 32, 127 - 137

Gardner G.C. (1990) Deep Swirling Flow Down a Plughole with Air Entrainment. Int. J. Multiphase Flow v16 n6 pp1003-1021.

Gardner G.C. and Kubie J. (1976) Flow of Two Liquids in Sloping Tubes: An Anologue of High Pressure Steam and Water. Int J Multiphase Flow. 2, 435-451.

Govier G.W. and Aziz K. (1972) The Flow of Complex Mixtures in Pipes. Van Nostrand Reinhold.

Graham E.J. (1967) The Flow of Air-Water Mixtures through Nozzles. NEL Report 308

Harris D.M and Shires G.L. (1973) Two-Phase Pressure Drop in a Venturi. NEL Report no 549 : "Two-Phase Flow through Orifices and Nozzles" Meeting 29/11/72. pp18-35.

Hart J, Ellenberger J and Hamersma P.J. (1988) Single and Two-Phase Flows through Helically Coiled Tubes. Chem Eng Sci. 43, 775-783.

Hawthorne W.R (1950) Secondary Circulation in Fluid Flow

Hayward A.T.J and Dallas J.T (1965) The NEL Universal Apparatus for Measuring the Gas Content of Liquids and Semi-Liquids. NEL Report No 189.

Helgeson N.L, Maddox J.P and Amend W.E. (1984) Recovery of Power from Flashing Gas-Hydrocarbon Solutions with the Biphase Turbine. Conf Fluid Machinery for the Oil Petrochemical and Rec Industries. pp235-245.

Hinze J.O. (1962) Momentum and Mechanical-Energy Balance Equations for a Flowing Homogeneous Suspension with Slip between the Two Phases. Appl Sci Res. all, pp33-46.

Hobbs (1990) Differential Pressure Meters. NEL Flow Measurement Course, Lecture Notes

Hwang S.T, Soliman H.M and Lahey R.T.jr. (1988) Phase Separation in Dividing Two-Phase Flows. Int. J. Multiphase Flow.. 14, 439-458.

Ince D.W. (1990) Using the Gamma Ray Densitometer for Density Measurements in Two-Phase Flow. Liverpool Univ. no. 60

Ishii M. (1975) Thermo-Fluid Dynamic Theory of Two-Phase Flow. Eyrolles, Paris

Ishii M. and Mishima K. (1982) Liquid Transfer and Entrainment Correlation for Droplet-Annular Flow. 7th Int Heat Transfer Conf Munich 1982. 5, 307-312.

ISO 5167 (1989) Measurement of Fluid Flow by means of Orifice Plates, Nozzles and Venturi Tubes inserted in Circular Cross-Section Conduits Running Full.

Ito D. (1959) Friction Factors for Turbulent Flow in Curved Pipes. Trans ASME D81, pp123-132

Jensen M.K, Pourdashti M and Bensler H.P. (1985) Two-Phase Pressure Drop with Twisted Tape Swirl Generators. Int. J. Multiphase Flow. 11, pp201-211.

Johnson M.W. (1989) The Computation of Secondary Flow in a 90° Rectangular Cross-Section Bend. To Be Published.

Jones O.C.jr and Delhaye J.M. (1976) Transient and Statistical Measurement Techniques for Two-Phase Flows: A Critical Review. Int. J. Multiphase Flow. 3, 89-116.

Kaji M, Mori K, Nakanishi S and Ishigai S. (1984) Flow Regime Transitions for Air-Water Flow in Helically Coiled Tubes. Multi-Phase Flow and Heat Transfer 3. Part a: Fundamentals ed. Veziroglu and Bergles. pp201-214.

Kalra S.P, Yao L.S and Davies W.E.R. (1983) Flow Behaviour in a Stationary Vane Centrifugal Separator - Simulation, Experiments and Analysis. 2nd Topical Meeting on Nuclear Reactor Thermal Hydraulics. Santa-Barbara Jan 11-14 ed. Merilo pp979-987

King N.W and Purfit G.L. (1984) Experiments on Oil/Gas Separation in Helical Passages. 2nd Int Conf on Hydrocyclones, Bath, 18-21 Sept 1984. f1, pp205-216.

Kinghorn F.C and McHugh A. (1981) The Performance of Turbine Meters in Two Component Gas/Liquid Flow. In Flow: Its Measurement and Control in Science and Industry, St. Louis, Missouri, March 1981, pp471-492

Kinghorn F.C. (1990) Measurement Uncertainty in Flowmeter Calibrations. Lecture Notes in "The Basic Principles and Practice of Flow Measurement", NEL.

Koutsky J.A and Adler R.J. (1964) Minimization of Axial Dispersion by use of Secondary Flow in Helical Tubes. Can J Chem Eng. 42, pp238-246.

Kowe R, Hunt J.C.R, Hunt A, Couet B and Bradbury L.J.S. (1988) The Effects of Bubbles on the Volume Fluxes and the Pressure Gradients in Unsteady and Non-Uniform Flow of Liquids. Int. J. Multiphase Flow. 14, pp587-606.

Kubie J and Gardner G.C. (1977) Flow of Two Liquids in a Helix: An Analogue of High Pressure Boilers. Int. J. Multiphase Flow. 3, pp353-366.

Kuo J.T. and Wallis G.B. (1988) Flow of Bubbles through Nozzles. Int. J. Multiphase Flow. 14, pp547-564.

Lockhart R.W and Martinelli R.C. (1949) Proposed Correlation of Data for Isothermal Two-Phase, Two Component Flow in Pipes. Chem Eng Progress. 45, pp39-48.

Lugt H. (1961) The Influence of Swirling Flow on the Discharge Coefficients of Standard Pressure Differential Flowmeters. Brennst-Warm-Kraft, 13(3), pp121-125

Maciaszek T. and Micaelli J.C. (1988) A Phase Separation Model for Tee Junctions Application to a PWR Safety Code. 25th Nat. Heat Transfer Conf, Houston, Tex 24-27 Jul 1988. 82-89.

Madden J.M. and St. Pierre C.C. (1970) Two-Phase Air-Water Flow in a Slot Type Distributor. Fluid Mechanics and Measurements in 2 Phase Flow Systems. Proc of a Symp., I.Mech.E and I.Chem.E; 24-25 Sept 1969. 184, pp174-184.

Mandhane J.M, Gregory G.A and Aziz K. (1974) A Flow Pattern Map for Gas-Liquid Flow in Horizontal Pipes. Int. J. Multiphase Flow. 1, 537-553.

Massey B.S. (1983) Mechanics of Fluids. Van Nostrand Reinhold. 5th Edition

McCreery G.E. and Banerjee S (1990) Phase Separation of Dispersed Mist and Dispersed Annular (Rivulet or Thin Film) Flow in a Tee 1 Experiments. Int. J. Multiphase Flow. 16, n3 pp429-445

McQuillan K.W and Whalley P.B. (1985) Flow Patterns in Vertical Two-Phase Flow. Int. J. Multiphase Flow. 11, 161-175.

Millington B.C. (1990) Private Communication

Murdock J.W. (1962) Two-Phase Flow Measurement with Orifices. Trans ASME. Dec 1962, pp419-433.

Nebrensky J.R, Morgan G.E and Oswald B.J. (1980) Cyclone for Gas/Oil Separation. Int Conf on Hydrocyclones BHRA Cambridge. pp167-178.

Oshinowo T and Charles M.E. (1974) Vertical Two-Phase Flow Part 1. Flow Pattern Correlations. Can. J. Chem. Eng. v52 pp25-35

Rippel G.R, Eidt C.M and Jordan H.B. (1966) Two-Phase Flow in a Coiled Tube. I&EC Process Design and Development. 5, pp32-38.

Rogers G.F.C and Mayhew Y.R. (1964) Heat Transfer and Pressure Loss in Helically Coiled Tubes with Turbulent Flow. Int J Heat Mass Transfer. 7, pp1207-1216.

Rouse H (1956) Seven Exploratory Studies in Hydraulics. Proc. ASCE v82, paper 1038

Rousseau J.C. and Ferch R.L. (1979) A Note on Two-Phase Separated Flow Models. Int. J. Multiphase Flow. 5, pp489-493.

Sasanow S. (1989) Wellheads on the Seabed. New Scientist 18 Mar 1989

Schrock V.E, Revankar S.T, Mannheimer R and Wang C-H (1986) Small Break Critical Discharge - The Roles of Vapor and Liquid Entrainment in a Stratified Two-Phase Region Upstream of the Break. NUREG/CR-4761 LBL-22024

Serizawa A. and Kataoka I. (1988) Phase Distribution in Two-Phase Flow. Conf. on Transient Phenomena in Multiphase Flow. Dubrovnik, 20-30 May pp179-224

Shoham O, Brill J.P and Taitel Y. (1987) Two-Phase Flow Splitting in a Tee Junction-Experiment and Modelling. Chem Eng Sci. 42, pp2667-2676.

Sim S.K and Lahey R.T. (1985) The Hydrodynamic Development Length for Lateral Void Distribution in a Triangular Conduit. ASME J Heat Transfer v47 pp125-130.

Smith L.T, Murdock J.W and Applebaum R.S. (1977) An Evaluation of Existing Two-Phase Flow Correlations for use with ASME Sharp Edge Metering Orifices. Trans ASME. July, pp343-347.

Smoglie C. (1984) Two-Phase Flow through Small Branches in a Horizontal Pipe with Stratified Flow. Karlsruhe KfK 3861 Dec 1984.

Smoglie C. and Reimann J. (1986) Two-Phase Flow through Small Branches in a Horizontal Pipe with Stratified Flow. Int. J. Multiphase Flow. 12, pp609-225.

Snoek C.W. (1988) A Review of Recent Advances in Multiphase Flow Measurements and Methods. Experimental Heat Transfer, Fluid Mechanics and Thermodynamics ed. Shah, Ganic and Yang pub Elsevier pp59-71.

Srinivasan P.S, Nandapurkar S.S and Holland F.A. (1968) Pressure Drop and Heat Transfer in Coils. The Chemical Engineer. no 218, pp113-119.

Srinivasan P.S, Nandapurkar S.S, Holland F.A. (1970) Friction Factors for Coils. Trans. Instn. Chem. Engnrs. 48, t156-t161.

Stuhmiller J.H. (1977) The Influence of Interfacial Pressure Forces on the Character of Two-Phase Flow Model Equations. Int. J. Multiphase Flow. 3, 551-560.

Svarovsky L. (1984) Hydrocyclones. pub Holt, Rhinehart and Winston.

Taitel Y, Bornea D and Dukler A.E. (1980) Modelling Flow Pattern Transitions for Steady Upward Gas-Liquid Flow in Vertical Tubes. AIChE Journal 26, pp345-354.

Taitel Y and Dukler A.E. (1976) A Model for Predicting Flow Regime Transitions in Horizontal and Near Horizontal Gas-Liquid Flow. AIChE Journal 22, pp47-55.

Tapucu A, Teydessou A, Troche N and Merilo M. (1989) Pressure Losses Caused by Area Changes in a Single Channel Flow under Two-Phase Flow Conditions. Int. J. Multiphase Flow. 15, pp51-64.

Thang N.T and Davis M.R. (1979) The Structure of Bubbly Flow through Venturis. Int J of Multiphase Flow. 5, pp17-37.

Usui K, Aoki S and Inoue A. (1983) Flow Behaviour and Phase Distribution in Two-Phase Flow around Inverted U-Bend. J Nuclear Science and Technology. 20, pp915-928.

Wallis (1969) One-Dimensional Two-Phase Flow. McGraw-Hill

Watanabe O, Tajima O, Nakano T and Shimoya M. (1986) Flow and Heat Hransfer of a Gas and Liquid Two-Phase Flow in Helical Coils. Nippon Kikai Gakkai Ronbunshu B Hen. 52, pp1857-1863.

Whalley P.B. (1980) Air-Water Two-Phase Flow in a Helically Coiled Tube. Int. J. Multiphase Flow. 6, pp345-356.

Whalley P.B. (1987) Boiling, Condensation and Gas-Liquid Flow. Oxford Press

White C.M. (1929) Streamline Flow through Curved Pipes. Proc. Royal Soc. (London) v123 pp645-663

Zuber N. (1980) Problems in Modelling of Small Break LOCA. NUREG - 0724; October 1980.

APPENDIX 1: ASSESSMENT OF UNCERTAINTY ON DIFFERENTIAL PRESSURE FLOWMETERS

A1.1 Orifice Plates

The mass flow through an orifice plate is given by the following equation

$$q_m = C\epsilon A_0 \left[\frac{2\rho\Delta P}{1-\beta^4}\right]^{0.5} \qquad \text{A1.1}$$

where

$$\beta = \frac{d}{D} \quad \text{and} \quad A_0 = \frac{\pi d^2}{4}$$

by substitution A1.1 becomes

$$q_m = \frac{C\epsilon\pi d^2}{4}\left[\frac{2\rho\Delta P}{1-\beta^4}\right]^{0.5}$$

$$\text{and if } k = \frac{C\epsilon\pi\ (2\rho\Delta P)^{0.5}}{4}$$

$$\text{then } q_m = kd^2(1-\beta^4)^{-0.5}$$

The overall uncertainty associated with a particular meter can be expressed as the root sum square of the individual

uncertainties associated with each component of equation A1.1 in the following manner.

$$e^2(y) = \left\{\frac{\partial y}{\partial x_1}\right\}^2 e^2(x_1) + \left\{\frac{\partial y}{\partial x_2}\right\}^2 e^2(x_2) + \ldots + \left\{\frac{\partial y}{\partial x_n}\right\}^2 e^2(x_n) \qquad \text{A1.2}$$

Each component of A1.1 has a sensitivity coefficient associated with it in equation A1.2, which is the partial derivative of q_m with respect to the component. For an orifice the partial derivatives are straightforward, with the exception of those for d and D which are derived below.

$$\frac{\partial q_m}{\partial d} = k\left[2d(1-\beta^4)^{-1/2} + \frac{d^2}{D} 2\beta^3 (1-\beta^4)^{-3/2}\right]$$

as $\dfrac{\partial \beta}{\partial d} = \dfrac{1}{D}$

re-arranging gives

$$\frac{\partial q_m}{\partial d} = 2kd(1-\beta^4)^{-1/2}\left[1 + \frac{\beta^4}{(1-\beta^4)}\right]$$

further re-arrangement and squaring gives

$$\left[\frac{\partial q_m}{\partial d}\right]^2 = \frac{4k^2d^2}{(1-\beta^4)^3}$$

and in percentage error terms

$$e^2(d)\left[\frac{\partial q_m}{\partial d}\right]^2 = \frac{4k^2d^4}{(1-\beta^4)^3}E^2(d)$$

$$\text{where } \frac{e^2(d)}{d^2} = E^2(d)$$

and, dividing by q_m^2, and re-arranging we get

$$e^2(d) = \frac{4}{(1-\beta^4)^2}E^2(d) \qquad \text{A1.3}$$

The sensitivity coefficient can be obtained for D by similar means, giving

$$e^2(D) = \frac{4\beta^8}{(1-\beta^4)^2}E^2(D) \qquad \text{A1.4}$$

The remaining coefficients are simply determined and their insertion into equation A1.2 gives

$$E^2(q_m) = E^2(C) + E^2(\epsilon) + \left[\frac{2\beta^4}{1-\beta^4}\right]^2 E^2(D) + \left[\frac{2}{1-\beta^4}\right]^2 E^2(d)$$

$$+ \frac{1}{4}E^2(\Delta P) + \frac{1}{4}E^2(\rho) \qquad \text{A1.5}$$

Equation A1.5 shows the sensitivity of the overall uncertainty to that of each component. For example, given that the β ratio is always less than 1 the uncertainty of an orifice plate is more sensitive to the bore diameter, d, than the pipe diameter, D.

A1.2 Venturimeters

The mass flow rate for a venturimeter is gained in a slightly different way to that for an orifice plate.

$$q_m = CA_1\left[\frac{2\rho\Delta P}{(1/\beta^2-1)^{1/2}}\right]^{1/2} \qquad \text{A1.6}$$

The sensitivity coefficients are found in a similar way to those for the orifice plate

$$\frac{\partial q_m}{\partial D} = k\left[\frac{2D}{(1/\beta^4-1)^{1/2}} + D^2.2\beta^3\frac{\partial\beta}{\partial D}(1/\beta^4-1)^{-3/2}\right]$$

$$\text{and} \quad \frac{\partial\beta}{\partial D} = \frac{-d}{D^2}$$

Re-arrangement gives

$$\frac{\partial q_m}{\partial D} = 2kD\left[\frac{1}{(1/\beta^4-1)^{1/2}} - \beta^{-4}.(1/\beta^4-1)^{-3/2}\right]$$

further re-arrangement reduces the equation to

$$\frac{\partial q_m}{\partial D} = \frac{-2kD}{(1/\beta^4-1)^{3/2}} \qquad \text{A1.7}$$

Squaring and multipling by the percentage error

$$e^2(D).\frac{\partial q_m}{\partial D} = \frac{4k^2D^2}{(1/\beta^4-1)^3}D^2E(D)$$

and dividing by q_m^2 gives

$$E^2(q_m) = \frac{4}{(1/\beta^4-1)^2}E^2(D) \qquad \text{A1.8}$$

APPENDIX 2: PUBLISHED PAPERS

EXPERIENCE WITH TWO DESIGNS OF DIFFERENTIAL PRESSURE FLOWMETERS IN TWO-PHASE FLOW

T.S. Whitaker & I. Owen

Department of Mechanical Engineering
University of Liverpool
PO Box 147, Liverpool, L69 3BX, UK.

ABSTRACT

Differential pressure flowmeters are the most widely used type of flowmetering device. In the quest to develop flowmeters for two-phase gas/liquid mixtures the suitability of two such devices is assessed in this paper. The flowmeters are an annular venturimeter and a variable orifice meter. The annular venturimeter was tested with air/water flows having void fractions up to 30% and the variable orifice meter with void fractions up to 40%. The two-phase discharge coefficient for the annular venturimeter was found to be independent of the void fraction but to fall from 0.95 to 0.92 in the two-phase Reynolds number range 90000 to 260000. The variable orifice meter was found to have a linear characteristic in two-phase flows with data within 7% of the corrected meter factor. The discharge coefficient and meter factor were calculated using the homogeneous density.

1.0 INTRODUCTION

Two-phase flows are frequently encountered in chemical engineering and oil production processes. Accurate metering of these gas-liquid flows is at present a difficult problem due to their unsteady and often violent nature. If simple flow meters, such as standard differential pressure devices which are readily available for single-phase flow metering, can be used under two-phase flow conditions, then these flow metering problems would be greatly eased. Two types of simple differential pressure flow meter which were available in the laboratory, were investigated for low void fraction two-phase flows, with the aim of producing a calibration for each.

Two-phase flows through differential pressure devices such as sharp-edged orifices have been investigated by several workers, notably Chisholm (1967) and Murdock (1962). Investigations of venturi tubes have been mainly limited to annular two-phase flow, Azzopardi and Govan (1985), and to examination of the flow structure, Thang and Davis (1979). The two flowmeters used in the present investigation were an annular venturimeter and a variable orifice meter.

This paper presents the experimental results obtained for the two flowmeters. For the annular venturimeter two-phase air/water flows with volume void fractions of up to 30% were investigated. The data gathered for the variable orifice meter were for void fractions of up to 40%. The two-phase discharge coefficient and the meter factor were found for the two devices respectively over the flow ranges investigated.

2.0 NOTATION

A_1 - Annulus Area
A_2 - Throat Area
Cd - Coefficient of Discharge
D - Diameter
E - Transducer Output
K - Meter Factor
P - Pressure
Q - Volume Flowrate
V - Mean Velocity
Re - Reynolds Number
x - Mass Quality
α - Volume Void Fraction
μ - Viscosity
ρ - Density

Subscripts

g - gas phase
l - liquid phase
m - mixture
tp - two-phase

3.0 EXPERIMENTAL ARRANGEMENT

3.1 Annular Venturimeter

The annular venturimeter was constructed from an aluminium centrebody of circular cross-section mounted concentrically inside a plain Perspex tube of 100 mm diameter (Fig 1). The centrebody was profiled to form an annular passage followed by a convergent section, a throat section and an annular diffuser. The differential pressure was measured using four pressure tappings equispaced around the outer throat diameter and, similarly, upstream of the converging section. Each set of tappings was connected with a piezometer ring in order to average out pressure variations through the annulus. For lower flow rates, a water manometer was connected across the tappings whilst at higher flow rates a mercury manometer was used. At all conditions the pressure at the inlet annular section tapping was also measured on a pressure gauge to enable the local air density to be determined.

The installation of the annular venturimeter was in a horizontal two-phase air/water flow rig (Fig 2). To ensure a consistent homogeneous flow pattern across the flow range being investigated, a perforated plate homogeniser was installed immediately before the annular venturimeter.

3.2 Variable Area Orifice Flowmeter

The variable area orifice flowmeter was constructed from the moving parts of a commercially available 50 mm meter. These were the shaft, supports, orifice plate, spring and contoured plug which were mounted in a specially manufactured Perspex body (Fig 3). This ensured that a visual assessment of the meter operation was possible. Pressure tappings were mounted in the upstream and downstream flanges of the flowmeter. The differential pressure was measured by a 4-20 mA output transducer, the output of which was recorded by a microcomputer.

The variable area orifice flowmeter was also installed horizontally in the two-phase air/water flow rig. No homogeniser was fitted prior to this meter as it was observed that the flow became homogeneous at all conditions as it was forced through the annulus between the orifice plate and the contoured plug.

3.3 The Test Facility

The horizontal test facility at Liverpool University is capable of single-phase water or two-phase air/water operation. It consists of three horizontal lines, each approximately 15 meters in length, of 50 mm, 100 mm and 150 mm diameter respectively (Fig 2). The water supply is from a 95 m^3 capacity tank giving a constant head of 37 metres of water. After exhaust from the rig, the water is pumped back up to the tank to form a closed loop. The level in the water supply tank can be kept constant to within 25 mm. The flow rate of water in the rig can be measured either by reference turbine and vortex shedding meters or by a gravimetric facility. For two-phase operation the air is injected after the reference meters and before the test section. The air supply is kept at a constant pressure of 100 psi and has a range of 1-2000 ℓ/min of free air, metered by a bank of variable area flowmeters.

3.4 Experimental Procedure

The experimental procedure for both types of flowmeter was essentially the same. The meters were each calibrated in single-phase flow against the reference meters to produce a baseline calibration on water. For two-phase flows, a water flow rate was set and then air flow added to achieve a predetermined volume void fraction. The air and water phases were mixed in the rig at the air injection points. The pressure differential across the meter was then measured for a known total volume flow rate and void fraction. The void fractions used were 5-30% for the annular venturimeter and 5-40% for the variable area orifice meter. A water or mercury manometer (depending on the flow range) was used to measure the pressure differential across the annular venturimeter. The differential pressure across the variable area orifice meter was measured using a pressure transducer.

4.0 RESULTS AND DISCUSSION

4.1 Annular Venturimeter

The theoretical volumetric flowrate through a venturimeter (annular or standard) is given by:

$$Q = A_1\left(\frac{2\Delta P}{\rho[(A_1/A_2)^2-1]}\right)^{1/2}$$

By dividing the experimentally measured flow rate by the theoretical value calculated for the same pressure differential, the discharge coefficient of the meter was found. For single-phase water flow, the fluid density was simply that of the water, whilst for the two-phase flow, the homogeneous mixture density was used and incompressible conditions within the meter were assumed. Thus the mixture density is given by:

$$\rho_m = \alpha\rho_g + (1-\alpha)\rho_l$$

For single phase flow, with Reynolds numbers between 60 x 10^3 and 300 x 10^3, the discharge coefficient was constant with a mean value of 0.975 and a standard deviation of 0.6%, Fig 4. For Reynolds numbers below this range, the value of the discharge coefficient was lower and the data had greater scatter. In BS1042 (1981), the discharge coefficient for a standard venturimeter of the same area ratio is 0.946, and similar trends for the data at lower Reynolds number are observed.

The two-phase flow data from the annular venturimeter does not appear to be influenced by the volume void fraction (Fig.5). Similar data for orifice plates, Chisholm (1967) and Smith et al (1977), also show this. The discharge coefficient decreases from a value of approximately 0.97 at a two-phase Reynolds number around 100 x 10^3 to about 0.92 at a Reynolds number of 260 x 10^3. The data has a standard deviation of 2.7%. From all the data acquired and using the two-phase Reynolds number the relationship

$$Cd_{tp} = 0.998 - 0.4054 \times 10^{-6}\ Re_{tp}$$

is established for $100000 < Re_{tp} < 260000$.

where

$$Re_{tp} = \frac{\rho_m DV}{\mu_m}$$

and

$$\mu_m = x\mu_g + (1-x)\ \mu_l$$

In a convergent section a flow tends to accelerate. In a two-phase gas/liquid flow the gas has less inertia than the liquid due to its much lower density, the inertia inbalance leads to the gas accelerating more quickly than the liquid. This is particularly true under separated flow

conditions. The homogeneous model assumes that there is no slip between the two-phases and, thus, no relative acceleration. This assumption will not necessarily be true in a contracting area duct. However, in an homogeneous type flow or bubbly flow, the inertia of the gas phase is increased by the virtual mass effect, Hinze (1962), Cook and Harlow (1984), Kowe et al (1988). Thus the acceleration difference between the two phases will be reduced, although the magnitude of the effect is difficult to quantify. The effects produced by the relative acceleration at the throat will be a relative velocity (slip) between the two phases and an increase in void fraction and thus a reduction in two-phase mixture density. The increase in void fraction is caused by the decrease in gas density at the throat due to the friction and momentum pressure drops between the annulus and the throat. The increase in void fraction will not be predicted by the homogeneous model, which assumes no change in mixture density between annulus and throat, and so the volume flow rate indicated by the meter will be greater than the actual flowrate through it for a given pressure drop. As the mass flux increases the changes in void fraction and slip will increase leading to an increasing over-prediction by the meter. This is manifest in the reduction of Cd with increasing mass flow rate.

The calibration given above is only applicable to low void fraction flows with homogeneous flow conditions. In fact the theory does not exactly predict the actual flow conditions even when the flow is apparently homogeneous. For flows which have greater slip between the phases, such as separated or annular flows, and for very violent flow regimes, such as slug or plug flows, it is apparent that the calibration will not be very effective. This is expected to be particularly true for separated flow regimes where liquid flows only on the pipe wall, when the pressure drop measured will be due to the velocity change in the air flow in the core of the passage.

The two-phase multiplier,Fig.6, appears to remain constant when the flow rate is increased with constant void fraction. However, the multiplier does increase with void fraction, varying from a value of 1.1 at a void fraction of 5%, to 1.7 at a void fraction of 30%. These values are small by comparison with those of Tapucu et al (1989) who obtained a value for the two-phase multiplier of 3 for a two-phase flow with a void fraction of 20% through smooth blockages of 20% and 40% blockage fractions. The blockage fraction of the annular venturimeter throat is

30%. Tapucu et al (1989) also predicted vena contracta coefficents for smooth blockages using two models. For low void fractions, 21% and less, these models predicted coefficents of greater than unity. This they interpreted as meaning that no vena contracta was formed. However, in the present use the flow did not form a jet and the loss-producing mechanism will therefore be different from that of Tapucu et al and so a different value for the two-phase multiplier would be expected.

4.2 The Variable Area Orifice Flowmeter

The variable area orifice flowmeter was firstly calibrated in single-phase liquid flow using a similar experimental technique to that for the annular venturimeter.

The attraction of the variable area orifice meter is that although it is a differential pressure device, the differential pressure produced is proportional to the flow rate. Using a linear differential pressure transducer, therefore, the electrical output (4-20 mA) is proportional to the flow rate. Thus

$$Q = K.E$$

where K is the meter factor. To correct the meter output for fluid densities other than that for which it was calibrated, the following correction is used:

$$Q = \sqrt{\frac{\rho_{cal}}{\rho_{fluid}}} .K.E$$

Therefore for the two-phase flow, the fluid density becomes the homogeneous mixture density.

Over the range 2 to 20 ℓ/s, the variable area orifice meter had a meter factor of 0.63 as shown in Fig.7. When tested with two-phase flow, the characteristics remained reasonably linear but with a different slope for each constant void fraction, Fig.8. However,if the meter factor is corrected for the mixture density as shown above, the actual volume flow rate shows reasonable agreement with the meter output, as shown in Fig. 9. The corrected meter output understates the actual flowrate, but by less than 7% with am RMS error of 4.92%, for all volume void fractions investigated. These results are comparable with those of Murdock (1962) for gas/liquid flows in a sharp edged orifice. A variable area orifice is

also a contraction in a flow. This leads to the same problems of accelerating flows as seen in the annular venturimeter. Due to the inadequacy of the homogeneous model in predicting slip and void fraction changes the flowmeter tends to understate the actual flowrate. The flow mixing is better than that seen in the annular venturimeter and so the understatement does not increase markedly with mass flow.

The analysis of the signal from the pressure transducer on the variable area orifice meter presented a problem. Due to the unsteady and violent nature of two-phase flows there was a great deal of noise on the signal. By sampling the signal 1000 times it was possible to find a reliable and repeatable mean value which could be used in the analysis. A distribution of a typical signal is shown in Fig.10. This mean value was used to eliminate the noise in the signal and give a reliable data value for the analysis. This type of distribution was typical at all the void fractions investigated, although at higher void fractions the distributions tended to be wider with less well defined means. This was due to the more violent and unsteady nature of higher void fractions flows causing an increase in signal noise. These more unsteady flows were not noticeably smoothed by passage through the contraction of the variable area orifice.

5.0 CONCLUSIONS

5.1 Annular Venturimeter

The annular venturimeter appeared insensitive to changes in void fraction from 5% to 30% in gas-liquid two-phase flow. The meter proved capable of calibration to provide a total volume flow rate. The discharge coefficient of the annular venturimeter increased from 0.975 at Re_{tp} of 90000 to 0.92 at Re_{tp} of 260000 in a linear relationship. The data collected was for the homogeneous flow regime only and thus the calibration is only of use in this flow regime. The annular venturimeter, therefore, will give a total volume flowrate and providing the void fraction is known will give flow rates of individual phases. The annular venturimeter could be useful as the meter in a two-phase flowmetering package. The flowmetering package would also require an upstream device for determining the void fraction of the two-phase flow, such as a gamma-ray densitometer.

5.2 Variable Area Orifice Flowmeter

The variable area orifice meter proved to retain its linearity under two-phase flow conditions. The meter factor was influenced by the void fraction of the gas-liquid two-phase flow ranging from 0.67 at 5% volume void fraction to 0.84 at 40%. The variable orifice tends to produce a well-mixed homogeneous flow regime even when the flow pattern at the inlet to the meter is separated; this removes the need for a flow conditioner. The variable area orifice meter will measure total volume flowrate of two-phase flows with void fraction from 5% to 40%, providing that the void fraction of the gas-liquid flow is known. The analysis of the signal removes fluctuations due to unsteady flow characteristics, and provides a reliable mean from the data which can be used to evaluate the volume flowrate through the meter. The variable area orifice meter could also find application as the metering device in a flowmeter package when combined with a void fraction meter.

6.0 REFERENCES

AZZOPARDI,B.J. and GOVAN,A.H. 1985. "Annular Two-Phase Flow in Venturis". European Two-Phase Flow Group Meeting, Marchwood Eng. Lab 4-7 June 1985.

CHISHOLM,D. 1967. "Flow of incompressible two-phase mixtures through sharp-edged orifices". J. Mech.Eng. Sci.,vol 9 No 1, pp 72-78

COOK, T.L. and HARLOW, F.H. 1984. "Virtual Mass in Multiphase Flow". Int.J. Multiphase Flow, Vol.10, No 6, pp 691-696.

HINZE, J.O. 1962. "Momentum and Mechanical energy balance equations for a flowing homogeneous suspension with slip between the two phases". Appl. Sci. Res., A11, 33-46.

KOWE, R. HUNT, J.C.R. HUNT A. COUET, B. and BRADBURY, L.J.S. 1988. "The Effects of Bubbles on the Volume Fluxes and the Pressure Gradients in Unsteady and Non-uniform Flow of Liquids". Int.J. Multiphase Flow, Vol. 14, No.5, pp 587-606.

MURDOCK, J.W. 1962. "Two-phase flow measurement with orifices". Trans.ASME Journal of Basic Engineering. Dec., pp 419-433.

SMITH, L.T. MURDOCK, J.W. and APPLEBAUM, R.S. 1977. "An Evaluation of Existing Two-Phase Flow Correlations for Use with ASME Sharp Edge Metering Orifices". Trans.ASME Journal of Engineering for Power, July 1977, p343-347.

TAPUCU, A, TEYSSEDOU, A. TROCHE, N and MERILO, M. 1989 "Pressure Losses Caused by Area Changes in a Single-Channel Flow under Two-Phase Flow Conditions". Int.J. Multiphase Flow Vol.15, No1, p51-64.

THANG, N.T. and DAVIES, M.R. 1979. "The Structure of Bubbly Flow through Venturis". Int.J. Multiphase Flow Vol.5, No.1,p17-37.

WALLIS, G.B. 1969. "One-Dimensional Two-Phase Flow". McGraw-Hill.

BS1042 1981 "Specification for Square Edge Orifice Plates, Nozzles and Venturi Tubes Inserted in Circular Cross-Section Conduits running Full".

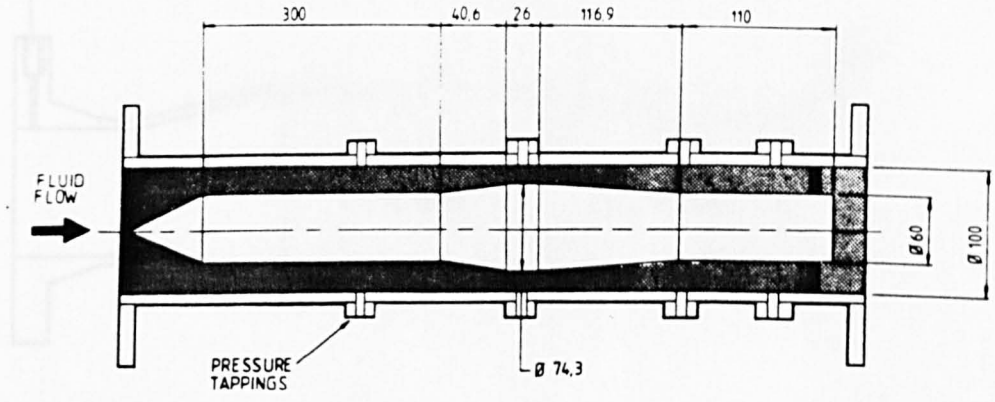

Fig.1 Annular Venturimeter

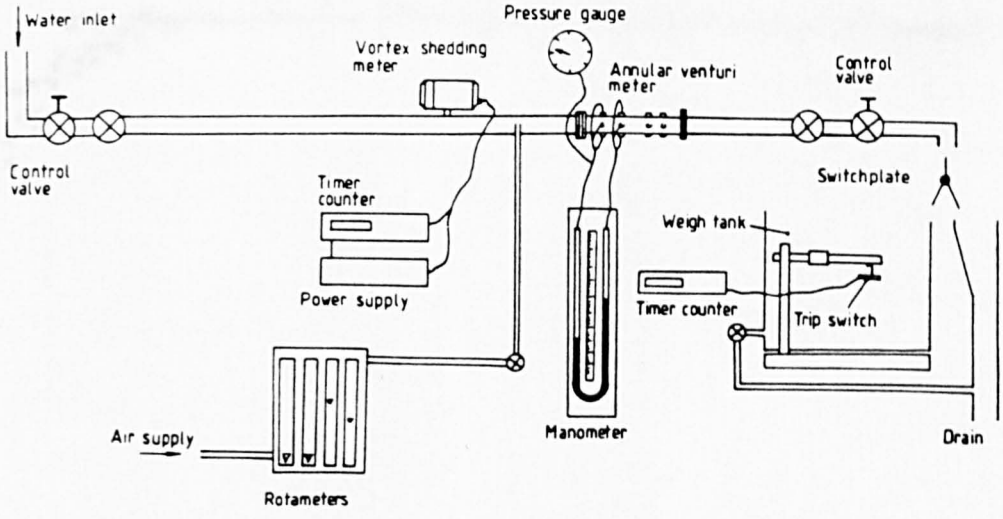

Fig.2 Two-Phase Air/Water Test Rig

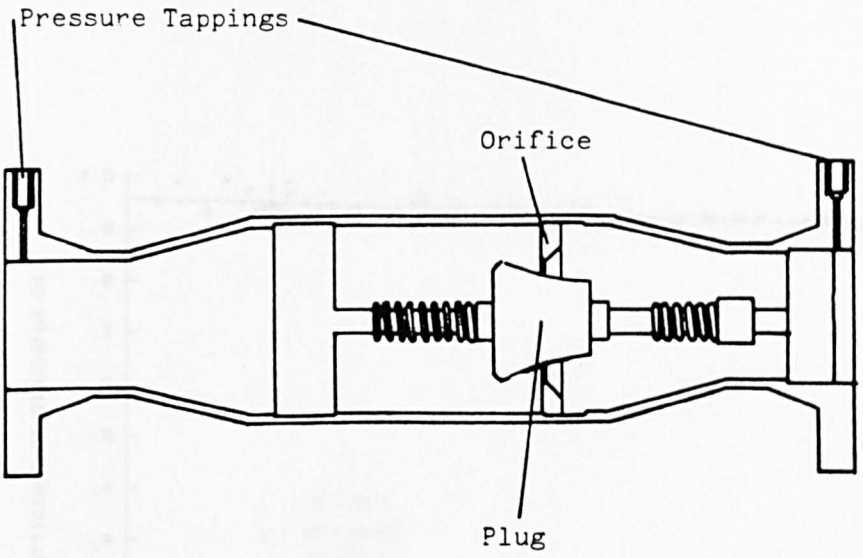

Fig.3 Variable Area Orifice Meter

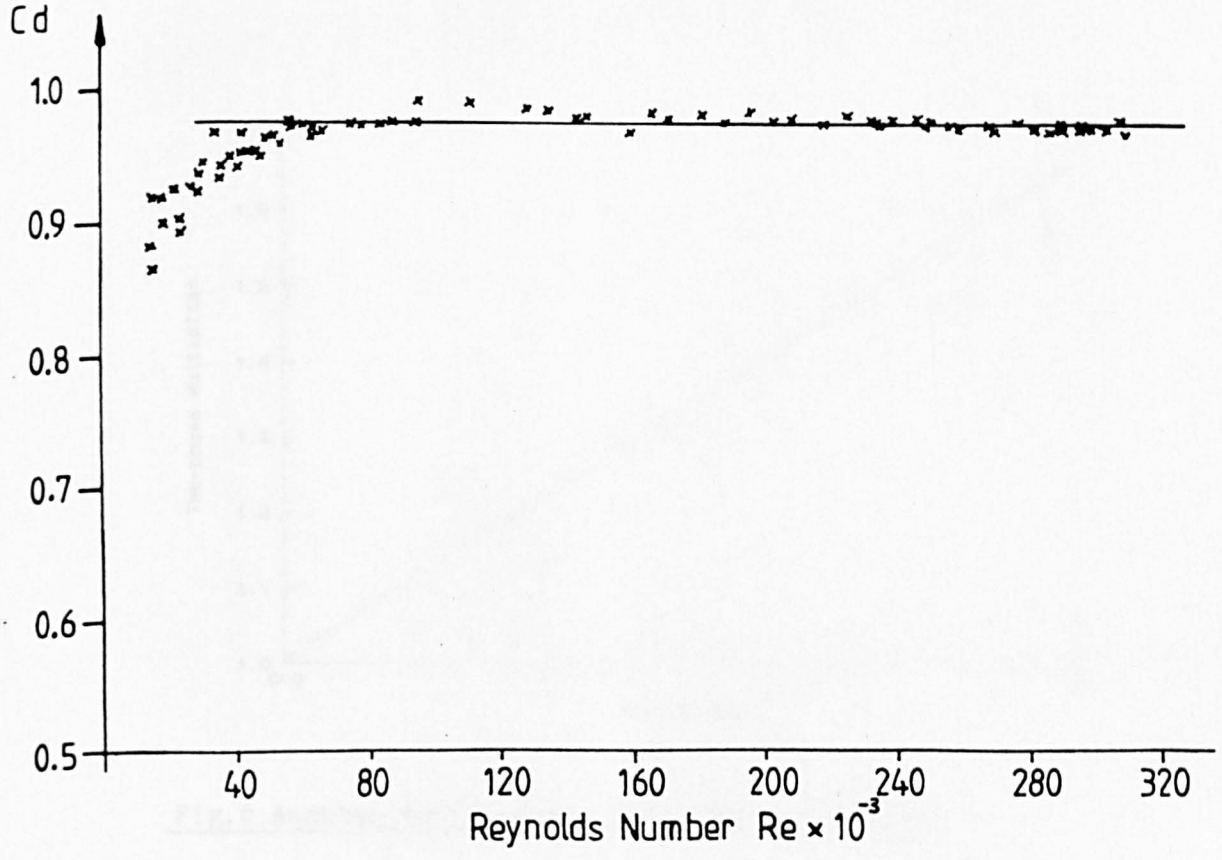

Fig.4 Annular Venturimeter Single-Phase Discharge Coefficient

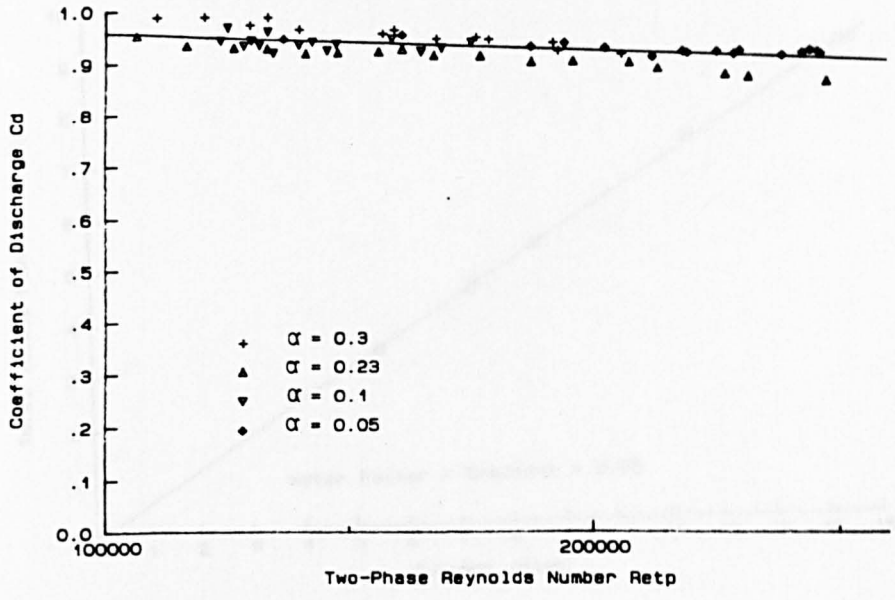

Fig.5 Annular Venturimeter Two-Phase Discharge Coefficient

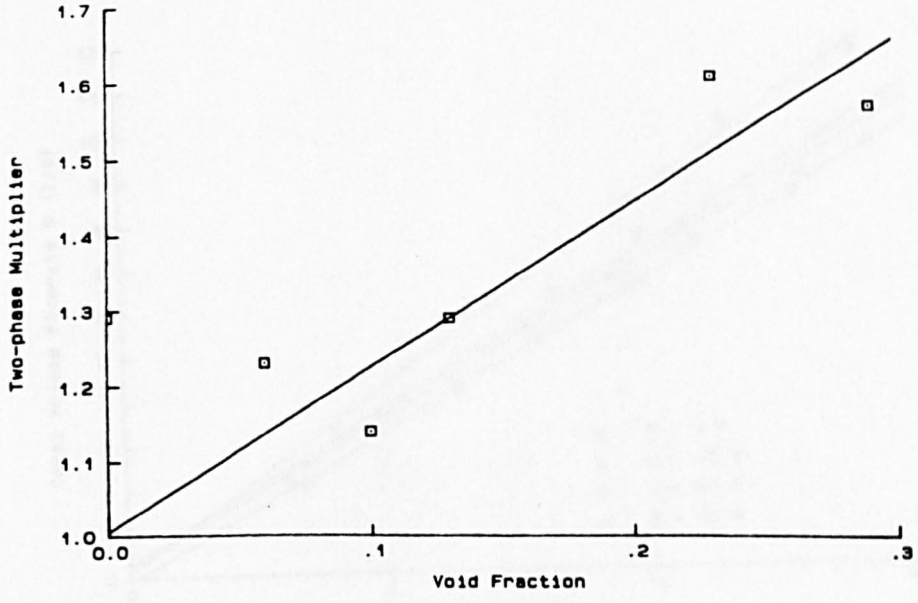

Fig.6 Annular Venturimeter Two-Phase Multiplier

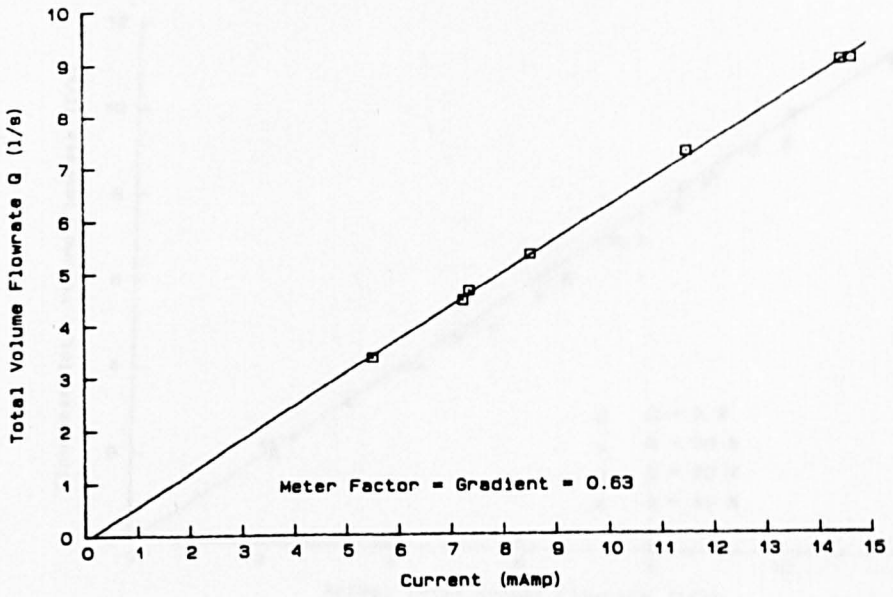

Fig. 7 Variable Area Meter Single-Phase Calibration

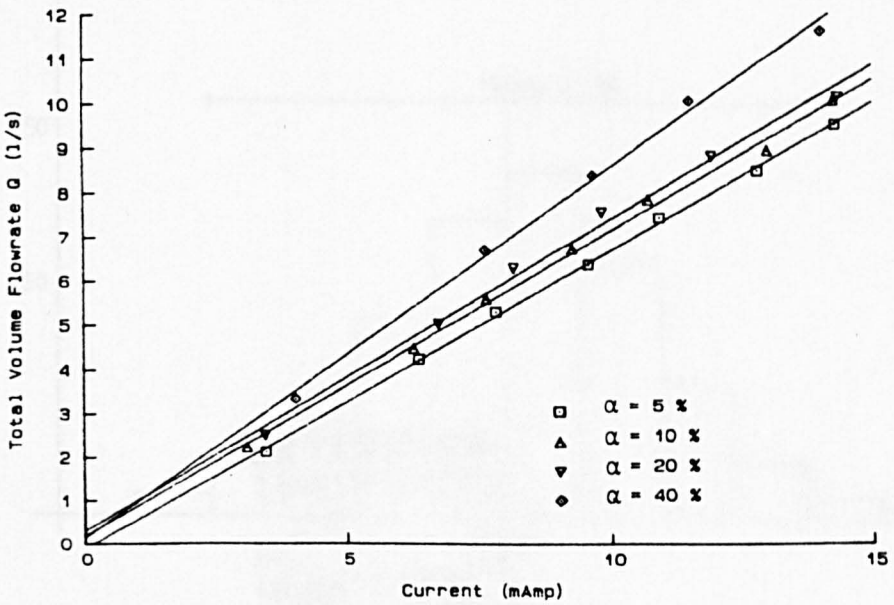

Fig. 8 Variable Area Meter Two-Phase Calibration

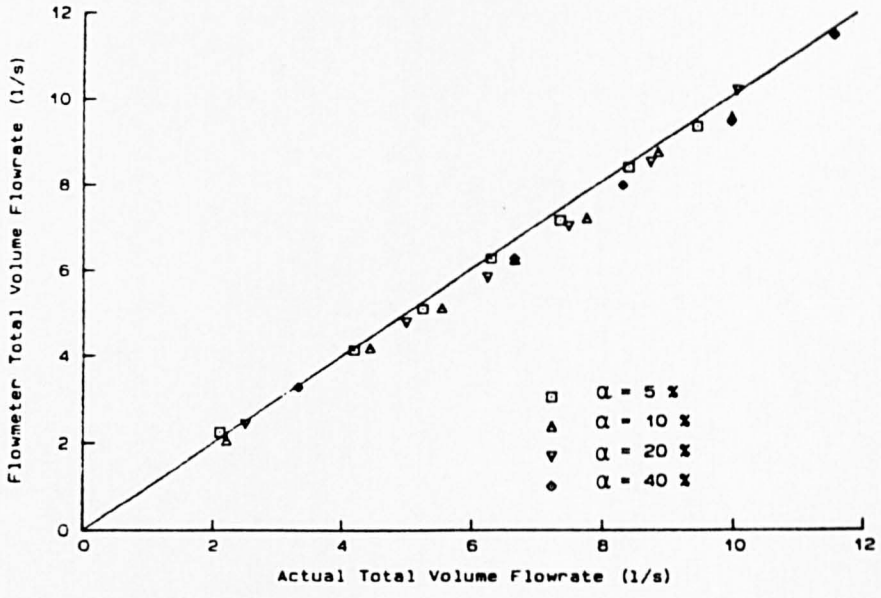

Fig. 9 Variable Area Meter Two-Phase Calibration with Homogeneous Mixture Density Correction

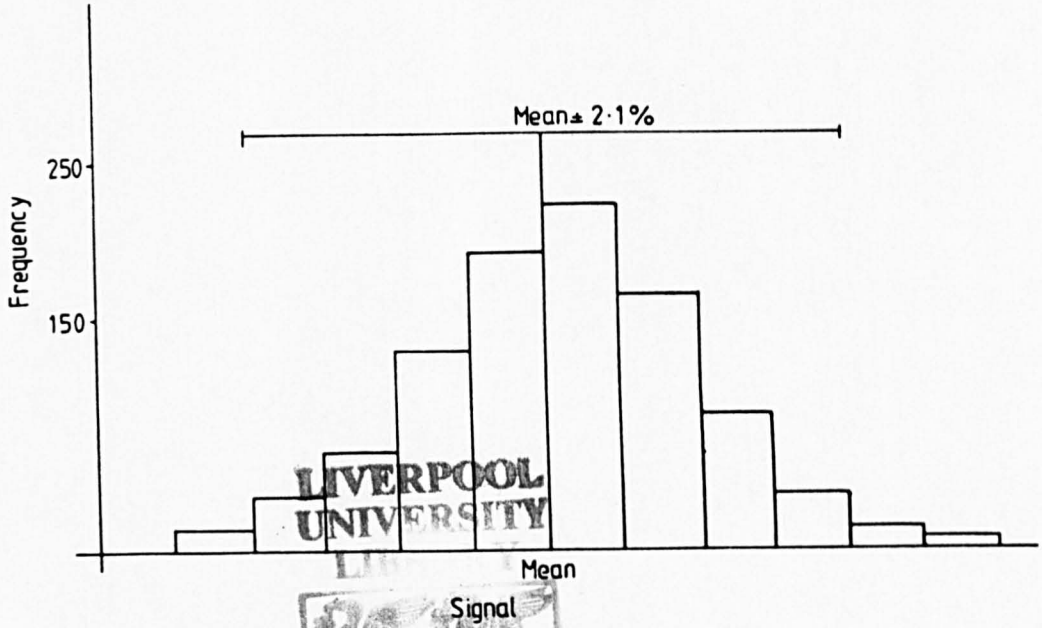

Fig. 10 Variable Area Meter Signal Distribution